Curso 2012/13
CIENCIAS Y TECNOLOGÍAS/44
I.S.B.N.: 978-84-15939-18-4

MANUEL PERGER

Una búsqueda de objetos de baja masa en regiones jóvenes de formación estelar

Directores
EDUARDO MARTÍN
DAVID BARRADO Y NAVASCUÉS

SERVICIO DE PUBLICACIONES
UNIVERSIDAD DE LA LAGUNA

SOPORTES AUDIOVISUALES E INFORMÁTICOS
Serie Tesis Doctorales

Resumen

La mejor herramienta y la más usada para caracterizar la formación de estrellas en un sistema cerrado es la función de masas. Muchas investigaciones en varias regiones, incluyendo Orion, muestran que su aspecto y su forma son más bien universales con un pico aproximadamente a 0.1 a 0.2 $M_{\odot}$. Sin embargo, hay excepciones importantes como la región de la formación estelar de Toro. En ésta, la distribución de las masas estelares muestra un pico aproximadamente a 0.8 $M_{\odot}$. Muchas estrellas de baja masa faltarían en esta región para que pudiera encajar la forma universal de la función. Esto podría darse debido a una de las características únicas de Toro como por ejemplo su baja densidad. Esta región es muy fácilmente accessible debido a su juventud y su proximidad. Numerosas investigaciones se han llevado a cabo buscando objetos nuevos en las nubes principales de la región. Sin embargo, algunas teorías proponen que muchos de los objetos de baja masa de Toro nacidos recientemente podrían ser expulsados de sus sitios de nacimiento, esto es, las nubes moleculares.

Nuestro objetivo es encontrar nuevos objetos de baja masa en Toro que pudieran proporcionar un nuevo enfoque sobre su función de masa. La región estudiada en este trabajo está localizada 5 *deg* al norte de las nubes principales y cubre aproximadamente 25 *sq.deg*. De esta manera, también contribuimos a resolver la pregunta si los objetos de baja masa se han movido desde su sitio de nacimiento o no. Puede que los objetos falten porque una gran parte de ellos ya no esté conectada con las partes más densas de las nubes principales de Toro. La meta fue encontrar tantos objetos como fuera necesario para identificar una diferencia en la función de masa y para poder constatar así una parte importante de miembros de Toro de baja masa lejos de las nubes. Para confirmar la relación entre la diferencia de la función de masa de Toro y su baja densidad de 1 $estrella \cdot pc^{-2}$, también hemos estudiado 15 *sq.deg*. de la región de Orion, de mayor densidad. En esa región buscamos nuevas asociaciones de estrellas para lograr construir sus funciones de masa completas hasta aproximadamente las mismas masas igual que realizamos en la investigación en Toro.

Para nuestra búsqueda hemos usado como base de datos el registro fotométrico de campo amplio e infrarrojo cercano UKIDSS GCS, el cual alcanza aproximadamente 3 magnitudes más en profundidad que 2MASS. Hemos investigado las características fotométricas de todos los 351 miembros de Toro ya conocidos y las hemos aplicado a esta base de datos para poder extraer posibles nuevos miembros. Debido a la baja densidad y la proximidad de la región, se aumentó el alcance de criterio de búsqueda mediante la construción de un mapa de extinción de alta resolución. Es más, fuimos capaces de tener acceso a movimientos propios y fotometría de infrarrojo mediano de una peque*ñ*a parte de la región estudiada. En total, se aplicaron 40 criterios de selección. En Orion se limpió la base de datos de posibles efectos de extinción y se hizo uso de diferentes métodos para identificar las asociaciones estelares que contiene la región. Para confirmar la pertenencia a una de las regiones de todas las fuentes selecionadas, se observaron tantos candidatos como fue posible mediante espectroscopia óptica de baja resolución. En este rango de longitud de onda, múltiples características de las líneas pueden revelar la juventud de una fuente. Para comparar dichas fuentes se observaron unos miembros de Toro ya conocidos y unas estrellas enanas de campo.

En Toro fueron observados 43 de 253 candidatos brillantes y 7 de 55 en Orion. El análisis fotométrico y espectral completo pudo identificar 7 y 4 de ellos como posibles nuevos miembros WTTS. Esto implica una cuota de éxito de observacin del 17% en Toro. Los objetos observados tienen tipos espectrales de hasta $M4.5$. En Orion hemos encontrado una nueva asociación estelar muy dispersa con la

función de masa universal. No obstante su existencia todavía no se puede establecer pues solamente se pudieron observar 7 fuentes. Los nuevos miembros de Toro no están conectados con ninguna nube molecular y se han movido desde su sitio de nacimiento a su sitio actual. Su existencia indica una significante población todavía desconocida de miembros de Toro lejos de las nubes principales. Nuestro proceso de búsqueda sin embargo está sesgado por magnitudes. Sólo tuvimos acceso a objetos con $12.0 < J < 15.5$ *mag* o $0.55 > M > 0.08\ M_{\odot}$. Dentro de este rango están localizados 104 miembros de Toro ya conocidos. Así pues, los 7 nuevos miembros contribuyen en un 10% a la función de masa. Teniendo en cuenta que sólo se observó el 17% de nuestra lista de canditatos, esperaríamos encontrar unos 41 miembros en la región estudiada dentro de este rango de magnitudes. Por tanto podemos concluir que los objetos de Toro de baja masa que faltaban están localizados lejos de las nubes principales de la región. Si esta región joven y cercana de formación estelar es única o no, se puede estudiar en sus partes externas. Toro es sin lugar a dudas de menor densidad y está más extendida a como se había asumido previamente.

Abstract

The best and most widely used tool to characterize the formation of stars in an enclosed stellar system is the mass function. Many investigations in various regions including Orion, point to a rather universal shape and form of it, peaking at around 0.1 to 0.2 $M_\odot$. Nevertheless, there are important exceptions, such as the Taurus star-forming region. There the distribution of stellar masses shows a peak at around 0.8 $M_\odot$. Many low-mass objects would be missing there in order to match the universal form of the function. This could be due to one of the unique characteristics of Taurus such as its low density. This region is very easily accessible because of its youth and proximity. Many investigations have been conducted to search for new sources in the main clouds of the region. However some theories suggest that many of the new born low-mass objects in Taurus might be ejected from their birth site, i.e. the molecular clouds.

We aim to find new low-mass objects in Taurus in order to get new insights on its mass function. The investigated area in this work is located 5 *deg* north of the main clouds and covers around 25 *sq.deg*. Thus, we also contribute to answer the question whether the low-mass objects have moved from their birth sites or not. Maybe the reason for the missing objects is that a large fraction of them is not anymore connected to the densest part of the main clouds of Taurus. We aimed to find as many objects as necessary to identify a difference in the mass function and to be able to claim such a significant fraction of off-cloud low-mass Taurus members. To probe the link between the difference of the mass function of Taurus and its low density of around 1 $star \cdot pc^{-2}$, we also studied 15 *sq.deg.* of the denser Orion region. There we searched for new stellar associations in order to construct their complete mass functions down to about the same masses as we did for the investigation in Taurus.

As database for our search we used the wide-field near-infrared photometric survey UKIDSS GCS, which reaches around 3 magnitudes deeper than 2MASS. We analyzed the photometric characteristics of all 351 already known Taurus members and applied them to this data set in order to extract new possible members. Due to the low density and the proximity of the region we increased the search criteria by constructing a high-resolution extinction map. Furthermore, we were able to access proper motions and mid-infrared photometry of a small part of our investigated region. All in all, we applied around 40 selection criteria. In Orion, the data set was cleaned from possible extinction effects and various methods were used to identify the stellar associations contained there. To probe the membership of all selected sources, we observed as many candidates as possible with low-resolution optical spectroscopy. In those wavelength ranges, many line features can reveal the youth of a source. To compare them, a set of already known Taurus members and field dwarfs were observed.

In Taurus and Orion, we observed 43 of 253 and 7 of 55 bright candidates, respectively. The complete photometric and spectral analysis revealed 7 and 4 of them as possible new WTTS members, which implies an observational success rate of around 17% in Taurus. The observed objects have spectral types up to $M4.5$. In Orion we found a very loose new stellar association showing the universal mass function. Its existence is however not yet well established, since we could observe only 7 sources. The new Taurus members are not connected to any molecular cloud and have moved from their birth site to their present location. Their existence indicates a significant unknown population of Taurus members away from the main clouds. Our search process was however biased by magnitudes. We only accessed objects with $12.0 < J < 15.5$ *mag* or $0.55 > M > 0.08$ $M_\odot$. 104 already known Taurus

members are located in this range. There, the 7 new members contribute around 10% to the mass function. Taking into account that we observed only 17% of our candidate list, we would expect around 41 new members in this magnitude range in our investigated region. Therefore, we conclude that the missing Taurus low-mass objects are located away from the main clouds of the region. The answer to whether this young and nearby star-forming region is unique or not can be found in its outer parts. The region is beyond doubt of lower density and more stretched out as previously assumed.

Acknowledgment

This research was funded by the European FP6 Marie Curie Research Training Network 'CONSTELLATION' under contract number MRTN-CT-2006-0358901. I would like to thank them and my two supervisors Eduardo and David for giving me the opportunity to work on the beautiful island of Tenerife. The 'Instituto de Astrofísica de Canarias', the 'Universidad de La Laguna' and the people I know there offered me a nice working place and atmosphere and provided me with everything I could ask for as a young researcher. I thank also the people which helped me with the thesis and with the life on the island, especially Mirjana and Karla. Of great scientific help was Nicolas, without whom I could not have done it. I thank the village of Almáciga for offering me a wonderful place to live. In Madrid, I would like to thank my collaborators Maria, Miriam, Hervé and David for the observations, the additional data and the help they gave me.

I thank my parents and my family for there financial help and their support throughout all those years of studies. I thank Anne for helping me with the English texts and my friends Nadja, Marion and Christoph for their love. Manuel, Jurek, Anna, Milan and Paul, I wish you the best in life! A special thank to Nela for loving me and for tolerating everything ... also the worst phases during the thesis.

But since it is made also for every reader, I would like to thank you. Whether you decided to read it out of pleasure, out of interest or just because you helped me getting through this PhD process.

Contents

List of Figures

List of Tables

Chapter 1

Introduction

1.1 Characterization of stellar formation

The formation of stellar and substellar objects is still a not completely understood topic in modern astrophysics. This is especially true for objects with masses larger than 8 solar masses ($M_{\odot}$) and less than 0.08 $M_{\odot}$. It takes place deep within Giant Molecular Clouds (GMC; Lada 1987), which form the denser regions of the interstellar medium of a galaxy. In general, they contain 10^5 to 10^7 $M_{\odot}$ of molecular hydrogen and show diameters of 100 to 1000 pc (Williams et al. 2000). Such huge clouds form the coldest objects in the universe with $10-50$ K and are highly structured into filaments, clumps and dense cores (Williams, Blitz & Stark 1995). The star-forming (SF) process begins, when the hydrostatic equilibrium of the cloud, i.e. the balance of its potential energy and gravity, fails. This happens if the mass of the cloud exceeds its Jeans mass, depending on its density and temperature. Allen et al. demonstrated in their 2007 review that most embedded young star clusters appear to be the densest regions of such much larger distributions that span the entire GMC. In the infrared wavelengths one can observe, that around 10% of the cloud mass is located in small clumps and clusters showing several hundreds of newly formed stars. Those include SF regions, open clusters and star associations which consist of stellar populations formed by the same material (i.e. same metallicity & gravity) and showing roughly same age and distance from the observer. The process of stellar formation involves the interplay of fragmentation from turbulent motions in the parental molecular cloud, gravity, dynamical motions of young stars, and the feedback from the youngest bright stars of type O and B. More complex distributions are delivered by the rotation of the young stars and, strongly connected to that, the influence of magnetism. The radiation of the larger stars and the ratio of binary formation are additional issues complicating the process. Nevertheless, it should be assumed that all objects of all different masses form in the same manner, resulting in a similar distribution of masses and luminosities for an enclosed stellar system. But many results point to a more complex explanation. Various numerical simulations have been dedicated to this problem (e.g. Bate et al. 2003, Bonnell et al. 2003), but their predictions are difficult to verify observationally. Important observational constraints are the spatial structure, the kinematics and the history of each cluster or molecular cloud.

And, since the work by Salpeter (1955), the Mass Function (MF) forms the one most important tool for constraining the formation of stellar objects. By looking at an enclosed stellar system, this function connects the number N of objects of a certain mass interval to their mass M. In those days, surveys reached down to around $V = 13$ mag or 0.5 $M_{\odot}$ and the relation found was:

$$\xi(logM) = dN/dlogM = 0.03 \cdot M^{-1.35}$$

It has been investigated during these decades in various environments and larger mass ranges to prove its universality or its dependency on age, density or galactic position of the investigated areas. Miller & Scalo (1979) and Scalo (1986) improved the accuracy of the form of the MF. Up to date different theoretical scenarios are able to reproduce it. Those investigations got separated into MF from the beginning of the star formation in a certain region (initial mass function or IMF) and the one observable in present days (system mass function or as we use it throughout this work, the MF). Recent results of large-scale surveys of open clusters suggest that it should be universal and not vary much with the initial conditions (Gutermuth et al. 2009). Latest data of the solar neighborhood and star clusters point towards a broken power-law or log-normal representation of the system MF and indicate no difference to the one formed by field stars (Kroupa 2002, Chabrier 2005, Larson 2005):

$0.08\ M_\odot < M < 1.00\ M_\odot$: $\xi(logM) = 0.076 \cdot exp[-(logM - log0.25)^2/(2 \cdot 0.55^2)]$
$1.00\ M_\odot < M < 3.47\ M_\odot$: $\xi(logM) = 0.044 \cdot M^{-4.37}$
$3.47\ M_\odot < M < 18.20\ M_\odot$: $\xi(logM) = 0.015 \cdot M^{-3.53}$
$18.20\ M_\odot < M < 63.10\ M_\odot$: $\xi(logM) = 0.00025 \cdot M^{-2.11}$

Note that the influence of binarity is very important. It is estimated that every third star in the galaxy is of such kind and orbits another star (Fender 2002). But in general, investigations of the system MF do not consider this effect.
Throughout this work, we will use the term low-mass objects (LMO) for low-mass stars ($< 0.5\ M_\odot$) and substellar objects ($< 0.08\ M_\odot$, hydrogen burning limit) like Brown Dwarfs (BD) and planetary-mass objects ($< 0.013\ M_\odot$, deuterium burning limit). Depending on the model, the stellar/substellar border for objects of $< 10\ Myr$ is equivalent to a stellar type of M6 (NextGen by Baraffe et al. 1998, AMES-Dusty by Chabrier et al. 2000 & COND by Baraffe et al. 2002). Thereby, we use the Morgan-Keenan or MK system, classifying stellar objects by the letters $O, B, A, F, G, K, M, L, T, Y$ (from hot to cool objects) and by a number between 0 and 9 as subclass[1] (Morgan & Keenan 1973). Around 75% of all stars in the Galaxy are classified as type M (Ledrew 2001). Stars of lower mass are generally smaller and of lower luminosity than larger ones. Therefore it is easier to reach down to the low-mass part of a MF in stellar associations close to Earth, since the detectability of its fainter members will be better.

Located beyond the substellar mass limit, BD were discovered and confirmed at the end of the last century (Rebolo et al. 1995, Nakajima et al. 1995). They form a large part of the uncertainties of the MF . BD cannot be classified as stars since they do not enter the hydrogen fusion process but only burn their deuterium for some 2 to 20 million years (Myr, Baraffe et al. 1998, Palla et al. 2005). Therefore, they are brightest in this relatively short time scale and hence best visible for the observer. To fill the gap in the knowledge of the MF in the low-mass range, it is therefore not only necessary to look for nearby regions, but also for young ones.
BD of late type M are characterized by cool (effective temperature $T_{eff} < 3500\ K$, Golimowski et al. 2004) cloudy atmospheres and red near-infrared (NIR) colors. Some of them show strong variable magnetic fields. Their optical spectra are dominated by large absorption bands (e.g. titanium oxide TiO, vanadium oxide VO, Morgan et al. 1943, Pavlenko et al. 2005). Besides the spectral type, there

[1] in diagrams and tables we translate the spectral types $O0, ..., M0, ..., Y0$ into the numbers $00, ..., 60, ..., 90$

are not many possibilities to distinguish them from young low-mass stars. In the so-called lithium test (Rebolo et al. 1992, Magazzu et al. 1993, Martin et al. 1994), BD are recognized by the presence of lithium line features in their spectra. This is due to the depletion of lithium in the hydrogen-burning stars. Note that this is only valid for BD with less than 0.065 $M_{\odot}$, the lithium burning limit and requests the usage of medium and high resolution spectra, which are up to date very time-intensive to obtain for such faint objects.

The objects of types L ($< 2700\ K$) and T ($< 1450\ K$) describe even cooler objects. They still show spectra dominated by the mentioned absorption bands. But in the spectra of the type L objects the influence of various metal hydride bands (e.g. FeH, CrH), water H_2O and carbon monoxide CO increase and various prominent alkali metal lines (e.g. NaI, KI, CsI) are visible. For the objects of type T, which are all BD, the influence of methane (CH_4) absorption gets very important (Pavlenko et al. 2005). Together with the water absorption bands it is so huge, that even the overall NIR colors get influenced and turn blue (Pinfield et al. 2008). Following this trend, the lowest mass BD of type Y were discovered just recently showing effective temperatures of less than 600 K (Cushing et al. 2011, Kirkpatrick et al. 2012). Those objects are supposed to show nearly no optical emission (Rodriguez et al. 2011). Beyond that spectral type only high mass planets are located. Young BD are still easily distinguishable from those objects, since they still burn their deuterium. If they get older it gets more difficult. Therefore, the mass of the deuterium burning limit is set to be the main separator between BD and planets.

For the formation of BD several mechanisms have been advocated (e.g. Whitworth et al. 2007). There is the stellar formation scenario (Padoan & Nordlund 2002), where they form via gravitational collapse and fragmentation of low-mass cores. As for low-mass stars, this process is followed by significant disk accretion. Here, the material would just not be sufficient to trigger the hydrogen fusion. Also, the protoplanetary disk could be destroyed early on by external influences. Such could be the radiation of bright OB stars in a massive star cluster or collisions with other stars. A second theory is the ejection scenario (Reipurth & Clarke 2001). Here, BD are ejected from their parent core and end up being starved for molecular material further away from the main cloud. This can happen e.g. in a system of multiple stars. Also, BD could form like planets by either core accretion or instabilities in the planetary accretion disk of a star and get ejected later on. Up to date there is no strong evidence, that there is any difference in their formation compared to stars. As we will point out further down, we aim to contribute to this question due to the location of our 'hunting ground' away from the center of the molecular clouds.

To complete our knowledge of the low-mass end of the MF, we explained why the regions to investigate should be not only nearby, but also relatively young. In such regions, the young stellar objects (YSO) are mostly still embedded in the gas and dust of the molecular cloud they were born in. So, the advantage of the improved detectability of BD is opposed by the disadvantage of the extinction of parts of their emitted light. As the sources get older, the gas and dust around them form an accretion disk, which emit mostly in the wavelength range longer than 3 μm. Going on in this evolution, the objects finally loose their accretion disk. This sequence gets also reflected in the classification done for YSO in literature: following Lada 1987, Andre et al. 1993 and Greene et al. 1994, they are generally divided by the slope α of their spectral energy distribution (SED, see Fig. 1.1):

$$\alpha = dlog(\lambda F_{\lambda})/dlog(\lambda)$$

- Class 0: faint for $\lambda < 10\mu m$
- Class I: $\alpha > 0.3$

- Flat spectrum: $0.3 > \alpha > -0.3$
- Class II: $-0.3 > \alpha > -1.6$
- Class III: $-1.6 > \alpha$

Up to Class I, the objects are classified as protostars, fully surrounded by the gas and dust they were born in. A Class III object then is already a young main-sequence star.

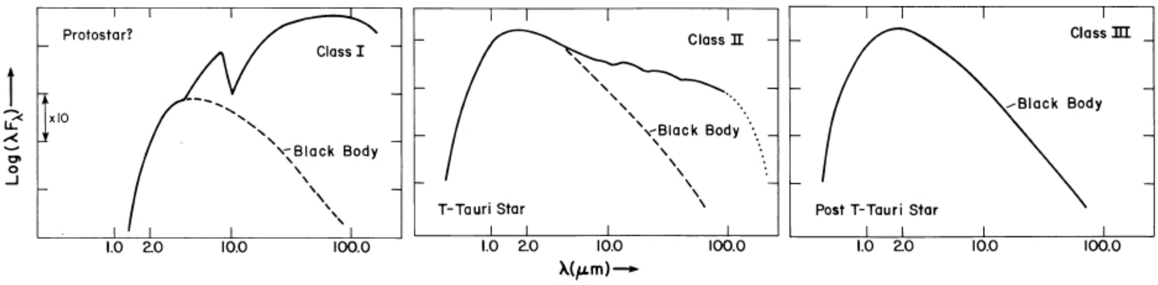

Figure 1.1: The classes of stellar objects by Lada (1987). In these sketches, the influence of the gas and dust surrounding the core of the protostar and later on the stellar object is illustrated by the SED of the object. The latter emits a blackbody radiation, whereas the gas and dust is cooler and emits in the mid-infrared wavelength range. A protostar, where the gas and dust is located all around the core is classified as Class I in this picture. A T-Tauri star with the gas and dust accreting around the stellar object is classified as Class II and a main-sequence or post T-Tauri star as Class III.

The young, low-mass, pre-main sequence stars of Class II are commonly referred to as T Tauri stars (TTS). The gas and dust around them form an accretion disk, which results for the observer into strong photometric variability. Also, an excess in the mid-infrared (MIR) occurs, since the cool material of the disks will emit their radiation mostly in this wavelength range. The disks of such objects are generally referred to as protoplanetary discs, since they are supposed to be progenitors of planetary systems. They show a strong chromospheric activity, resulting in large hydrogen ($H\alpha$, $Br\gamma$, $Pa\beta$) and metallic (*CaII* infrared triplet) emission lines. In contrast to main sequence stars, they show a high abundance of lithium. After that 'classical' stage of the T Tauri phase (CTTS), they begin to loose their accretion disk and, due to the absence of the strong emission lines, are then referred to as weak-lined T Tauri stars (WTTS). They still show at least hydrogen in emission, but less broad and only due to chromospheric activity. Barrado et al. (2003a) state an empirical 50 to 5% of stars showing disks in stellar associations of ages of 1 to 10 *Myr*, respectively.
Those Class II YSO are not yet that compact and hence show larger radii than main-sequence stars of same mass. This results in a smaller value for the local gravity compared to more evolved objects. Their energy source is the gravitational contraction. If they get older, they get therefore smaller and their rotational velocity increases. The gravity is thereby a very important tool to distinguish younger from older sources and can be measured by absorption lines resulting from transitions of e.g. sodium (*NaI*) or potassium (*KI*) in the optical and infrared wavelengths.

1.2 Investigated regions

As we have pointed out, it is necessary to look deep into nearby and young enclosed stellar associations to access the complete MF formed of one molecular cloud. With nearby, we refer to distances up to 1 *kpc* from Earth. With young, we refer to regions containing stellar populations with an age of less than 20 Myr, where BD are supposed to still burn their deuterium. In our own Galaxy such regions have been investigated intensively to find answers to the questions related to the form and shape of the low-mass part of the MF. Many new members in this mass range were found in all of them. We give an overview of some important regions used or mentioned in this work in Tab. 1.1. We give distances, ages and references to publications describing searches for new low-mass members or the investigation of the MF.

name	distance [pc]	age [Myr]	Reference
Taurus-Auriga	140	≈1	see text
Trapezium/ONC (Orion)	480	≈1	Slesnick et al. 2004, Muench et al. 2002, Hillenbrand et al. 2000
σOrionis (Orion)	350-440	3-8	Bejar et al. 2011, Lodieu et al. 2009, Hernandez et al. 2007
			Kenyon et al. 2005, Zapatero Osorio et al. 2003
IC 348 (Perseus)	315	2	Burgess et al. 2009, Luhman et al. 2003a, Muench et al. 2003, Lada et al. 1995
Alpha Per (Perseus)	182	90	Lodieu et al. 2005, Deacon et al. 2004, Barrado et al. 2002, Stauffer et al. 1999
Upper Sco (Scorpius-Centaurus)	145	≈5	Lodieu et al. 2011a, Slesnick et al. 2008, Lodieu et al. 2008
			Lodieu et al. 2007b, Slesnick et al. 2006b
IC 4665 (Ophiuchus)	350	27	Lodieu et al. 2011b, Cargile et al. 2010, Manzi et al. 2008, de Wit et al. 2006
Chamaeleon I (Chamaeleon)	165	2-6	Luhman et al. 2008a, Luhman et al. 2008b, Luhman 2007
Pleiades	134	125	Lodieu et al. 2007a, Bihain et al. 2006, Moraux et al. 2003, Stauffer et al. 1998

Table 1.1: Distances and ages of some important SF regions used or mentioned in this work. We give the names of the region and the name of the greater area in brackets.

The outcome of those investigations form in the most cases a quite consistent and universal view. Their system MF mostly show peaks at around 0.1 to 0.3 $M_{\odot}$. Only few regions do not fit into it. In Fig. 1.2 we show MF of three different clusters. Two of them show the universal behavior, whereas the other function differs by very much. Those variations in the peak mass or the overall shape of the MF were mostly connected to the different densities of the regions.

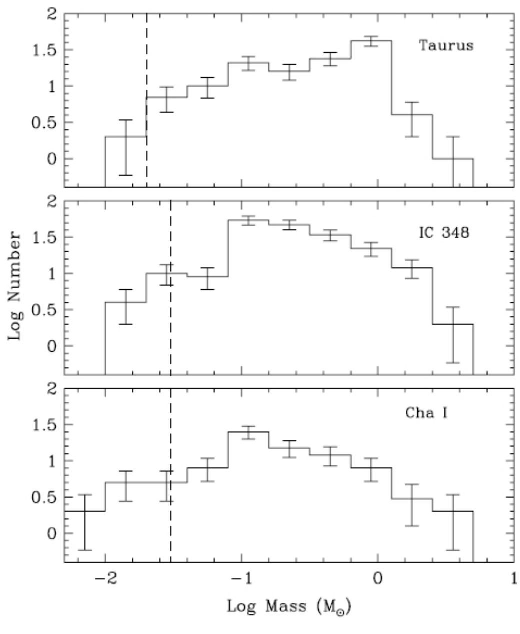

Figure 1.2: The MF of Taurus, IC 348 and Chamaeleon I by Luhman (2007). Except Taurus, they show the peaks at around 0.1 $M_{\odot}$ ($log(M) = -1$) following the 'universal' MF. They differ from Taurus in their higher density. The difference in the peak value of Taurus forms one of the strongest arguments against the proposed universality of the MF and its connection to the density of the region.

The main database used in this work to achieve the explained goals is designed especially for those

purposes: the Galactic Cluster Survey (GCS), a sub-survey of the UKIRT Infrared Deep Sky Survey (UKIDSS). It observed four SF regions and six open clusters far deeper as the substellar limit in those nearby regions.
Our main investigations were done in the Taurus-Auriga SF region. As requested, it is very young (1 *Myr*) and nearby (140 *pc*, e.g. Kenyon et al. 1994, Bertout et al. 1999). Also, it is the best example for the very low density (1 to 10 $star\ pc^{-3}$, Scelsi et al. 2007) variation. It has been investigated intensively especially in the search for new low-mass members in the last decades (e.g. Kenyon et al. 1995, Luhman 2004a & 2006, Luhman et al. 2003b, 2006, 2009a & 2009b, Güdel et al. 2007, Scelsi et al. 2007 & 2008, Quanz et al. 2010). Up to date, it contains 351 confirmed members (Kenyon et al. 2008, Luhman et al. 2010). The region is very unique since it is very spread out ($> 20\ sq.deg$) and of very low mass ($3.5 \cdot 10^4 M_\odot$). We show an overview of the region, its surroundings and its main stellar sub-associations in Fig. 1.3.

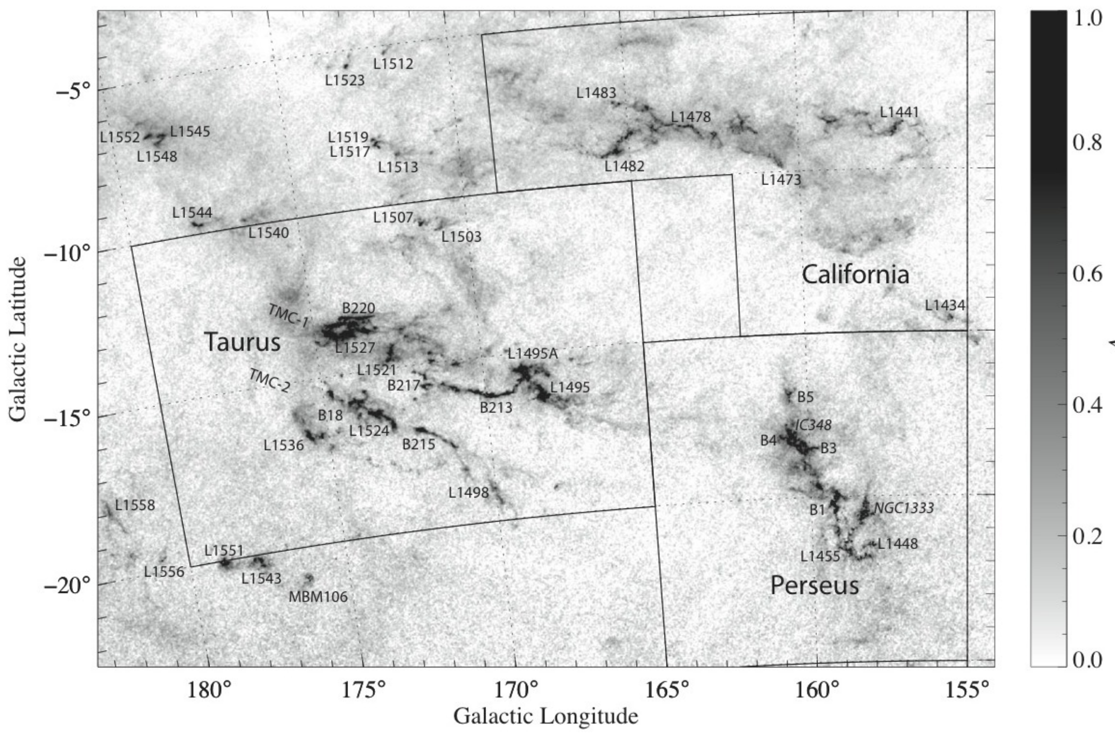

Figure 1.3: An overview of the greater Taurus region with the extinction map by Lombardi et al. (2010). The two main clouds of Taurus are marked with TMC-1 and TMC-2 in the image.

Monin et al. (2010) state a $41 \pm 12\%$ and $58 \pm 9\%$ percentage of objects showing disks for BD and TTS in Taurus, respectively. The members of the area show solar-type metallicity with $[Fe/H] = -0.01 \pm 0.05$ (D'Orazi et al. 2011) and proper motions of (μ_α,μ_δ)=(-5.0 to 15.0,-35.0 to -5.0) mas/yr (Quanz et al. 2010). Most importantly, the region is quite unusual in the distribution of its stellar masses: the peak of its MF is located at around 0.8 $M_\odot$ (Luhman et al. 2009a, see Fig. 1.2).
This fact forms one of the strongest arguments against the proposed universality of the MF. Assuming that the function is indeed universal, there would be many low-mass stars missing. On the UKIDSS GCS Working Group web page[2] they calculate the expected numbers for BD in the region assuming different MF. For a power law with a value of the exponent of [+1,0,−1], they expect [256,38,6] BD, whereas for a log-normal function only 2 BD are expected. Of the 351 known

[2]http://www.roe.ac.uk/ nch/gcs/

members, 65 (19%) are of spectral type $M6$ or later. Following the ejection model, the missing objects could therefore be located further away. But so far, all searches for new members were concentrated on the main clouds. Therefore it is not surprising that they are strongly related to the filaments they were born in. Luhman et al. (2009a) state that all members up to spectral type $M5$ should be known in those parts of the region. On the other hand, if the MF is not universal, its form could be related to one of the unique characteristics of Taurus. The part of the UKIDSS GCS covering the Taurus region investigated in this work is located 5 *deg* to the north of the two main clouds (see Fig. 1.3). Therefore, we will contribute to the interesting question of the formation process due to the location of this 'hunting ground'.

To be able to compare the outcome of this investigation in Taurus especially related to the density of the area, we also considered the Orion SF region. This complex is the nearest and best studied region of ongoing star-formation containing many substructures, star clusters and molecular clouds. Supernovae remnants from massive stars, ultraviolet radiation and stellar winds triggered there the process of star formation and formed molecular clouds surviving with an overall bubble-like structure (Bally 2008). It consists of two main structures known as Orion A and B clouds.
In this rich region, all stages of star-formation can be observed, from very young, embedded clusters, to older, fully exposed young stars. It consists of dense star clusters as well as widely spread populations in low density areas (Briceño 2008). Around the areas of Orions hot OB stars, which are the prime sites for star-formation (Briceño et al. 2007), the stars can be divided into groups of different ages that are partially superimposed along the line-of-sight (Blaauw 1991). They are all 1 to 5 *Myr* old and are located 350 to 460 *pc* away (Caballero 2009). Assuming a power law with a exponent of $[+1, 0, -1]$, there are $[816, 151, 29]$ BD expected on the UKIDSS GCS Working Group web page. For a log-normal function 11 BD are expected.
Orion OB1d population forms the Orion Nebula Cluster (ONC) or Trapezium Cluster, located 480 *pc* away and 1 *Myr* old (Herbig et al. 1986). The OB1a population is located in the north-east of the Orion belt. It shows a peak in the MF at around 0.1 to 0.2 $M_\odot$ (Gutermuth et al. 2009). In this work we will concentrate on the UKIDSS GCS covered part between the ONC, the σ Orionis cluster and Orion A and B clouds. This area consists predominantly of the OB1b and OB1c populations. The first, containing the σ Orionis Cluster, is concentrated on the Orion belt. It is supposed to be around 2 *Myr* old and located at a distance of 440 *pc* (Brown et al. 1994). The cluster around the $O9.5$ star σ Orionis shows a peak of the MF of around 0.1 $M_\odot$ and proper motions of the members of around (μ_α, μ_δ)=$(3.52, -0.20)$ *mas/yr* (Kharchenko et al. 2005). It is at a distance of 350 to 440 *pc* and of 3 *Myr* age.
Orion OB1c is located 460 *pc* away, in front of the ONC and is around 4.5 *Myr* old (Brown et al. 1994). Therefore, if necessary, we will adopt a distance of 450 *pc* to the UKIDSS GCS covered part of the Orion SF region. So far, no difference in the MF of those two subgroups have been measured (Briceño 2008). We give an overview of the whole Orion SF region in Fig. 1.4. In recent studies,it becomes clearer that there is a so far less investigated distributed populations as numerous as the ones inside the molecular clouds (Briceño et al. 2005). In the area covered by the UKIDSS GCS, most studies have been carried out in the ONC (e.g. Preibisch et al. 2005) or σ Orionis Cluster (Barrado et al. 2003b, Lodieu et al. 2009). As described, both of them show the 'universal' form and peak of the MF. Up to date, only few studies searched for LMO in the off-cloud populations of the Orion OB1 association (Béjar et al. 2003, Downes et al. 2006 & 2008).

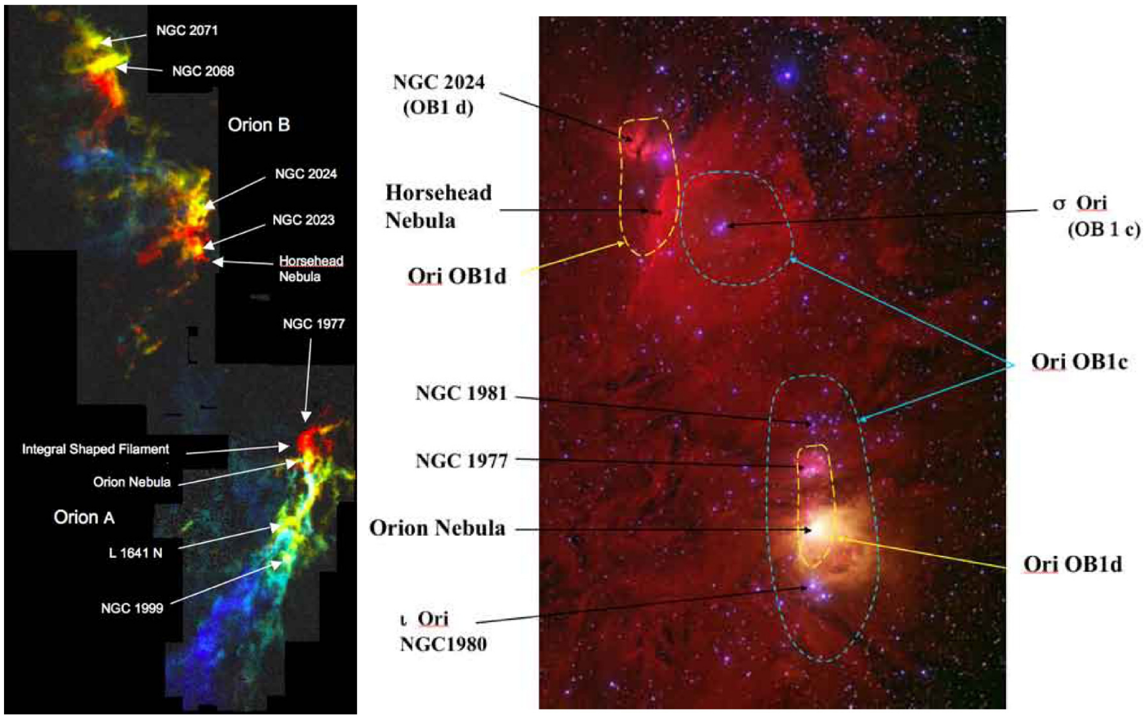

Figure 1.4: Orientation in the larger Orion SF region by Bally 2008. On the left side an overview of the cloud structure is given indicating the different star clusters distinguishable in the region (110 GHZ ^{13}CO $J = 1 - 0$ transition image, colored via Doppler shifts). On the right side, the optical image shows the different star clusters and populations overlaid in the region.

1.3 Aims and structure of this thesis

In this work, we want to determine the complete MF of an enclosed stellar system formed by a single molecular cloud. Since up to date the only chance to achieve this is in young and nearby areas, we investigate in this thesis mainly the Taurus-Auriga SF region. With a distance of 140 pc and an age of around 1 Myr, the members of this area form the low-density example of such regions. Its MF differs in the peak and the form to the 'universal' MF marked by other SF regions. We use as main database the UKIDSS GCS, which observed in the yet unexplored north of Taurus' two main clouds. If we find many new members there, we might fill the gap of the missing LMO and redraw the MF. Thereby we could identify evidence for a true universality of the MF, independent of any characteristics of the regions investigated. If we do not find many new members, the evidence that the MF is indeed connected to the density of the region would increase. Therefore, we additionally investigate parts of the high-density Orion SF region. There, we want to find a new small stellar clump in between Orion A and B clouds. Then we could investigate its complete MF and find thereby comparable data for this theory. In both cases, we contribute by this work to the interesting question of the BD formation, since the new found members in Taurus would be far away from the clouds and filaments they were born in. With a velocity of around 20 mas/yr, they could have moved from their birth site, the molecular filaments, and reached their present location, 5 deg to the north in around 1 Myr. Also, we should be able to reach significantly deeper in magnitude as the searches for LMO done so far in literature with 2MASS data.

LMO emit their radiation mainly in the infrared wavelengths. Additionally, the gas and dust which surrounds newly formed stars, absorbs much of the optical outflow. But the infrared can reveal those sources. Therefore, this wavelength range is excellent to identify such newly formed stars and to investigate in general the formation of stars and LMO. To find new members in Taurus, the already known members and their different characteristics will narrow down possible search criteria for the NIR photometry of the UKIDSS GCS. We will investigate in detail the MF drawn by the already known members. With the help of this knowledge, new LMO members should reveal themselves by various characteristics:

- same location in color-magnitude (CMD)- and color-color (CCD)- diagrams
- similar proper motion
- red NIR colors
- MIR excess (if with accretion disks)
- photometric variability (if with accretion disks)

Since our 'hunting ground' will be of very low density , we have to find very few new members hidden in a significant number of background stars. So, the criteria we apply have to be very strict and use every data available. We explain all data sets in Chap. 2 of this thesis. To increase the number of possible search criteria, we calculate an extinction map, which effects the colors and the luminosities of the candidates. This step let us compare our selections not only to the empirical data marked by the already known Taurus members, but also to model data. This is done in Chap. 3. To identify a new stellar clump in the Orion region, we use the described criteria extracted from the members of the σ Orionis Cluster. Using also the extinction map, we can compile an unbiased density map. The methods to find, quantify and qualify such clumps then includes NIR photometric analysis, star count maps, nearest neighbor (NN) calculations and the construction of the Minimal Spanning Trees (MST, e.g. Gutermuth et al. 2009). We will use similar methods with our data set. We describe in Chap. 4 all applied search criteria.

To prove the status assumed from those characteristics, we observed the new member candidates via optical spectroscopy. It was sufficient to use low-resolution observations, since the youth of the objects should result in small gravity features. Also, CTTS should reveal themselves by large emission lines resulting from the excitation of hydrogen and calcium in the accretion disk. With the help of those spectra, we should be able to assign spectral types, measure the mentioned line features and estimate the surface gravity at least empirically. This data then is sufficient to discuss the membership of the candidates. We will not investigate the abundance of lithium of the observed objects, since the resolution of the spectra will be too low. We describe the observations made in Chap. 5 of this thesis. Due to the knowledge of similar studies, we expect a 30% success rate to discover new members in our candidate selections. This is a typical number for a benchmark region such as Taurus.

We give a complete analysis of the observations in Chap. 6 and discuss the results in Chap. 7. In Chap. 8 we give a short summary and an outlook of the future work regarding the search for LMO in Taurus with the UKIDSS GCS data. All large tables and images will be shown in the appendices sorted by the chapters from App. A to App. D.

Chapter 2

Database

2.1 UKIDSS Galactic Cluster Survey

Our main database for this research is the UKIRT Infrared Deep Sky Survey (Lawrence et al. 2007). Its data was collected with the Wield-Field CAMera WFCAM (Casali et al. 2007) on the United Kingdom InfraRed Telescope (Hawaii)[1]. It consists of various galactic and extragalactic subsurveys: the shallow Large Area Survey (LAS), the Deep Extragalactic Survey (DXS) and the Ultra Deep Survey (UDS) reach down to 18.4, 21.0 and 23.0 *mag* in K band, respectively. In this work we use the Galactic Cluster Survey (GCS). Together with the Galactic Plane Survey (GPS) it is one of the shallow galactic subsurveys of UKIDSS, reaching down to 18.7 and 19.0 *mag*, respectively. We show the coverage of all surveys in Fig. 2.1.

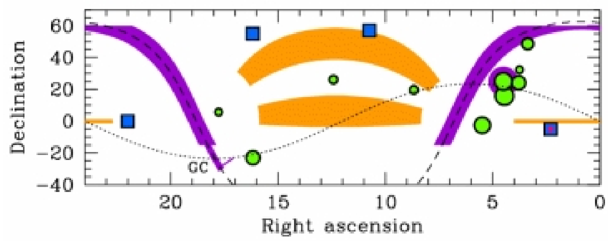

Figure 2.1: Final UKIDSS sky coverage as planned. Right ascension is given in hours, declination in degrees. The dashed line marks the Galactic plane, the dotted line the ecliptic. The colors yellow, violet, green, blue and red represent the coverage of the LAS, GPS, GCS, DXS and UDS (image from www.UKIDSS.org).

Once finished, the GCS will cover around 1000 *sq.deg* of $ZYJHK$ passband photometry (Hewett et al. 2006, see Fig.2.2) of four nearby SF regions (Taurus-Auriga, Orion, Sco and Per-OB2) and six open clusters (Pleiades, Alpha Per, Praesepe, IC 4665, Hyades and Coma-Ber). This includes second epoch K band photometry to be able to derive proper motions. It is designed to identify faint low-mass members of the clusters and explain thereby the variations between their characteristics including their MF. Its mass limit is with around 25 M_{Jup} well below the stellar/substellar border of 80 M_{Jup}. For the objects analyzed in this work, the Data Releases 4 to 6 (DR4 to DR6, see Tab. 2.1) were used.

We accessed the data via the WFCAM Science Archive (WSA[2]) using a free form SQL (Structured Query Language). It includes astrometric positions, observational data and the photometry and

[1] operated by the Joint Astronomy Center on behalf of the Science and Technology Facilities Council of the United Kingdom
[2] http://surveys.roe.ac.uk/wsa/index.html

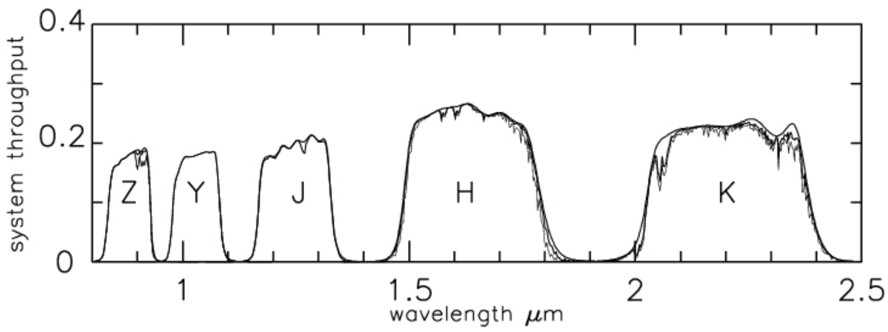

Figure 2.2: The UKIDSS *ZYJHK* filters (from Hewett et al. 2006).

DR9	October 25th 2011	323 sq.deg
DR8	September 3rd 2010	234 sq.deg
DR7	February 25th 2010	172 sq.deg
DR6	October 13th 2009	167 sq.deg
DR5	April 6th 2009	≈160 sq.deg
DR4	July 1st 2008	≈150 sq.deg
DR3	December 6th 2007	≈140 sq.deg
DR2	march 1st 2007	≈90 sq.deg
DR1	July 2006	≈70 sq.deg
Early DR	February 2006	-

Table 2.1: The dates and the *ZYJHK* coverage of the various UKIDSS GCS data releases

its errors from the five UKIDSS filters. The data was cross-matched with the Two Micron All Sky Survey (2MASS, Cutri et al. 2003) for brighter sources. Using the time difference and astrometric errors of $\Delta = 90$ *mas* for both surveys in both directions[3], we were able to calculate proper motions and their errors via (U and M for UKIDSS and 2MASS, respectively):

$$\mu_\alpha = \frac{RA_U - RA_M}{t_U - t_M} \cdot \cos(Dec_U) \pm \frac{\Delta}{t_U - t_M} \cdot \sqrt{2 \cdot cos^2(Dec_U) + (RA_U - RA_M)^2 \cdot sin^2(Dec_U)}$$
$$\mu_\delta = \frac{Dec_U - Dec_M}{t_U - t_M} \pm \frac{\Delta}{t_U - t_M} \cdot \sqrt{2}$$

We calculate very high average errors of $(\Delta\mu_\alpha, \Delta\mu_\delta) = (9.4, 6.6)$ *mas/yr*. We define the saturation and completeness limits by the magnitudes where its logarithmic distribution (binned with the average photometric error 0.1 *mag*) is linear (see e.g. Fig.2.4). The detection limit was applied, where the first bin was empty. The 3σ limit is the magnitude of the brightest source showing an error of 3 times the average magnitude error of the whole sample. We show the calculations and values for each region in the upcoming sections.

One of the aims of the GCS survey is the finding of LMO. Therefore, Hewett et al. (2006) provide photometry in the UKIDSS filters for field stars later than type M. We show those values down to $T8$ type in the appendix in Tab. A.1 corrected for the distance of Taurus ($d = 140$ *pc*) via

[3]For 2MASS, H.L. McCallon states an error of 86 *mas* at http://web.ipac.caltech.edu/staff/hlm/2mass/catvsuc/catvsuc.html. For UKIDSS, despite the smaller observational aperture, Deacon et al. (2009) state an error of 100 *mas* for sources with $J < 10.5$ *mag* and applies cuts to UKIDSS GCS/2MASS cross-matched sources differing more than 60 *mas*.

$$K = (M_K - 5) + 5 \cdot \log(d).$$

2.2 Taurus

2.2.1 UKIDSS GCS DR8

The UKIDSS GCS in the Taurus-Auriga SF region was designed to discover the missing LMO and to prove the variation from the universality of the MF in the region. The observations were not only centered at the molecular clouds of the region, but reach very generously into outer parts. Due to the observational schedule the survey up to DR8 only covered a part of around 25 *sq.deg* about 5 *deg* to the north of Taurus' main clouds. This region is the primary 'hunting ground' of this work and is unexplored until now. But to demonstrate the treatment of the GCS data, we show the example of the DR8. The just recently published DR9 contains even more data in ZYJ bands to the southeast of the DR8. The latter covers an area of 45 *sq.deg* (at least in $ZYJK$ filters) and includes the main clouds where most of the already known members are located (see Fig. 2.3).

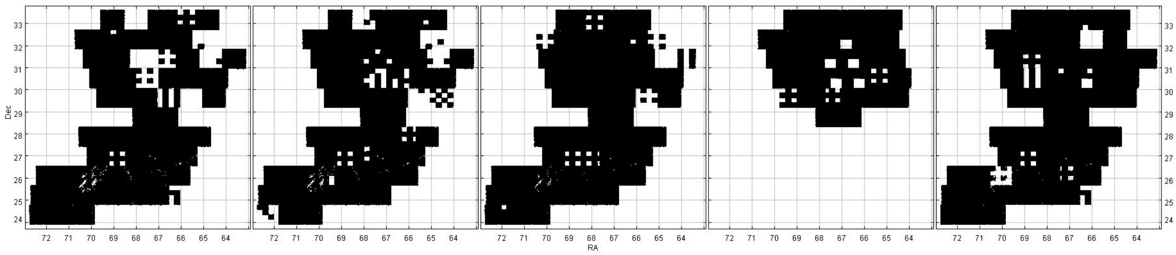

Figure 2.3: The $ZYJHK$ filter coverage (from left to right) of the UKIDSS GCS DR8 in Taurus. The H band coverage represents approximately our region A.

We consider the area above 28.3 *deg* in declination as our 'hunting ground' (already covered in previous UKIDSS GCS data releases) and name it region A throughout this work. In detail, this is the region where UKIDSS GCS point source data are available inside 63.0 to 73.0 *deg* in right ascension (RA, $4h12m$ to $4h52m$) and 23.5 to 34.0 *deg* in declination (Dec). We calculated a completeness limit of $J < 19.35$ *mag* ($\tilde{3}0\ M_{Jup}$, see Tab. 2.2 and Fig. 2.4), which is 3.5 *mag* deeper than for 2MASS.

filter	Z	Y	J	H	K
wavelength range [μm]	0.83-0.925	0.97-1.07	1.17-1.33	1.49-1.78	2.03-2.37
2MASS completeness limit [*mag*]	-	-	15.8	15.1	14.3
initial data points	1125304	1228748	1294904	850852	1951931
final data points	776502	794876	800850	535536	835662
detection limit [*mag*]	22.05	21.85	21.25	20.45	20.45
3σ-limit [*mag*]	21.27	21.02	20.35	19.63	19.41
completeness limit [*mag*]	20.45	20.05	19.35	18.85	18.05
saturation limit [*mag*]	10.95	11.05	10.45	10.75	9.45

Table 2.2: Photometric limits of the UKIDSS GCS DR8 in Taurus with average errors from 0.087 *mag* (in Z) to 0.106 *mag* (in K). 'Initial data points' refer to the number of objects downloaded from the WSA. The 'final data points' are the number of objects with photometry in the shown limits (2MASS limits from http://www.ipac.caltech.edu/2mass/releases/allsky/doc/explsup.html). For the definition of the various limits see previous section.

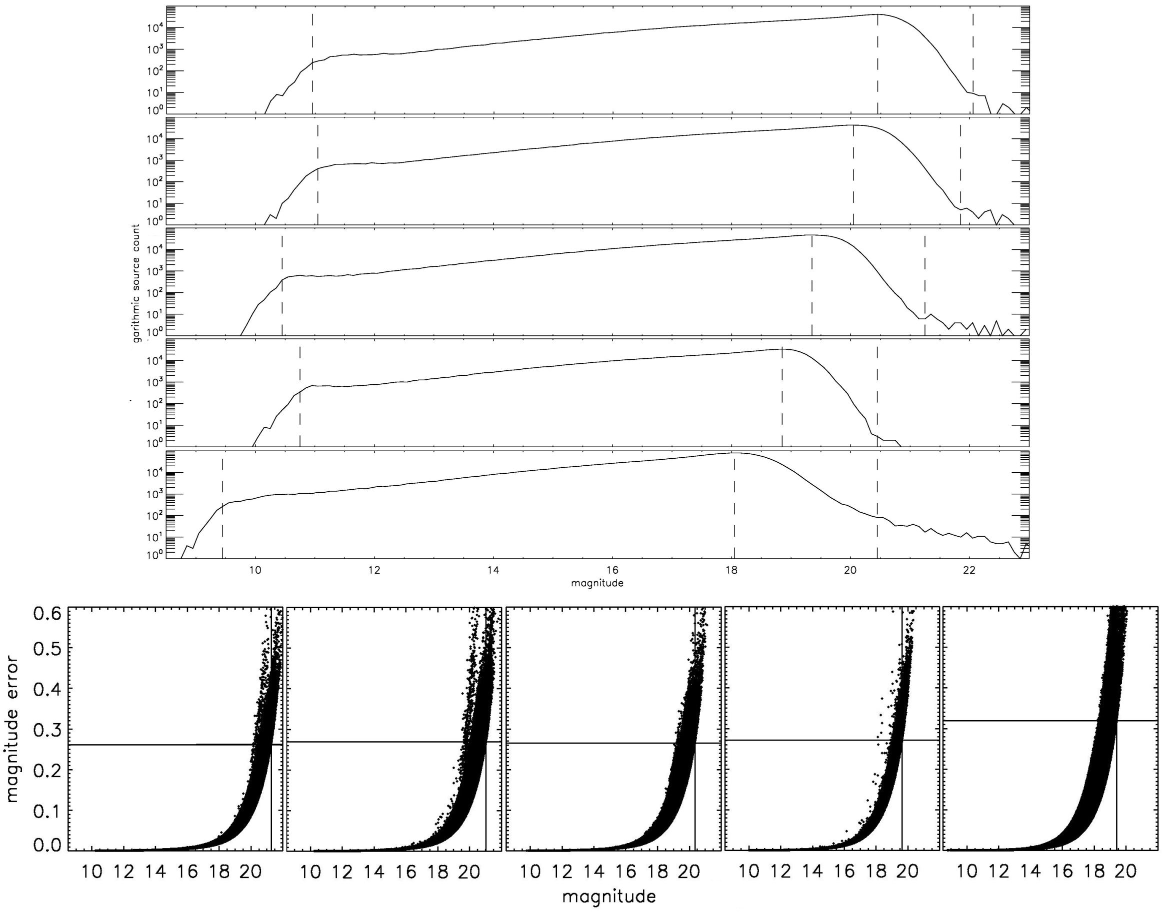

Figure 2.4: top: saturation-, completeness- & detection limits of $ZYJHK$ filters (from top to bottom), bottom: 3σ limits in $ZYJHK$ filters (from left to right).

By applying the saturation and completeness limits in all five filters, we receive the data of 1421387 sources. We request either $ZYJH$ filter data, since the region is already completely covered by the survey in K band. We receive 967875 sources as our main UKIDSS GCS DR8 database in the Taurus-Auriga SF region. The area north of 28.3 *deg* contains 621083 sources and south of that declination 347143 sources. 452861 sources show 2MASS data. Of those, many show values beyond the 2MASS completeness limits. The cross match by WSA is done by searching for the nearest neighbor of both data sets. High proper motion stars or connections in high density regions are doubtful. Also, the photometry of the UKIDSS survey is based on observations which have a four times smaller aperture with around 1 *arsecond* (2MASS is 4 *arcsec*[4]). Therefore, we try to clean this data set. We calculate the magnitude differences of the two surveys in the JHK filters and apply a 1σ limit to those intrinsic average colors. Those limits are: $[J_U - J_M, H_U - H_M, K_U - K_M]$=[$-0.6622$ to 1.8431,-0.5897 to 2.0437,-0.5477 to 1.7437] *mag*. After cleaning the data set we are left with 88139 sources showing reliably both UKIDSS and 2MASS photometry. Hewett et al. (2006) state the following relations between 2MASS and UKIDSS photometry for dwarf stars. They hardly differ from a linear relation (see Fig. 2.5):

$J_M = J_U - 0.073(J_U - H_U) - 0.01$
$H_M = H_U - 0.069(H_U - K_U)$

[4]http://www.ipac.caltech.edu/2mass/releases/allsky/doc/sec4$_4$*c.html*

$K_M = K_U + 0.073(H_U - K_U)$

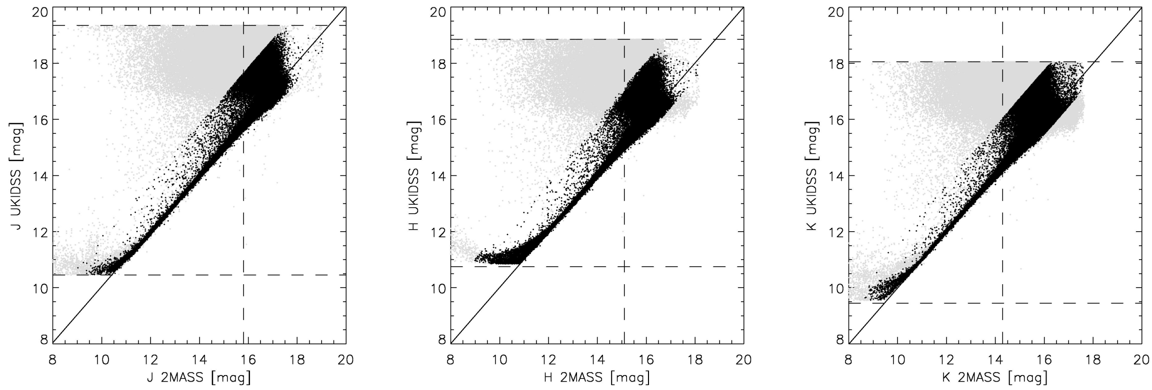

Figure 2.5: UKIDSS GCS and 2MASS photometry comparison. The gray data points represent all available UKIDSS data. The black dots show this data set in the described limits. The dashed lines indicate the saturation and completeness limits of the UKIDSS GCS DR8 data set and the completeness limit of the 2MASS survey. The full line shows the connection of the photometry of the two surveys described by Hewett et al. (2006).

2.2.2 Taurus members and their characteristics

To define characteristics of the region, we searched for all available data of already known Taurus members. The census of its stellar population is best described in Luhman et al. (2010) which is an updated version of the one by Kenyon et al. (2008). We include all 351 sources in the appendix in Tab. A and show their location in Fig. 2.7. Note, that for consistency purposes, we always try to give the 2MASS name of a source if available. Many publications were used to fill the data known of those stars, including as well the SIMBAD database (operated at CDS, Strasbourg, France). We give an overview of the data by showing lowest and highest values in Tab. 2.3.

column	RA	Dec	type	T_{eff}	μ_α	μ_δ	A_V	J_M	H_M	K_M
unit	*deg*	*deg*		*K*	*mas/yr*	*mas/yr*	*mag*	*mag*	*mag*	*mag*
lower limit	60.955	15.496	L0	2200	−17	−49	0	5.9	5.1	4.2
upper limit	76.980	30.828	B5	10500	+31	+11	24	18.2	16.1	15.4
column	*B*	*V*	*R*	*I*	[3.6]	[4.5]	[5.8]	[8.0]	[24.0]	
unit	*mag*	*mag*	*mag*	*mag*	*mag*	*mag*	*mag*	*mag*	*mag*	
lower limit	6.3	6.3	7.0	6.9	5.9	5.0	2.6	2.8	0.5	
upper limit	21.4	24.9	20.6	19.9	15.3	14.3	13.6	13.8	11.1	

Table 2.3: Summary of the data of the 351 Taurus members. Note that not every source shows data in all columns. The numbers mark the lowest and highest value available in the data set.

The Taurus clouds are distributed in an area of around 60 *sq.deg*. For the 351 known members in 140 *pc* distance, this corresponds to a density of around 1.0 $star \cdot pc^{-2}$. We compare the known members and the UKIDSS GCS data set by their 2MASS positions (< 0.001 *deg* or < 3.6 *arcsec*) and *JHK* photometry (< 0.5 *mag*). This is necessary to avoid wrong counterparts resulting from high proper motion objects or the different aperture of the two surveys. Only 143 objects show 2MASS *JHK* band photometry larger than the UKIDSS GCS saturation limits of 10.45, 10.75, and 9.45 *mag*, respectively. Also, only 109 members are located in the part covered by the UKIDSS GCS DR8.

53 members show both criteria and only the $M4.5$ type 2MASSJ04163048+3037053 is located north of 28.3 deg. This objects is provided with all available 2MASS and UKIDSS photometry. Not considering the 2MASS saturation limit, we find UKIDSS GCS data of 82 already known members. We show this data in the appendix in Tab. A. Note, that this data was not yet available for the search criteria applied later on in this work. The just recently published UKIDSS GCS DR9 would not include many more members except the $M5.25$ type star 2MASSJ05064662+2104296 at $(RA, Dec) = (76.6943, 21.0749)$.
With the data of the 351 already known members of Taurus, we construct the MF of the region for masses less than 1 $M_{\odot}$. To derive masses, we use the 2MASS J band photometry of the objects as observed and the evolutionary models described in sec. 2.4. Note, that the data are not corrected for extinction effects. Of all the members, 11 do not show the requested photometric value. 69 sources have $J < 9.63$ mag, which get translated by the models to masses > 1 $M_{\odot}$. We include published data of the Pleiades (Lodieu et al. 2007a), the σ Orionis Cluster (Lodieu et al. 2009) and IC 4665 (Lodieu et al. 2011) for comparison. We show all calculations in Tab. 2.4. Thereby, we calculate the number of objects dN in a certain mass $M_C \pm \Delta M_C$ or magnitude range $J_C \pm \Delta J_C$ (translated by the evolutionary models used in this work). The variation dM is $2 \cdot \Delta M_C$. The different MF in Fig. 2.6 confirm the unusual behavior of the Taurus-Auriga SF region. We include data made available to us by A. Bayo from σ Orionis (Caballero et al. 2007 & 2009), the 2 Myr old NGC 6611 (Oliveira et al. 2009) and the 5 Myr old λ Orionis (Barrado et al. 2005, Bayo et al. 2011) and Upper Sco (Lodieu et al. 2007b). The peak of the MF of Taurus is the only one located beyond 0.7 $M_{\odot}$, whereas for the other regions the value is located roughly in between 0.1 and 0.4 $M_{\odot}$.

The data of the already known members can also be used to demonstrate the connection between various parameters. We show the diagrams of the spectral type vs. the effective temperatures T_{eff} of stellar objects in the appendix in Fig. A.1, where we find the formula $T_{eff} = -143 \cdot (spectraltype) + 12415$. Besides the connection of the spectral type and their J band values (without extinction effects), we also calculate the luminosity function (see Tab. 2.5) and show it in those diagrams. We find a peak of $J = 10.25$ mag, corresponding to masses between 0.8 and 0.9 $M_{\odot}$ following the model described by Baraffe et al. (1997 & 1998).

region	J_C $[mag]$	M_c $[M_\odot]$	dN	dN/dM $[M_\odot]^{-1}$	$log(\frac{dN}{dlogM})$	region	J_C $[mag]$	M_c $[M_\odot]$	dN	dN/dM $[M_\odot]^{-1}$	$log(\frac{dN}{dlogM})$
Taurus	9.850	0.950	26.0	260.0	2.755	Pleiades	12.250	0.605	13.5	160.6	2.349
Taurus	10.315	0.850	27.0	270.0	2.722	Pleiades	12.750	0.529	21.1	305.7	2.570
Taurus	10.815	0.750	35.0	350.0	2.781	Pleiades	13.250	0.456	31.4	407.2	2.630
Taurus	11.300	0.650	28.0	280.0	2.621	Pleiades	13.750	0.375	49.2	585.7	2.702
Taurus	11.630	0.585	13.0	433.3	2.766	Pleiades	14.250	0.293	58.6	724.0	2.685
Taurus	11.970	0.535	22.0	314.3	2.587	Pleiades	14.750	0.222	63.0	1049.2	2.727
Taurus	12.350	0.475	9.0	180.0	2.294	Pleiades	15.250	0.169	55.5	1206.0	2.669
Taurus	12.620	0.425	9.0	180.0	2.245	Pleiades	15.750	0.131	42.6	1420.0	2.630
Taurus	12.875	0.375	13.0	260.0	2.351	Pleiades	16.250	0.104	28.4	1182.2	2.450
Taurus	13.125	0.325	11.0	220.0	2.216	Pleiades	16.750	0.084	17.5	1027.8	2.295
Taurus	13.390	0.275	5.0	100.0	1.800	Pleiades	17.250	0.070	16.0	1524.5	2.388
Taurus	13.705	0.225	19.0	380.0	2.292	Pleiades	17.750	0.060	6.0	687.7	1.979
Taurus	13.985	0.188	3.0	120.0	1.714	Pleiades	18.250	0.053	3.2	504.0	1.789
Taurus	14.210	0.163	2.0	80.0	1.475	Pleiades	18.750	0.046	6.2	789.0	1.914
Taurus	14.445	0.140	3.0	150.0	1.684	Pleiades	19.250	0.040	9.3	2394.1	2.338
Taurus	14.695	0.120	8.0	400.0	2.042	Pleiades	19.750	0.036	19.3	6881.4	2.760
Taurus	14.900	0.105	6.0	600.0	2.161	Pleiades	20.250	0.034	10.9	3882.9	2.477
Taurus	15.060	0.095	6.0	600.0	2.118	Pleiades	20.750	0.031	72.9	31695.7	3.354
Taurus	15.245	0.085	4.0	400.0	1.893	Pleiades	21.250	0.029	268.1	297926.7	4.304
Taurus	15.395	0.078	0.0	0.0	-						
Taurus	15.480	0.074	1.0	333.3	1.751						
Taurus	15.535	0.071	1.0	500.0	1.912						
Taurus	15.700	0.065	4.0	400.0	1.776						
Taurus	15.920	0.058	1.0	200.0	1.423						
Taurus	16.100	0.053	1.0	200.0	1.383						
Taurus	16.485	0.045	7.0	700.0	1.859						
Taurus	17.360	0.035	5.0	500.0	1.602						
Taurus	19.680	0.025	1.0	100.0	0.754						
σ Orionis	12.250	0.418	43.0	292.5	2.444	IC 4665	13.468	0.565	38.0	200.4	2.411
σ Orionis	12.750	0.295	44.0	449.0	2.480	IC 4665	14.072	0.390	88.0	550.0	2.687
σ Orionis	13.250	0.208	39.0	506.5	2.379	IC 4665	14.689	0.255	101.0	918.2	2.725
σ Orionis	13.750	0.140	32.0	542.4	2.234	IC 4665	15.308	0.168	100.0	1538.5	2.768
σ Orionis	14.250	0.089	15.0	348.8	1.843	IC 4665	15.880	0.114	80.0	1904.8	2.694
σ Orionis	14.750	0.057	22.0	1100.0	2.155	IC 4665	16.491	0.076	62.0	1550.0	2.405
σ Orionis	15.250	0.042	24.0	2181.8	2.317	IC 4665	17.061	0.052	12.0	1333.3	2.172
σ Orionis	15.750	0.032	6.0	800.0	1.772	IC 4665	17.493	0.040	4.0	444.4	1.604
σ Orionis	16.250	0.026	3.0	576.9	1.535	IC 4665	17.887	0.032	4.0	571.4	1.616
σ Orionis	16.750	0.021	6.0	1176.5	1.748	IC 4665	18.315	0.025	3.0	500.0	1.456
σ Orionis	17.250	0.016	6.0	1463.4	1.733						
σ Orionis	17.750	0.013	1.0	370.4	1.035						
σ Orionis	18.250	0.010	1.0	454.6	1.031						
σ Orionis	18.750	0.008	3.0	588.2	1.529						

Table 2.4: Data for the calculation of the MF of Taurus, the Pleiades (Lodieu et al. 2007a), the σ Orionis Cluster (Lodieu et al. 2009) and IC 4665 (Lodieu et al. 2011b). The connection between J band magnitude and masses are given by the evolutionary models from Baraffe et al. (1997 & 1998) and Chabrier et al. (2000).

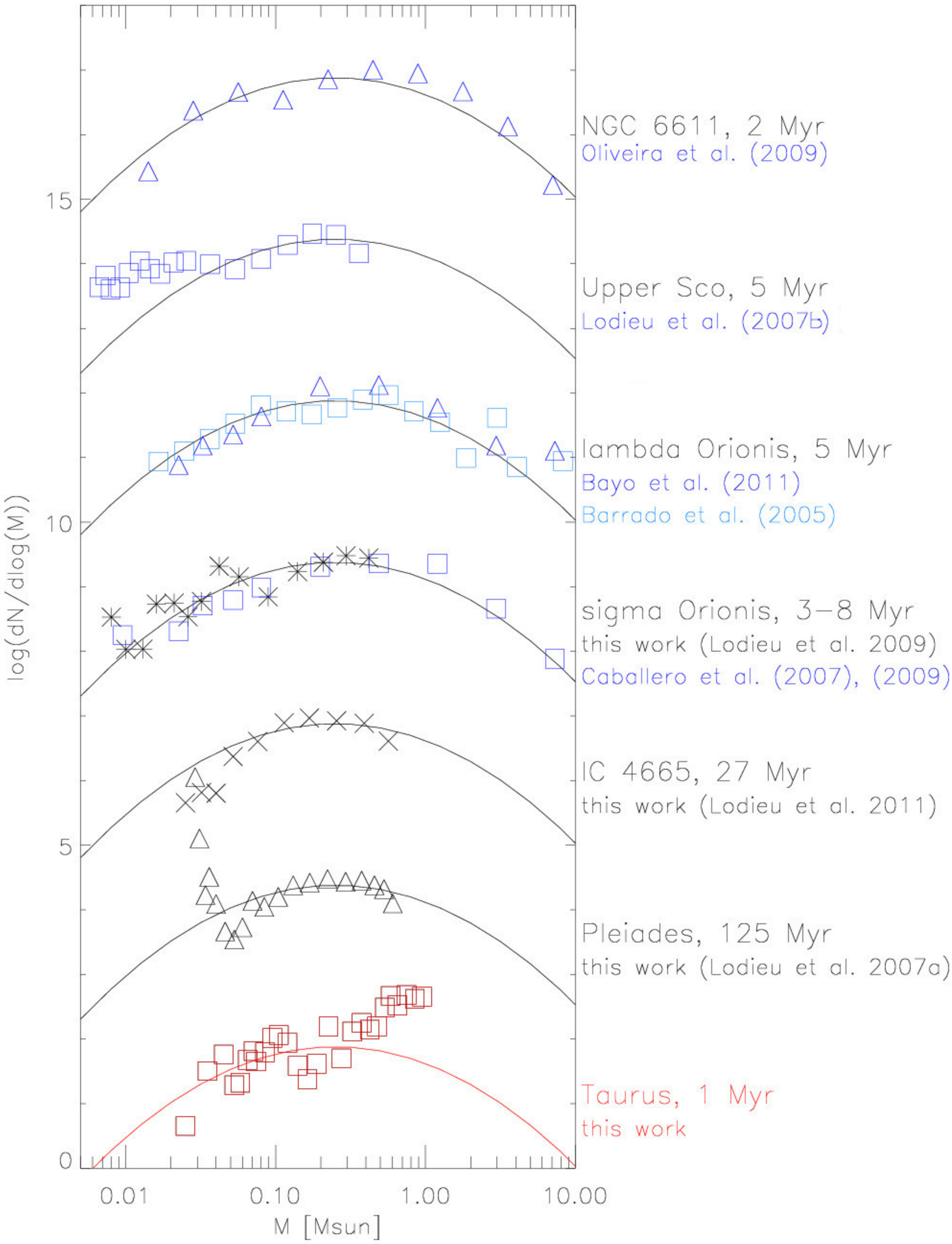

Figure 2.6: The MF calculated in this work of the 351 known Taurus members in red and in black from the Pleiades (Lodieu et al. 2007a), the σ Orionis cluster (Lodieu et al. 2009) and IC 4665 (Lodieu et al. 2011b). The blue points for σ Orionis, λ Orionis, upper Sco and NGC 6611 are based on data made available to us by A. Bayo. We indicate the reference and the age of the associations. Values are shifted along the ordinate. The black line represents the log-normal function from Chabrier (2003) for LMO. Except Taurus, the shown MF show peaks in between $0.1\,M_{\odot} < M < 0.4\,M_{\odot}$. Taurus' peak is located beyond $0.7\,M_{\odot}$. Note the very unusual behavior of the Pleiades values in the low-mass end.

J_c [mag]	dN	J_c [mag]	dN	J_c [mag]	dN
5.25	0	10.25	34	15.25	3
5.75	2	10.75	31	15.75	8
6.25	0	11.25	30	16.25	5
6.75	4	11.75	22	16.75	4
7.25	2	12.25	17	17.25	1
7.75	4	12.75	24	17.75	0
8.25	10	13.25	17	18.25	1
8.75	20	13.75	12	18.75	0
9.25	32	14.25	11	19.25	0
9.75	31	14.75	15	19.75	0

Table 2.5: Data for the calculation of the Taurus luminosity function

2.2.3 Additional data

Assuming an even lower density than in Taurus' main clouds, we do not expect many new members in region A. Our only reference are the already known Taurus members. Besides their NIR photometry delivered by the UKIDSS GCS and the 2MASS survey, we are provided with their optical and MIR photometry. To be able to use as many characteristics of the Taurus members as possible, we searched for any such available survey data in region A.

2.2.3.1 Optical wavelengths

No deep optical survey like e.g. the Sloan Digital Sky Survey (SDSS, Adelman-McCarthy et al. 2008) are conducted in region A. But we found BVR filter photometry (Johnsons filter system) delivered by the Naval Observatory Merged Astrometric Data set (NOMAD, Zacharias et al. 2005). This is a merge of various shallow optical surveys such as Hipparcos, Tycho-2, UCAC-2 and USNO-B1 catalogs. By cross-matching the UKIDSS GCS data of region A by 2MASS positions (< 0.001 deg) and JHK photometry (< 0.5 mag) we received 240674 sources showing at least one of the optical magnitudes. The cross-match between the NOMAD and the 2MASS data delivers proper motions with errors from 10 to 20 mas/yr. We give an overview of the data on Tab. 2.6.

column	RA	Dec	B	V	R	J_M	H_M	K_M
unit	deg	deg	mag	mag	mag	mag	mag	mag
lower limit	60.933	28.281	8.4	8.3	8.1	5.2	4.4	4.1
upper limit	70.477	33.575	25.0	18.0	20.9	19.1	18.2	17.6

Table 2.6: Summary of the NOMAD data of region A in the Taurus SF region. Note that not every source shows photometry in all filters. The numbers mark the lowest and highest value available in the data set.

2.2.3.2 MIR wavelengths

MIR data is very important in the search for new LMO, since many young sources are supposed to show accretion disks. Those emit most of their radiation in this wavelength range. The MIR data improves the chances of detections and/or membership confirmation. That is why most searches for LMO in the Taurus region made use of the Spitzer/IRAC (InfraRed Array Camera)) $I1$, $I2$, $I3$, $I4$ (3.6, 4.5, 5.4, 8.0 μm) & MIPS (Multiband Imaging Photometer for SIRTF) $M1$ (24.0 μm) data (Fazio et al. 2004). But the space telescope did not observe fully region A. Maria Morales Calderon[5] and collaborators provided us with Spitzer data of a small part southeast of region A (see Fig. 2.7). We show an overview of the 42800 sources in Tab. 2.7. The photometry provided is given to us with only one decimal and contains large errors.

column	RA	Dec	[3.6]	[4.5]	[5.8]	[8.0]	[24.0]
unit	*deg*	*deg*	*mag*	*mag*	*mag*	*mag*	*mag*
lower limit	64.045	28.281	8.5	7.7	7.1	6.3	2.7
upper limit	69.895	30.700	20.9	20.8	18.3	17.1	12.0

Table 2.7: Summary of the Spitzer/IRAC data of region A of the Taurus SF region. Note that not every source shows photometry in all filters. The numbers mark the lowest and highest value available in the data set.

In April 2011, the very interesting MIR data of the Wide-field Infrared Survey Explorer (WISE[6], Wright et al. 2010) satellite was published. It covers 57% of the whole sky including region A. It was not available to us during the work on this thesis. We will discuss the data late on in the text (see Sec.7.3.2).

2.2.3.3 SIMBAD cross-match

No other surveys were conducted in region A. Nevertheless, we made a search in the SIMBAD database. Again, we searched for counterparts to the UKIDSS GCS data set with a < 0.001 *deg* variation in location and < 0.5 *mag* in 2MASS JHK photometry. All together 163 sources were found. Of them 37 are galaxies and 123 stars from type $B0$ to $M4.5$. Interestingly, we find three objects classified as TTS in the data set. We give their data summary in Tab. 2.8 and include them in Fig. 2.7. We observed the $M3.5$ field star 2MASSJ04391586+3032074 (see Chap. 5).

[5] Spitzer Science Center, California Institute of Technology, Pasadena, USA and Centro de Astrobiología (INTA-CSIC), ESAC campus, Villanueva de la Canada, Madrid, Spain

[6] A joint project of the University of California, Los Angeles, and the Jet Propulsion Laboratory/California Institute of Technology, funded by the National Aeronautics and Space Administration

name	2MASS J04204982+3009155	2MASS J04391586+3032074	2MASS J04155138+3100356
spectral type	K8	M3.5	G6
RA [*deg*]	65.207650	69.816200	63.964017
Dec [*deg*]	30.154358	30.535600	31.009914
B [*mag*]	15.80	-	13.25
V [*mag*]	14.74	-	12.36
R [*mag*]	13.80	-	11.70
Z_U [*mag*]	12.34	13.57	11.42
Y_U [*mag*]	11.99	13.20	11.27
J_U / J_M [*mag*]	11.42 / 11.50	12.65 / 12.68	10.64 / 10.48
H_U / H_M [*mag*]	10.87 / 10.74	12.10 / 12.07	- / 10.05
K_U / K_M [*mag*]	10.52 / 10.51	11.80 / 11.83	10.17 / 9.89
[3.6] [*mag*]	-	11.50	-
[4.5] [*mag*]	-	11.50	-
[5.4] [*mag*]	-	11.40	-
[8.0] [*mag*]	-	11.40	-
μ_α [mas/yr]	-3.4	-5.0	-3.6
μ_δ [mas/yr]	-6.6	-30.8	7.1

Table 2.8: UKIDSS GCS DR8 data of three TTS identified in region A of Taurus

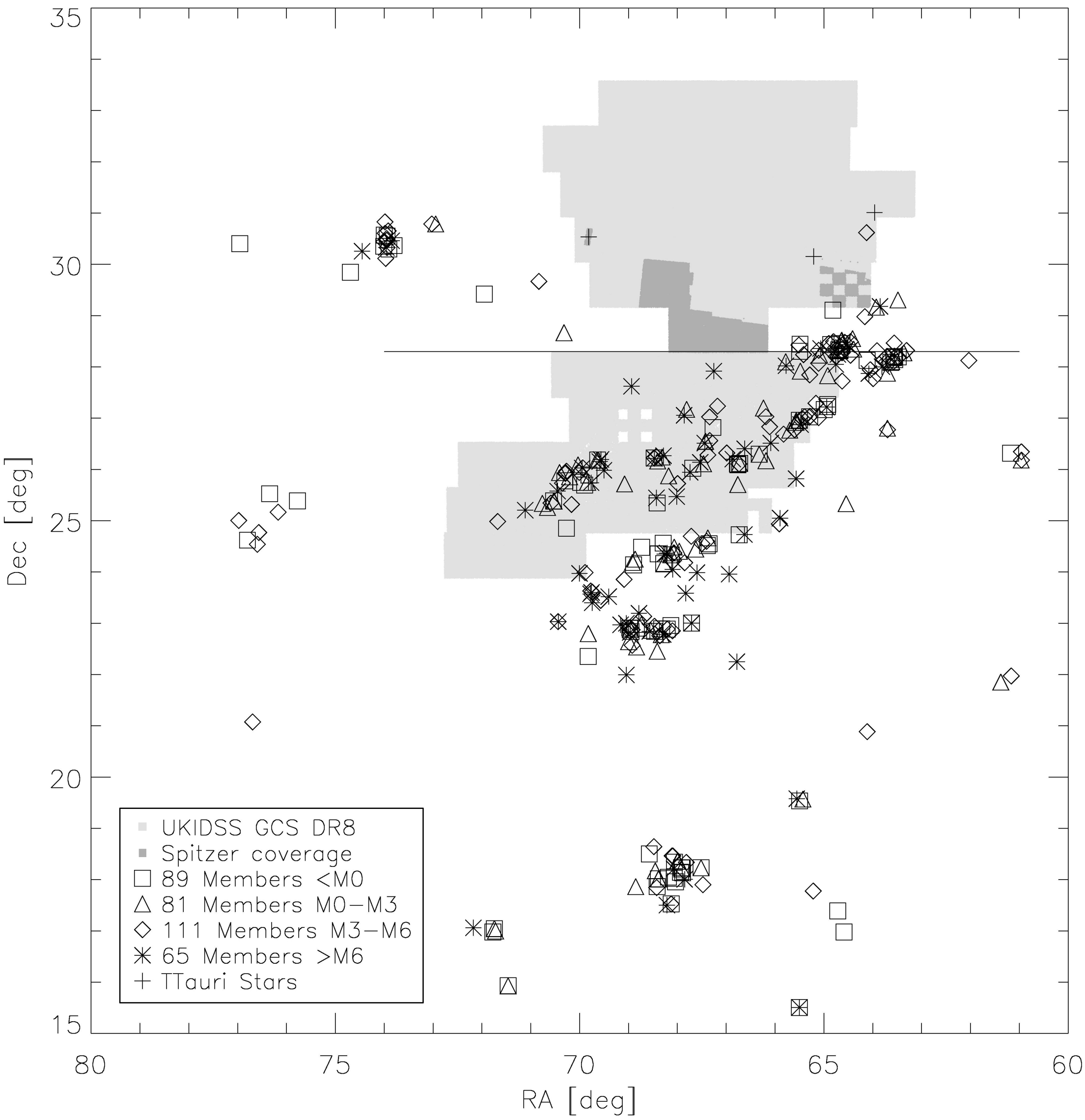

Figure 2.7: The location of already known Taurus members (separated by spectral type), the UKIDSS GCS DR8, the Spitzer data set and the three known TTS located in region A. The horizontal line divides the data set into region A and the southern part already covered by various searches.

2.3 Orion

2.3.1 UKIDSS GCS DR5

For the work in Orion, we used as main database the UKIDSS GCS DR5. It covers around 15 *sq.deg* in $ZYJHK$ filters in between Orion A and B clouds. It includes parts of the Orion Nebula Cluster (ONC) and the star cluster around σ Orionis. We show the different distributions for each filter in Fig. 2.8

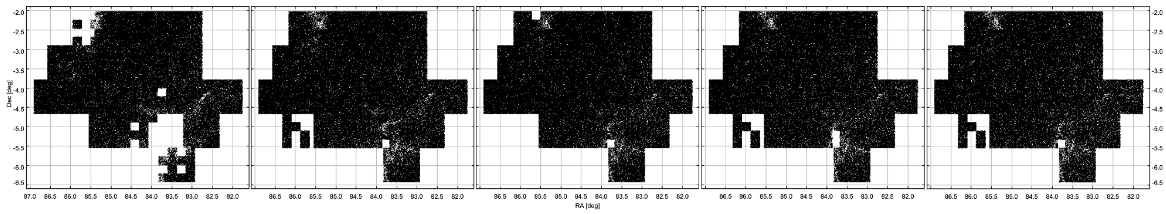

Figure 2.8: The $ZYJHK$ filter coverage (from left to right) of the UKIDSS GCS DR5 in Orion.

We requested all point source data available from 81.7 to 87.0 *deg* in RA ($5h26m$ to $5h48m$) and from -6.5 to -1.9 *deg* in Dec. All sources show JHK photometry, since we want to apply a NIR extinction map in those filters. We calculated a completeness limit of $J < 19.55$ *mag* ($\tilde{4}5$ M_{Jup}, see Tab. 2.9 and Fig. 2.9).

filter	Z	Y	J	H	K
wavelength range [μm]	0.83-0.925	0.97-1.07	1.17-1.33	1.49-1.78	2.03-2.37
2MASS completeness limit [*mag*]	-	-	15.8	15.1	14.3
data points	161380	181497	186930	186930	186930
detection limit [*mag*]	22.25	21.55	21.15	20.25	21.85
3σ-limit [*mag*]	21.24	20.95	20.42	19.86	19.17
completeness limit [*mag*]	20.35	20.05	19.55	18.55	18.05
saturation limit [*mag*]	10.75	10.85	10.35	10.95	9.45

Table 2.9: Photometric limits of the UKIDSS GCS DR5 in Orion with average errors from 0.097 *mag* (in Z) to 0.114 *mag* (in K).

By applying the saturation and completeness limit in all five filters in this region, we receive the data of 186930 sources. Those form our main database in the Orion region. Of those, 87025 sources show 2MASS photometry. We clean this data by the limits calculated for this data set: $[J_U - J_M, H_U - H_M, K_U - K_M] = [-0.5621$ to $1.4970, -0.6040$ to $1.4849, -0.6830$ to $1.4840]$ *mag* (for Taurus see Sec. 2.2.1). We are left with 73945 sources, which have both UKIDSS and 2MASS photometry. We show the location of the final data in Fig. 2.10.

2.3.2 Additional data

The area covered by the UKIDSS GCS DR5 was already observed by various optical, NIR and MIR surveys. We made a search in the SIMBAD database and found many sources belonging mostly to the ONC and the σ Orionis cluster. We show the data of four TTS counterparts identified in the UKIDSS covered area with the usual deviance of < 0.001 *deg* in location and a < 0.5 *mag* in 2MASS JHK photometry in Tab. 2.10 and Fig. 2.10.

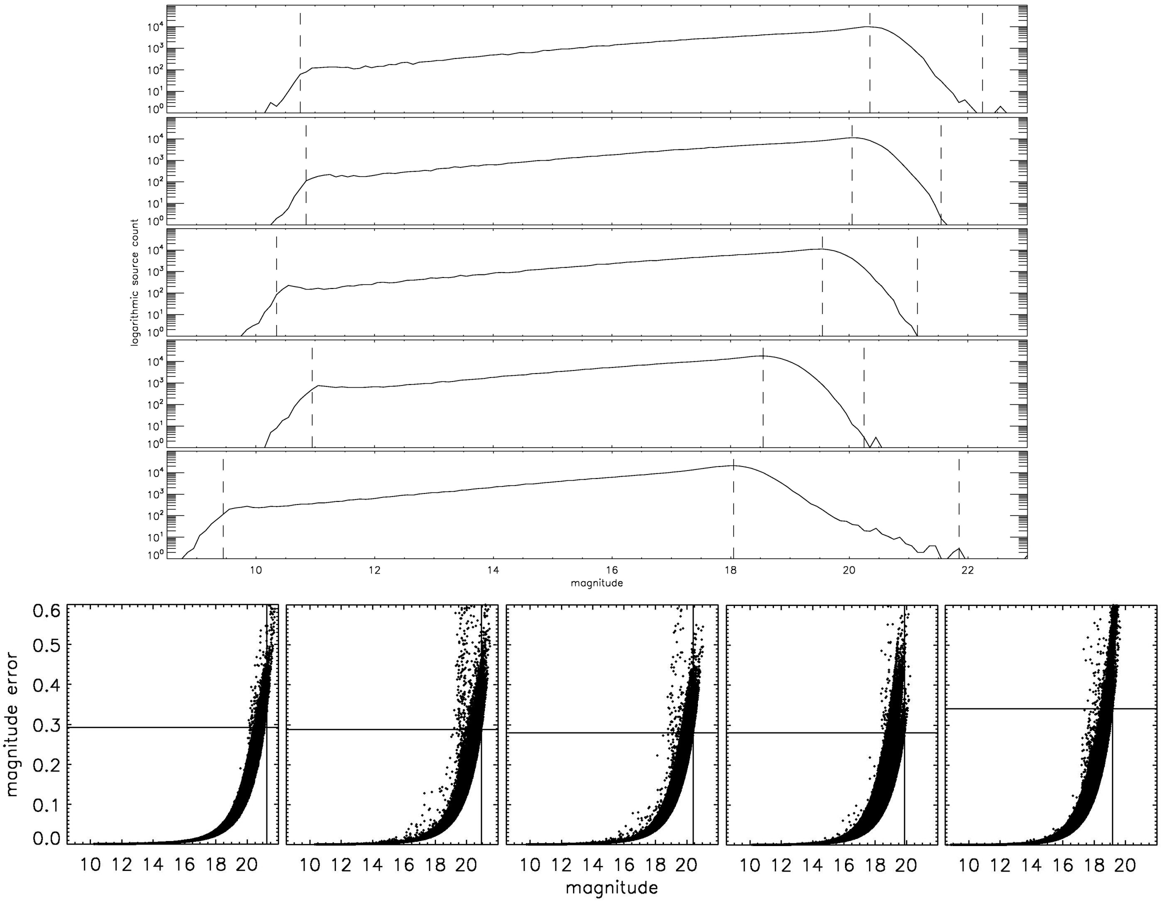

Figure 2.9: top: saturation-, completeness- & detection limits of *ZYJHK* filters (from top to bottom), bottom: 3σ limits in *ZYJHK* filters (from left to right).

Name	spectral type	RA [*deg*]	Dec [*deg*]	Z_U [*mag*]	Y_U [*mag*]	J_U [*mag*]	H_U [*mag*]	K_U [*mag*]	μ_δ [*mas/yr*]	μ_α [*mas/yr*]
2MASSJ05360406−0201296	M0	84.016913	−2.024881	13.00	12.71	12.21	11.66	11.32	−14.80	16.89
2MASSJ05345650−020533	M0	83.735462	−2.092600	12.94	12.64	12.13	11.65	11.29	6.34	−8.36
2MASSJ05404753−0212109	G7	85.198036	−2.203030	13.29	12.93	12.34	11.67	11.38	−3.12	2.78
2MASSJ05354409−0508376	K6	83.933704	−5.143766	-	14.97	14.31	13.39	12.71	−7.03	13.31

Table 2.10: UKIDSS GCS DR5 data of four TTS identified in Orion

2.3.3 σ Orionis

Lodieu et al. (2009) provide a complete census of the σ Orionis cluster with the UKIDSS GCS DR4. We show an overview of the 287 member candidates found by them in Tab. 2.11 and Fig. 2.10. They are all located inside a circle of 30 *arcmin* diameter around the $O9.5$ star σ Orionis ([*RA*,*Dec*] = [84.6875,−2.6000] *deg* = [$5h38m45s$,$-2deg36'0''$]).

column	RA	Dec	Z_U	Y_U	J_U	H_U	K_U
unit	*deg*	*deg*	*mag*	*mag*	*mag*	*mag*	*mag*
lower limit	84.195	−3.079	12.8	12.5	12.0	11.4	10.3
upper limit	85.161	−2.125	20.9	20.2	19.0	18.1	17.3

Table 2.11: Summary of 287 UKIDSS GCS DR5 counterparts of σ Orionis member candidates by Lodieu et al. (2009). The numbers mark the lowest and highest value available in the data set.

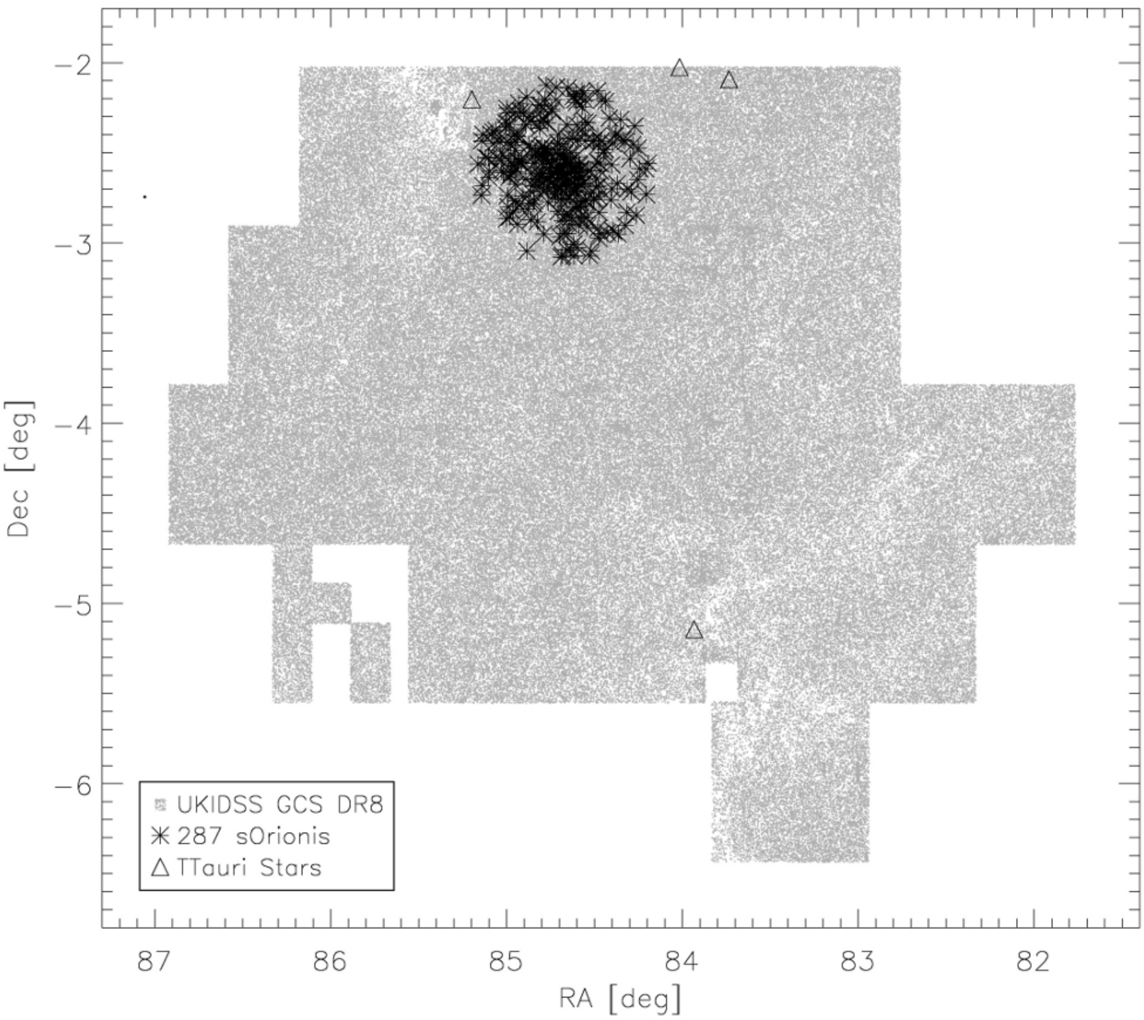

Figure 2.10: The location of the UKIDSS GCS DR5 data set in Orion, the UKIDSS counterparts of the σ Orionis cluster candidates by Lodieu et al. (2009) and the four TTS identified in the UKIDSS data set.

2.4 Evolutionary models

We make use of different theoretical models. They describe the photometry of stellar objects for different masses, ages, metallicities and gravities. For sources from solar masses down to the sub-stellar/stellar border, Baraffe et al. (1997 & 1998) deliver values in $VRIJHK$ filters for metallicities of $[Fe/H] = -0.5$ to 0.0 and ages from 2 Myr to 13 Gyr. Chabrier et al. (2000) reach deeper into the substellar region down to 0.01 $M_{\odot}$. They describe $VRIJKLM$ photometry of objects with ages from 100 Myr to 10 Gyr. We use both models with solar metallicities, youngest available common ages and photometry corrected for the distances of Taurus and Orion, respectively. The most recent model data is available on F. Allard's homepage[7]. We use them in various CMD and CCD and for the relation of magnitudes and masses for LMO.

2.5 Optical reference spectra

Our ultimate goal is to confirm membership via optical spectroscopy. With such observations, we will be able to characterize the sources we select as photometric member candidates. We have several options to assign spectral type. The most common one is to compare observed spectra to reference spectra of sources of similar age. Such a database was made available to us by K. Luhman[8]. It consists of 33 spectra from the Chamaeleon I SF region (2 to 6 Myr, Luhman 2004b & 2007), the Upper Sco association (5 Myr, Luhman et al. 2007) and Taurus (Briceño et al. 1998). The spectra are covering the spectral types from $M0.5$ to $M9.5$ in steps of 0.25 subtypes missing $M0.75$, $M4.25$, $M6.75$, and $M9.25$. We show the spectra in Fig. A.2 and their data collected from the SIMBAD database in Tab. A.4 in the appendix. The range of spectral types is sufficient, since our search for new members will be focused on M type candidates only.

[7] http://perso.ens-lyon.fr/france.allard/

[8] Department of Astronomy and Astrophysics & Center for Exoplanets and Habitable Worlds, Pennsylvania State University, USA

Chapter 3

High-resolution extinction maps

Young SF regions are still filled with the gas and dust their members were born into. The effect of such clouds on the stars embedded in them and on the stars in their background is the wavelength dependent absorption of their emitted light. If we take into account the observational detection limits, it is obvious, that the dust column density of the cloud is proportional to the surface density of the detectable stars. This fact is used in the star count method (Bok & Cordwell 1973). There, the surface density of an extincted (on-cloud, N_{on}) and an unextincted (off-cloud, N_{off}) field on the sky get compared. The visual extinction A_V of the first can then be estimated by (Lada et al. 1994, b_V as the slope of the cumulative luminosity function of the filter V.):

$$A_V = b_V^{-1} \cdot log(N_{off}/N_{on})$$

In the star count method we use the information of non-detected sources. More efficient and precise is the use of the reddened photometry of the detected sources. Here, it is not only the luminosity which can be used to calibrate the extinction, but also its wavelength dependency reflected in the colors of each object. This was done by Lada et al. (1994) who developed the Near-Infrared Color Excess (NICE) method. They use the extinction laws by Rieke & Lebofski (1985). But the UKIDSS JHK filters show a slightly different central wavelength as the ones of the 2MASS survey. Also, the UKIDSS ZY filters were not yet considered in those approximations. Therefore, we calculated our own relations using linear regression of the $VJHK$ band relations from the mentioned authors (see Fig. 3.1). We find ([λ]=μm):

$$log_{10}\frac{A_\lambda}{A_V} = -1.6002 \cdot log_{10}(\lambda) - 0.4095$$

and show the results in Tab. 3.1.

filter	Z	Y	J	H	K	[3.6]	[4.5]	[5.8]	[8.0]
λ_c [μm]	0.8775	1.02	1.25	1.635	2.2	3.545	4.442	5.675	7.760
A_λ/A_V	0.480	0.377	0.273	0.175	0.114	0.064	0.054	0.047	0.044

Table 3.1: The extinction relations of the five UKIDSS filters calculated via linear regression and the ones for the four IRAC filters calculated by the laws from Indebetouw (2005).

NICE then uses the relations $ZYJHK_{observed} = ZYJHK_{intrinsic} + A_{ZYJHK}$ to calculate the visual extinction via the photometric colors:

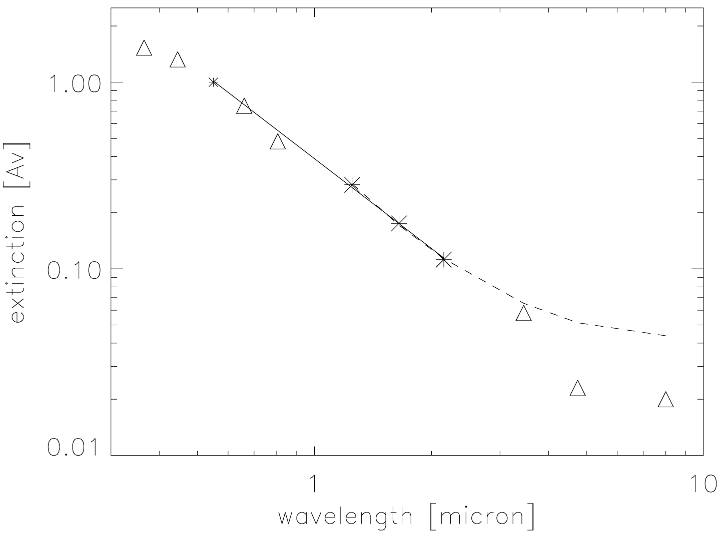

Figure 3.1: Illustration of the extinction law calculation. The triangles mark the relations from 0.365 to 8.0 μm found by Rieke & Lebofski (1985). The asterisks mark the ones for V, J, H and K band, with which we calculated our own law for the UKIDSS filters (full line). The dashed line represents the law found by Indebetouw et al. (2005) for wavelengths from 1.2 to 8.0 μm ($log_{10}\frac{A_\lambda}{A_V} = 0.61 - 2.22 \cdot log_{10}(\lambda) + 1.21 \cdot (log_{10}(\lambda))^2$).

$$A_V = 9.62 \cdot ((Y-J)_{obs} - (Y-J)_{int})$$
$$A_V = 10.20 \cdot ((J-H)_{obs} - (J-H)_{int})$$
$$A_V = 6.29 \cdot ((J-K)_{obs} - (J-K)_{int})$$
$$A_V = 16.39 \cdot ((H-K)_{obs} - (H-K)_{int})$$

The intrinsic colors can be determined again by the use of a control field. Then, as for the star count method, the observed region gets divided into a small grid of which each rectangle should contain around 10 to 15 sources. This is the amount of sources approximated by the authors leading to a large enough distribution of intrinsic stellar colors. In these squares, the observed color of all stars get averaged and a visual extinction estimated. Hence, in each square there have to be sufficient stars, so that their average color is homogeneous and depends only on the extinction and not on the stellar types of the objects in the square. This criteria can be difficult to maintain for a distant region, since foreground stars could dominate the color average. And since they are not effected by the extinction, it would result in a higher value for A_V.

Lombardi et al. (2001) generalized NICE and incorporated other colors in their NIR Color Excess Revisited (NICER) technique. They even perfected it in Lombardi (2009) for small-scale structures to the NICEST technique. All those methods are originally based on 2MASS photometry, even for the Taurus SF region (Lombardi et al. 2010). But the UKIDSS GCS delivers a better instrument to calculate such NIR extinction maps, since it is around 3.5 mag deeper. Therefore, its stellar surface density is much higher and so is the resolution of the extinction map. Lombardi (2005) shows that the photometric technique is more efficient as the star count method for low density regions. We do not apply the most sophisticated NICEST technique, since we do not expect any small scale structures and it does not seem very useful to be more precise without cleaning the data set (see also Goodman et al. 2009). In the following, we describe the NICER technique used in this work. We generalize the relations:

$$(H-K)_{obs} = (H-K)_{int} + 16.39^{-1} \cdot A_V \qquad \text{to} \qquad c_{i,obs} = c_{i,int} + k_i \cdot A_V$$

and state the weighted dependency (by factors b_1, b_2) of the extinction estimator ($\hat{A}_V$) by two colors (c_1, c_2) with

$$\hat{A}_V = b_1 c_{1,obs} + b_2 c_{2,obs}.$$

We request the value of the estimator to be unbiased i.e. to be the true extinction. This leads to the two conditions

$$b_1 k_1 + b_2 k_2 = 1 \qquad \text{and} \qquad b_1 \langle c_{1,int} \rangle + b_2 \langle c_{2,int} \rangle = 0$$

The estimator of the extinction has to show minimum variance f.

$$f(b_1, b_2) = Var(\hat{A}_V) = [\hat{A}_V - \langle \hat{A}_V \rangle]^2$$

We include the two conditions described above with Lagrange parameters and introduce the matrix **C** with

$$\begin{pmatrix} [c_{1,obs} - c_{1,int}]^2 + \sigma_1^2 & [c_{1,obs} - c_{1,int}][c_{2,obs} - c_{2,int}] + \sigma^2 \\ [c_{1,obs} - c_{1,int}][c_{2,obs} - c_{2,int}] + \sigma^2 & [c_{2,obs} - c_{2,int}]^2 + \sigma_2^2 \end{pmatrix}$$

In the case of $c_1 = J - H$ and $c_2 = H - K$, $\sigma_1^2 = \sigma_J^2 + \sigma_H^2$, $\sigma_2^2 = \sigma_H^2 + \sigma_K^2$ and $\sigma^2 = -\sigma_H^2$. Then, we can determine the parameters b via:

$$\vec{b} = (\mathbf{C}^{-1} \cdot \vec{k}) / (\vec{k} \cdot \mathbf{C}^{-1} \cdot \vec{k})$$

With a denominator D this leads to:

$$D = k_1 k_2 (C_{12} + C_{21}) - k_1^2 C_{22} - k_2^2 C_{11}$$
$$b_1 = \tfrac{1}{D}(k_2 C_{12} - k_1 C_{22}) \qquad \text{and} \qquad b_2 = \tfrac{1}{D}(k_1 C_{21} - k_2 C_{11})$$

In contrast to the NICE method, we do this for every single star not considering the intrinsic color defined by its stellar type. Those preliminary visual extinctions per star ($A_V(x_i)$) get averaged by spatial smoothing via

$$\bar{A}_V = \frac{\sum W(x - x_i) \cdot A_V(x_i)}{\sum W(x - x_i)}, \text{ with}$$
$$W(x - x_i) = exp(a \cdot [(x - x_0)^2 + (y - y_0)^2]) \qquad \text{and} \qquad a = 2 \cdot ln(0.5)/FWHM^2$$

We chose the Full Width Half Maximum ($FWHM$) of the Gaussian W to correspond to the square size used in the NICE technique containing the mentioned 10 to 15 sources. We include the influences of all stars if they do contribute at least the 3σ limit (0.03%) of W. The intrinsic colors used in the calculations are again the averaged colors of an off-cloud control field.

3.1 Taurus

We want to include as many criteria as possible to narrow down the search for new LMO in Taurus. The main source to do so is the UKIDSS GCS photometry. Because of that, we calculate the described high-resolution NIR extinction map via the NICER technique. With the map, we are not only able to compare the UKIDSS photometry to the values of the already known Taurus members, but also to compare the dereddened magnitudes to models and field star data. The region covered by the UKIDSS GCS does not seem to cover a great amount of gas and dust besides a small part in the

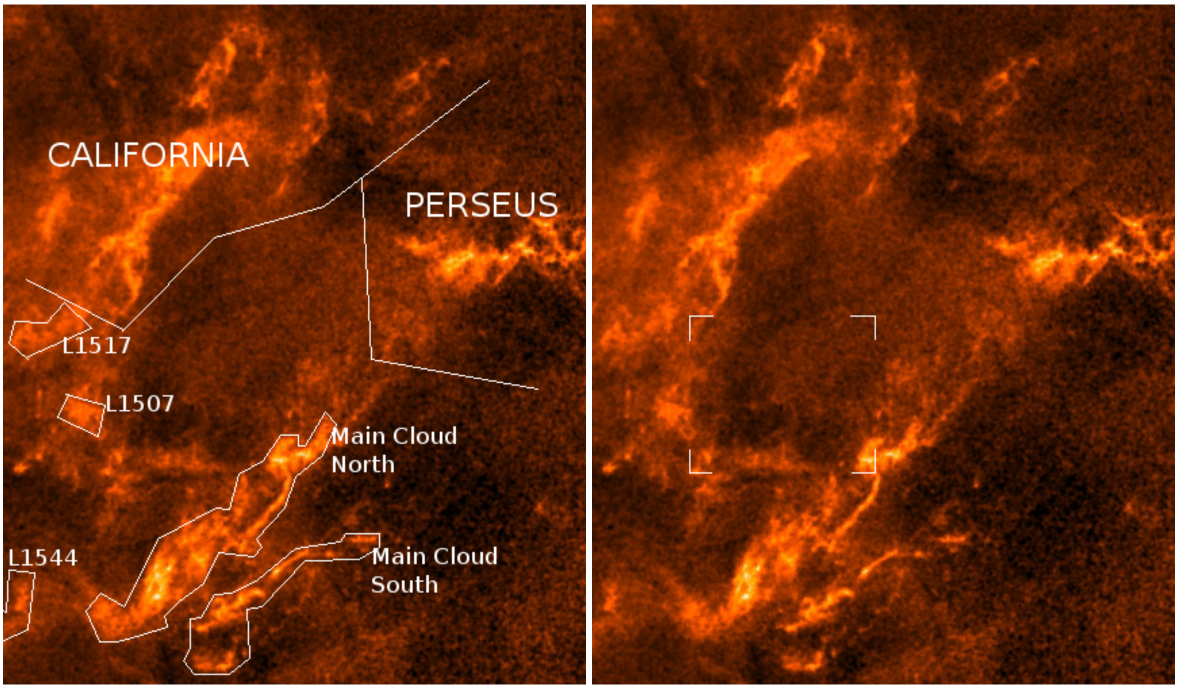

Figure 3.2: The images show the extinction map of the Taurus-Auriga SF region and its surroundings in galactic coordinates (Dobashi et al. 2005, 6 *arcmin* resolution). On the left, we mark the main clouds of the region and separate it from the California and Perseus complexes. On the right side our region A is marked. Note, that it does not include any already known clouds. Only in the southeastern part a small cloud is visible. South is to the bottom, east to the left.

southeast (see Fig. 3.2).

To identify the control field and to define the $FWHM$ of the Gaussian, we calculate a preliminary extinction map with the star count and NICE techniques. Applying a grid on the data, we find an average of 11 and 12 stars for a square size of $1.5'$ x $1.5'$ (0.025 *deg* x 0.025 *deg*) for JHK and YJK filters, respectively. We choose therefore $FWHM = 0.025$ *deg*. This leads to an influence of 0.1% of the Gaussian for distances of 0.04 *deg* (2.4 *arcmin*). All objects inside a circle of that diameter around each source contribute therefore to the smoothed extinction of each object in a 3σ limit (0.27%). The resolution of that map is 4 times smaller than the 6 *arcmin* achieved by Dobashi et al. (2005). We identify the control field in the square degree between RA from 66.5 to 67.5 *deg* and Dec from 32.5 to 33.5 *deg* (see Fig. 3.4). This field contains 20320 and 20244 sources showing JHK and YJK photometry, respectively. We find the following intrinsic colors:

$$(Y-J)_{int} = 0.4969 \pm 0.1486\ mag$$
$$(J-K)_{int} = 0.7679 \pm 0.2614\ mag$$
$$(J-H)_{int} = 0.5615 \pm 0.1685\ mag$$
$$(H-K)_{int} = 0.2086 \pm 0.1661\ mag$$

For our original search of LMO in region A, $H-K$ and $J-H$ colors of 376648 sources providing JHK photometry were used to calculate A_V. For the DR8 data, we had to calculate differently, since the area south of 28.3 *deg* is not covered in H band. We used the 665588 sources showing $Y-J$ and $J-K$ colors and YJK photometry. In those two different extinction maps, we calculate negative extinctions for various objects. We set those values to 0, since the negativity is of no sense. We do this for 67777 sources in the JHK map and for 28128 sources in the YJK map. For 334061 sources we calculate two values for the visual extinction via the two different filter sets. We compare them in

Fig. 3.3.

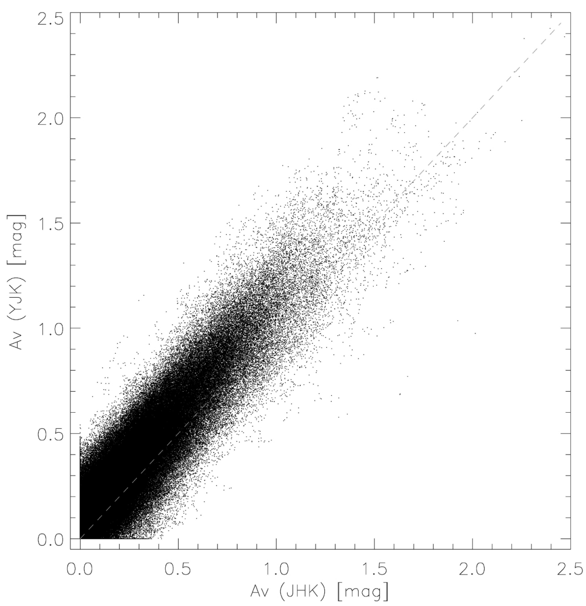

Figure 3.3: Comparison of the different extinction map values calculated for 334061 sources of region A via YJK and JHK photometry. There is a small difference for the values visible by the variation to the dashed line marking $A_{V,YJK} = A_{V,JHK}$.

The calculation for the YJK photometry seems to deliver slightly larger values. This might be due to the uncertainty of the extinction law for the Y band. This difference is also visible in the final extinction maps, which we show in Fig. 3.4. Nevertheless, the results are in good agreement with the map calculated via NICEST by Lombardi et al. (2010, see Fig.1.3).

Including the zero values, we find the following average visual extinctions in region A for the two maps:

$A_{V,JHK} = 0.26 \pm 0.25$ mag

$A_{V,YJK} = 0.34 \pm 0.28$ mag

Those values indicate the small influence of molecular clouds on region A. As an error for the visual extinction of every source, we calculate the Gaussian error of the uncertainties of the used colors from the control field. For the YJK map this is $\sqrt{(\Delta((Y-J)_{int}))^2 + (\Delta((J-K)_{int}))^2} = \sqrt{0.1486^2 + 0.2614^2}$ $mag \approx 0.30$ mag. For the JHK map this is 0.24 mag. Separating the northern main cloud of Taurus containing 164096 sources, we find an average of $A_{V,YJK} = 1.02 \pm 0.50$ mag. This is a significant difference to the average values calculated for region A. We deredden the UKIDSS GCS photometry of all five filters via the relations $ZYJHK_{observed} = ZYJHK_{intrinsic} + A_{ZYJHK}$ and the visual extinction calculated by the JHK NICER technique. By this, we increase the number of criteria for our search process in the following chapter.

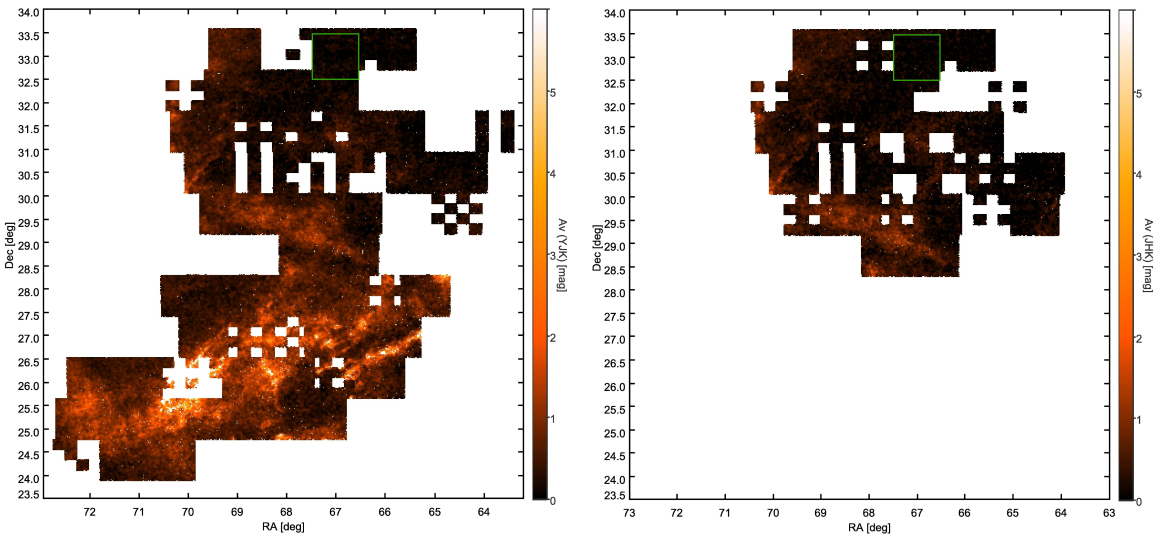

Figure 3.4: The high-resolution NIR extinction maps (1.5 *arcmin*) in Taurus calculated with the NICER technique and YJK (left) and JHK (right) photometry, respectively. Note the slightly smaller values for the latter map. The control field is marked green.

3.2 Orion

In Orion, we calculate the extinction map to be able to identify and diminish the influence of molecular clouds present in the UKIDSS GCS data set. We want to have an unbiased view on the clustering in the region to find possible new stellar associations. In the area covered by the survey we have the opportunity to probe this dereddening effect by the presence of the σ Orionis cluster. We show the greater region in Fig. 3.5.

We calculated a preliminary extinction map with the star count and NICE techniques to find a control field and to define the FWHM of the Gaussian used in the smoothing process. Applying a grid on the data, we find an average of 11 stars for a square size of 2.1′ x 2.1′ (0.035 *deg* x 0.035 *deg*) for JHK filters. We choose therefore $FWHM = 0.035\ deg$. The control field we identify in the square degree between RA from 83.5 to 84.5 deg and Dec from -3.0 to $-2.0\ deg$ (see Fig. 3.6). This field consists of 14246 sources. There, we find the following intrinsic colors:

$$(J-H)_{int} = 0.56 \pm 0.18\ mag$$
$$(H-K)_{int} = 0.21 \pm 0.19\ mag$$

The values are the same as for the Taurus region. The error of the visual extinction for each source is 0.26 *mag*. At the time of the research done in this region, we were not aware of the more sophisticated NICER method and applied the NICE technique using $J-H$ and $H-K$ colors. We calculated the two values in the described grid of $148x128$ (= 18944) data points, formed the average of them and set 8372 to zero, due to their negativity or their location outside the UKIDSS coverage. We overlaid the data set containing every stellar object and assigned the visual extinctions to the stars located in each grid. Including the zero values, we calculate $A_V = 1.12 \pm 0.19\ mag$ for the whole map. We show the final extinction map in Fig. 3.6.

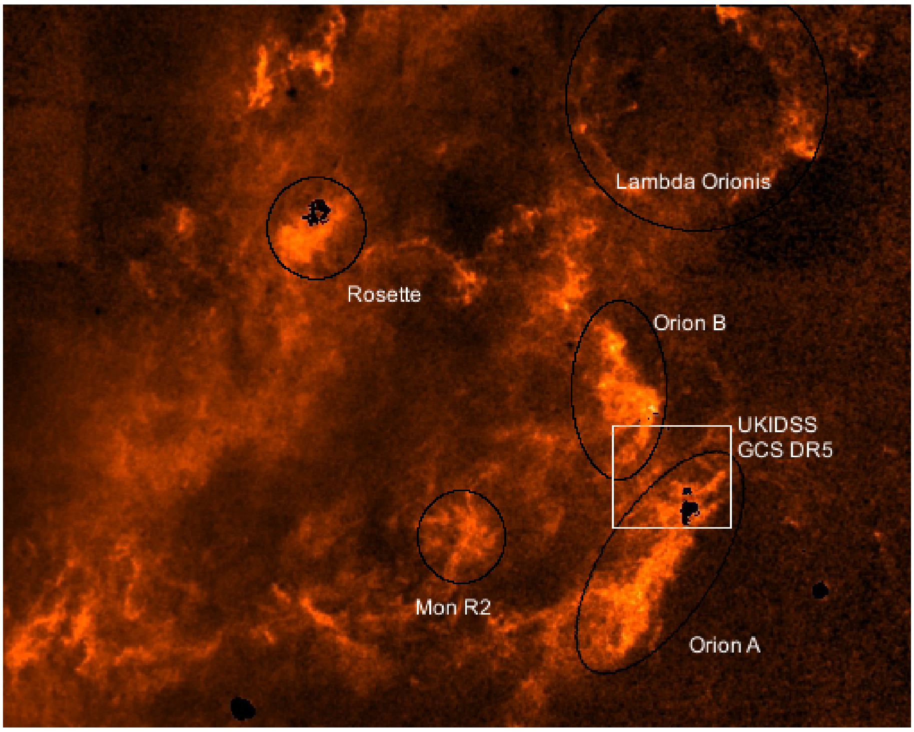

Figure 3.5: The image shows the extinction map of the Orion region and its surroundings in 6 *arcmin* resolution published by Dobashi et al. (2005). We mark and name the main parts and the area observed by the UKIDSS GCS survey. South is to the bottom, east to the left.

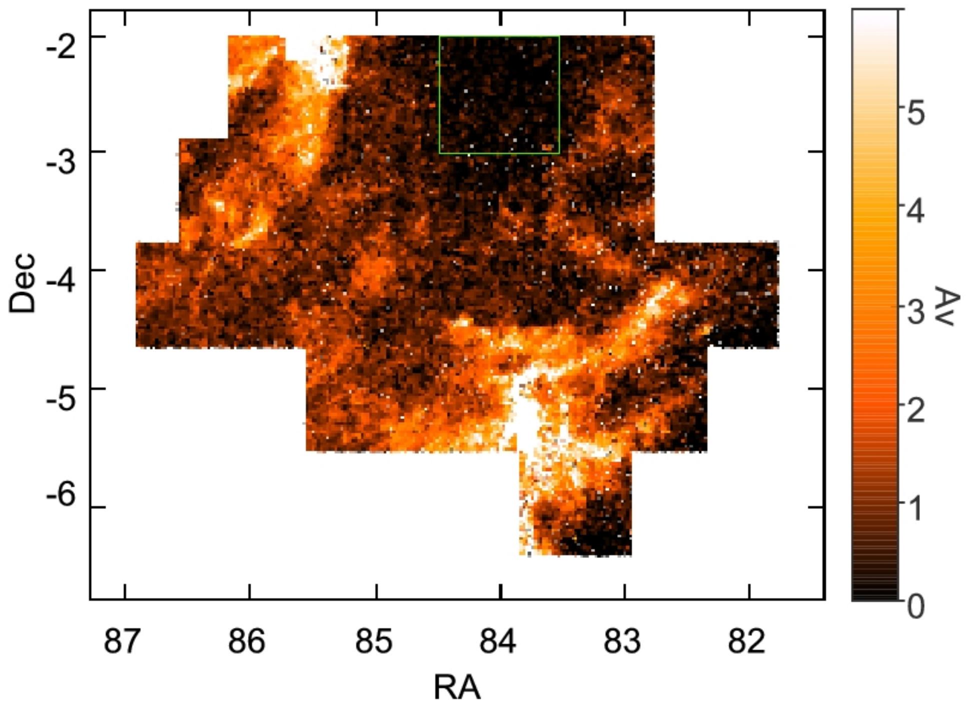

Figure 3.6: The high-resolution 2.1 *arcmin* NIR extinction maps in Orion calculated with the NICE technique and *JHK* photometry. The control field is marked green. In the southwest, we see the A cloud surrounding the ONC (central region is left out in the UKIDSS GCS data due to its brightness). On the northeastern part, the Orion B cloud is visible.

Chapter 4

The search for new low-mass objects

4.1 Different searches in Taurus

In this section, we describe the techniques to search for new LMO in Taurus . All members of Taurus are supposed to be born in the molecular clouds in which the already known members are located. But region A is located 5 *deg* north to its main clouds. Only in its southeastern part, we identified a less dense molecular cloud by the extinction map (see Fig. 3.4). Therefore, we will mostly select candidates not related to the gas and dust of that area. They could have been ejected early on from their birth sites following the embryo ejection formation model. The UKIDSS GCS data set contains mostly objects behind Taurus, since the region is nearby and of very low density. Assuming a density of 0.25 stars pc^{-2} (4 times smaller than in the main cloud), we expect only around 40 new Taurus members in our region A. Due to the proximity of the region, the foreground stars do not contaminate our sample by very much.

We conclude, that we have to apply a very detailed search to identify the few new members the area could contain. The criteria we will use depend on the values of the already known Taurus members and the UKIDSS GCS data set. Also, we use the described evolutionary models and photometric model data sets. The extinction map was derived to be able to compare even more precisely those values and deredden the ones from the UKIDSS GCS data set. Only one already known member is located in region A (see Fig. 2.7). That is why the UKIDSS GCS photometry before DR8 was of no help in those searches. Nevertheless, we give their photometric values in the appendix in Tab. A, including as well the part south of 28.3 *deg* and the 81 members located there.

4.1.1 Photometric search for objects of type M and L

We search for new low-mass members of spectral type M and L of Taurus via their location in various CMD and CCD. As an example, we show the $J-K$ vs. J diagram of the members of Taurus in Fig. 4.1. The sequence marked by the members is slightly redder than the one from the field dwarfs and the evolutionary models. This is due to the extinction caused by the gas and dust the members are embedded in. The members mark a certain area in the diagram ($J < 16.5$ *mag*, $0.5 < J-K < 3.5$ *mag*), which we will use as reference for our search. Hereby, we follow the work by Lodieu et al. But the low stellar density of Taurus and the location of region A let all diagrams be dominated by background stars. In contrast to e.g. Lodieu et al. (2007b) in UpperSco or Lodieu et al. (2009)

in σ Orionis, we are not able to separate the member sequence visually. This is mainly due to the lower density of members in Taurus compared to the regions investigated by those authors. The first restriction we made to our selection is the detection in at least three UKIDSS filters. This allows us to incorporate more than just one photometric selection criteria. Of the 967875 and 620766 sources in the whole area and region A, 836599 (86%) and 509413 (82%) show such values, respectively. In the following we describe the various CMD cuts made to select new member candidates in Taurus.

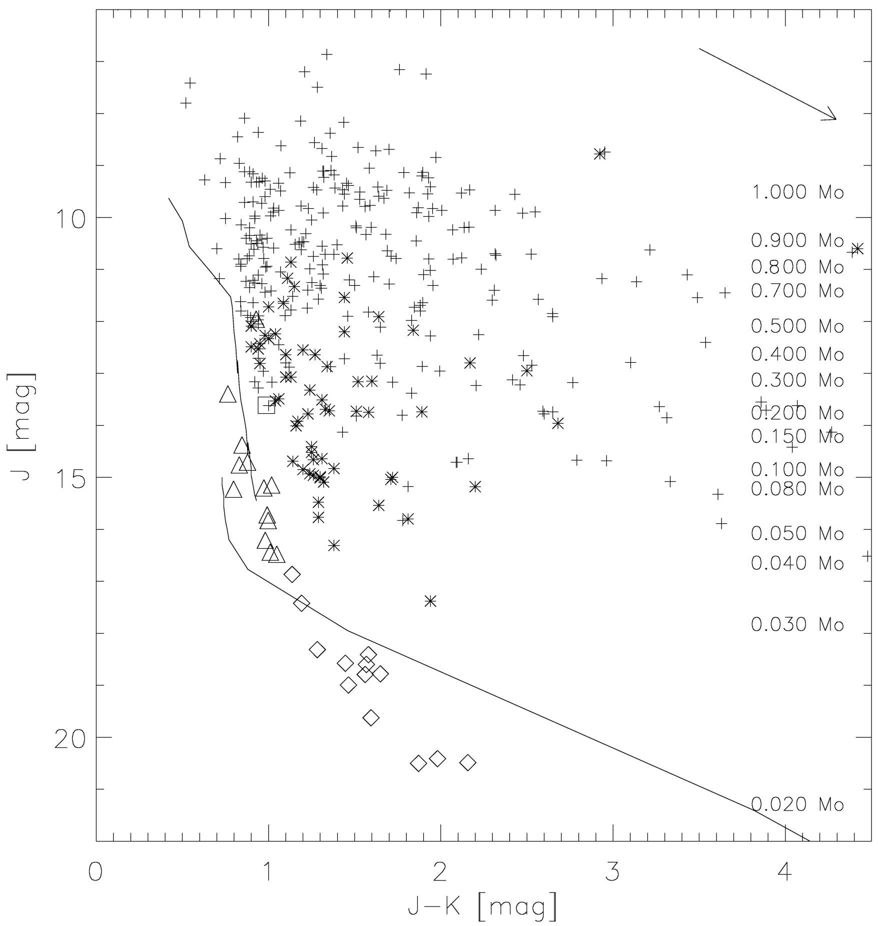

Figure 4.1: The $J-K$ vs. J CMD of the already known members of Taurus $< M6$ (plus), $> M6$ (asterisk), the field dwarfs described by Hewett et al. (2006) of type M (triangle) and of type L (diamond). Additionally, we show the tracks of the evolutionary models for earlier types by Baraffe et al. (1998) and for later types by Chabrier et al. (2000). On the right side, we give the corresponding masses from the models (assuming a distance of 140 pc and no interstellar reddening). Note, that the members form a certain region in the diagram which is redder than the model data. The arrow on the upper right side marks an extinction of $A_V = 5$ mag.

4.1.1.1 Selection 1: UKIDSS & 2MASS JHK photometry

The 2MASS JHK photometry of the Taurus members let us define the location of members in the $J-H$ vs. J, $J-K$ vs. J and $H-K$ vs. H CMD, and in the $H-K$ vs. $J-H$ CCD. We can apply limits in those diagrams not only to the UKIDSS JHK photometry of the UKIDSS data set, but also to their 2MASS counterparts. In all the CMD the UKIDSS data set forms a triangle-like distribution. This is an overlay of various populations in various distances in the line-of-sight of the observations. On the blue faint side of the diagrams, old distant background stars are located. On the red side, besides the member of Taurus, distant galaxies are located. The members of the SF region should be located around the hypotenuse of the triangle only dislocated due to the effects of the extinction. There, they form the main sequence of young nearby objects. We chose our limits to include all known Taurus members and to exclude all unextincted older model field dwarfs. As a less strict criteria, we follow the density lines of the CMD (see Fig. 4.2 and in the appendix Fig. B.1). By that we find the following cuts (an overview of all selection criteria including mass and magnitude ranges are shown in Tab. B in the appendix):

$$J < 8.80 \cdot (J-K) + 5.30 \; mag$$
$$J < 3.70 \cdot (J-K) + 12.15 \; mag$$
$$J < 15.50 \cdot (J-H) + 4.30 \; mag$$
$$J < 7.20 \cdot (J-H) + 11.60 \; mag$$
$$H < 18.00 \cdot (H-K) + 8.55 \; mag$$
$$H < 6.60 \cdot (H-K) + 13.20 \; mag$$
$$J-H > 0.50 \; mag$$
$$H-K > 0.15 \; mag$$
$$J-H < 1.37 \cdot (H-K) + 0.6445 \; mag$$

In general, we find two cuts in every diagram. The steeper one follows the member sequence and the M field dwarf models. On the other hand, we explored the magnitude ranges beyond the 2MASS detection limit, where only the L field dwarf models helped to find the cuts. This is of course less reliable. But we risk to loose some candidates in order to diminish the selection. Especially, because this faint part of the UKIDSS data set is highly populated. We select 53066 of 836599 (6%) and 20107 of 509413 (4%) sources for the whole data set and region A, respectively. We confirm the statement of Luhman et al. (2006), who describe the following limits in the $H-K$ vs. $J-H$ diagram for Taurus members later than $M6$:

$$0.60 \; mag < J-H < 1.30 \; mag$$
$$H-K > 0.35 \; mag$$
$$H-K > 0.73 \cdot (J-H) - 0.1975 \; mag.$$

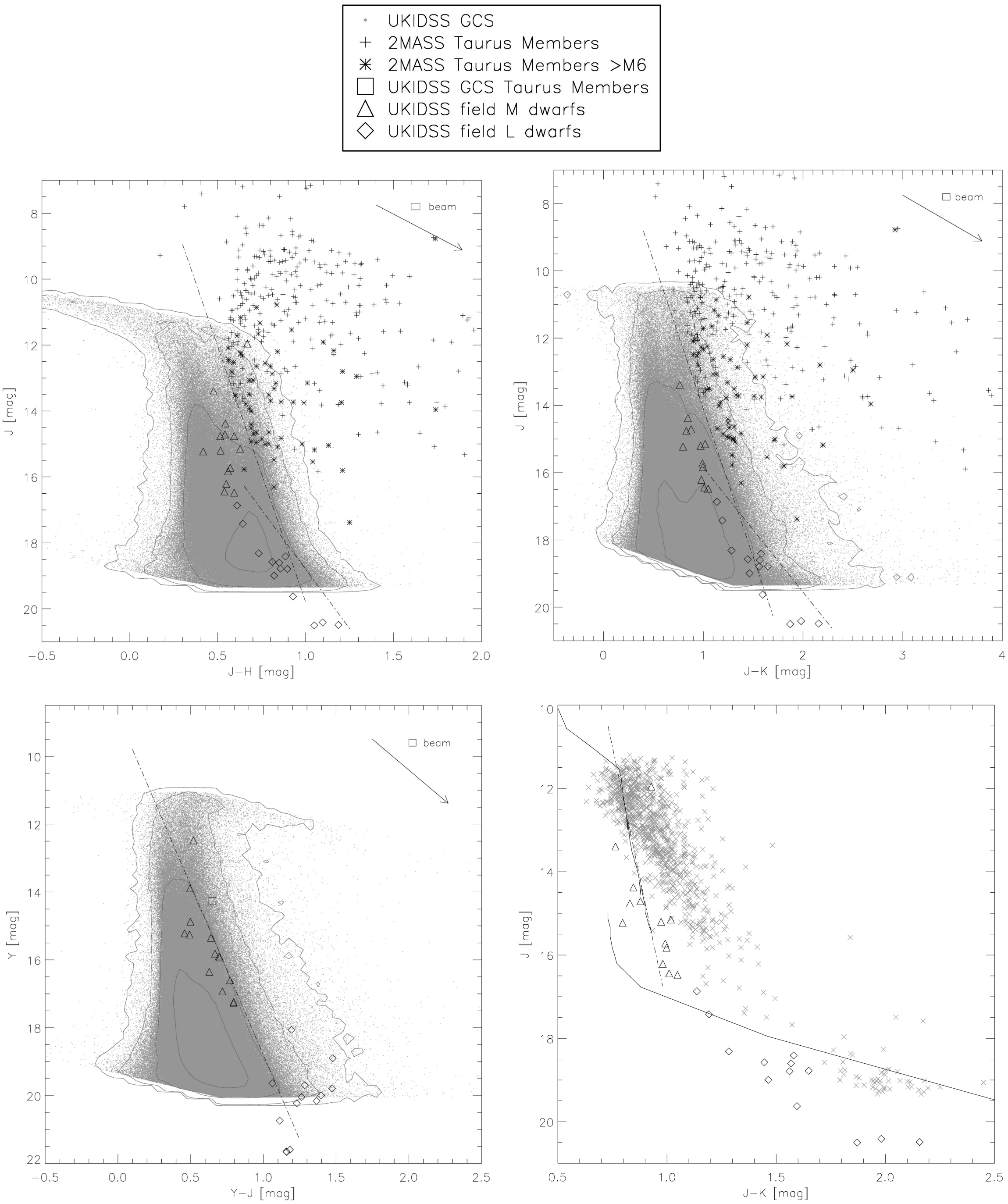

Figure 4.2: As examples, we show the $J-H$ vs. J (upper left) and the $J-K$ vs. J (upper right) of selection 1, the $Y-J$ vs. Y (lower left) of selection 2 and the dereddened photometry in the $J-K$ vs. J (lower right) CMD of selection 5. The signs are like in Fig. 4.1 and get explained at the top of the images. In the dereddened $J-K$ vs. J diagram we show the evolutionary models used in this work (no extinction, distance of 140 *pc*). Additionally, we show the one Taurus member already identified in region A (square). The whole UKIDSS GCS data set is shown in gray dots. To better understand its distribution in the image, we calculate density lines for areas containing > 5, > 50, > 500, and > 2500 sources. The beam resolution of those lines is given in the upper part of each image. Also, we show the arrow of $A_V = 5$ *mag*. The dash-dotted lines show the cuts we have made. For further selection diagrams see Fig. B.1 to Fig. B.7 in the appendix.

4.1.1.2 Selection 2: UKIDSS *ZYJHK* photometry

For the other CMD including the *ZY* UKIDSS filters, we did not have the values of the already known members except one. Instead, we used the field dwarf models and the density lines of the UKIDSS data to estimate conservative cuts. In filters of shorter wavelength, the colors are more affected by the extinction. This suggests a sequence of members more clear than with the *JHK* photometry. The *Z* band central wavelength of 0.8825 μm corresponds to a maximum output of a blackbody of $T_{eff} = 2897.8\ K/\lambda[\mu m] \approx 3300\ K$. For every body hotter than that, all used colors should be red. This is also reflected in the location of the field dwarfs (see Fig. 4.2 and in the appendix Fig. B.2 and Fig. B.3). We find the following limits in the diagrams:

$$
\begin{gathered}
Z < 9.00 \cdot (Z - Y) + 11.10\ mag \\
Z < 5.70 \cdot (Z - J) + 8.75\ mag \\
Z < 5.70 \cdot (Z - H) + 6.30\ mag \\
Z < 3.65 \cdot (Z - K) + 7.85\ mag \\
Y < 10.00 \cdot (Y - J) + 8.80\ mag \\
Y < 7.90 \cdot (Y - H) + 5.50\ mag \\
Y < 4.80 \cdot (Y - K) + 7.70\ mag
\end{gathered}
$$

We select 15361 of 53066 (29%) and 2106 of 20107 (10%) sources in the whole data set and in region A, respectively.

4.1.1.3 Selection 3: proper motions

Besides the selections made with the photometry, we set proper motion limits for the new member candidates. If an object moves within the velocity limits of a stellar association it is a strong indication of its membership to that association. Our data set is distributed with a Gaussian around the zero movement point. No indication of a separate overlaid distribution at the velocities of Taurus can be distinguished. The literature limits given by Quanz et al. (2010) are $(-5, -35) < (\mu_\alpha, \mu_\delta) < (15, -5)$ mas/yr. In our own data, the 351 members are located in a square of $16x16$ $(mas/yr)^2$ around the center of $7.4/-20.4$ mas/yr (see Fig. 4.3). But the average errors we calculated from the UKIDSS/2MASS comparison are very high with $(\Delta\mu_\alpha, \Delta\mu_\delta) = (9.4, 6.6)$ mas/yr. They are even higher for the NOMAD sources. Adding 10 mas/yr as uncertainties to the described limits, we are not able to exclude the zero movement point. But there, the objects contaminating our selection are located. Besides background sources, these are distant galaxies which show red colors such as the Taurus members. It would have been essential for this selection criteria to exclude the zero movement point to be the important one it represents in literature. But with our data, we only can exclude high proper motion sources. We apply the following limits to the sources: $(-18.6, -46.4) < (\mu_\alpha, \mu_\delta) < (33.4, 5.6)$ mas/yr for the UKIDSS/2MASS calculation and $(-30.0, -60.0) < (\mu_\alpha, \mu_\delta) < (40.0, 10.0)$ mas/yr for the NOMAD/2MASS calculation. We select 10492 of 15361 (68%) and 1368 of 2106 (65%) sources in the whole data set and in region A, respectively. We divide the data into (see e.g. Tab. B.2)

- candidates with proper motions inside the limits described by the already known members (membership probability 1), and
- candidates with proper motions inside the limits set by this work (membership probability 2)

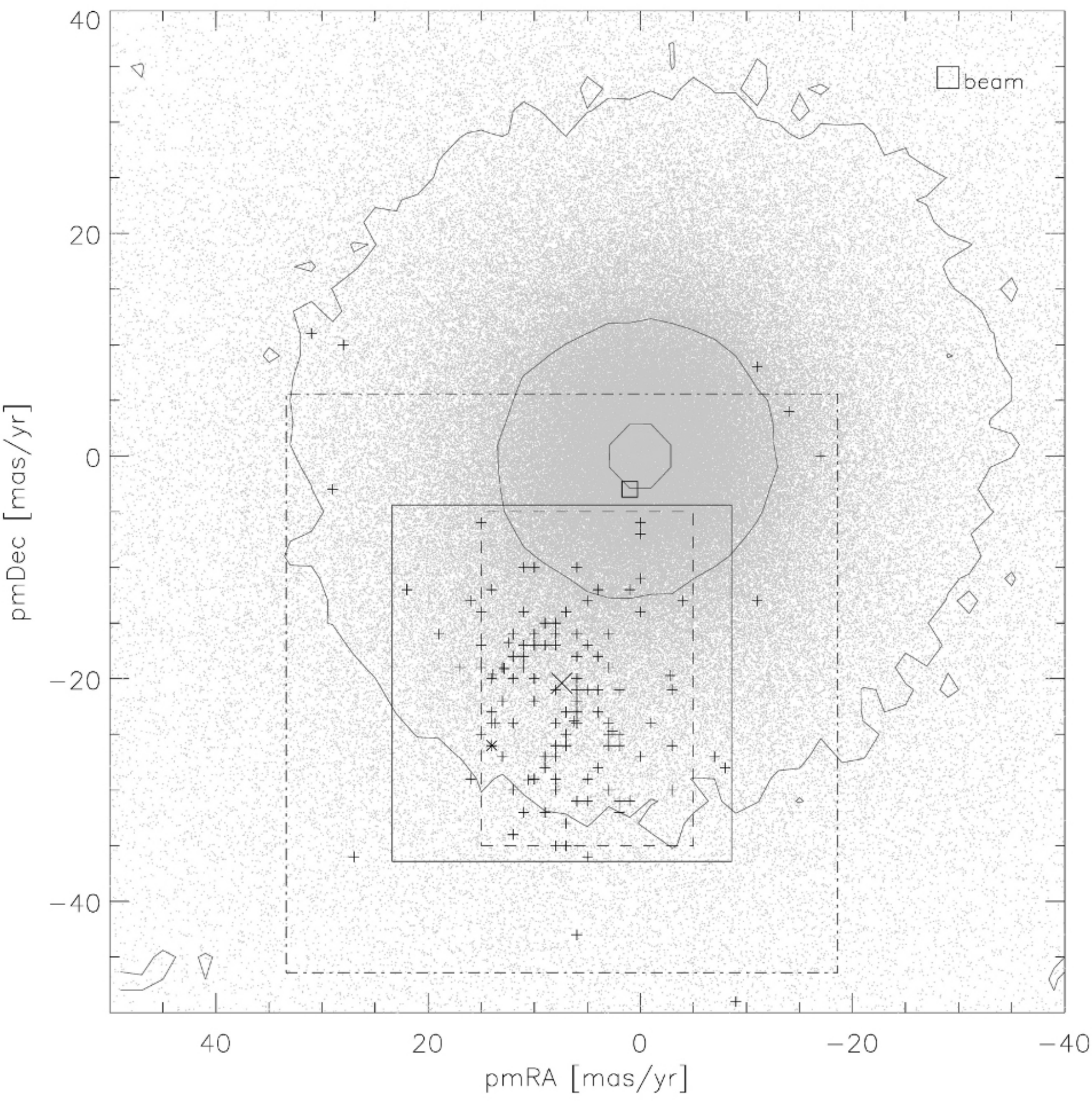

Figure 4.3: We show the proper motion plot μ_α vs. μ_δ or *pmRA* vs. *pmDec*. The signs are like in Fig. 4.2. We show the limits defined by Quanz et al. (2010, dashed line) and the limits identified by the data of the already known Taurus members (full line). The selections made for the UKIDSS/2MASS calculated proper motions by adding 10 *mas*/*yr* errors to the latter are shown by the dash-dotted line. They include the (0/0) point, where background stars and distant galaxies are located. Note, that there is no visible distribution in the UKIDSS data on the average Taurus location marked by the large cross.

4.1.1.4 Selection 4: NOMAD *BVR*- and Spitzer MIR photometry

We select sources of region A in the CMD constructed with optical and/or MIR photometry. There, the data of the already known Taurus members does not reveal the member sequence clearly. Nevertheless, we try to find conservative cuts in our search for new member candidates. In this chapter, we use the Spitzer MIR data only to compare it to the already known members. More detailed searches with this photometry are done later on in this chapter. There, we use it to identify MIR excess due to the possible presence of transition disks. We draw the following cuts:

$$B < 9.00 \cdot (B-V) + 12.00\ mag$$
$$B-R > 0.75\ mag$$
$$V-R > 0.00\ mag$$
$$[3.6]-[4.5] > -0.15\ mag$$
$$[3.6]-[5.4] > -0.15\ mag$$
$$[3.6]-[8.0] > -0.15\ mag$$
$$[3.6]-[24.0] > -0.15\ mag$$

Except for the B vs. $B-V$ diagram, we only find lower limits for the colors (see Fig. B.4 and Fig. B.5 in the appendix). In the CMD of the Spitzer MIR photometry, we chose as ordinate only the [3.6] filter. By these criteria, we select 10419 of 10492 and 1295 of 1368 sources in the whole data set and in region A, respectively.

4.1.1.5 Selection 5: extinction corrected, dereddened photometry

We dereddened the photometry of all filters as described, using the extinction map derived from the UKIDSS *JHK* photometry. The selection made in this section is therefore limited to region A. The effect and the outcome of the dereddening process is shown in Fig. 4.4.
Together with the model field dwarf data and the evolutionary models, the dereddened photometry let us identify more cutting lines in all the CMD and CCD. This is done very conservative, since our extinction values show large uncertainties. We try to include the field dwarf data into our cuts and define only lines, which affect the remaining selection (see Fig. 4.2 and in the appendix Fig. B.6 and Fig. B.7). The following lines are found:

$$Z < 24.14 \cdot (Z-Y) + 5.36\ mag$$
$$Z < 7.50 \cdot (Z-Y) + 12.55\ mag$$
$$Z < 8.67 \cdot (Z-J) + 5.80\ mag$$
$$Z < 5.15 \cdot (Z-J) + 9.88\ mag$$
$$Z < 5.70 \cdot (Z-H) + 5.75\ mag$$
$$Z < 4.94 \cdot (Z-K) + 4.86\ mag$$
$$Y < 23.33 \cdot (Y-J) + 0.53\ mag$$
$$Y < 7.27 \cdot (Y-K) + 4.36\ mag$$
$$J < 27.50 \cdot (J-H) + 0.18\ mag$$
$$J < 25.00 \cdot (J-K) - 7.75\ mag$$
$$H < 32.00 \cdot (H-K) + 3.96\ mag$$
$$H < 13.20 \cdot (H-K) + 9.71\ mag$$

We select 9868 of 10419 (95%) and 746 of 1295 (58%) sources in the whole data set an in region A, respectively. This selection step just affects our region A.

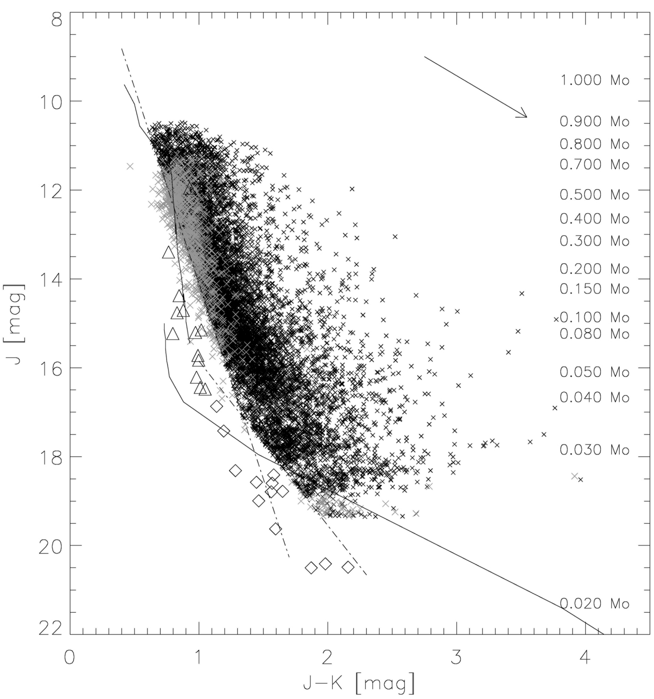

Figure 4.4: The image shows the $J-K$ vs. J CMD (see Fig. 4.1). Besides the evolutionary models and the field dwarf data the remaining sources of our selection are shown (black X). The gray X indicate the dereddened values, using the visual extinction calculated via the UKIDSS JHK photometry. We can observe how those data points fit better the evolutionary models and the model field dwarf data. The signs are like in Fig. 4.1 and 4.2.

4.1.1.6 Final selection of a bright and a faint LMO candidate sample

So far, we selected candidates of the whole UKIDSS GCS DR8 data set. We found some hundred sources in region A and some thousand south of it, where the UKIDSS H band is missing. That filter would be crucial to improve the search there. With that southern data of the DR8, the selection criteria for the whole data set could be improved. We will discuss later (see Sec. 7.3.1) how the additional UKIDSS photometry of the southern 81 already known Taurus members could improve the selections 1 (Sec. 4.1.1.1) & 2 (Sec. 4.1.1.2).

The objects used for observations in this work are located in region A. And we are not able to create more selection criteria for the southern part. From here on, we will describe only the treatment for the remaining 746 candidates of region A. We request a detection in the UKIDSS JHK filters. Thereby we make sure, that the most important selections based on the already known Taurus members are used and that an extinction value was calculated. Following the evolutionary models, we set a limit to the magnitudes of LMO. For a star of 0.5 $M_\odot$ in a distance of 140 pc this is around 12 mag in J band.We set it both to the UKIDSS and to the 2MASS photometry. We select 377 of the 746 (51%) sources by those two criteria. The remaining objects got checked for the reliability of their photometry. We checked the UKIDSS GCS J band images for wrong detections. These could result from image damages, image border problems or overlapping of two or more sources (visual binarity). The images in all filters are provided by the WSA accessible via the www.UKIDSS.org web page. As examples we show the 47 images of $30x30$ $arcsec^2$ in filter J of the finally observed candidates in the appendix in Fig. B.8, Fig. B.9 and Fig. B.10. By this, we ruled out 57 of the objects and were left with 320 candidates.

At this point of the candidate selection, we had to consider the feasibility of the optical follow-up observations. We divided the remaining selection into a faint and a bright subsample. We had access to 4m-class telescopes like the WHT. There, we find $I < 18.5$ *mag* to be an upper feasibility limit, resulting in an exposure time of about one hour. Using the evolutionary models, this corresponds approximately to $J < 15.5$ *mag*. This magnitude defines the separation we make between the two subsamples. It is already covered by the 2MASS survey. Therefore, we request for the bright subsample a detection in all three 2MASS filters. Then, we applied the limit to both 2MASS and UKIDSS passbands. To be more precise in our photometric selections, we requested errors in the UKIDSS passbands of less than 0.01 *mag*. This limit is extremely low for the whole UKIDSS GCS data and still very strict for this bright subsample. It reduces the large number of candidates to a smaller sample of sources with more precise photometry. Finally, our bright sample of region A consists of 253 sources. Following the proper motion criteria, 112 of them (44%) are of membership probability 1. We give an overview of the data in Tab. 4.1.

column	B_N	V_N	R_N	Z_U	Y_U	J_U	H_U	K_U	J_M	H_M	K_M
unit	*mag*	*mag*	*mag*	*mag*	*mag*	*mag*	*mag*	*mag*	*mag*	*mag*	*mag*
lower limit	15.83	14.53	13.73	12.93	12.57	12.00	11.27	10.80	12.03	11.08	10.75
upper limit	21.83	17.97	20.09	16.83	16.12	15.30	14.56	14.12	15.39	14.46	14.04
column	[3.6]	[4.5]	[5.8]	[8.0]	$A_{V,YJK}$	$A_{V,JHK}$	$\mu_{\alpha,U}$	$\mu_{\delta,U}$	$\mu_{\alpha,N}$	$\mu_{\delta,N}$	
unit	*mag*	*mag*	*mag*	*mag*	*mag*	*mag*	*mas/yr*	*mas/yr*	*mas/yr*	*mas/yr*	
lower limit	10.8	10.8	10.8	10.8	0	0	-16.25	-44.06	-20.0	-58.0	
upper limit	13.6	13.5	13.5	13.3	1.54	1.34	33.37	5.34	34.0	10.0	

Table 4.1: Summary of 253 bright LMO Taurus member candidates. Note that not every source shows data in all columns. The indices [N,U,M] refer to the surveys [NOMAD,UKIDSS,2MASS].

The reason to construct a faint subsample of our candidate list is the access granted to the GTC/OSIRIS instrument in 2009. We had the opportunity to reach down beyond the limit set by the 4m-class telescopes. It was also the opportunity to access the advantage of the deeper UKIDSS GCS photometry compared to 2MASS. 55 of the selected 320 (17%) objects show $J > 15.5$ *mag*. We request no 2MASS counterpart and errors in the UKIDSS passbands of less than 0.15 *mag*, since they rise with fainter magnitude. We select 19 sources for our faint sample and give an overview of the data in Tab. 4.2.

column	Z	Y	J	H	K	$A_{V,YJK}$	$A_{V,JHK}$
unit	*mag*	*mag*	*mag*	*mag*	*mag*	*mag*	*mag*
lower limit	19.48	18.49	17.41	16.27	15.41	0	0
upper limit	19.48	19.87	19.34	18.25	17.29	2.90	2.45

Table 4.2: Summary of 19 faint LMO Taurus member candidates. Note that not every source shows data in all columns.

Finally, we observed 43 new Taurus member candidates of the bright- and 4 of the faint subsample. They were chosen randomly out of the candidate lists. All the data available for each source is shown in Tab. B, Tab. B.2 and Tab. B.4.

However, we still expect the selected candidates to be contaminated. We probably have selected many background stars and galaxies, since Taurus and even more the region A are of such low density. We expect less than the usual success rate of 30% in such searches for LMO. A large distribution of MIR data as provided by the WISE survey could help with the search. We will discuss later (see Chap. 7.3.2), how our selection could be improved by this new data set. We also note, that the second epoch K band data of the UKIDSS GCS will provide much clearer proper motions for the sources. But due to the unclear future of the UKIRT telescope, it is still in discussion if those observations will be made. We remind, that an overview of all the selection criteria is given in Tab. B in the appendix.

4.1.2 Search for sources showing MIR excess

Another approach to search for new low-mass members in Taurus uses the MIR data in the small part southeast of region A. With that photometry, we searched for infrared excess produced by the accretion disks many of the young members of Taurus show. We applied color and magnitude limits to the Spitzer data in collaboration with Miriam Aberasturi Vega[1], who made the final selection we observed. To narrow down the search, we selected firstly all sources showing the 4 IRAC and the 5 UKIDSS filters. These are 2872 of 42800 sources (7%). We give a summary of the data in Tab. 4.3.

column	Z	Y	J	H	K	[3.6]	[4.5]	[5.8]	[8.0]
unit	*mag*	*mag*	*mag*	*mag*	*mag*	*mag*	*mag*	*mag*	*mag*
lower limit	11.42	11.36	10.63	10.86	9.76	8.66	7.67	7.06	6.98
upper limit	20.34	19.73	19.14	18.47	17.89	17.00	17.20	16.00	15.00

Table 4.3: Summary of the data of the 2872 sources with IRAC and UKIDSS photometry.

4.1.2.1 Selection 1: MIR CCD and CMD

We used the relations described by Barrado et al. (2007) to classify the 2872 candidates and the 351 already known Taurus members by their MIR colors. The data of those MIR wavelengths indicate the behavior of warm gas in the surroundings of the objects. The authors distinguish the different classes in the [5.8] − [8.0] vs. [3.6] − [4.5] CCD, which we show in Fig. 4.5. 19 already known Taurus members do not show all the IRAC passbands. We find 31 and 37 possible protostars (Class I) in the candidate sample and the member database, respectively. 283 and 150 objects get classified as TTS (Class II) and 97 and 2 stars are in between those two classes (Class I/II). We identify 2461 and 143 more evolved stars (Class III). Therefore, the derived classes do not justify a new selection criteria. But the members should all be very young. The results are shown in the appendix in Tab. A for the members and are added to every table of data of observed objects (see appendix B).

The candidate sample contains many extragalactic sources. Gutermuth et al. (2008) describe a method to identify broad-line Active Galactic Nuclei (AGN) and objects with strong Polycyclic Aromatic Hydrocarbon (PAH) emission in various CCD and CMD. We show the criteria in the following and illustrate them in Fig. 4.6:

$$[3.6] - [5.8] < 1.5\ mag$$
$$[4.5] - [8.0] > 1.0\ mag$$
$$[3.6] - [5.8] < 0.75 \cdot ([4.5] - [8.0] - 1.0)\ mag$$
$$[4.5] - [5.8] < 1.05\ mag$$

[1]Centro de Astrobiología (INTA-CSIC), ESAC campus, Villanueva de la Canada, Madrid, Spain

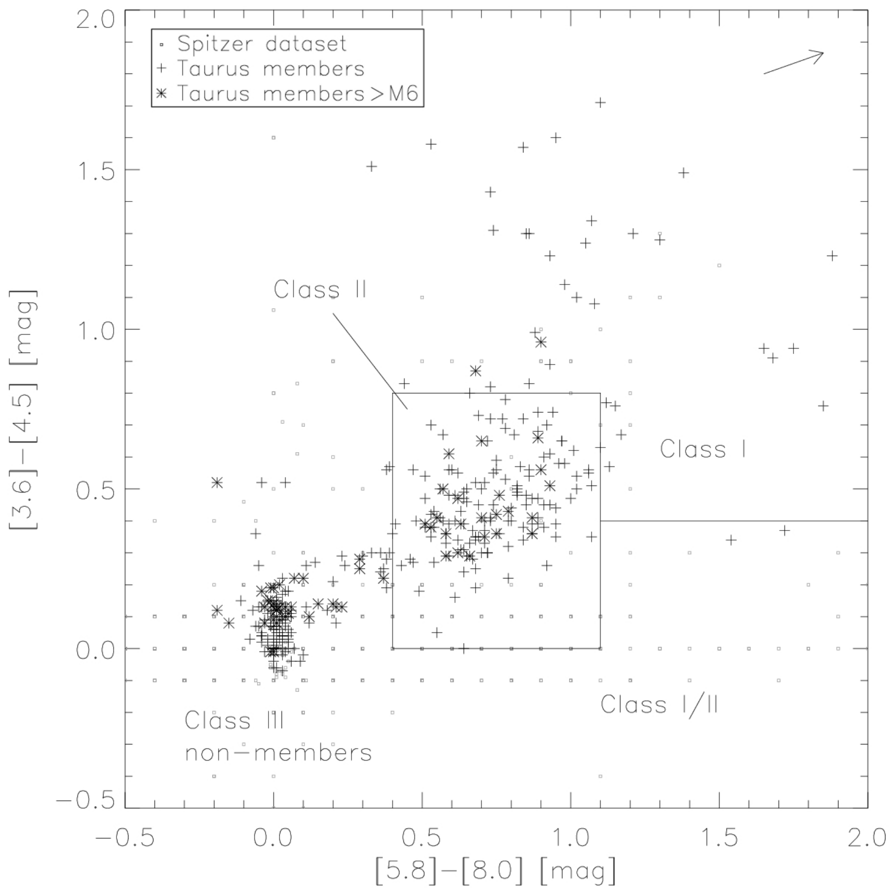

Figure 4.5: We show the $[5.8]-[8.0]$ vs. $[3.6]-[4.5]$ CCD which enable to distinguish the different stellar classes marked by the lines (Barrado et al. 2007). We plot the candidates showing all IRAC and UKIDSS filters (small squares), the already known members of Taurus (plus & asterisk) and an arrow of 20 *mag* visual extinction.

$$[5.8]-[8.0] > 1.0\ mag$$
$$[4.5]-[5.8] < 0.875\cdot([5.8]-[8.0]-1.0)\ mag$$
$$[4.5] > 13.5\ mag$$
$$[4.5]-[8.0] > 0.5\ mag$$
$$[4.5] > 13.5+([4.5]-[8.0]-2.3)/0.4\ mag$$

We exclude by those criteria 235 possible galaxies and are left with 2637 of 2872 (92%) candidates. We use also the tool by Bouy et al. (2009) to exclude Quasi Stellar Objects (QSO). They use the relation $(i-J) > 1.12(J-[3.6])-1.0\ mag$ and combine thereby optical, NIR and MIR photometry. Instead of their filter i, we use the optical filters available for our sources. Those include Johnsons BVR and UKIDSS Z filters. We do not find more contaminants by this method.

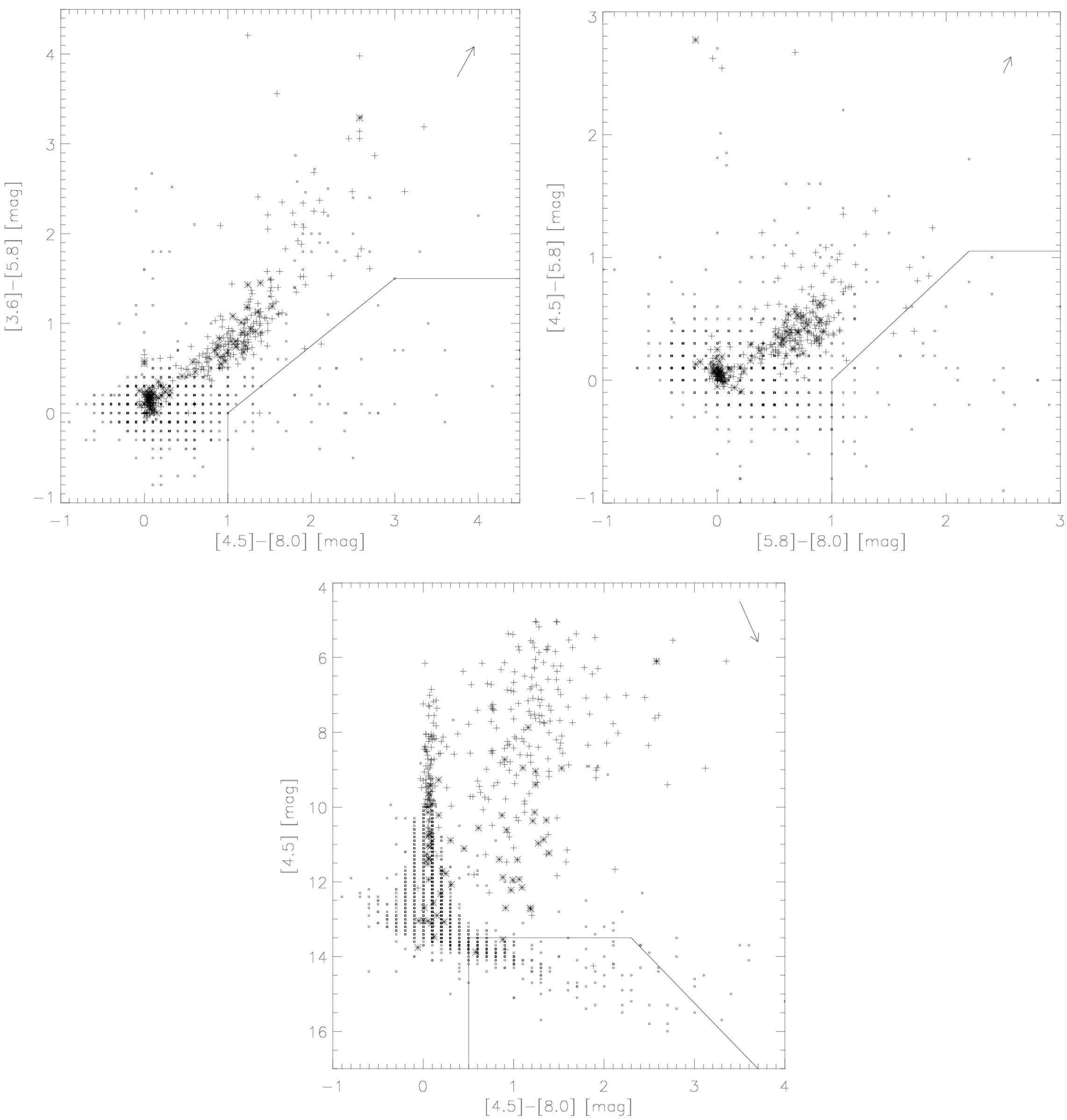

Figure 4.6: We show the [4.5] – [8.0] vs. [3.6] – [5.8] (top left) and the [5.8] – [8.0] vs. [4.5] – [5.8] (top right) CCD and the [4.5] – [8.0] vs. [4.5] (bottom) CMD. The applied cuts to exclude extragalactic sources are marked by the lines (see Gutermuth et al. 2008). A visual extinction of 20 *mag* is indicated by the arrow. Signs are like in Fig. 4.5.

4.1.2.2 Selection 2: MIR slope

Another selection criteria used in literature is the slope the four IRAC filters form in the SED. Its shape contains information about the warm dust surrounding the stars. Lada et al. (2006) describe limits to distinguish between
- stars with strong MIR excess from optically thick accretion disks,
- stars with a weaker excess indicative of evolved disks,
- stars with no measurable excess associated with a lack of disk material within 1 AU.

We calculate the slope of each star from a least-square fit to a power law of the four passbands via the following relations[2]:

$$\alpha_{IRAC} = dlog(\lambda F_\lambda)/dlog(\lambda)$$
$$F_\lambda = F_{0,\lambda} \cdot 10^{-0.4 \cdot m_{filter}}$$
$$(F_{0,[3.6]}, F_{0,[4.5]}, F_{0,[5.8]}, F_{0,[8.0]}) = (6.601, 2.731, 1.064, 0.3053) \cdot 10^{-11} W m^{-2} \mu m$$

We show the result in Fig. 4.7. The upper limit for sources without disk is $\alpha_{IRAC} = -2.56$ and the limit between thin and thick disks is $\alpha_{IRAC} = -1.8$. Due to the uncertain values of the IRAC photometry of our sample, we extend the limit of diskless stars down to -2.62. Applying this criteria, we are left with 712 of 2637 (27%) Taurus member candidates showing signs of accretion disks.

[2] zero points from the IRAC instrument handbook on http://irsa.ipac.caltech.edu/data/SPITZER/docs/irac/

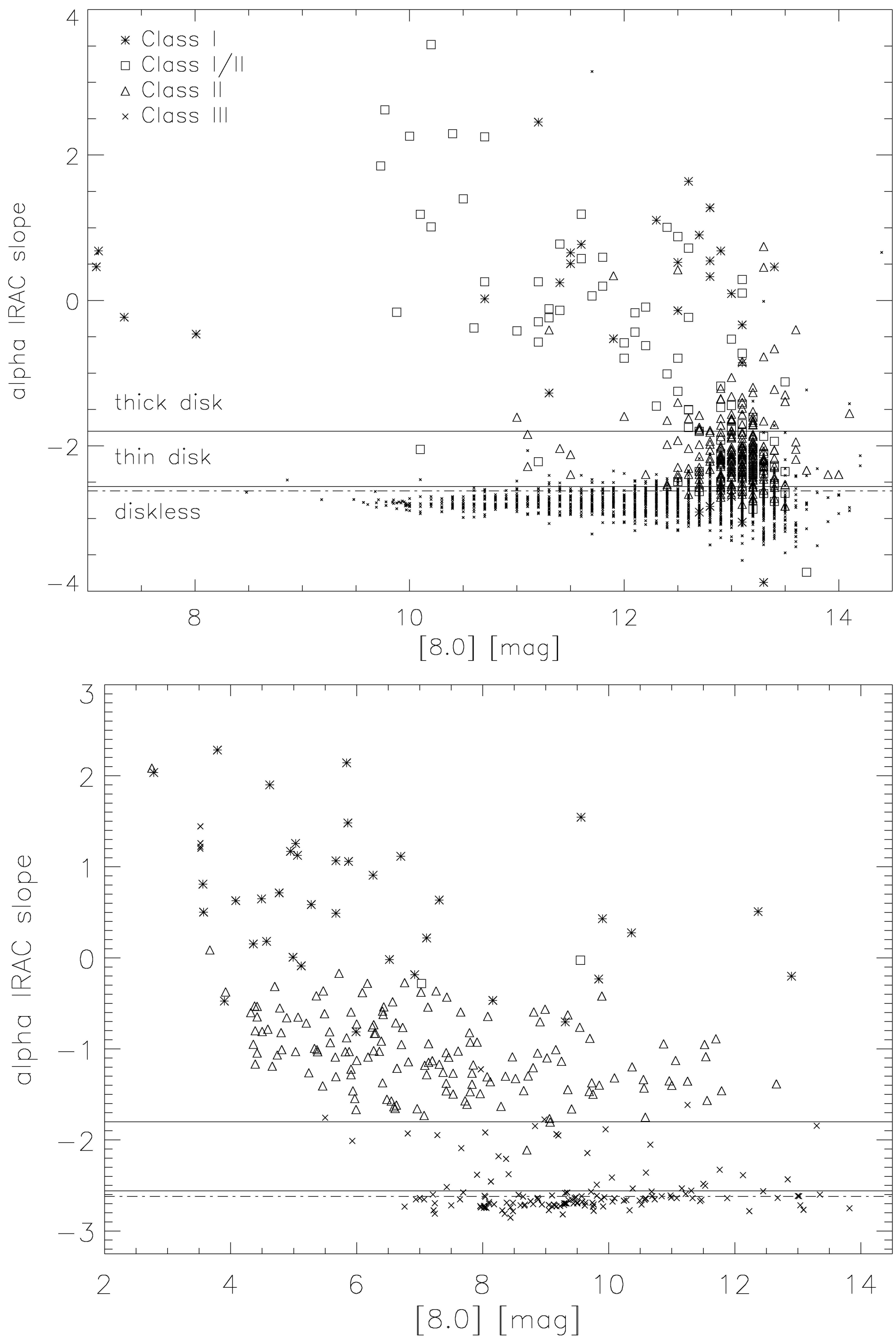

Figure 4.7: We show the [8.0] vs. α_{IRAC} diagram of the whole candidate sample showing IRAC and UKIDSS passband photometry (top) and of the already known Taurus members (bottom). We divide each data set into the different classes derived in this section. Especially the members fit very well into this division and get separated by the limits of Lada et al. (2006) marked by the full lines. We show the lower limit cut used to select sources by the dash-dotted line. The signs get explained in the image.

4.1.2.3 Additional criteria and final selection

To increase our success rate, we request a JHK detection in the 2MASS filters. We restrict the sample by $12.0 < J < 15.5$ *mag* in both UKIDSS GCS and 2MASS filter, due to the observational feasibility and the LMO magnitude limits (see Sec. 4.1.1). Errors in the UKIDSS filters are chosen to be < 0.01 *mag* and < 0.2 *mag* in the IRAC filters (Gutermuth et al. 2008). The candidates were also checked for the UKIDSS GCS J band images. As well, we constructed the SED of the sources including all available photometry of the 2MASS, UKIDSS GCS & IRAC surveys. We show those criteria for the 22 objects finally selected and observed in the appendix in Fig. B.11 and Fig. B.12. Those last procedures and the final selection were done with the help of M. Aberasturi Vega. Applying those last criteria, we are left with 644 of 712 sources (90%). We give an overview of this sample in Tab. 4.4. We show all the data available to each observed source in the appendix in Tab. B and Tab. B.6. An overview of the selection criteria is shown in Tab. B in the appendix.

column	B	V	R	Z	Y	J	H	K	J_M
unit	*mag*	*mag*	*mag*	*mag*	*mag*	*mag*	*mag*	*mag*	*mag*
lower limit	13.81	14.25	13.97	12.71	12.43	12.01	11.58	11.35	12.02
upper limit	21.85	17.97	19.7	16.77	16.12	15.44	14.91	14.65	15.44
column	H_M	K_M	[3.6]	[4.5]	[5.8]	[8.0]	$A_{V,YJK}$	$A_{V,JHK}$	
unit	*mag*	*mag*	*mag*	*mag*	*mag*	*mag*	*mag*	*mag*	
lower limit	11.53	11.32	11.1	11.1	9.6	10.9	0	0	
upper limit	14.85	14.55	15.1	14.0	14.1	13.5	2.01	1.65	

Table 4.4: Summary of 644 MIR excess Taurus candidates. Note that not every source shows data in all columns.

4.2 Search of new stellar clumps in Orion

The clustering of sources visible in the UKIDSS GCS data reflects the location of molecular clouds. This fact is used by the extinction map calculated by the star count method. There, the number of stars is proportional to the visual extinction. To find stellar associations clustered in the distance of a certain region we therefore have to correct for these effects. The σ Orionis Cluster is an example of an association which is not connected to a molecular cloud, since the central bright star has blown the gas away. It is located in the part of the Orion SF region covered by the UKIDSS GCS. Lodieu et al. (2009) described this data and found 287 member candidates. We cross-correlate them with our UKIDSS GCS data set and find 281 counterparts. The 6 missing sources were not selected by us due to the completeness limit of the survey in the region. We follow the procedures done in the previous chapters and search for new member candidates in various CMD and CCD. We define cuts in the diagrams, so that the 281 σ Orionis member candidates get selected. By using the dereddened photometry, the influence of the extinction gets diminished. Thereby, the clustering in the Orion distance becomes visible. Lodieu et al. (2009) found their candidates with the following limits:

$$J < 12\ mag$$
$$J - K > 0.75\ mag$$
$$J < 5.33 \cdot (J - K) + 12.00\ mag$$
$$Z < 7.50 \cdot (Z - J) + 7.50\ mag$$
$$Z < 5.56 \cdot (Z - J) + 9.83\ mag$$
$$Y < 19.92 \cdot (Y - J) + 4.03\ mag$$

$$Y < 7.78 \cdot (Y - J) + 11.94 \; mag$$

We modify those criteria, add the ones we found for the $J-H$ vs. J ad $H-K$ vs. H diagrams and define new ones for the dereddened values (marked with 'd', see Fig. B.13 and Fig. B.14 in the appendix):

$$J - K > 0.80 \; mag$$
$$J < 5.83 \cdot (J-K) + 10.83 \; mag, \qquad J_d < 15.00 \cdot (J_d - K_d) + 4.00 \; mag$$
$$J - H > 0.45 \; mag, \qquad J_d - H_d > 0.40 \; mag$$
$$J < 14.00 \cdot (J-H) + 9.20 \; mag, \qquad J_d < 20.00 \cdot (J_d - H_d) + 8.00 \; mag$$
$$H - K > 0.25 \; mag, \qquad H_d < 50.00 \cdot (H_d - K_d) + 1.00 \; mag$$
$$H < 14.00 \cdot (H-K) + 9.50 \; mag, \qquad H_d < 15.00 \cdot (H_d - K_d) + 11.50 \; mag$$
$$Z < 7.00 \cdot (Z-J) + 7.80 \; mag, \qquad Z_d < 5.00 \cdot (Z_d - J_d) + 12.00 \; mag$$
$$Y < 15.00 \cdot (Y-J) + 6.00 \; mag, \qquad Y_d < 13.33 \cdot (Y_d - J_d) + 9.33 \; mag$$
$$Y < 8.33 \cdot (Y-J) + 10.67 \; mag$$

By this procedure, we select 3941 of 186930 sources (2%). We recover only 197 member candidates of the σ Orionis Cluster described by N. Lodieu. On the other hand, we find 96 additional member candidates located in less than 30 *arcmin* distance of its central star (293 in total). Most of the sources selected by us show $J > 18$ *mag*. Only 1028 of 3941 sources and 203 of 293 σ Orionis Cluster member candidates are brighter. We use those data sets to identify the stellar clumps in the region (see Fig. 4.8). An overview of the selection criteria is shown in Tab. B in the appendix.

We identify three clusters in our data which are not connected to the residuals from the A or B cloud of Orion. We recover the σ Orionis Cluster, containing 203 sources (in 30 *arcmin* distance of the central star). We find the NGC 1981 cluster at $(RA, Dec) = (83.7875, -4.4317)$ *deg* (e.g. Wu et al. 2009, Maia et al. 2010) containing 76 sources. But most importantly, we find a new clump in the northwestern part of the area around $(RA, Dec) = (83.2, -2.25)$ *deg* containing 55 sources. By a SIMBAD search, we find the remnant molecular cloud (visible because they reflect light from B stars) [OS98]24 (Ogura et al. 1998) in this region, located at $(RA, Dec) = (5h : 32m : 31s, -2^{\odot} : 10.1') = (83.129, -2.168)$ *deg*. In the following chapters, we describe the observations of 7 members of this clump and investigate the identified three clusters in detail (see Chap. 6.6). We show the UKIDSS GCS DR5 J band images of the 7 objects in Fig. B.15 and the available data in Tab. B in the appendix.

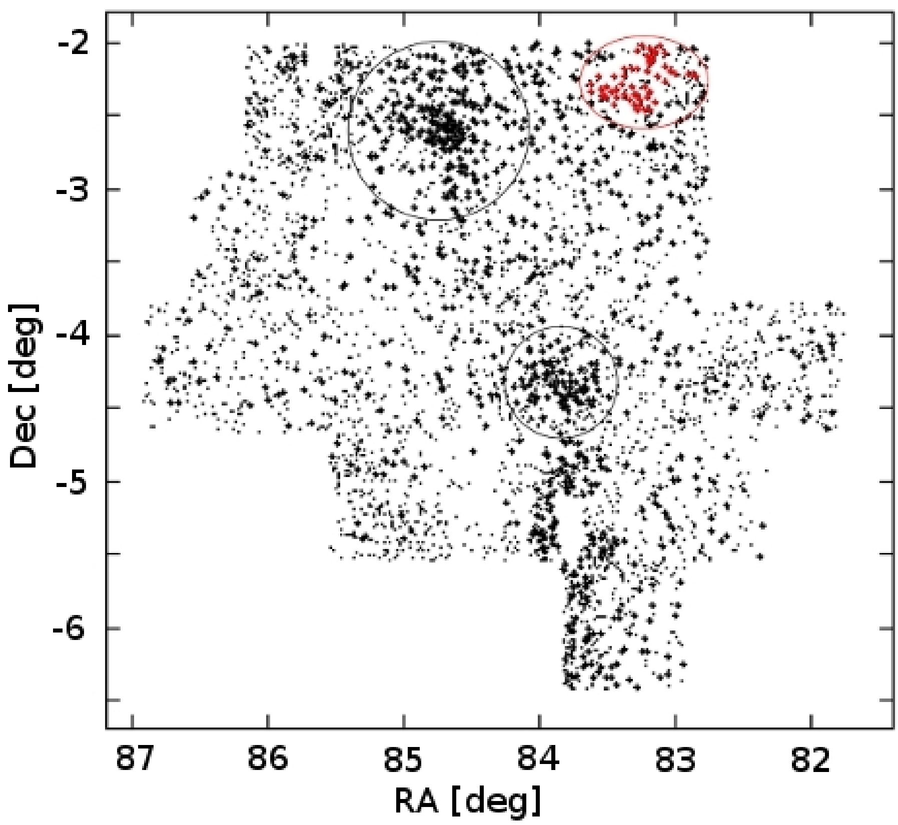

Figure 4.8: We show the unbiased clustering in the Orion region covered by the UKIDSS GCS. We show all 3941 sources selected by our photometric criteria (small black dots) and highlight the 1028 objects with $J < 18$ *mag* (black plus signs). We identify the σ Orionis Cluster (large black circle) containing 203 bright sources, and the NGC 1981 cluster (small black circle) with 76 bright sources. In the northwestern part, we find a new star cluster containing 55 bright members. Around the ONC in the southwest and around Orion B cloud in the northeast we see residuals of the dereddening process.

Chapter 5

Observations

5.1 Telescopes and instruments

Spectroscopic observations were made to verify the membership of our candidates. We used telescopes of the Observatorio del Roque de los Muchachos on the Canary Island of La Palma:

- the Gran Telescopio Canarias (GTC) is a reflector telescope run by the Instituto de Astrofísica de Canarias (IAC). With its 10.4 *m* mirror it is one of the largest Earth-based optical telescope. We used the Optical System for Imaging and low Resolution Integrated Spectroscopy (OSIRIS, Cepa et al. 2000) mounted at its Nasmyth-B focus.
- the William Herschel Telescope (WHT) is part of the Isaac Newton Group of Telescopes (ING). The Intermediate dispersion Spectrograph and Imaging System (ISIS), mounted at its Cassegrain focus was used.
- the Nordic Optical Telescope (NOT) with its Andalucia Faint Object Spectrograph and Camera (ALFOSC) obtained more data. The instrument is owned by the Instituto de Astrofísica de Andalucia (IAA) and is operated jointly under agreement between the IAA and the NBIfAFG of the Astronomical Observatory of Copenhagen by Denmark, Finland, Iceland, Norway, and Sweden.

The most data come from various runs obtained from 2005 to 2009 at the Centro Astronómico Hispano Alemán (CAHA). There, we used both telescopes of the Calar Alto Astronomical Observatory near Almeria, Spain, which are operated jointly by the Max Planck Institut für Astronomie (MPIA) and the Instituto de Astrofísica de Andalucía (CSIC).

- we obtained spectra with the Cassegrain TWIN Spectrograph, mounted at the Cassegrain focus of the 3.5 *m* telescope
- we used the imager and spectrograph Calar Alto Faint Object Spectrograph (CAFOS) at the 2.2 *m* telescope
- a few supplemental spectra were observed in the NIR with the 3 *m* Shane reflector telescope at LICK observatory, Mt. Hamilton, California. There, at the Cassegrain focus, we used the Gemini Twin-Arrays Infrared Camera.

For further details on the various telescopes, instruments, observational runs and their outcome, see Tab. 5.1.

telescope	instrument	type	configuration	RON $[e]$	gain $[e/ADU]$	disp. $[\AA/pix]$	Slit $['']$	date date	λ $[\mu m]$	res.	objects	STD	comment
GTC	OSIRIS	opt. spec.	R300R	3.5	1.18	7.05/7.91	1.0	6-12.2009-8.1.2010	var.	var.	4 faint LMO	var.	dark problems
NOT	ALFOSC	opt. spec.	grism5	5.3	0.736	3.17	1.0	19.12.2009	0.50-0.90	2400	8 bright LMO 7 Orion	J0948...	-
CAHA2.2	CAFOS	opt. spec.	grism10, R200	5.06	20.0	4.28	1.0	10.-11.11.2009	0.62-1.02	1800	31 bright LMO 11 MIR excess 4 Taurus mem. 1 field dwarf	J2319...	PI: M. Aberasturi Vega
WHT	ISIS	opt. spec.	R600R, GG495	5.0	1.16	4.5	1.0	31.10.-1.11.2009	0.58-0.72	1700	11 MIR excess	J0404...	PI: H.Bouy
NOT	ALFOSC	opt. spec.	grism5	5.3	0.736	3.14	1.0	24.08.2009	0.51-1.00	2400	4 bright LMO	J2211...	service time
WHT	ISIS	opt. spec.	R158R, GG495	5.06	1.16	3.62	1.0	23.12.2008	0.48-1.05	2100	2 bright LMO 1 Taurus mem.	J0235...	-
LICK	GEMINI	NIR spec.	-	-	-	-	-	8.11.2008	1.08-2.45	-	4 bright LMO	J0441...	PI: H.Bouy, reduced
CAHA2.2	CAFOS	opt. spec.	grism10, R200	5.06	20.0	4.4	1.3	30.11.-4.12.2007	0.62-1.04	1700	27 Taurus mem. 18 field dwarfs	-	PI: D.Barrado, reduced
CAHA3.5	TWIN	opt. spec.	T11 grating	3.825	50.0	10.7	1.5	22.11.2006	0.57-0.99	700	2 bright LMO	-	PI: D.Barrado, reduced
CAHA3.5	TWIN	opt. spec.	T11 grating	3.825	50.0	10.7	1.5	22.-24.11.2005	0.56-1.04	700	3 bright LMO 12 field dwarfs	-	PI: D.Barrado, reduced

Table 5.1: Data of the various telescopes and instruments used for this work. They are sorted by their observational date. Note, that unsuccessful runs and rejected proposals are not listed. The names of the standard stars (STD) are shortened.

5.2 Remarks on the observations

For the proposals of optical spectroscopy we used the relation $I = 1.4 \cdot J - 3.8$ *mag* described by the evolutionary model data for LMO. This was done to estimate the I band magnitude of the objects and thereby the feasibility of their spectroscopic observation. We tried to achieve minimum signal-to-noise ratios of 20. All observations of the different years took place in the months from September to March, since both Taurus and Orion are located in that direction.

All together, we observed 144 objects with 148 optical low-resolution spectra and 4 additional NIR spectra in JHK filters. Of those, 32 spectra of 31 field dwarfs and 37 spectra of 37 already known Taurus members were observed as comparison. We obtained 22 spectra of 22 MIR excess candidates for the search in Taurus and 7 spectra of 7 candidates for the search in Orion. Most importantly, 50 spectra were obtained from 47 candidates for the search for LMO via the UKIDSS GCS photometry. We give the various observational logs in detail in the appendix from Tab. C.2 to Tab. C.9.

Besides the candidates and the already known Taurus members, we observed for comparison some field dwarfs. We show their data in Tab. C.1 in the appendix. One of them is the $M3.5$ type TTS 2MASSJ04391586+3032074, which is located in the region covered by the UKIDSS GCS DR8. We show this additional data in Tab. 5.2 and its UKIDSS J band image in Fig. 5.1.

$RA = 69.816090\ deg$			
$Dec = 30.535347\ deg$	$H_U = 12.104\ mag$	$[5.8] = 11.400\ mag$	$\mu_{\alpha,U} = -4.974 mas/yr$
$Z_U = 13.566\ mag$	$K_U = 11.805\ mag$	$[8.0] = 11.400\ mag$	$\mu_{\delta,U} = -30.782 mas/yr$
$Y_U = 13.196\ mag$	$[3.6] = 11.500\ mag$	$A_{V,YJK} = 1.229\ mag$	$\mu_{\alpha,N} = 6.000 mas/yr$
$J_U = 12.652\ mag$	$[4.5] = 11.500\ mag$	$A_{V,JHK} = 1.059\ mag$	$\mu_{\delta,N} = -34.000 mas/yr$

Table 5.2: UKIDSS GCS DR8 data of the $M3.5$ type field TTS 2MASSJ04391586+3032074

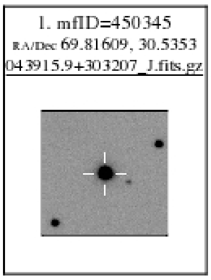

Figure 5.1: UKIDSS GCS DR8 image of the $M3.5$ type field TTS 2MASSJ04391586+3032074

5.3 Data reduction

For the reduction of all kinds of observed spectra, we used the Image Reduction and Analysis Facility (IRAF)[1]. We explain in the following the techniques used to reduce the spectra obtained

[1] written and supported by the IRAF programming group at the National Optical Astronomy Observatories (NOAO) in Tucson, Arizona. NOAO is operated by the Association of Universities for Research in Astronomy (AURA), Inc. under cooperative agreement with the National Science Foundation

in the optical and in the NIR wavelengths. For all observations we observed standard stars for instrumental response and flux corrections and to correct for telluric absorption lines. We show their data in Tab. C.10 in the appendix, where we also show their fully reduced spectra in Fig. C.1. The one used in the NIR observations is shown in Fig. 6.10 in Chap. 7.

5.3.1 Optical spectra

For the reduction of the optical spectra we used standard procedures. We observed calibration images such as bias frames (output of the CCD without light exposure), flat field frames (instrumental response to a uniform light exposure of the CCD) and calibration lamp images. Each set of those calibration images were combined by the IRAF *imcombine* task to form a master bias-, flat field-, and calibration lamp image using both gain and read-out-noise (RON) of each observation. The task forms the median flux on every pixel on the images. We show examples of those master frames in Fig. 5.2.

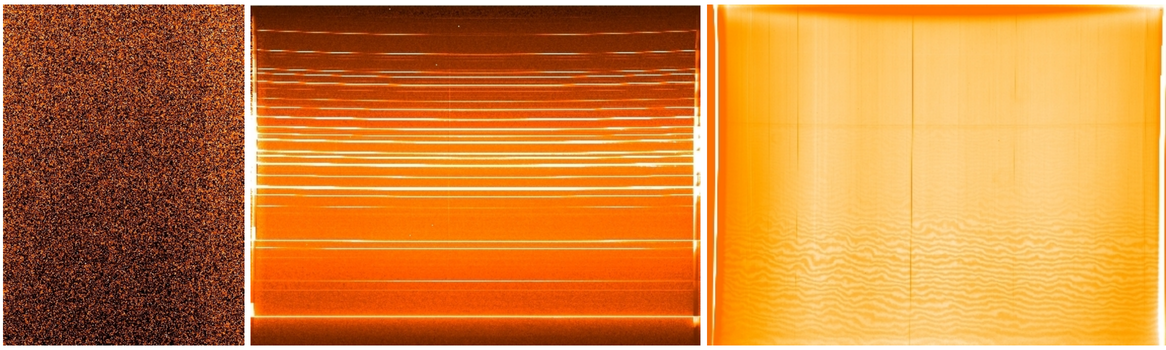

Figure 5.2: A master bias (left) and calibration lamp (middle) frame from the optical data reduction. On the right side, a normalized master flat field is shown. The images come from the CAHA/CAFOS observations conducted in November 2009 in the wavelength range from 0.62 to 1.02 μm with a resolution of 1800.

All images include the instrumental output of the CCD. By subtracting the master bias frame from all images we correct for this effect. After trimming and cutting them, we fitted a high order function alongside the dispersion axis of the master flat field by the *response* task. After correcting the flat field for that function and normalizing it, we divided each image by that calibration frame. Thereby, we correct for the different response of the pixels of the CCD to light exposure. The next step was to extract each spectra by the *apsum* task, where again the RON and the gain of the observations were necessary as input. This was done also for the master calibration lamp frame. The task sums up the fluxes of the different pixels of each column alongside the wavelength axis. The three-dimensional image gets transformed to a two-dimensional spectra. Using an optical line list given by IRAF, we identified the different emission lines in the calibration lamp image with the *identify* task. Thereby, we calibrate the dispersion axis and convert the pixel scale of the images into wavelengths. The science spectra were then corrected with this calibration with the *refspec* and *dispcor* tasks. For the correction of the instrumental response and the calibration of the flux, we observed standard stars of early type of the IRAF database. With the *standard* and *sensfunc* tasks, we determined the relation between the observed flux in counts and the standard star flux of the IRAF database in W/m^2 in small wavelength intervals. Then, the *calibrate* task translated this calibration to each science spectra. The final spectra were trimmed for display purposes and normalized at 7500 $\AA$ as usual in literature. We show them after the analysis in Fig. D.1 to Fig. D.12 in the appendix.

The data of the GTC/OSIRIS run were difficult to reduce. This is due to the dark current problems the instrument had at its first semester of observation. Nevertheless, we show all the spectra we were able to reduce. Problematic were as well the spectra observed with the WHT/ISIS instrument in November/December 2009. The standard star shows a very unusual spectra and the reduced data is not of great reliability. Note as well, that the optical spectra of the observations done before December 2008 were given to us already fully reduced by the PI D. Barrado.

5.3.2 Near-infrared spectra

The data were delivered to us by H. Bouy already fully reduced up to the standard star calibration. We received the spectra of four sources in the three passbands JHK of the Lick/Gemini instrument. As standard star the $A0$ type 2MASSJ04412412+4818033 was used. In contrast to the optical light, the infrared light of stellar objects reaches Earth only in some clearly defined wavelength intervals. Also, the spectra observed are full of telluric lines resulting from the absorption of the light in the atmosphere. The standard star observation is used to correct for those effects. This is done by dividing the science spectra by the standard star spectra. Then it gets multiplied by the blackbody radiation of same temperature (in our case $T = 9500\ K$) with the IRAF task *imarith*. Thereby, only the influence of the telluric lines gets eliminated. After combining the spectra of the three filters, we normalize the flux at 1.6 μm. We describe the calculations with

$$F = (F_{science} \cdot F_{blackbody})/(F_{standard} \cdot F_{1.6\mu m})$$
$$F_{blackbody} \approx \lambda^{-5} \cdot (exp[hc/\lambda kT] - 1)^{-1}$$

We show the final spectra in Fig. 6.10 in Chap. 7.

Chapter 6

Analysis

6.1 Spectral types from optical spectra

In this section, we derive the spectral types of the sources observed with optical spectroscopy. The light emitted by a stellar object depends on its effective temperature T_{eff} and on its chemical composition. The first defines the large-scale structure and overall slope of the spectrum connected theoretically with the blackbody radiation described in Planck's law, where

$$F_\lambda \propto \lambda^{-5} \cdot [exp(\frac{hc}{\lambda kT}) - 1]^{-1}.$$

The wavelength of the maximum output is defined by Wien's displacement law via $\lambda_{max} = 2898.8$ $T_{eff}^{-1} \mu mK$. A maximum output at the wavelengths covered by our spectroscopic observations of $(0.5/0.75/1.0)$ μm is expected for stars with $T_{eff} = (5800/3900/2900)$ K. A flat spectra in those wavelengths should therefore compare theoretically to spectral types of $(G2-G8/K9-M0/M5.5-M6.5)$ (scales by Ammler et al. 2005, Luhman et al. 2003a). Since our search was done for LMO of M type or later, we expect most of the observed objects to have significant more flux at the longer observed wavelengths.

On the other hand, the chemical composition is responsible for structures of smaller scale such as lines (narrow) and bands (extended) of absorption and emission features. The LMO we were searching for show numerous neutral metal lines, such as CaI, FeI, NaI, or KI. And they show very prominent molecular bands such as TiO or VO beginning its influence in mid-M type stars. These facts are the reason to observe our candidates in the optical wavelengths, where those bands influence most. The shape and form of them help to define the spectral type of the observed stars using various techniques.

6.1.1 Relative comparison

We visually sort all observed spectra by comparing them to our reference spectra (see Sec. 2.5) and to each other. Considering also the literature types of the observed already known Taurus members and field dwarfs, we find three distinct groups (e.g. Comerón et al. 2010, see Fig. 6.1):

- for the hotter stars up to the late K stars the slope of the spectra is the only criteria to distinguish them in our observations. They point downwards (for longer wavelengths) for the G type stars, get flatter and finally begin to point upwards at about the transition from K to M stars. For the later K type stars, the influence of the TiO absorption bands from 6550 to 6850 and from 7050 to 7300 $Å$ increase. They begin to form a little characteristic bump from 6850 to 7200 $Å$. Beyond 7400 $Å$ the described types are flat and do not show any larger features.

- the late K to early M type stars show increasing absorption in the described wavelength bands. But here, the TiO and VO absorption bands from 7600 to 7850 $Å$ and from 7850 to 8000 $Å$ increase their influences, respectively. The slope from 7200 to 7500 $Å$ is getting steeper but remains a straight linear line.
- in the spectra of early- to late M type the described absorption bands increase their influence. But we identify discontinuities in their slopes at 7350 (beginning at around type $M3.5$) and 8000 (beginning at type $M3.5$ to $M3.75$) $Å$. There, the VO absorption bands begin to dominate the spectral shape and depress the continuum flux level. The observed $M8$ field dwarfs then, show already a very steep upward pointed Planck slope in the observed wavelength range.

We notice that in many cases the already known Taurus members do distinguish themselves from the field dwarfs in the emission of various spectral lines. When comparing them to our reference spectra, many show an inclination of the slope. This is due to the wavelength dependent extinction resulting from the gas and dust located in the line-of-sight towards the sources. The effect gets larger for shorter wavelengths in the optical and NIR. This translates to a steeper slope of the spectra for reddened sources. For the sorting process and the determination of the spectral type, we correct for this effect (Fig. 6.2). The flux F of an object at a wavelength λ is

$$log(F_\lambda) = -\frac{1}{2.5} \cdot (M_\lambda + A_\lambda - ZP_\lambda)$$

Considering the extinction law derived in Sec.3, a reddened observed flux can therefore be dereddened by

$$F_{\lambda,dered} = F_{\lambda,ext} \cdot 10^{A_\lambda/2.5}, \text{ with}$$
$$log\frac{A_\lambda}{A_V} = -1.6002 \cdot log(\lambda) - 0.4095$$

A minimal extinction of 0.1 mag was considered. We show all sorted spectra from Fig. D.1 to Fig. D.12 in the appendix. We assign spectral types only for the spectra which resemble the reference ones beginning with type $M0.5$. The derived types and used visual extinctions are shown in the appendix in Tab. D. A summary of the number of spectra showing types and extinction values is shown in Tab. 6.1.

sample	LMO bright	LMO faint	Taurus members	field dwarfs	MIR	Orion
# all spectra	45	5	37	32	22	7
# $< M0.5$ type	16	-	12	17	22	-
# $> M0.5$ type	29	-	25	15	-	7
# $A_V > 0$ mag	29	-	18	14	-	2
A_V range [mag]	1.0 - 4.0	-	0.2 - 6.3	0.2 - 3.0	-	0.2 - 0.3

Table 6.1: Summary of the type sorting process of the observed optical spectra

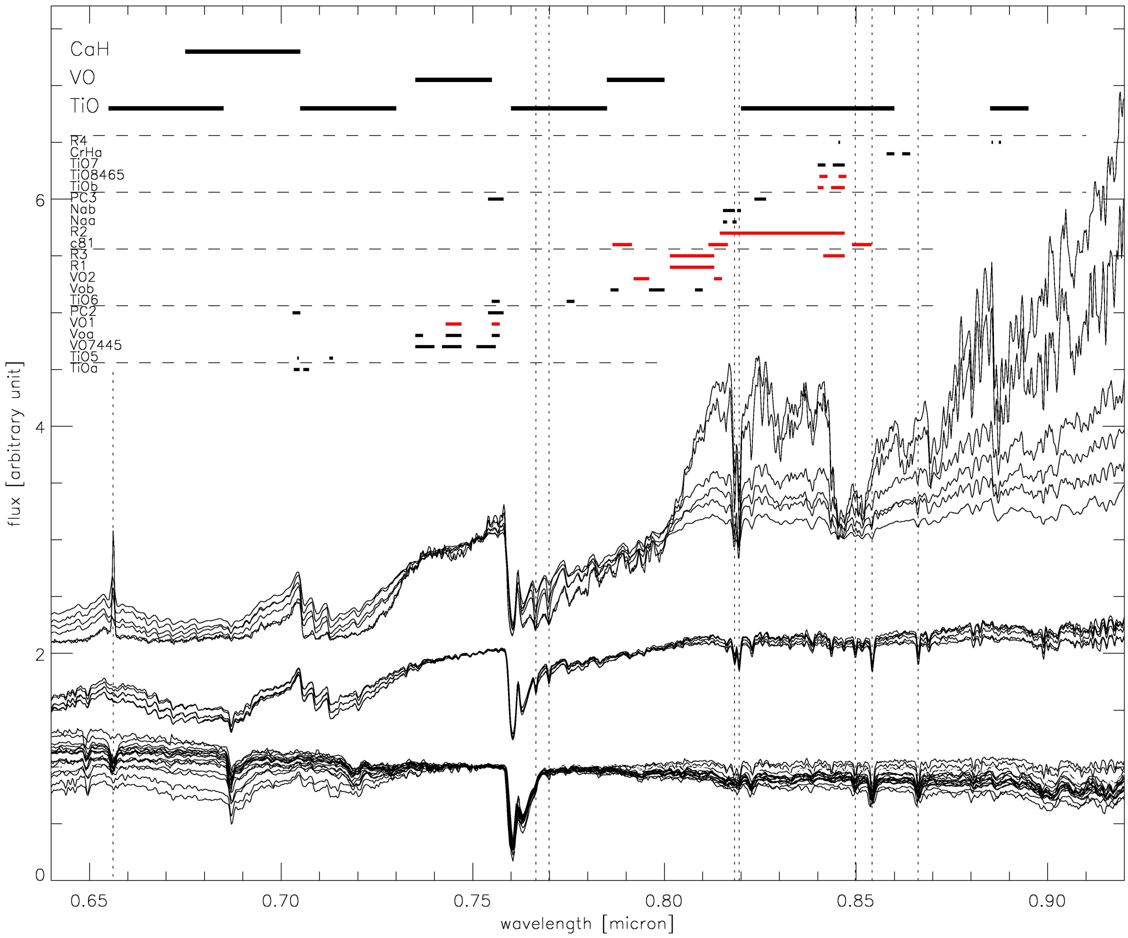

Figure 6.1: An illustration of the sorting criteria applied to our optical observations using 29 observed field dwarf spectra. They should show only small if any extinction compared to the Taurus members. There are 6, 6, and 17 objects in the lower (earlier types to late *K* types), middle (late *K* to early *M* types), and upper (early to late *M* types) group, respectively. They get explained in the text. In the upper part of the image, the location of the main absorption bands of *TiO* and *VO*, and the various spectral indices are marked (dashed lines for display purposes only). The ones marked red get used in Sec. 6.1.2 to define the spectral types of the objects. We show all spectra in the wavelength range from 0.64 to 0.92 μm, since all objects are observed in this range, and the important features of *M* type stars are located there. We indicate the location of the $H\alpha$ (6563 $\AA$) line, the *KI* (7665 & 7699 $\AA$) and *NaI* (8183 & 8195 $\AA$) doublets and the *CaII* infrared triplet (8498, 8542 & 8662 $\AA$) by vertical dashed lines. All spectra are normalized at 7500 $\AA$ and shifted along the ordinate if necessary.

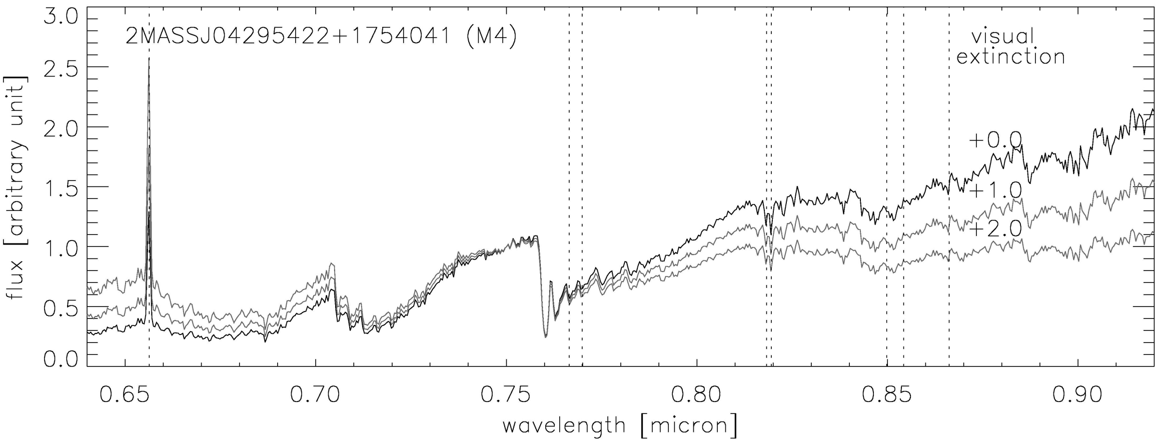

Figure 6.2: An illustration of the dereddening process. We show the Taurus member 2MASS J04295422+1754041 (Luhman et al. 2010) of literature type $M4$ as observed (top, +0.0) and dereddened by visual extinctions of $+1.0$ and $+2.0$ *mag* as indicated. The spectra are normalized at 7500 $\AA$. Note, that the $H\alpha$ emission line at 6563 $\AA$ is quite strong with this object ($EW(H\alpha) = -25.08\,\AA$). The wavelengths of the KI and NaI doublets, and the $CaII$ triplet are marked from left to right by the dashed vertical lines.

6.1.2 Spectral indices

A technique to calculate spectral types is delivered by the spectral indices. We use the ones described in the literature by Martín et al. (1999) and Riddick et al. (2007). They all compare the flux of two or more wavelength intervals of the optical spectra. Thereby, they measure the influence of various absorption bands. The values strongly depend on the extinction, growing with larger wavelength separation of the two intervals. But we are interested in finding the values independently of the visual comparison done in the previous chapter. Therefore, we do not consider the extinction values found there. The smaller the wavelength intervals, the more uncertainty is included to the indices due to the the resolution and the signal-to-noise ratio of the spectra. Only stars of type M or later get affected by the VO and TiO absorption bands. That is why most of the indices get important for types later than $M2$ to $M3$. Nevertheless, we considered all indices with a given type-index relation in the mentioned publications (Tab. 6.2).

name	Range of validity	Numerator [Å]	Denominator [Å]	spectral type index relation
TiO6	M0-M8	7550-7570	7745-7765	type $=60.91754+14.578\cdot(x-1.108)-27.808\cdot(x-1.108)^2+26.199\cdot(x-1.108)^3-7.9521\cdot(x-1.108)^4$
PC2	M2-M8	7540-7580	7030-7050	type $=60.95891+8.7890\cdot(x-1.156)-6.0903\cdot(x-1.156)^2+1.8529\cdot(x-1.156)^3$
TiO7	M2-M8	8440-8470	8400-8420	type $=62.2993-27.642\cdot(x-0.941)-94.586\cdot(x-0.941)^2-140.74\cdot(x-0.941)^3$
R1	M2.5-M8	8025-8130	8015-8025	type $=62.8078+21.085\cdot(x-1.044)-53.025\cdot(x-1.044)^2+60.755\cdot(x-1.044)^3$
R3	M2.5-M8	(8025-8130)+(8415-8460)	(8015-8025)+(8460-8470)	type$=62.8379+19.708\cdot(x-1.035)-47.679\cdot(x-1.035)^2+52.531\cdot(x-1.035)^3$
c81	M2.5-M8	8115-8165	(7865-7915)+(8490-8540)	type $=62.4331+8.0558\cdot(x-1.036)-6.8171\cdot(x-1.036)^2+3.0567\cdot(x-1.036)^3$
R2	M3-M8	8145-8460	8460-8470	type $=62.9091+10.503\cdot(x-1.035)-14.105\cdot(x-1.035)^2+8.5121\cdot(x-1.035)^3$
TiO8465	M3-M8	8405-8425	8455-8475	type $=63.2147+8.7311\cdot(x-1.085)-10.142\cdot(x-1.085)^2+5.6765\cdot(x-1.085)^3$
TiO-b	M3-M8	8400-8415	8435-8470	type $=62.9069+13.841\cdot(x-1.067)-23.646\cdot(x-1.067)^2+17.787\cdot(x-1.067)^3$
VO-b	M3-M8	(7860-7880)+(8080-8100)	7960-8000	type $=63.4875+29.469\cdot(x-1.017)-156.53\cdot(x-1.017)^2+394.28\cdot(x-1.017)^3-325.44\cdot(x-1.017)^4$
VO1	M0-M8	7430-7470	7550-7570	type $=61.0285-52.770\cdot(x-0.961)-205.48\cdot(x-0.961)^2-349.44\cdot(x-0.961)^3$
R4	M3-M8	8854-8857	(8454-8458)+(8873-8878)	type $=62.7907+11.124\cdot(x-1.065)-14.937\cdot(x-1.065)^2+10.609\cdot(x-1.065)^3$
TiO5	M3-M8	7126-7135	7042-7046	type $=60.47587-14.907\cdot(x-0.862)-28.702\cdot(x-0.862)^2-37.843\cdot(x-0.862)^3$
TiO-a	M3-M8	7033-7048	7058-7073	type $=61.0810+9.8651\cdot(x-1.05)-4.9939\cdot(x-1.05)^2+1.4823\cdot(x-1.05)^3$
VO2	M3-M8	7920-7960	8130-8150	type $=62.6102-7.9389\cdot(x-0.963)-8.3231\cdot(x-0.963)^2-14.660\cdot(x-0.963)^3$
PC3	M3-M8	8235-8265	7540-7580	type $=62.0395+24.61\cdot(x-0.956)-50.292\cdot(x-0.956)^2+39.489\cdot(x-0.956)^3$
CrH-a	M3-M8	8580-8600	8621-8641	type $=61.4801-46.29\cdot(x-1)-37.824\cdot(x-1)^2$
VO-a	M5-M8	(7350-7370)+(7550-7570)	7430-7470	type $=65.0705+11.226\cdot(x-0.982)+6.7099\cdot(x-0.982)^2$
VO7445	M5-M8	0.5625(7350-7400)+0.4375(7510-7560)	7420-7470	type $=65.0881+17.121\cdot(x-0.982)+13.078\cdot(x-0.982)^2$

Table 6.2: The relations between spectral indices and spectral types as described by Riddick et al. (2007). The x in the formula is the value of the spectral index. They are sorted by the range of validity and divided by their usefulness determined in this section. The upper part was used to calculate types, whereas the indices in the lower part were rejected.

We compare the behavior of the spectral types derived by the visual comparison to those relations in Fig. 6.3 (used in this work) and in the appendix in Fig. D.13 (rejected by this work). Since no candidate is of type later than $M5$ we did not include the indices VOa and $VO7445$ in the calculations of the spectral type due to their range of validity. The scatter of the data is too large for the indices $CrHa$, $PC3$, $R4$, & $VO1$ and the relations do not seem to be very accurate for our data with the $PC3$, $VO2$, $TiO5$, $TiOa$ & $R4$ indices. We use all the other indices to calculate the spectral types. In Fig. 6.1 we can see, that the indices used in this work cover the whole range of the observed wavelength range. They include the VO and TiO absorption bands in wavelengths longer than 0.76 μm. We show all values derived in this section for the objects comparable to our reference spectra in Tab.D in the appendix. The types calculated from the indices are only shown, if they match the validity range given by the authors.

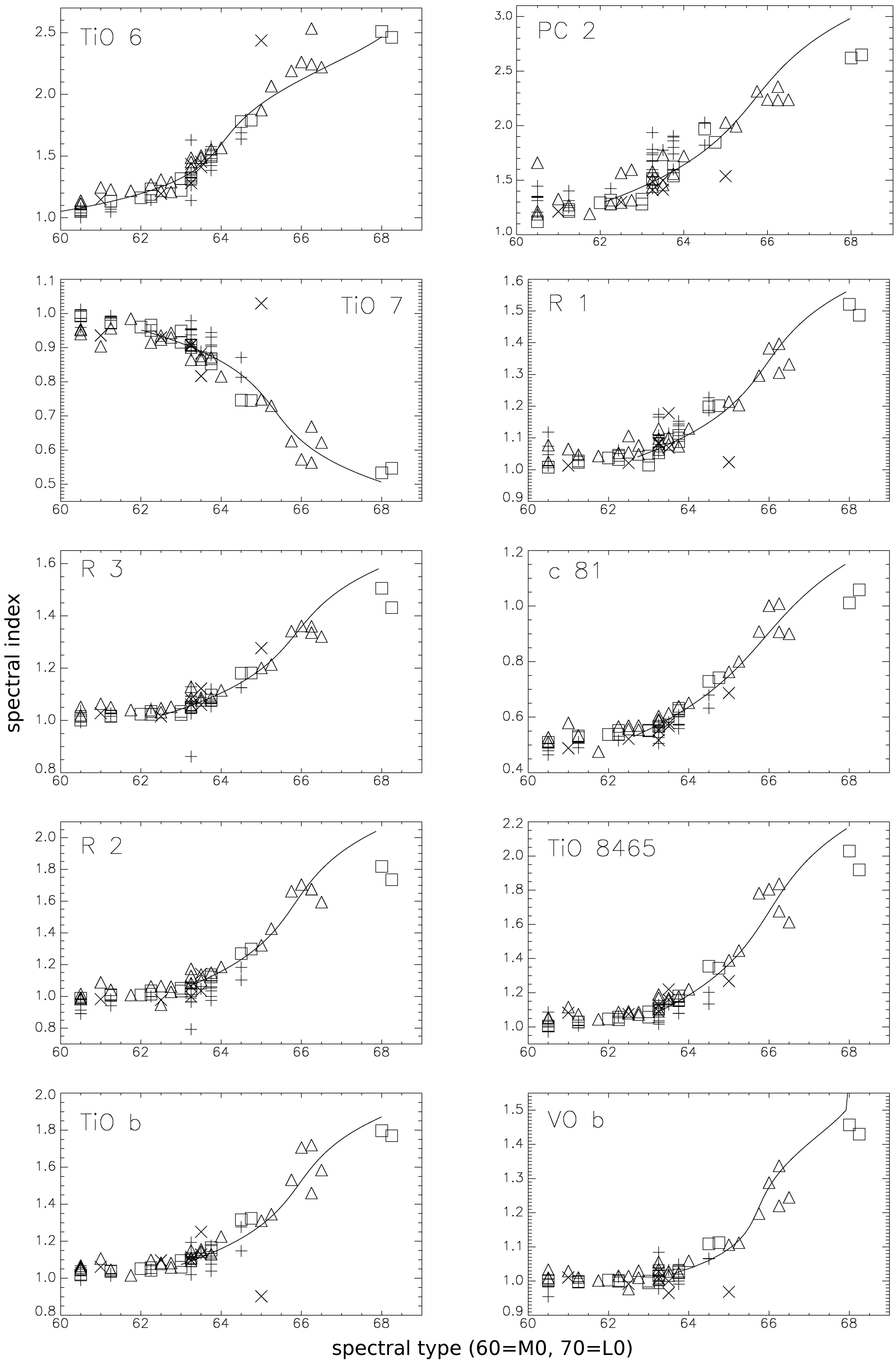

Figure 6.3: The spectral indices used to calculate spectral types. We show the indices calculated for the Taurus members (triangle) and field dwarfs (square). Also we show the ones for Taurus (plus) and Orion (cross) member candidates for which we derived a spectral type in the previous chapter. The relation of the indices and the types described by Riddick et al. (2007) are illustrated as a full line drawn only in their respective validity range. As already explained, the spectral types *G*0, *K*0, *M*0 get translated throughout this work with the numbers 50, 60, 70.

6.1.3 Remarks on the spectral typing

We compare differences of spectral types to the visual extinction estimated by the visual comparison of the spectra. We found *PC*2 and *R*1 very dependent on those values (Fig. 6.4). At least for the first one this is due to the larger wavelength separation of the two used intervals. The adopted spectral types from the visual comparison match in general very well with the ones calculated by the indices. Also, we find good internal consistency in the spectral types derived from the indices. The most uncertain values are the types found in literature (Fig. 6.4).

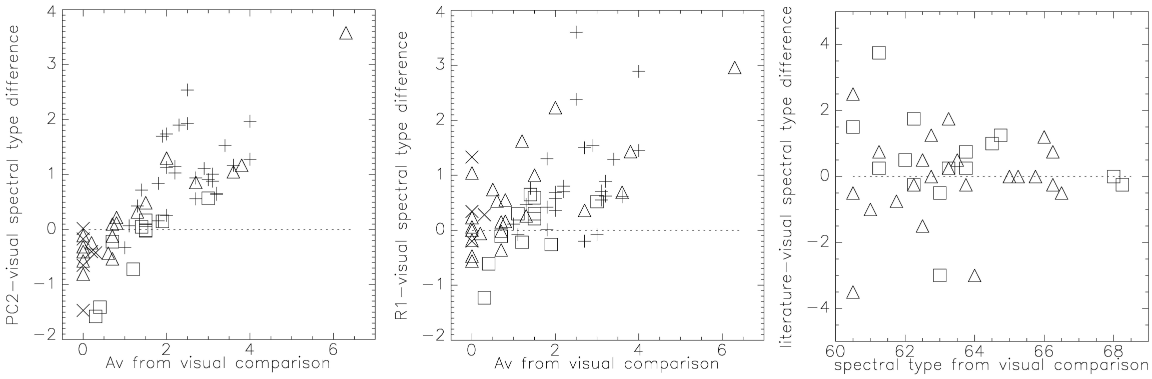

Figure 6.4: We compare differences of derived spectral types to the visual extinction (left & middle) and to the spectral types derived by the visual comparison (right). We compare the differences of the types derived by the visual comparison and the *PC*2 index (left), the *R*1 index (middle) and the literature values (right). We show the data of the observed Taurus member candidates (plus), the Orion member candidates (cross), the already known Taurus members (triangle) and the field dwarfs (square). Only sources which resembled one of the reference spectra are shown. The dotted line marks the zero value.

6.2 Line features in the optical spectra

We adopt the thesis from Barrado et al. (2003a) that we can identify accreting stars in low-resolution optical spectra by their hydrogen and calcium emission. If we confirm candidates as accreting stars, it is very likely that they are young and belong to the Taurus or Orion SF region, respectively. To probe this youth, we also access proxy of the surface gravity of the objects. Since young objects are still in the formation process, their material is not yet fully contracted and compact. Therefore, we expect low gravities in the order of $log(g) = 3.5$ to 4.0 for such objects. Indicators for this value in optical spectra are the potassium (7665 and 7699 $\AA$) and sodium (8183 and 8195 $\AA$) doublets. Other lines, like *LiI* at 6708 $\AA$ (Rebolo et al. 1996) or *HeI* could distinguish even better between members and non-members, CTTS and WTTS. But with the low-resolution spectra obtained in this work, they are not detectable and clearly distinguishable from the background noise.

To measure the line features, we calculate their equivalent widths (EW). This is the width of a rectangle with the same pseudo-continuum level of the flux density (referred to as 'flux' in astronomy and throughout this work, in $W/m^2/\mu m$) and the same flux (the integrated flux density in W/m^2) as the measured line. The pseudo-continuum is the approximation of a continuum level without the line feature. We use the IRAF task *splot* to calculate the values. There, we choose the wavelength interval of the integration and the one used to approximate the pseudo-continuum. The task then fits a spline3 function of 2nd order to the continuum and a Gaussian to the line feature and delivers eventually the EW (see Fig. 6.5). The values are positive for an absorption and negative for an emission line. Since the wavelength ranges of all line features are very small, extinction affects them very little.

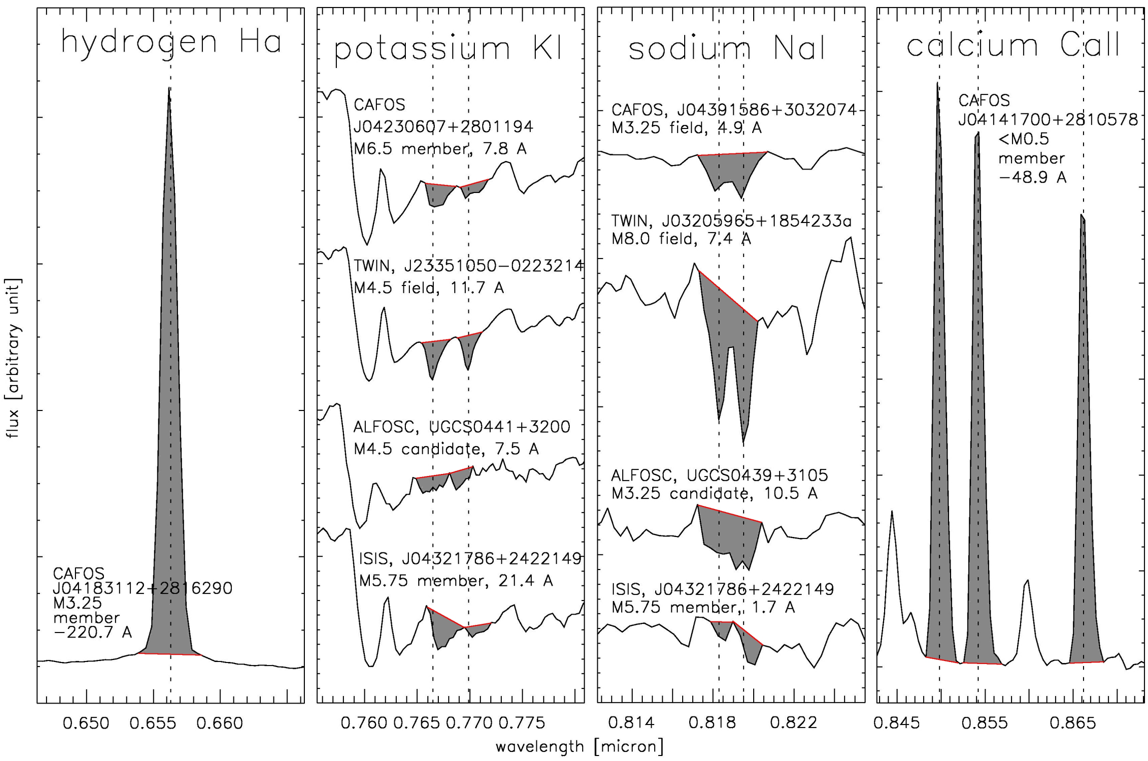

Figure 6.5: The different line features of this work. They get measured by fitting a pseudo-continuum (red line) and calculating the area under the curve (gray area). The latter gets approximated by a Gaussian with the IRAF task *splot*. The $H\alpha$, *KI* and *CaII* lines get resolved by all instruments. The *KI* doublet gets measured by fitting two separate Gaussians. The *NaI* doublet does not get resolved in the ALFOSC observations. We try to measure those two lines by fitting two Gaussians simultaneously, but some got fitted by two separate ones (e.g. 2MASSJ04321786+2422149 in the image). We give the instrument, name (2MASS name shortened), our spectral type, category and EW for each shown spectra and feature. The dotted horizontal lines represent the literature values of the corresponding feature. The strong emission line identified at 8598.3 $\AA$ in the spectra of 2MASSJ04141700+2810578 is *CaIII* (see Atomic Line List: *http://www.nist.gov/pml/data/asd.cfm/*)

6.2.1 The calcium triplet *CaII*

We analyze our spectra at the wavelengths of the calcium infrared triplet (*CaII* IRT) at 8498, 8542 and 8662 $\AA$. Those lines are strong in emission for CTTS. They are produced by accretion shocks very close to the stellar surface (Batalha et al. 1996) or, with much lower intensity, by chromospheric activity. An intrinsic variability is expected. To analyze the EW of the lines, all available numbers get summed up. In all our observed spectra, 12 of 37 (32%) already known Taurus members show the lines in emission (Tab. 6.3). 8 of 37 (22%) of those objects show the lines in absorption, such as do 26 of 31 (84%) field dwarfs, 11 of 22 MIR excess candidates, 5 of 6 (83%) faint LMO candidates, 28 of 45 (62%) bright LMO candidates, and 2 of 7 (29%) Orion candidates. Those results seem to be independent of spectral type (Fig. 6.6). Mohanty et al. (2005) give a formula to calculate the mass accretion rate via the line with the longest wavelength with $log(\dot{M}_{acc}) = 1.06 \cdot log(-F_{CaII8662}) - 15.40$. For completeness reasons, we show the numbers of the 12 emitters in Tab. 6.3 and the rest of the EW in Tab. D in the appendix.

name	*CaII* (8662 Å) [Å]	*CaII* IRT [Å]	$log(\dot{M}_{acc})$ $[log(M_{\odot}/yr)]$	type
2MASSJ04292373+2433002	-27.3	-82.3	-13.9	- (K5.00)
2MASSJ04141700+2810578	-14.7	-48.9	-14.2	- (K3.00)
2MASSJ04224786+2645530	-14.0	-47.6	-14.2	- (M1.00)
2MASSJ04555938+3034015	-8.3	-26.2	-14.4	- (G2.00)
2MASSJ04215563+2755060	-6.4	-21.9	-14.5	M1.75 (M1.00)
2MASSJ04183112+2816290	-6.3	-21.2	-14.6	M3.25 (M3.50)
2MASSJ04321606+1812464	-2.0	-11.9	-15.1	M6.25 (M6.00)
2MASSJ04474859+2925112	-2.6	-7.8	-15.0	- (K5.00)
2MASSJ04270280+2542223	-1.9	-5.8	-15.1	M1.25 (M2.00)
2MASSJ04215943+1932063	-1.7	-4.8	-15.2	- (K0.00)
2MASSJ04141458+2827580	-0.8	-3.5	-15.5	M3.25 (M5.00)
2MASSJ04333405+2421170	-1.0	-3.3	-15.4	- (K7.00)

Table 6.3: All objects showing the *CaII* IRT in emission. For the numbers of the *CaII* IRT, the EW of the three lines get summed up. They are all already known Taurus members and are most probably CTTS. We give the spectral types derived by this work and the ones from Luhman et al. (2010) in brackets.

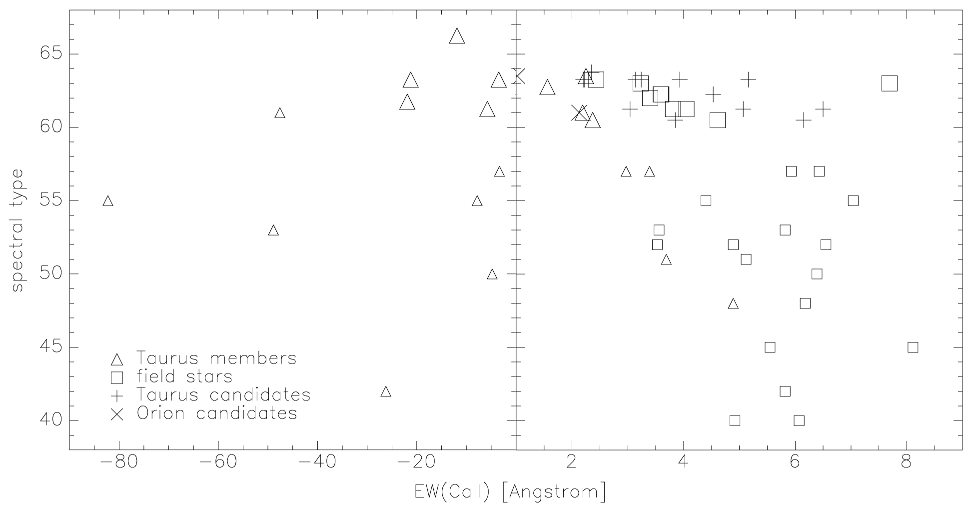

Figure 6.6: The *CaII* IRT EW values of all observed spectra vs. the spectral types derived in this work (large signs) or from literature (small signs). Note again, that the numbers (40, 50, 60) indicate the types ($G0, K0, M0$) throughout this work. The different signs get explained in the image. Only 12 Taurus members show the lines in emission resulting in negative values (left side). The objects with the lines in absorption are shown on the right side. The member candidates of our searches of type earlier than $M0.5$ are not shown in the diagrams. All values are listed in Tab. D in the appendix.

6.2.2 Hydrogen emission $H\alpha$

CTTS are characterized by strong hydrogen emission exceeding at least 20 $\AA$ in EW. WTTS should still show a narrower version of the $H\alpha$ line at 6563 $\AA$ exceeding 5 $\AA$. The low-resolution spectra obtained in this work does not allow to compare the widths of the line. Similar to the *CaII* IRT, this line can be due to chromospheric activity. It then shows an empirical limit dependent on spectral type via $log(-EW(H\alpha)) = 0.0893 \cdot (spectraltype) - 4.5767$. Also, the line can be a sign for disk accretion (Barrado et al. 2003a). There, the level of emission depends strongly on the spectral type of the observed object. We give the CTTS lower limit values defined by the authors in Tab. 6.4.

type	$EW(H\alpha)$ [$\AA$]	type	$EW(H\alpha)$ [$\AA$]	type	$EW(H\alpha)$ [$\AA$]	type	$EW(H\alpha)$ [$\AA$]
K0	-3.9	K7	-6.6	M4	-14.7	L1	-190.4
K1	-3.9	K8	-7.2	M5	-18.0	L2	-279.6
K2	-4.0	K9	-7.8	M6	-24.1	L3	-328.9
K3	-4.1	M0	-8.7	M7	-41.9	L4	-436.4
K4	-4.4	M1	-10.1	M8	-53.0	L5	-698.3
K5	-5.1	M2	-11.2	M9	-87.9		
K6	-5.9	M3	-12.2	L0	-148.2		

Table 6.4: Lower $H\alpha$ EW limits for CTTS with a maximum of $log(g) = 4.0$ corresponding to the saturation limit at $L(H\alpha)/L_{bol} = -3.3$ (Barrado et al. 2003a).

WTTS are considered to show $H\alpha$ resulting from chromospheric activity and little influence from the disk. This is observable in the differences of the CTTS lower EW limits and the formula given above (Fig. 6.7). We consider a source emitting this line due to matter accreting in a disk around it as young object. It has a strong indication of being a member of the molecular cloud of Taurus or Orion, respectively. We show all measured values in Tab. D in the appendix.

One of the field dwarf spectra, namely 2MASSJ03205965+1854233a of type $M8.0$ shows an emission at 6563 $\AA$ larger than 20 $\AA$. 2MASSJ03205965+1854233b ($M8.25$) and 2MASSJ01592349+5831162 ($M3.75$) exceed the 5 $\AA$ level. All three objects are cool enough that the emission could be produced only by the chromosphere, which is not unusual (see e.g. West et al. 2008). Only 3 more such objects show small emission lines, but 12 objects of types $< M0.5$ show it in absorption. The situation is different for the Taurus members. 21 spectra show values above 20 $\AA$ and another 8 still exceed 5 $\AA$. 2MASSJ04183112+2816290 and 2MASSJ04334871+1810099 show values beyond 200 $\AA$ and 2MASSJ04321606+1812464 and 2MASSJ04442713+2512164 beyond 100 $\AA$. It was suggested that it is not obligatory for young sources to show $H\alpha$ emission to prove cloud membership (Martín et al. 2010). But our own observations verify the opposite. Throughout all types, the already known Taurus members show the line in emission. Only the $G8$ Taurus member 2MASSJ04341803+1830066 does not. Due to the intrinsic variability of the line, the limits given in literature are not considered very strictly in this work. Nevertheless, of the observed Taurus LMO candidates, 9 early type objects show a small absorption line at the wavelength not exceeding 2 $\AA$. 6 objects show a small emission line and for 12 spectra of spectral types $M3.25$ to $M4.5$, the value exceeds 5 $\AA$. It reaches 17 and 26 $\AA$ for the $M3.75$ type UGCSJ0429+3237 and the $M3.25$ type UGCSJ0437+3056, respectively. Both objects are considered the best candidates to be CTTS without CaII emission. The spectra of UGCSJ0441+3101a, a faint LMO candidate shows $H\alpha$ in absorption, as do all IRAC candidates. 5 Orion candidates show EW larger than 5 $\AA$, and UGCSJ0532-0208 is located next to the CTTS region in the diagram. We accessed EW values as small as 0.65 $\AA$.

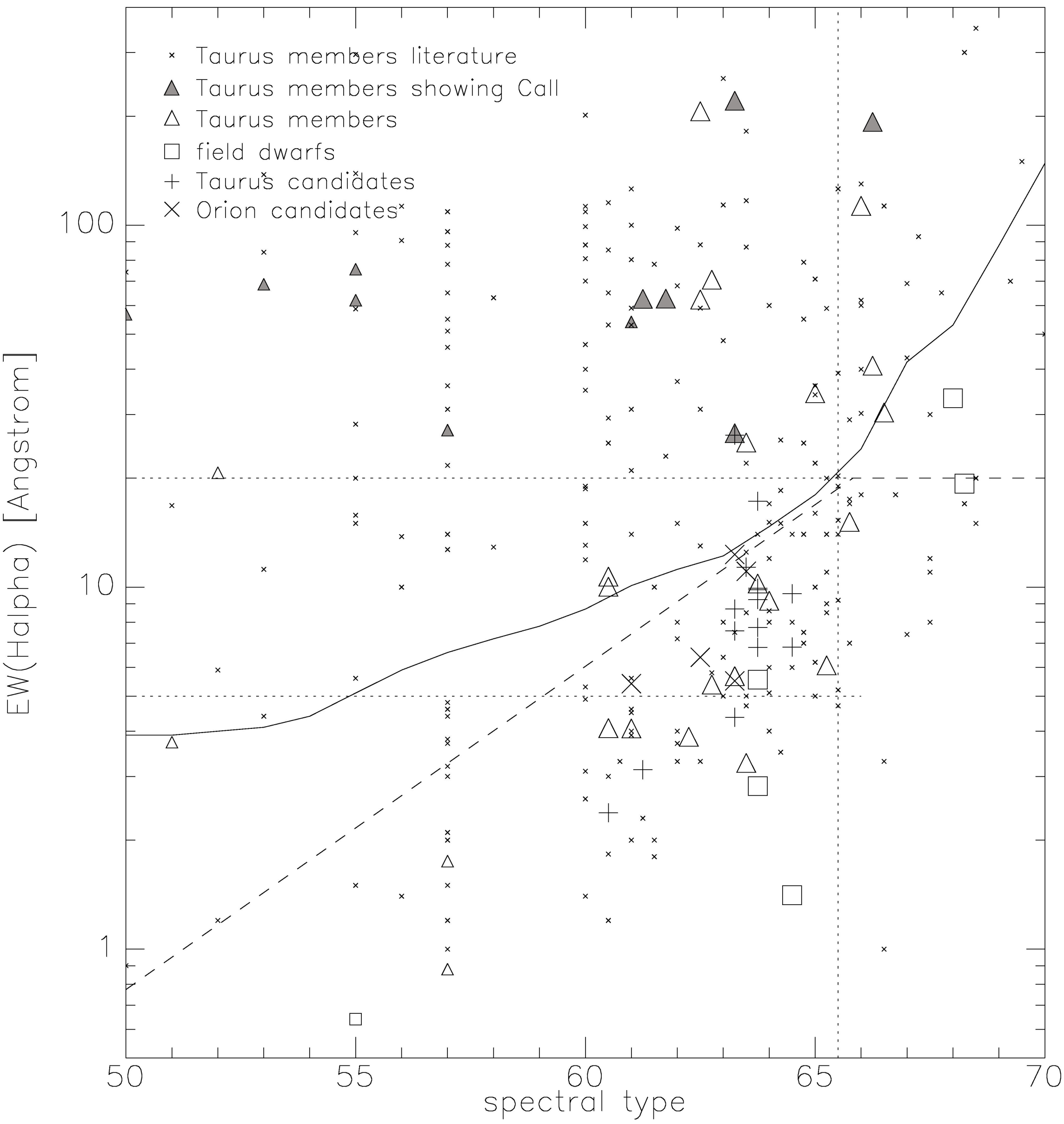

Figure 6.7: The negative $H\alpha$ EW values of all observed sources vs. the spectral types derived by this work if available (large signs) or from literature (small signs). We include measurements of 230 sources from the literature to show the huge scatter of data available for Taurus members (small cross, see Tab. A for references). The different signs get explained in the image. The dotted lines represent the 5 and 20 $\AA$ limits marking the lower limits of the chromospheric activity and disk accretion, respectively. More in detail, the dashed line gives the limit of the first one depending on the spectral type. The full drawn curve then represents the lower limits defined by Barrado et al. (2003a) for the disk accretion. All objects showing *CaII* emission (filled gray symbol) are located in the CTTS area. But many already known Taurus members (triangle) show values lower than the defined limits. The data of no field dwarf (square) and of only two Taurus candidates are located above the lower limit expected for disk accretion. Note, that the candidates (plus for Taurus and cross for Orion) of type earlier than *M*0.5 do not show in the diagram. For the values see Tab. D in the appendix.

6.2.3 The sodium and potassium doublets *NaI* & *KI*

We measure both absorption lines of the potassium (*KI*) and sodium (*NaI*) doublets at 7665 and 7699, & 8183 and 8195 *Å*, respectively. Both are indicators for the strength of the surface gravity (Martín et al. 2004). They are supposed to show small influence on the Taurus and Orion members, since young objects should not yet be that compact as more evolved ones. We consider the behavior of those line features as indicators for the youth of the objects. They form another criteria to probe the membership to the young SF regions (Guieu et al. 2006).

We show the values depending on the spectral type in Fig. 6.8 and in the appendix in Tab. D. With our data we can confirm that the young Taurus members show in general smaller values of both doublets than the older field dwarfs. This is much clearer with the *NaI* lines, where the members do not exceed 3.5 *Å*. The differences increase with later spectral types and begin to be measurable for *M* type objects. For the *KI* doublet, we find a large value for the Taurus member 2MASSJ04321786+2422149 of type *M*5.75, which does not fit in the theory. For this doublet it is much more difficult to find differences. It is not possible to clearly separate our candidates into young and old objects by just comparing this feature with the field dwarfs and Taurus members. We reach down to values of around 0.12 and 0.28 *Å* for the EW of the *KI* and *NaI* doublet, respectively. We set an empirical upper limit of 4 *Å* for the *NaI* doublet for a candidate to be a member of Taurus or Orion. Compared to the dwarf stars we are searching for in this work, giants of same type show lower gravity. But due to the low-resolution spectra, we can hardly distinguish both types. Nevertheless, the candidate samples will contain many giant stars.

6.2.4 Additional correlations and membership

We plot the different spectral features against each other to be able to identify further membership criteria for the candidates (Fig. 6.9). We find the described connection between the age of the objects, the strength of the lines emitted by the accretion disk ($H\alpha$, *CaII*) and the ones emitted by the surface, indicating the gravity there (*KI*, *NaI*). The first pair does show a relation compared to each other following $EW(H\alpha) = 1.8 \cdot EW(CaII) - 8.4Å$. Since the EW of the *KI* doublet is of such low reliability, the connection between the second pair is more difficult to describe. Interesting might be as well the diagrams connecting one of the doublets with the CaII triplet. There, we find well defined regions for the location of the Taurus members. But without further analysis of those relations, we do not find any more reliable membership criteria for our candidates in the diagrams.

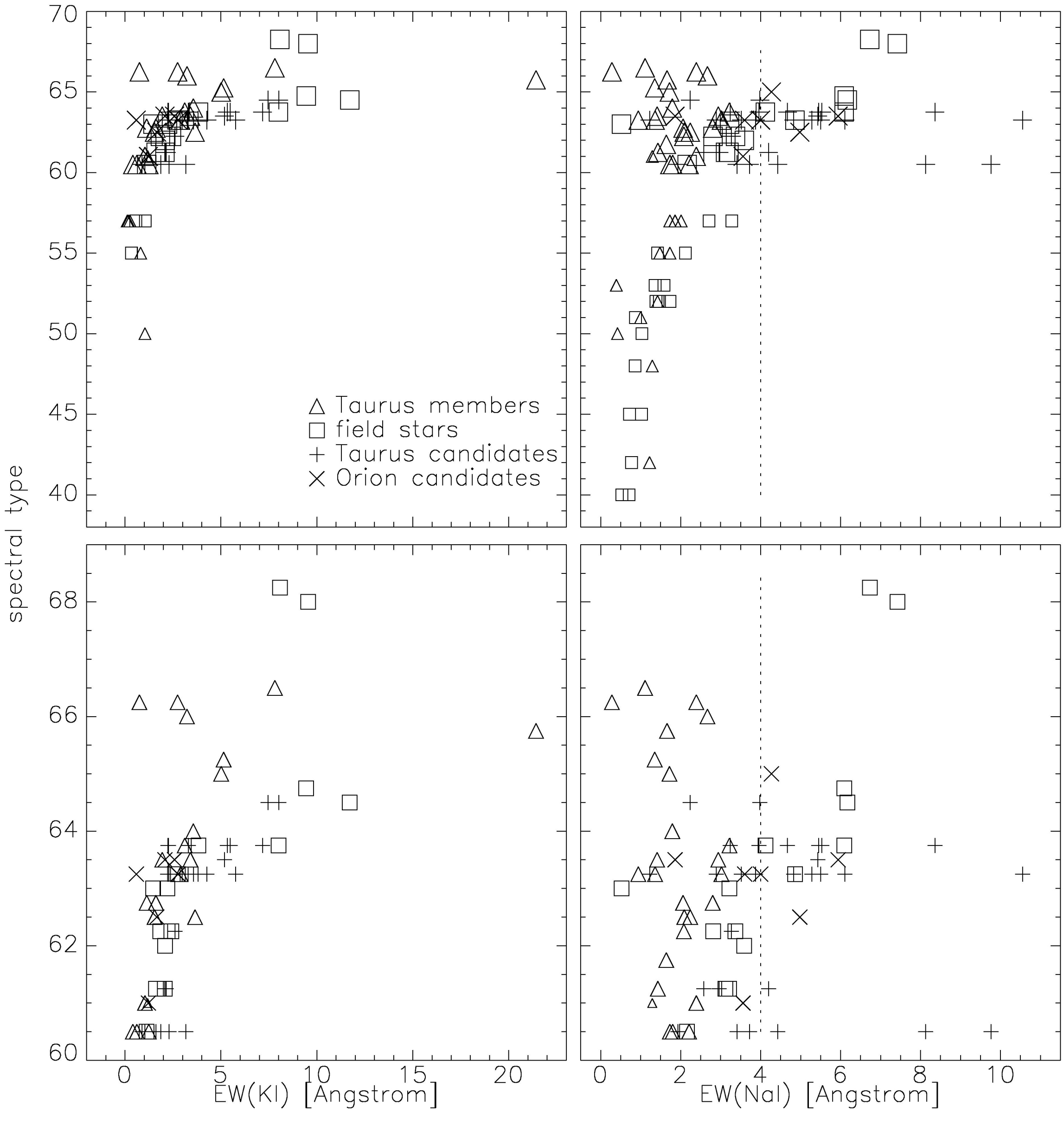

Figure 6.8: The values of the *KI* (left diagrams) and *NaI* (right diagrams) EW plotted against our derived spectral types (large signs) or from literature (small signs). The different signs get explained in the image. In the upper half, we include all data, whereas in the lower part, only objects of type *M* are shown (numbers 60 to 69). The *NaI* doublet is much clearer in separating between the young already known members of Taurus and older field stars. The dotted line marks the empirical limit set in this work. Note, that the candidates of type earlier than *M*0.5 do not show in the diagram. For all values see Tab. D in the appendix.

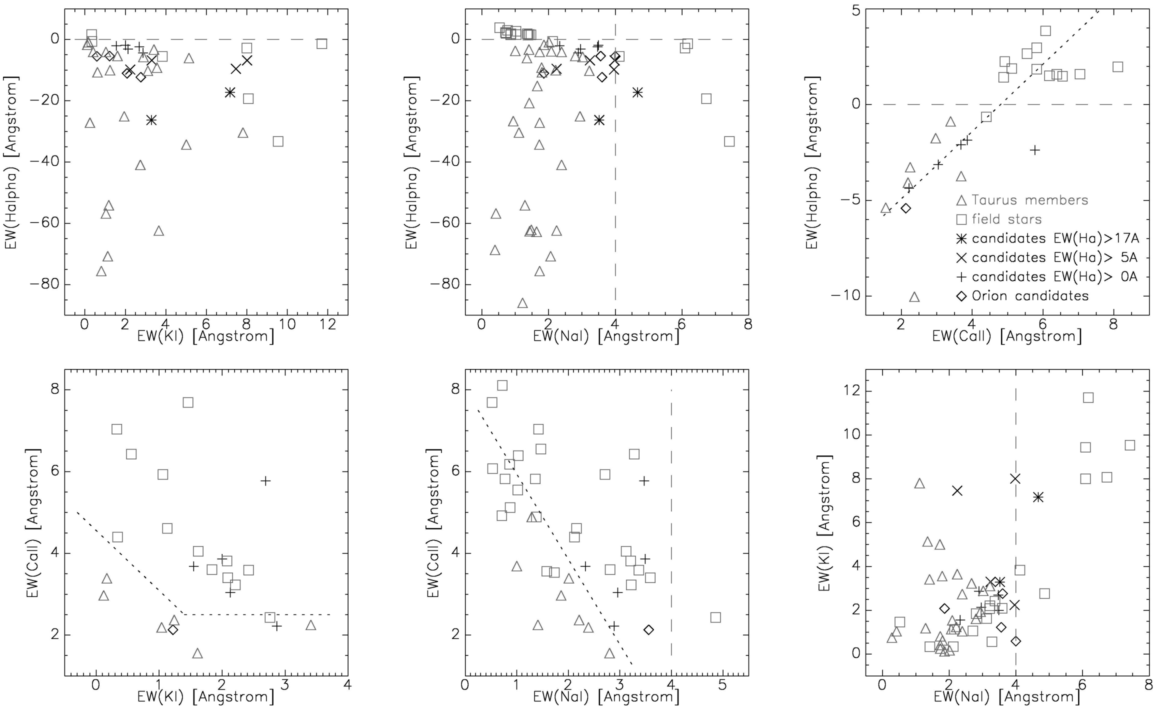

Figure 6.9: In this image all measured EW are plotted against each other. We show all observed Taurus members (triangle) and field dwarfs (square). We put only the 11 and 4 candidates not ruled out already to be new Taurus and Orion (diamond) members, respectively, by their hydrogen and/or sodium EW (see Chap. 7). We sort the Taurus candidates by their different $H\alpha$ EW. The different signs get explained in the image. The connection between the lines emitted by the accretion disk (top: $H\alpha$, bottom: *CaII*) and the ones emitted by the surface (left: *KI*, middle: *NaI*) are shown in the left and in the middle pair of the image. In the pair on the right side, the connections between the two features caused by the same effects are shown. We mark the limits used as membership criteria by the dashed lines (Note, that UGCSJ0429+3237 exceeds the sodium upper limit but is included due to its high $H\alpha$ EW). In the diagrams there are regions only occupied by members or by field dwarfs and regions, where the data of both are located. We mark possible new relations found by this fact by the dotted lines. In no diagram we can reliably learn more about a possible membership of the candidates. Note, that not every source shows every line feature.

6.3 Sources with additional NIR spectra

We analyze the four spectra delivered from the Gemini instrument in the NIR *JHK* filters (see Sec. 5 and Tab. 5.1). They were the first observations done for this work and are of very low quality and resolution. The objects observed do not reveal themselves by any larger absorption and/or emission features. We show the spectra together with their optical counterpart in Fig. 6.10.

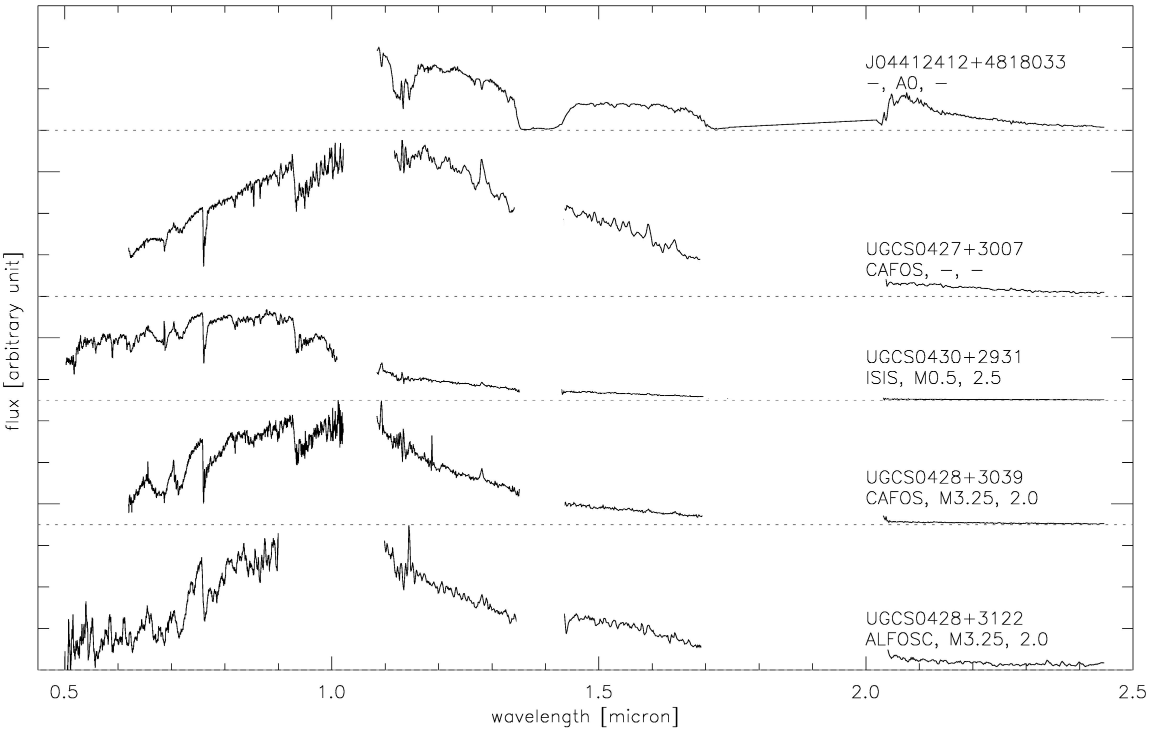

Figure 6.10: The four objects observed by NIR spectroscopy and the standard star used for calibration (top, 2MASS name shortened). They are sorted by spectral type and dereddened by the visual extinction derived from their optical spectra. We show names, instruments of the optical observations, the derived spectral types and visual extinctions. For display purposes the optical spectra of UGCSJ0427+3007, UGCSJ0430+2931 and UGCSJ0428+3039 and the NIR spectra of UGCSJ0427+3007 and UGCSJ0428+3039 were smoothed.

The objects with an optical reference spectra deliver a spectral type and a visual extinction. They can be analyzed by the overall shape of all the available spectra. Although *M* dwarfs do not resemble blackbodies, the overall shape can give a hint for the spectral type and is at least useful for comparison of the four sources. We can locate the maximum flux output between 0.75 and 0.9 μm for UGCSJ0430+2931 and between 0.9 and 1.1 μm for UGCSJ0428+3039 and UGCSJ0428+3122. After Wien's displacement law this translates to temperatures between 3200 and 3900 K on the one hand and 2600 to 3200 K on the other hand. Following the temperatures scale from Luhman et al. (2003a), we would reach down to a $M4.5$ star for UGCSJ0430+2931 and types of $M4.5$ to $M8.25$ for the other two objects. UGCSJ0427+3007 is even cooler and of later type, since its maximum flux output is between 0.9 and 1.2 μm. All types derived here are cooler than the ones delivered by the optical spectra. There we got a $M0.5$ and two $M3.25$ type stars, corresponding to 3700 to 3800 K and 3300 to 3400 K, respectively. Those values would again translate to maximum flux output at 0.77 and 0.87 μm.

6.4 Virtual Observatory SED Analysis

We analyze all observed candidates by their SED. This includes 43 Taurus candidates of the bright LMO sample, 3 of the faint LMO sample, 22 from the MIR excess sample and the 7 Orion candidates. We use the interactive Virtual Observatory SED Analysis (VOSA[1], Bayo et al. 2008) tool. The tool requests as input the distance, the visual extinction and the magnitude and its error in a defined photometric filter. For the NOMAD *BVR* photometry, we use the ones described by Johnson[2]. The filters for the 2MASS, UKIDSS and IRAC values are included into the tool. For the Taurus objects, a distance of 140 *pc* is used and for the Orion candidates 450 *pc*. The photometric errors of the UKIDSS and 2MASS photometry are given, whereas we use errors of 0.05 mag for the IRAC values due to our uncertain values. For the optical filters, we do not include errors nor do we include visual extinctions. Based on this multiphotometric input, the tool delivers approximations and fits for the effective temperature, gravity, bolometric luminosity, age and mass of the objects. Besides the evolutionary models already described in this work (NextGen: Baraffe et al. 1998, Hausschildt et al. 1999 and COND: Chabrier et al. 2000, Baraffe et al. 2002), we also use the DUSTY model, described by Chabrier et al. (2000) and Allard et al. (2001). We use the set limits for the model variables of the VOSA tool. Those are

- Nextgen: $T_{eff} = 1600\ K$ to $10000\ K$, $logg = 3.5$ to 5.5, age= 1 Myr to 8 Gyr, $M = 0.02$ to 1.4 $M_{\odot}$
- DUSTY: $T_{eff} = 500\ K$ to $3900\ K$, $logg = 3.5$ to 6.0, age= 1 Myr to 10 Gyr, $M = 0.001$ to 0.1 $M_{\odot}$
- COND: $T_{eff} = 100\ K$ to $4000\ K$, $logg = 2.5$ to 6.0, age= 1 Myr to 10 Gyr, $M = 0.001$ to 0.1 $M_{\odot}$

We show the outcome of the calculations in Tab. D in the appendix. There, we also show the SED of each object from Fig. D.14 to Fig. D.18. Note, that VOSA only operates with an input of more than 3 photometric filters. With the outcome of the SED fits, we are also able to construct the Hertzsprung-Russell-Diagram (HRD) comparing the bolometric luminosity to the effective temperatures of the objects. We show it in Fig. 6.11.

Not all sources are located in the set model limits. For those, no ages and masses get calculated. Since we did not limit our input parameters, this might be due to a wrong distance value for sources in reality located in the background of the respective SF region. The 22 candidates selected by their possible MIR excess are probably such sources. On the other hand, all 11 good Taurus candidates and all the Orion candidates are located in the model data range. But the resulting ages are all older as expected. The spectral types found by VOSA are generally much cooler than the ones found by this work via visual comparison with reference spectra. Those differences of spectral types, ages and location in the HRD are probably related to the missing input of visual extinction values into the fitting process.

[1]developed under the Spanish Virtual Observatory project supported from the Spanish MICINN through grant AyA2008-02156

[2]http://svo.cab.inta-csic.es/theory/filters/

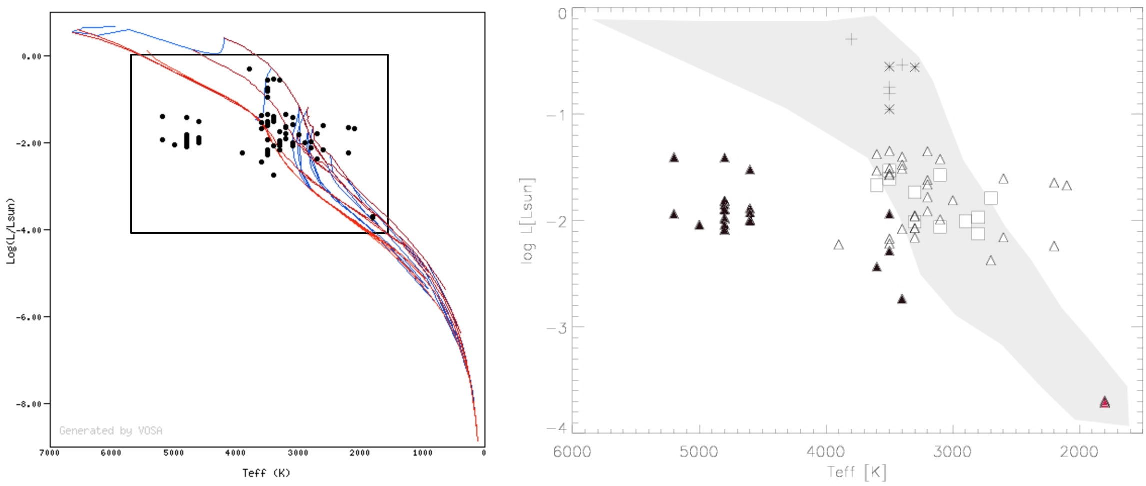

Figure 6.11: HRD of 75 observed sources delivered by the analysis of VOSA:
left: HRD from VOSA. The red lines show from dark to light models with ages from 0.001, 0.01, 0.1, 1.0 and 10 Gyr. From dark to light, the blue lines show models with masses from 0.001, 0.01, 0.05, 0.01, 0.5, 1.4 $M_{\odot}$. The evolutionary models included are NEXTGEN (T_{eff} from 3000 to 7000 K), DUSTY and COND ($T_{eff} < 3000\ K$).
right: highlight of the location of the data points. We show 11 good Taurus candidates (big square), 32 possible Taurus non-members (empty triangle), 22 MIR excess candidates (black triangle), 3 faint LMO candidates (red), 4 good Orion candidates (plus) and 3 possible Orion non-members (asterisk). The area covered by model data is marked gray.

6.5 Comments on individual observed sources

6.5.1 Taurus candidates

- the two spectra of the bright LMO Taurus candidate UGCSJ0439+3032 were observed with ALFOSC and CAFOS and show both low resolution (2400/1800 for the ALFOSC/CAFOS observation, respectively). We sort them to reference spectra of same type $M0.5$, but use different values for the visual extinction of 2.3 and 4.0 *mag*. The spectral types from the spectral indices deliver the same values for both spectra, but are generally too cool with types from $M2.4$ to $M3.4$. The NaI EW differ by very much with 8.1 and 1.9 $Å$, respectively (error is approximately 0.3 $Å$). This huge difference should be due to the difference in resolution of both spectra.

- for the two spectra of the bright LMO Taurus candidate UGCSJ0440+3156, the similarity in spectral type $M3.75$ is better than for UGCSJ0439+3032. We even used the same value for the visual extinction of 2.2 *mag* to resemble the reference spectra. They are both observed with the ALFOSC instrument, but due to different observation dates, we were not able to sum them up. The spectral types calculated from the spectral indices deliver similar and consistent values compared to the one derived visually ($M2.6$ to $M4.8$, $M2.2$ to $M4.9$). Only the EW of the various line features do not fit that perfectly in this very consistent image ($EW(H\alpha) = -7.7$ and -9.9 $Å$, $EW(KI) = 5.3$ and 2.3 $Å$, $EW(NaI) = 8.4$ and 5.5 $Å$). This could be due to the line variability and the unresolved NaI doublet.

- the two sources UGCSJ0441+3126 and UGCSJ0440+3004 of the faint LMO sample cannot be sorted into the M dwarf group although their shapes would resemble $M1.25$ and $M3.25$ types, respectively. But there slope is inclined towards smaller wavelengths due to the problematic GTC/OSIRIS observations. Because of to the lack of emission lines, the probability for them to be new members of Taurus is quite low.

6.5.2 Already known Taurus members

- the spectra of the Taurus member 2MASSJ04292373+2433002 (GV TauA+B) of literature type $K5$ (Luhman et al. 2010) is full of emission lines. Due to the unclear trajectory of the continuum level, it was not possible to sort it clearly into our relative sorting order.
- the $G8$ Taurus member 2MASSJ04341803+1830066 (HBC 407) does not show any $H\alpha$ emission and a rather high $CaII$ IRT absorption with 4 $Å$. Only the gravity features indicate a possible youth and membership, with KI not detectable (< 0.1 $Å$) and NaI of 1.3 $Å$.
- we find a large value for the KI doublet (21.4 $Å$) for the Taurus member 2MASSJ04321786+2422149 (CFHT Tau7) of type $M5.75$. This does not fit in our theory. The observations made with the ISIS instrument do in general not show great fringing at this wavelength range. The other measured EW of this source do show a consistent image and indicate the Taurus membership ($EW(H\alpha) = -15.2$ $Å$, $EW(NaI) = 1.7$ $Å$,). It seems, that the KI doublet could not be measured properly.
- the unusually high visual extinction ($A_V = 6.3$ mag) of the $M0.5$ type star 2MASSJ04293606+2435556 (XEST13-010) is probably responsible for the large difference to the literature spectral type of $M3$. The spectral indices do rather show values similar to the literature type ($M1.0$ to $M4.1$), but are as always suggesting one or two subtypes too cool.
- the visual comparison delivered a spectral type of $M0.5$ type for the Taurus member 2MASSJ04345542+2428531 (AA Tau). The literature described in this thesis states a type of $K7$ and our spectral indices indicate as always an even cooler type ($M1.0$ to $M3.3$). The visual extinction found for this source affects with 0.8 mag not very much the derivation of the spectral type. But a search in the SIMBAD database delivered a spectral type $M0.0$ matching much better with our measurement.
- the difference in spectral types is even larger for HV TauC. In literature, a spectral type of $M1.0$ is stated, whereas we state a $M4.0$ type. The spectral indices follow quite closely the latter ($M3.9$ to $M4.6$). The visual extinction used was 1.3 mag and should not affect the type determination by very much. A search in the SIMBAD database delivers a type of $K6.0$ (Terada et al. 2007). But the source is the circumstellar disk of the $M2$ star HV Tau (Sestito et al. 2008). Since we did not observe this spectrum by ourselves, we cannot be sure, if it is not a mixture of two or more spectra.

6.5.3 Field dwarfs

- the field dwarf HIP16242 of literature type $K7$ (Koen et al. 2010) shows a spectrum inclined to the smaller wavelengths. If corrected for this effect, it resembles an $M0.5$ type object. No spectral indices and visual extinction were derived for this object.
- the two spectra observed for the literature $M8.0$ BD 2MASSJ03205965+1854233 (LP412-31) deliver types of $M8.0$ and $M8.25$ by our visual comparison. Thereby, we use similar visual extinction to fit the spectra to the reference ones with 0.3 and 0.4 mag, respectively. They are both observed with the TWIN instrument, but due to different configurations, we were not able to sum them up. The types delivered by the spectral indices are cooler with $M6.6$ to $M7.5$ and $M6.3$ to $M8.0$, but similar for the two spectra. The EW show a quite consistent picture. The difference in the $H\alpha$ value (19 and 33 $Å$) might be due to line variability.

- the field dwarfs 2MASSJ00180010+4400293 (GJ015) and 2MASSJ00005477+3249321 (HIP76) do both show a large difference in the spectral type delivered by this work and the ones stated in literature. $M5.0$ and $M0.0$ in literature are opposed to $M1.25$ and $M3.0$ by our visual comparison. In both cases, the spectral indices point to the latter values with $M1.3$ to $M2.7$ and $M2.6$ to $M3.3$. Visual extinction values derived are 0.7 and 0.2 *mag*.

- the observed TTS field dwarf 2MASSJ04391586+3032074 does not show any $H\alpha$ or *CaII* emission. We find our spectral type $M3.25$ similar to the one found by literature ($M3.5$). The *NaI* EW is beyond our limit with 4.9 *Å*, as expected for field dwarfs. The TTS status of the source is at least doubtful due to the absence of any emission line.

6.6 Cluster analysis in Orion

We identified three clusters in our Orion candidate sample. Thereby, the radius of the σ Orionis Cluster was set to 30 *arcmin* around the central star following Lodieu et al. (2009). It contains 203 sources with $J < 18$ *mag*. The clumping, the radius of NGC 1981 containing 76 sources, and the new found star cluster containing 55 sources will be described in the following.

6.6.1 Nearest neighbor Methods

The spatial distribution of stars by the star count method is limited by the resolution of the grid square size (see Chap. 3). To avoid this influence, we applied the nearest neighbor (NN) distance method (Gutermuth et al. 2009). Here, we derive the typical spacing between each star and its n-th closest neighbor, where n is 1 and 5 and the methods are called NN2 and NN6. Peaked NN2 distance distributions suggest a sub-region of uniform, elevated surface density. By this method, we searched for clumping in our data set. We found the mentioned clusters and were able to define their radius by setting a 1.5σ limit. We derived a new center defined as the average of the positions of all stars. Furthermore, the NN6 distance can be used to estimate the overall object density or local surface density via $\rho = (N-1)/(\Pi r^2)$ (N is the number of stars, r is the radius of the association). We illustrate the distribution in Fig. 6.12 and give values in Tab. 6.5.

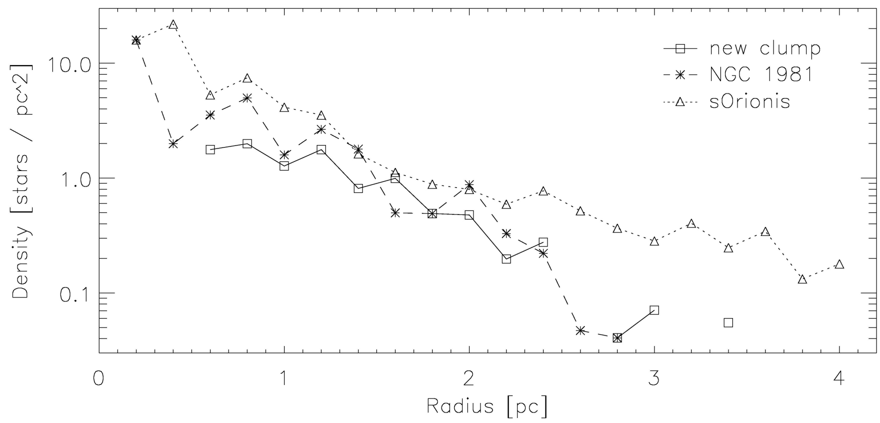

Figure 6.12: The density distribution of the cluster member candidates in Orion. We show the number density of the UKIDSS GCS candidates in σ Orionis, NGC 1981 and the one found by this work. The signs are as indicated in the image.

6.6.2 Minimal Spanning Tree

By setting a NN2 threshold, we isolate a locally dense population without grouping more than a few of the sources together. We performed another algorithm to isolate the closely spaced populations and immediately group them together. The most complete and convenient characterization of the spectrum of source spacing can be obtained by the Minimum Spanning Tree (MST, e.g. Cartwright et al. 2004, Schmeja et al. 2006, Bastian et al. 2007 & 2008) of the source positions. This mathematical algorithm performs a near-identical analysis to the Path Linkage Criterion (Battinelli 1991). The MST is defined as the network of lines, or branches, that connect a set of points together such that the total length of the branches is minimized and there are no closed loops. For detailed comparison to the NN2 and NN6 methods see Gutermuth et al. (2009). This method is not fixed to any specific form of the clusters but permit them to be circular or elliptical, or even two circles. We show the visual outcome of the MST in Fig. D.19, Fig. D.20 & Fig. D.21 in the appendix.

The method allows us to derive important values which make it possible to compare the clusters. We show them in Tab. 6.5. There is the normalized correlation length $\bar{s}$. This is the mean separation of each star to every other one divided by the overall radius of the cluster. It is a good indicator of the extent to which a smooth cluster is centrally concentrated. For a density distribution of $\rho \approx r^{-\alpha}$, it decreases with rising α. In our case, the values resemble the ones for the IC 2391 and Chamaeleon cluster found by Cartwright et al. (2004). The values therefore indicate a less centrally concentrated cluster as for e.g. Taurus, where $\bar{s} = 0.55$ is stated. This value can quantify, but cannot distinguish between a smooth large-scale radial density gradient and multi-scale (fractal) subclustering. The same is true for the mean edge length m, which is the mean length of all the branches in the MST. The normalization is done by dividing it by $\sqrt{(\Pi N r^2)/(N-1)}$. The Q factor is the division of both values $\bar{s}$ and the normalized mean edge length $\overline{m}$. It does both quantify and classify the clusters. A limit of $Q = 0.8$ is stated for centrally condensed clumps like our σ Orionis cluster (and e.g. IC 348: 0.98, Ophiuchus: 0.85). Substructures show smaller values, as do NGC 1981 and the new cluster (IC 2391: 0.66, Chamaeleon: 0.67, Taurus: 0.45, values from Cartwright et al. 2004).

6.6.3 Mass function and various data distributions

Following the investigation done with the already known Taurus members, we form the MF of the three clusters and show it in Fig. 6.13. Also, we form the luminosity function of the clusters and show them in Fig. D.22 in the appendix. They all follow the normal or universal behavior of clusters with a peak of the MF at lower masses as for Taurus.

We show the plot of the proper motions of the member candidates in Fig. 6.14. There is no difference visible compared to the zero movement point in none of the clusters. But the proper motions of the members of the σ Orionis cluster are with $(\mu_\alpha, \mu_\delta) = (3.52, -0.20)$ mas/yr (Kharchenko et al. 2005) also in this range. The distribution in a square of 30 mas/yr around the zero movement point of all the selected sources is still a sign of possible membership.

cluster name	σ Orionis	NGC 1981	new clump
objects number	203	76	55
center RA [deg]	84.67882	83.81870	83.26841
center Dec [deg]	-2.59013	-4.35317	-2.27805
radius [deg]	0.504	0.333	0.424
area [$sq.deg$]	0.797	0.348	0.564
density [$stars/sq.deg$]	254.7	218.3	97.5
NN2 range [$arcmin$]	0.28-5.70	0.51-4.75	0.60-4.44
NN2 mean [$arcmin$]	2.14±1.19	1.93±0.89	2.36±1.03
NN6 range [$arcmin$]	3.43-10.21	2.51-7.43	3.35-14.07
NN6 mean [$arcmin$]	5.64±1.19	4.64±0.89	6.09±1.03
density NN6 [$stars/sq.deg$]	180.2	265.9	154.5
radius [pc]	3.96	2.61	3.33
area [pc^2]	49.17	21.48	34.80
density [$stars \cdot pc^{-2}$]	4.1	3.5	1.6
NN2 range [pc]	0.02-0.37	0.03-0.31	0.04-0.29
NN2 mean [pc]	0.14	0.13	0.15
NN6 range [pc]	0.22-0.67	0.16-0.49	0.22-0.92
NN6 mean [pc]	0.37	0.30	0.40
density NN6 [$stars \cdot pc^{-2}$]	11.7	17.2	10.0
mean edge length m [$arcmin$]	2.331±1.437	2.210±0.983	2.795±1.206
mean edge length m [pc]	0.153	0.145	0.183
normalized mean edge length $\overline{m}$	0.617±0.380	0.537±0.239	0.452±0.195
normalized correlation length $\overline{s}$	0.727±0.173	0.694±0.135	0.641±0.129
Q=$\overline{m}/\overline{s}$	0.849	0.775	0.705

Table 6.5: Data for the Orion clusters in the UKIDSS GCS region

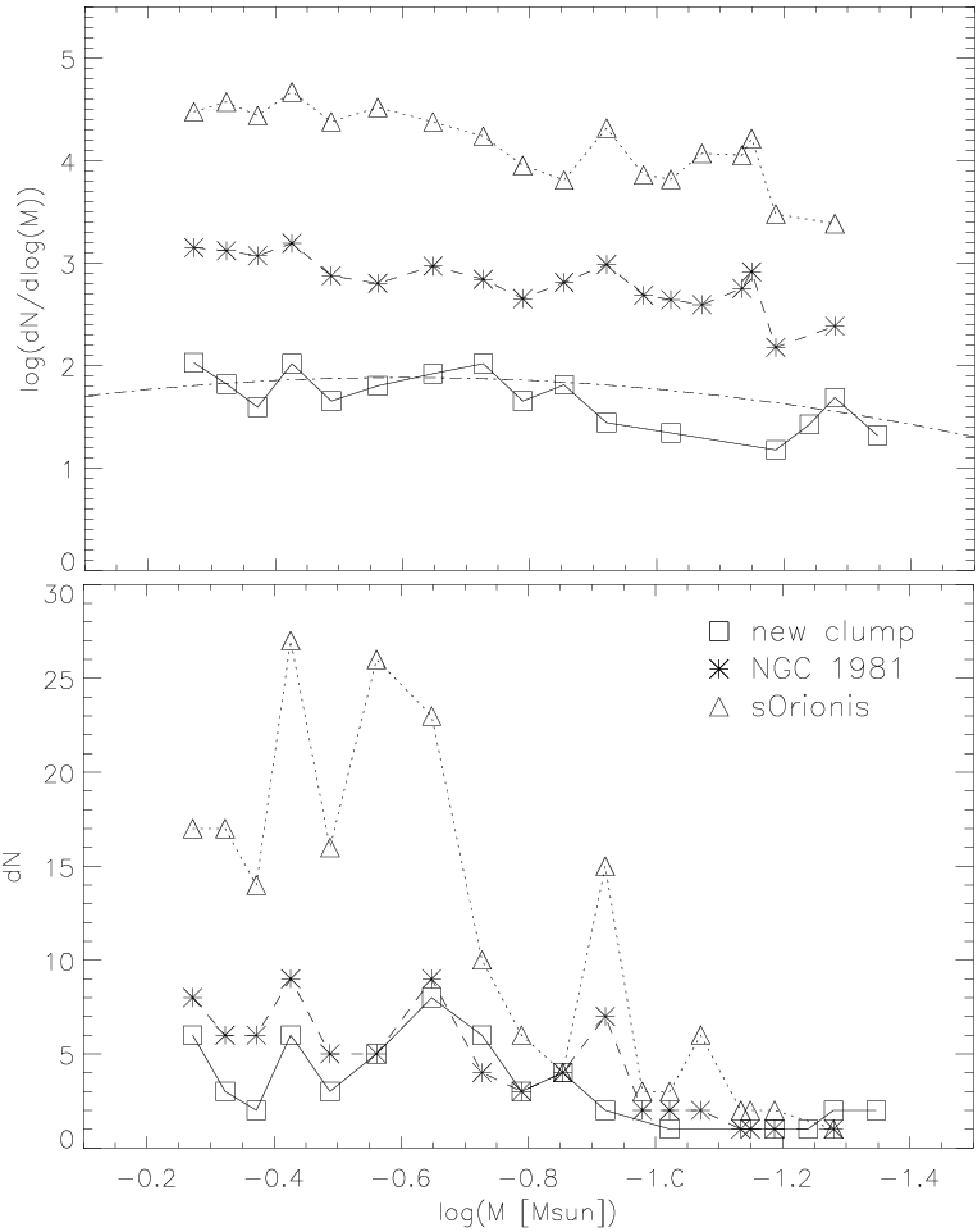

Figure 6.13: The MF of 203 selected σ Orionis cluster candidates (triangle), 76 candidates of NGC 1981 (asterisk) & 55 candidates of the new stellar clump (square). The MF all show peaks in between $-0.65 < log(M) < -0.25$ or $0.2 < M < 0.6\ M_{\odot}$. They all follow the normal or universal form of the MF (dash-dotted black line is the log-normal function from Chabrier (2003) for LMO). We show the classical logarithmic distribution of the function in the top image. On the bottom, we show the number distribution. For more details see Fig. 2.6.

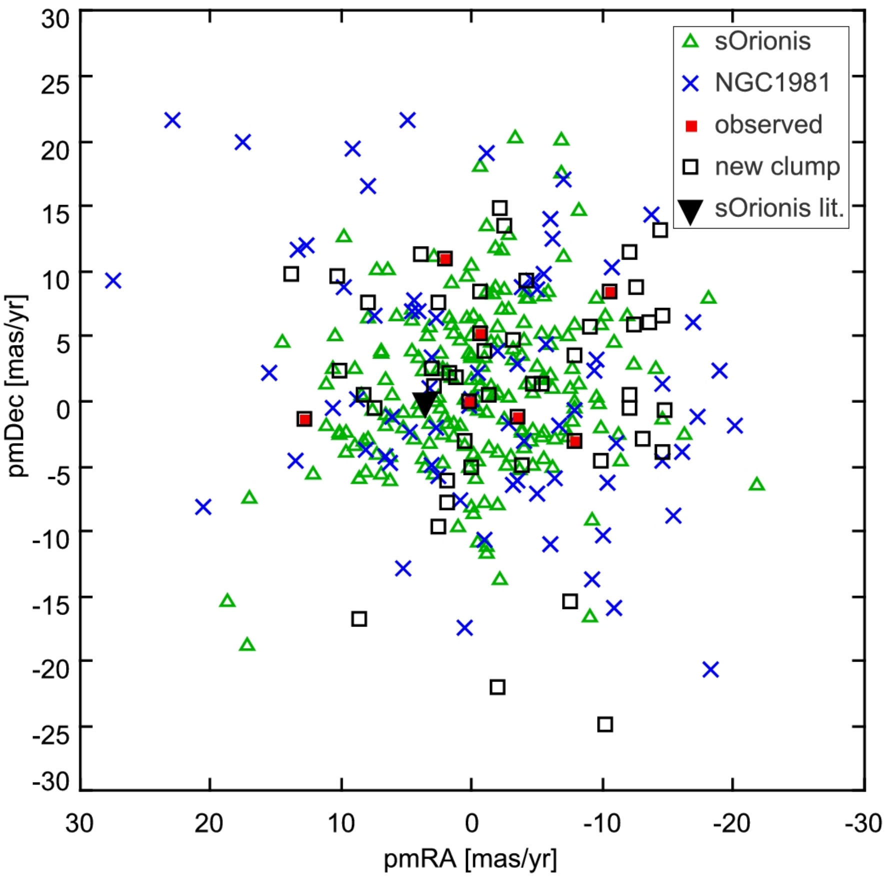

Figure 6.14: The distribution of the proper motions of NGC 1981 (blue cross), the new clump (black square) and σ Orionis (green triangle). We indicate the observed sources of the new cluster by the filled red squares and the average movement of the σ Orionis cluster by the filled black triangle.

Chapter 7

Results and discussion

7.1 Results

- **High-resolution NIR extinction maps**
were calculated for the UKIDSS GCS covered parts of Taurus and Orion. With a resolution of 1.5 ans 2.1 *arcmin* those are the most detailed maps of that kind so far. We did not use the most sophisticated calculation due to the approximative character of the whole theory. A quite large error of 0.24 to 0.30 *mag* was estimated. But since we constructed two maps of Taurus, based on a different set of photometric filters, the values are very reliable. In any case, we were able to detect and distinguish the molecular clouds in those regions. Their huge effect on the photometry and on the colors of the stars was eliminated in our search process by including the dereddened photometry into the selection criteria. This approach is not common in comparable studies, although the search for LMO is mostly based on such molecular clouds. Especially for the search for young BD, the approximation and consideration of the extinction seems necessary. We can see on the map of Orion how successful the dereddening process can eliminate the effects of the clouds.

- **The outcome of the search process:**
the main selection in Taurus was done using the UKIDSS GCS NIR data. We selected 253 bright and 19 faint LMO candidates. Both samples fulfill around 40 photometric criteria. This is due to the multiphotometric approach including MIR, NIR, and optical wavelengths of both the already known Taurus members and the possible candidates. For the 644 transition disk candidates this number is much smaller but still more than in most comparable studies. In Taurus the large number of criteria was necessary to improve the search due to its low density, which in region A, away from the main clouds, is expected to be even lower. We compensate the conservatism of the photometric cuts with this large number of criteria. Unfortunately, we could not use the proper motions as the strong membership criteria it represents in comparable studies. The errors were too large too be able to exclude the zero movement point, where the most contaminating and distant objects are located. But we divided the candidates into higher and lower membership probability due to their proper motions. In Orion, the photometric search was not meant to be that detailed. We tried to eliminate obvious non-members and cleaned the data set of the influence of any molecular clouds with the help of the dereddened photometry. We successfully recover two known stellar associations in the area and find a third, yet unknown cluster.

- **Reaching deeper with the UKIDSS GCS:**
  the UKIDSS GCS data set reaches 3 to 4 magnitudes deeper into the NIR filters than 2MASS. It was an aim of this work to use this advantage in the search for new LMO in Taurus. The comparison data of already known Taurus members does not cover those fainter magnitude range. This made the selection criteria in that part less reliable. But the biggest disadvantage is the fact, that optical spectroscopy of sources with $J > 15.5$ *mag* ($I \approx 18.5$ *mag*, $M \approx 0.07\ M_{\odot}$) is very time-intensive ($> 1\ h$), even with 4 *m* telescopes. But such observations are necessary to probe the youth and the cloud membership of candidates even for regions as near as Taurus. The 2MASS completeness limits is given with 15.8 *mag* in this filter. With the GTC, having a mirror of 10.4 *m*, we observed in 20 to 30 minutes objects with sources of up to $J = 18.2$ *mag* ($I \approx= 21.7$ *mag*, $M \approx 0.03\ M_{\odot}$). To make use of the described UKIDSS advantage, it is necessary to observe with the largest optical telescopes.

- **Spectral typing:**
  we find a good internal consistency for the spectral types derived from the indices. Compared to the spectral types derived from the visual comparison, they generally seem to suggest one or two subtypes cooler. This effect might be due to the extinction of the sources, which was not considered in the calculation of the indices, but in the visual comparison. We were able to assign spectral types for 36 observed candidates. The literature values of already known Taurus members and field dwarfs confirm in 23 of 40 (58%) cases the spectral type derived from the visual comparison (±0.5 subtypes).

- ***CaII* IRT and $H\alpha$ emission lines:**
  our observations confirm that only young Taurus members with accretion disks emit the *CaII* IRT and that evolved main sequence field stars do not. Only 12 already known Taurus members of our sample do show the lines. For all of them we find strong hydrogen emission. They are confirmed by this method to be CTTS. None of our candidates show the *CaII* IRT in emission. But due to our results, they are no requirement for the Taurus and Orion membership. We find 22 of 37 Taurus member spectra showing $H\alpha$ above the limits set by Barrado et al. (2003a). 18 bright LMO Taurus- and 5 Orion candidates show the line in emission. These are considered to be good candidates to be WTTS members of the respective region. 2 of 18 Taurus candidates could still produce their hydrogen emission in accretion disks ($EW(H\alpha) > 17$ Å).

- ***KI* and *NaI* absorption doublets:**
  the observed spectra are not able to deliver very distinguishable values for $EW(KI)$ and $EW(NaI)$. Our chosen resolution was too low. This gets reflected in the large scatter of the data and the fact, that we were not able to extract any conclusions out of the potassium doublet. As a proxy for surface gravity, it should reveal the age of the sources more clearly. We consider objects showing $EW(NaI) < 4$ Å to be possible members, based on the fact that 7 of 32 (22%) observed non-members have larger values. 31 bright LMO candidates, 5 faint LMO candidates, and 4 Orion candidates do fulfill this criteria.

- **VOSA:**
  the 75 observed candidates show a large scatter in the HRD calculated by VOSA. For the non-members this could be because of the wrong input of the distance. For the possible members, this is due to the missing input of the extinction, resulting in cooler spectral types. The Analyzer derives ages and masses for 35 of 75 (47%) observed candidates. We find 15 sources showing temperatures translated to *K* type stars. And only 8 of the 35 (23%) *M* type objects confirm

the spectral type of our observations (±0.5 subtypes). 5 of them are located in Taurus. But VOSA estimates ages of $> 50\ Myr$ for them. For the possible member UGCSJ0429+3237 of type $M3.75$, it delivers an age of 63 Myr, a mass of 0.2 $M_{\odot}$, and a $M3.7$ type. The other 3 better estimations of VOSA are located in Orion. It calculated ages of 2.6 and 1.6 Myr, masses of 0.48 and 0.40 $M_{\odot}$, and spectral types of $M2.3$ and $M3.0$ for the $M2.5$ type UGCSJ0532-0212 and the $M3.25$ type UGCSJ0533-0224, respectively. It is difficult to trust the outcome, because of the generalized input of distances especially in Orion and the lack of extinction values. Those problems are observable in the separated location of Taurus and Orion sources in the HRD. Since small changes in those critical input values affect the outcome by very much, it seems not very useful to use this tool in the search for new low-mass members.

- **The already known members of Taurus:**
  the photometry of the 351 already known Taurus members was used in this work to approximate the location of members in various CMD and CCD. We could not make use of the photometry of their UKIDSS $ZYJHK$ filters but the 2MASS JHK filters. For comparison, we observed 37 of 351 (11%) already known Taurus members with optical spectroscopy. Of those, 22 (59%) show strong hydrogen emission. Assuming that the line is partly emitted by the material of an accretion disk, this results in a disk fraction of 59%. This value resembles the one found by Monin et al. (2010) for TTS with 58% (see Chap. 1). 12 (32%) of those sources are identified as CTTS showing the $CaII$ triplet in emission. All of the observed members show $EW(NaI) < 4\ \AA$.

- **Observational outcome:**
  we observed 43 sources of the 253 bright and 4 sources of the 19 faint LMO candidates. All together, we observed 17% of the selected member candidates. Of 43 objects, 11 (26%) are possible new members of Taurus, since they show $H\alpha$ in emission and NaI comparably small. This success rate is slightly lower as expected for the benchmark region Taurus (with 30%). As we searched in a region, where we even expected less members than for the low-density region on the molecular clouds of Taurus, this outcome is very satisfying. 27 of 43 (63%) observed sources show a membership probability 1 following the proper motion criteria (inside the limits set by the already known Taurus members, see Sec. 4.1.1.3). 8 of the 11 possible new members show those values.

- **MIR excess and faint LMO candidates:**
  the search for candidates with signs of transitional disks by their MIR excess was completely unsuccessful. We observed 22 sources out of 644 candidates (3%). Our data was very unreliable, showing an error of 0.1 mag Also, the final selection included the visual inspection of the SED of the objects. This might have also misled us, considering the outcome of VOSA in this work. The spectra observed with the ISIS instrument are very doubtful (see also the $A4$ type standard star 2MASSJ04043412+2508517 in Fig. C.1). The same is true for the GTC observations, where we were not able to clear the dark frame problems of that semester. The poor data of the IRAC filters has to be combined with NIR photometry to identify more reliable candidates. But even for the LMO candidates found in regions covered by our IRAC data, there was no match between both selections.

7.2 Achievements and implications

7.2.1 Possible membership of 11 Taurus and 4 Orion sources

We cannot confirm to have found any CTTS showing both the $CaII$ and $H\alpha$ lines in emission and low KI and NaI EW. But of the 18 and 5 sources emitting $H\alpha$, 10 and 4 objects match the limit for the NaI doublet ($EW(NaI) < 4\,Å$) for Taurus and Orion, respectively. Additionally, we include UGCSJ0429+3237 due to its strong hydrogen line ($EW(H\alpha) = -17.3\,Å$), although it shows a slightly larger sodium absorption ($EW(NaI) = 4.7\,Å$) as our limit. We consider those 11 and 4 sources as possible new members of the respective region. In Fig. 7.1 and Fig. 7.2 we compare the shape of those spectra in the KI and NaI wavelength range to the ones of the already known Taurus member and field dwarf of same spectral type. Of the 8 possible new Taurus members with spectral types assigned, UGCSJ0431+3111, UGCSJ0433+2912, UGCSJ0421+3052 and UGCSJ0441+3200 have a similar shape at the KI wavelengths as the already known member of same type. We consider them, together with UGCSJ0438+3119, UGCSJ0427+2836 and UGCSJ0437+3005 the best 7 candidates. For the NaI doublet only UGCSJ0431+3111 and UGCSJ0433+2912 seem to resemble those spectra. Both of them show proper motion values inside the limits set by the already known members (probability 1, see Sec. 4.1.1.3)). For the Orion sources, the NaI doublet delivers more reliable data. None of the possible new members resemble the shape of an already known Taurus member. If the sources are indeed new members, they are WTTS, showing only small, if any, influence from an accretion disk. The source UGCSJ0428+3039 Of type $M3.25$ was also observed in the NIR wavelengths indicating a spectral type from $M4.5$ to $M8.25$. 8 of 11 (72%) possible new Taurus members show a membership probability 1.

To summarize, we assigned membership to the young region due to the following criteria:
- similar BVR, JHK, and IRAC photometry as already known members
- same proper motions as already known members
- redder $ZYJHK$ colors as model field dwarfs
- dereddened $ZYJHK$ colors fitting the adequate evolutionary models
- large $H\alpha$ emission typical for young accreting sources
- small NaI absorption typical for young sources

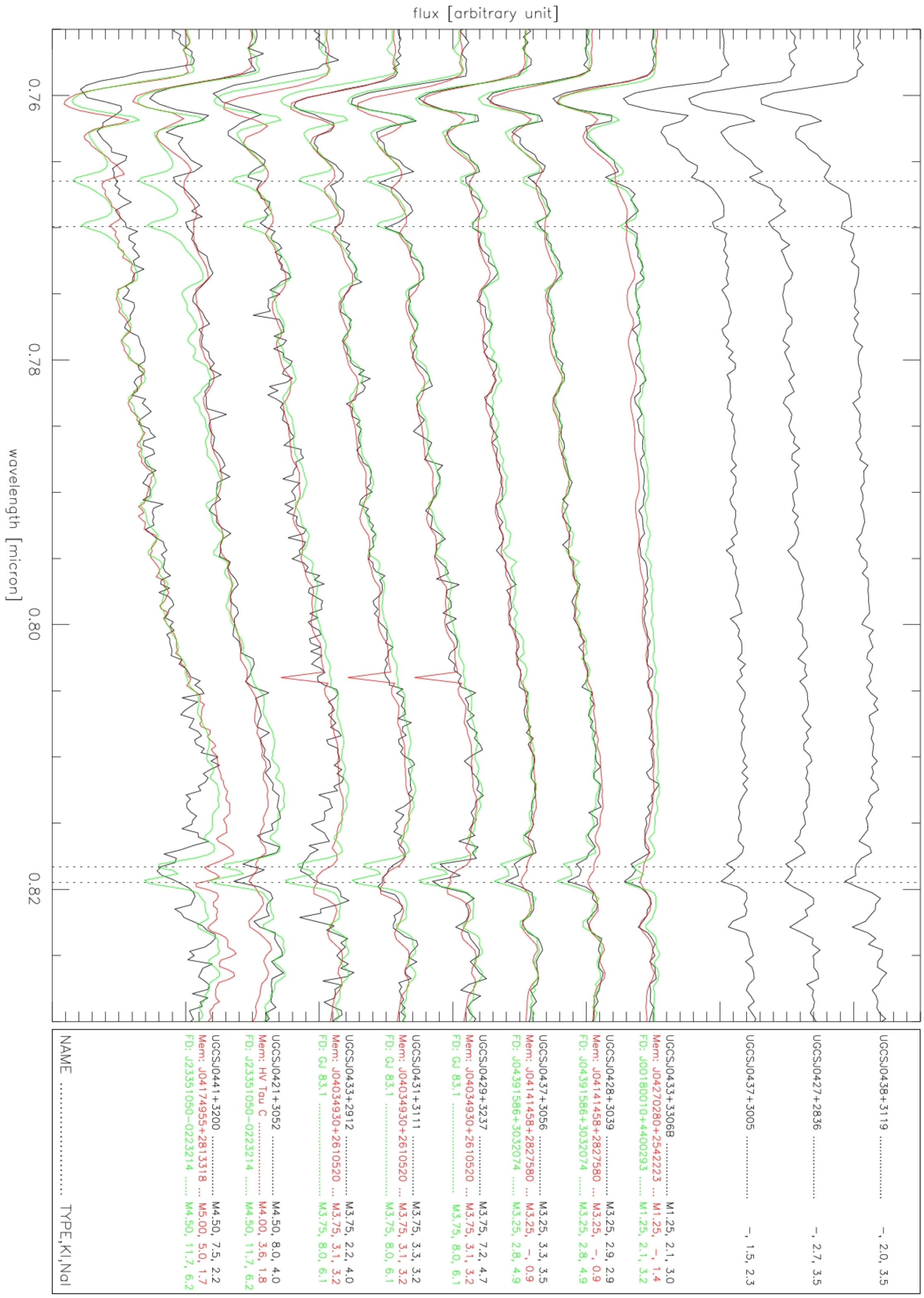

Figure 7.1: We compare in detail the wavelength ranges of the *KI* (7615 & 7749 $\AA$) and *NaI* (8133 & 8245 $\AA$) doublets indicated by the vertical dotted lines. We show the spectra of the 11 possible new Taurus members with $H\alpha$ in emission (black curve). 10 of them have $EW(NaI) < 4\,\AA$, whereas UGCSJ0429+3237 was selected due to $EW(H\alpha) = -17.3\,\AA$. If they resembled a reference spectra in the visual comparison (i.e. if we assigned a spectral type to them), they get compared to a already known Taurus member (red) and a field dwarf (green) of same type. On the right hand side, we give the name (2MASS names shortened), our spectral type, and the EW in $\AA$ of the *KI* and the *NaI* doublet of the candidates (black), the Taurus members (red, marked 'Mem') and the field dwarfs (green, marked 'FD') they get compared to. The spectra are sorted by their spectral type (early to late from top to bottom. Note, that we did not observe an already known $M4.5$ Taurus member. We consider only the first 3 and the last 4 as good candidates due to this diagram.

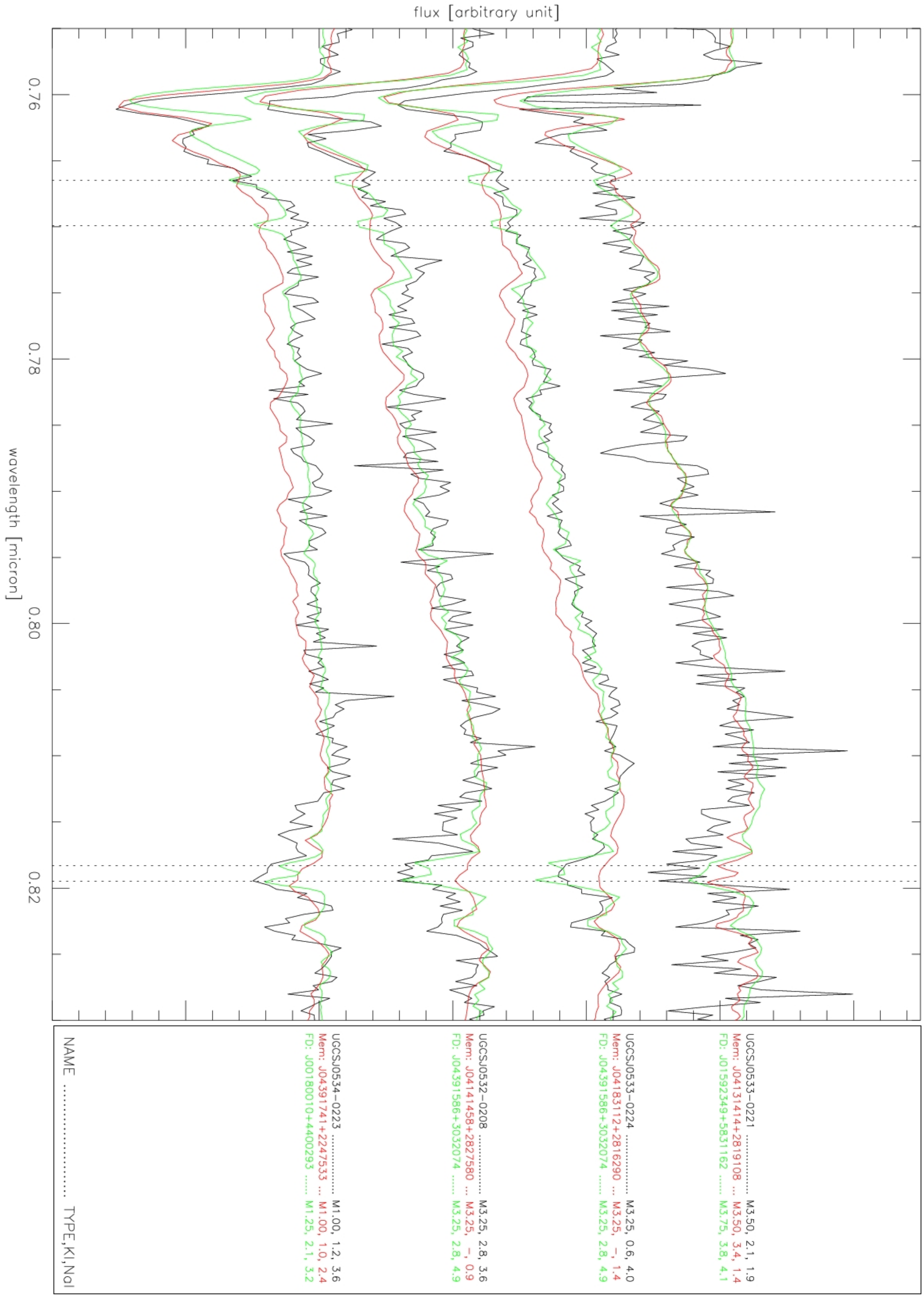

Figure 7.2: The spectra of the 4 Orion candidates with $H\alpha$ in emission and $EW(NaI) < 4\,\AA$ (black curve). For further explanations see Fig. 7.1. Note, that we did not observe field dwarfs of type $M1.0$ and $M3.5$. Due to this diagram it is doubtful how many members were discovered, since they all resemble field stars rather than Taurus members.

7.2.2 Location of the new Taurus members

All selected candidates, all observed objects and the 11 possible new members in Taurus are shown in Fig. 7.3. Their location is not connected to the main molecular clouds. Those are located around 5 deg to the south. If the membership of the 11 sources is true, they have certainly moved from their birth site in the south to their present location. In the 1 Myr existence of the region, they would have moved with a velocity of 18 mas/yr. We see two possibilities. Although the region is very young, it could be due to dynamical mass segregation (Bastian et al. 2010, Portegies Zwart et al. 2010), where associations loose their low-mass members to the field over time. On the other hand it could be due to the embryo ejection model, where young LMO get ejected before they fully accrete their material. It would be very interesting to reach down to the magnitudes of BD in the region and compare the BD to star ratio. If we would find a larger value as on the main clouds, it could be a sign in favor of this formation theory. Both described possibilities suggest many of the missing low-mass members of Taurus to be located further away from its center. But since our search is very much biased in the magnitude range ($12 < J < 15.5$ mag or $0.55 < M < 0.08$ $M_{\odot}$ for the bright LMO sample), we could not access the members of higher or lower mass. However the region is certainly more stretched out as previously assumed. Already of low density, the region seems to fade out into space more slowly. The members are even located beyond the detectable molecular clouds and their birth sites. With 351 members in 60 $sq.deg.$, we derived a density of around 1 $star \cdot pc^{-2}$. To estimate a new density of Taurus, we include the 7 new members and do not consider the fact, that we observed only 17% of our candidate list. They are located inside the 25 $sq.deg.$ covered by the UKIDSS GCS, which represent around 12.5% (one out of $3x3 - 1 = 8$ parts) of the outer regions of Taurus. This would lead us to 407 members in 260 $sq.deg.$ or around 0.3 $star \cdot pc^{-2}$. To fully understand the formation of stars and BD in Taurus, the exploration of those outer parts is necessary.

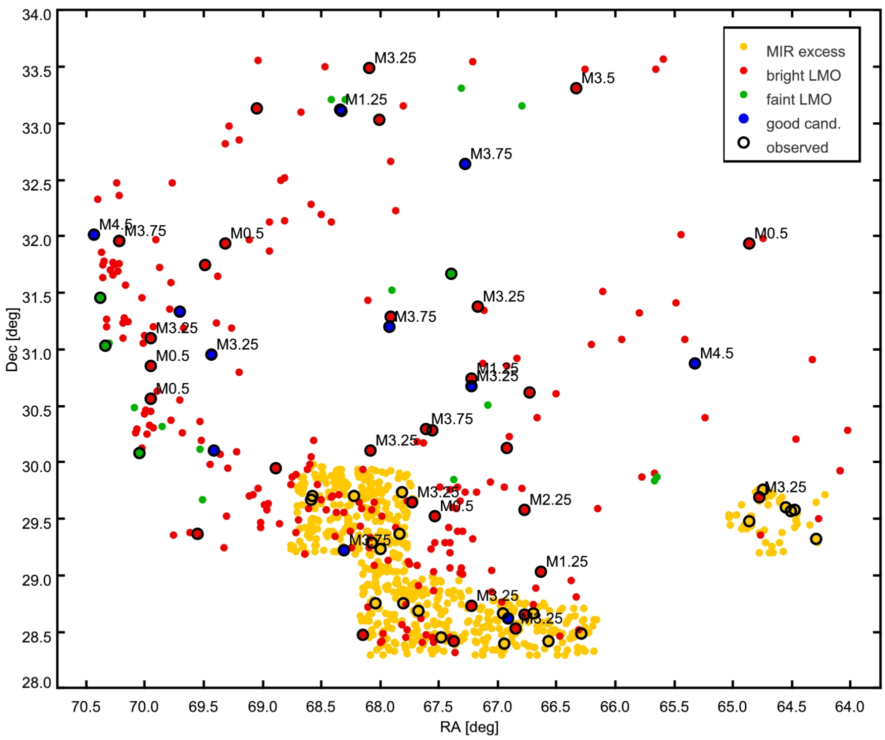

Figure 7.3: Spatial distribution of the various candidates selected in the Taurus SF region covered by the UKIDSS GCS (region A). We mark the sources observed (black circle), the possible new members (blue dot) and show the determined spectral types. The different signs get explained in the image.

7.2.3 Implications on the mass function

The main goal of this work was to discover the missing Taurus low-mass members. We hoped to find at least a number of objects which could result in an observable difference in the MF. Considering the low density of possible new members, the finding of at least 7 such candidates is a success. They represent around 16% of the observed 43 bright LMO candidates. If we account for the fact, that we only observed 17% of our 253 candidates, we expect however around 41 new Taurus members in our investigated area. In the magnitude range we accessed in our search for bright LMO ($12.0 < J < 15.5$ mag or $0.55 > M > 0.08$ $M_{\odot}$) 104 already known Taurus members are located. Those numbers show that the population of Taurus is much more numerous. And the previous assumption that there are no more members of types $< M5$ is wrong. A look at the new drawn MF (see Fig. 7.4) does not prove any change in its form, the number of added objects is just too small. There however, we contribute only around 10% to the existing MF in the mentioned mass range. If we could include 41 new members, the MF would change significantly. We could furthermore account for the fact, that we searched only around 12.5% of the outer regions of Taurus. Assuming 41 new members in each of that 8 regions around Taurus, 328 new members in the mentioned mass range could be located away from the main clouds. They would be located in area of $8x25 = 200$ $sq.deg.$. By these numbers it seems clear, that there is an unknown population comparable to the size of the 351 already known Taurus members in the main clouds. The missing LMO of the area are located away from the main clouds. Most of the new members located in those outer parts should be fainter than $J = 12$ mag, assuming that it would have been more obvious to include them in previous investigations. Therefore, those members would fill the gap of the missing LMO. Our findings clearly point towards a more universal form of the MF, as previously reported.

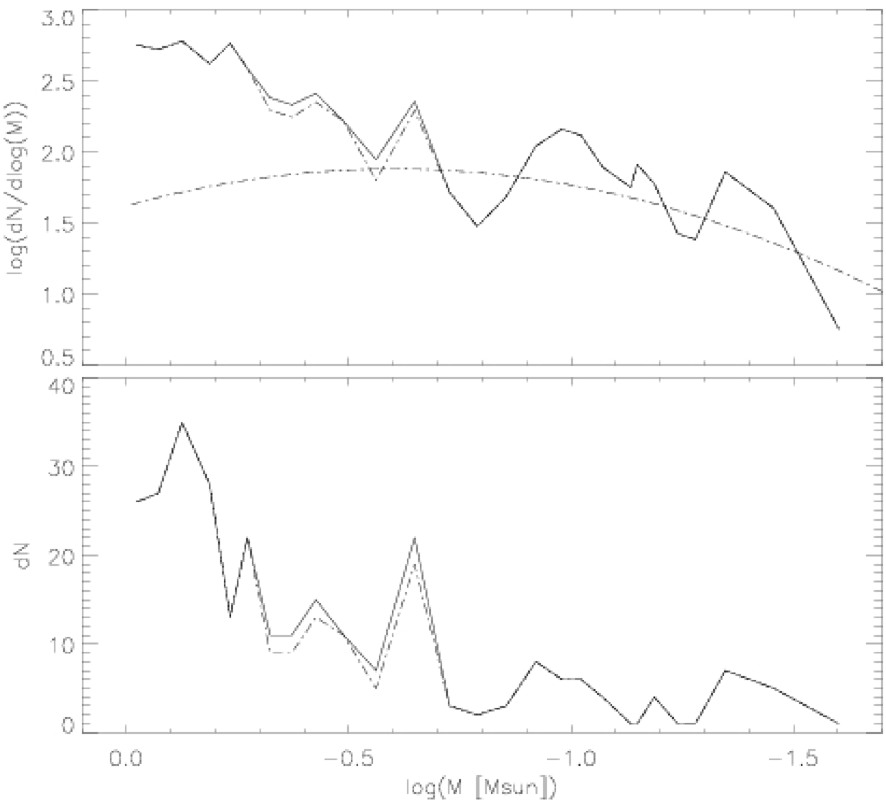

Figure 7.4: MF of 351 already known Taurus members (dash-dotted line), and the one including the 11 possible new members identified in this work (full line). In the top image, we show the logarithmic ordinate, whereas in the bottom image, the linear relation is shown (see Fig. 2.6 for Taurus & Fig. 6.13 for Orion). In the top image, we show the log-normal field MF described for the low-mass range (Chabrier 2005).

7.2.4 Stellar associations in Orion

We searched for candidates in Orion showing similar $ZYJHK$ photometry (observed and dereddened) as 203 possible σ Orionis members of the same data set. Reducing the influence of the Orion A and B clouds with the help of the extinction map, we identified three associations. They all show a significantly higher (1.5σ) stellar density than the background. We constructed the MF and find the universal log-normal shape proposed by Chabrier (2005) for σ Orionis, NGC 1981, and our new clump. To probe the membership of the sources, we observed 7 of the 55 (13%) possible members of the latter. The observational outcome was very successful. 4 of those 7 show signs of membership to the region with a strong $H\alpha$ emission and a weak NaI absorption. Although their membership is doubtful due to their spectra in the KI and NaI range, this would be an observational success rate of 57%. But the new clump with its 55 members already shows a much smaller stellar density than the other two. Also, the Q-factor is lower (0.705) and indicates an even looser agglomerate not centrally condensed. If only 57% of the 55 sources would associate with each other, the clump of 31 members would probably be lost in the background. On the other hand, the clump could contain many sources fainter than our J band magnitude limit of 18 *mag*. We also remind, that our selection could be contaminated by the remnant molecular cloud [OS98]24. Up to date, no clear statement can be made to the existence of the clump. More possible members could only be found by observing the rest of the candidates. For an overview, we show the location of the three clusters in Fig. 7.5.

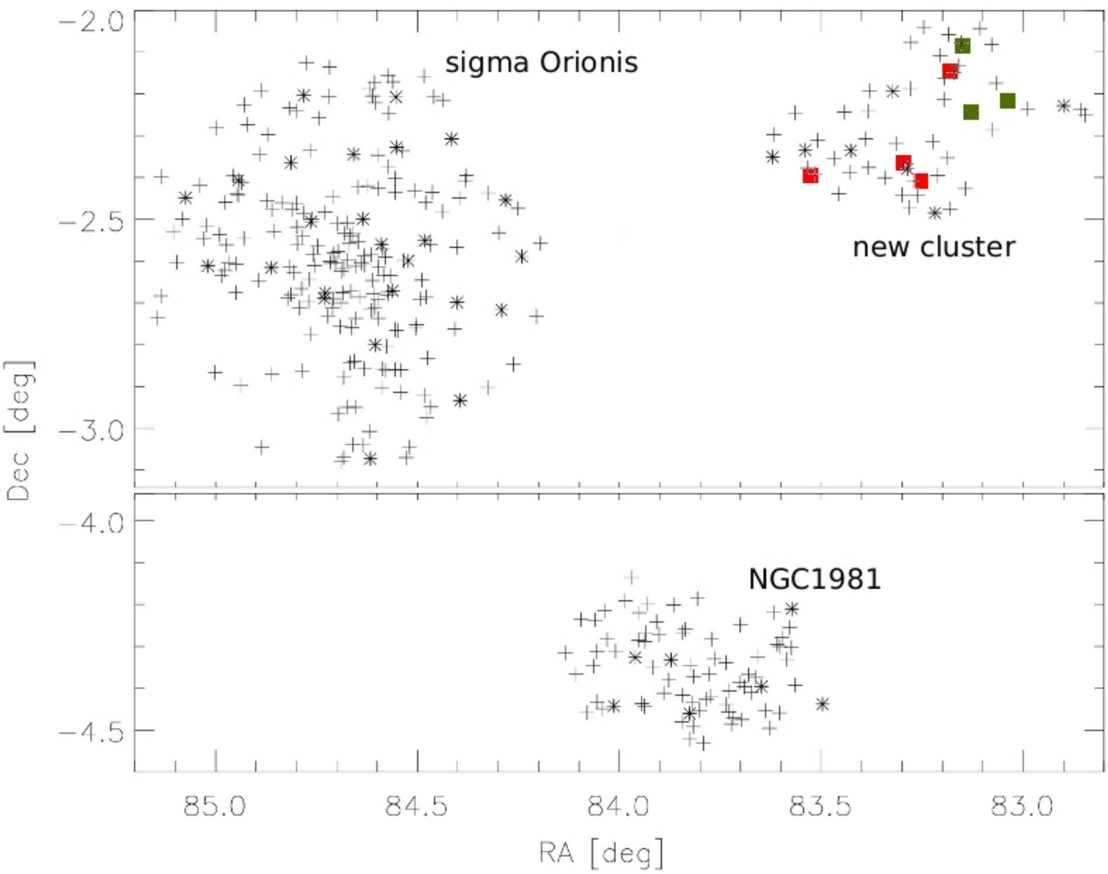

Figure 7.5: The spatial distribution of σ Orionis (top left), the newly found cluster (top right) and NGC 1981 (bottom). We show the sources with $J < 15$ *mag* (plus) and the fainter ones (asterisk). In the new cluster, we indicate the observed sources. Red marks the possible new members, green marks possible non-members.

7.3 New data in Taurus

7.3.1 UKIDSS GCS DR8 of Taurus members

With the DR8 of the UKIDSS GCS, the survey covers finally the part of Taurus, where the main clouds and the already known members are located. This data was not yet available in our research. We show CMD and CCD of the data to learn, how the additional *ZY* photometry of the members can improve and influence the search process. In Fig. 7.6 we can observe, how the filters help to define much stricter cutting lines in the CMD.

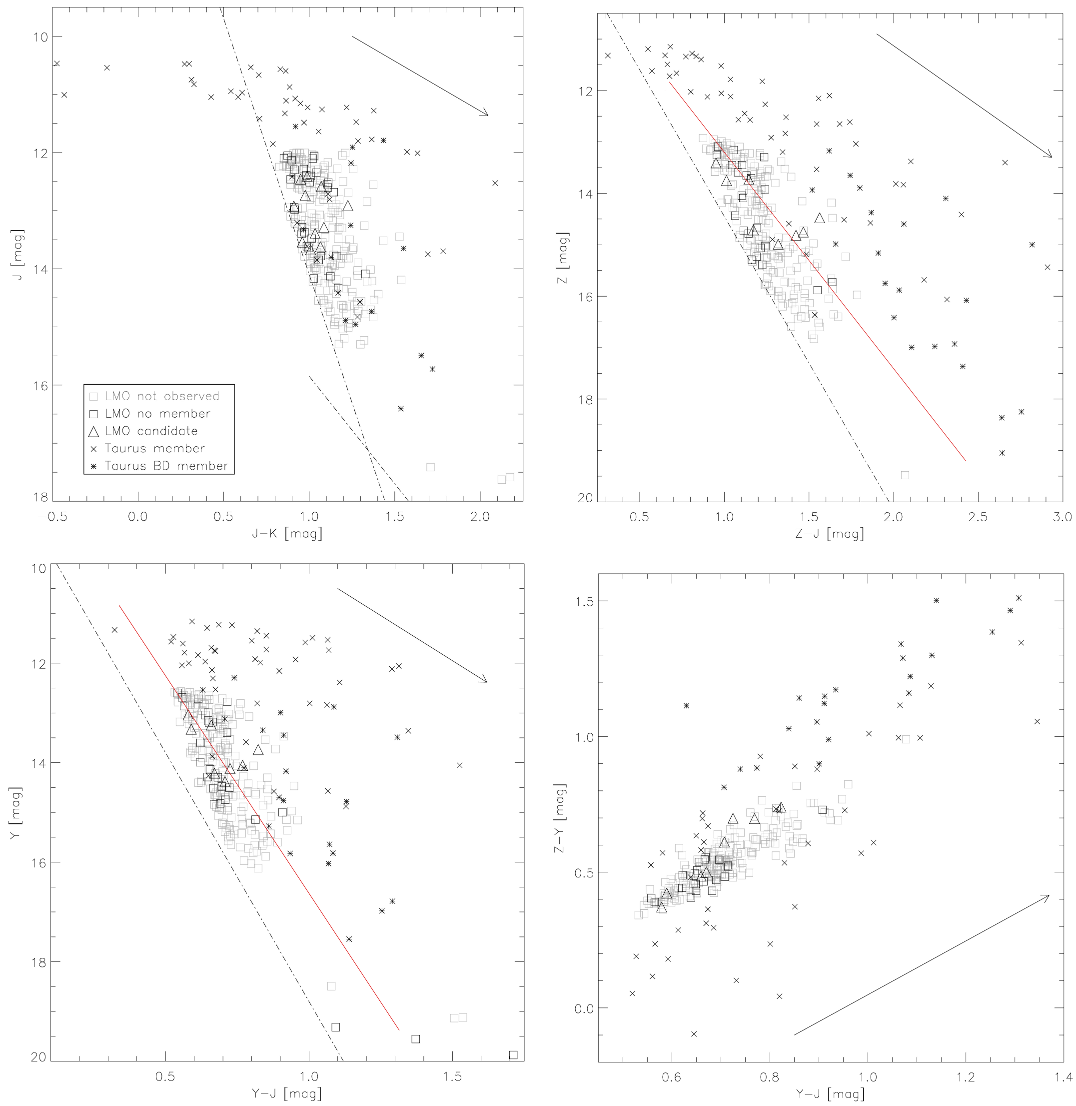

Figure 7.6: CMD and CCD of UKIDSS GCS DR8 photometry of the 272 bright and faint LMO candidates (light gray square), the 47 observed ones (dark gray square) & the 11 possible new members (triangle). We include the cutting lines by which they were selected (dash-dotted line, see also Chap. 4, Fig. 4.2, Fig. B.2 & Fig. B.3). We compare them to the data of the 82 already known Taurus members covered by the UKIDSS GCS DR8 (cross & asterisk for BD, see Tab. A). On the top left image, the $J-K$ vs. J is shown. Here, the 2MASS and UKIDSS photometry seem to describe similar limits. The $Z-J$ vs. Z CMD is shown on the top right and the $Y-J$ vs. Y CMD on the bottom left. In both diagrams, the already known Taurus member indicate a much stricter cutting line (red line) as the ones used in this work. On the other hand, some of the 11 possible members would not be selected by such criteria. On the bottom right, the $Y-J$ vs. $Z-Y$ CCD is shown. The signs get explained in the image. The arrow indicates a visual extinction of $A_V = 5\ mag$.

On the other hand, some of our 11 possible new Taurus members would not have been selected by those modified search criteria. Only in the two diagrams, where we have chosen new cuts, we would exclude at least four (36%) of them (namely UGCSJ0438+3119, UGCSJ0427+2836, UGCSJ0429+3237 and UGCSJ0421+3052). Especially UGCSJ0421+3052 is located outside our cuts in both diagrams and considered by our spectra to be a new member. Including this criteria, we downsize the number of possible new members from 7 to 6. It is very useful to investigate the UKIDSS GCS DR8 data of the already known Taurus members in detail. It would make the extraction of candidates much better in such important diagrams for the LMO search as e.g. the $Z-J$ vs. Z diagram (see publications by Lodieu et al.).

7.3.2 WISE MIR data

The data of the MIR survey WISE covers both our region A and the Taurus main clouds. It provides images and photometry in the four filters $W1$, $W2$, $W3$, $W4$ (3.4, 4.6, 12.0, 22.0 μm). At least the first two should deliver comparable data with the IRAC filters $I1$ & $I2$ at 3.6 & 4.5 μm, respectively. The last one is more similar to the MIPS filter $M1$ at 24.0 μm. The research with the data is ongoing (e.g. Aberasturi et al. 2011) to be able to characterize fully LMO with those filters. It is an interesting attempt to find locations in CCD and CMD where the different classes are located (e.g. Kirkpatrick et al. 2011). Also, the slope of the MIR passbands could be interesting. We cross-match the WISE data with our sample consisting of 272 bright and faint Taurus LMO candidates. We find counterparts for 257 objects. They all show photometry in all four filters. For our observed sources, we find 40 of 43 sources of the bright and 2 of 4 sources of the faint LMO sample. Of the 11 possible new Taurus members, 10 show counterparts. We show the data in different plots in Fig. 7.7.

The candidates are located along a straight line in the shown CMD which indicates the consistency of our search. In the $W1-W2$ vs. $W1$ and $J-W3$ vs. J diagrams, the 10 possible new members form a steeper cut. Such characteristics should be investigated precisely in the future. The cross-match with the already known Taurus members and their IRAC photometry could be an interesting work to define the new MIR data of WISE.

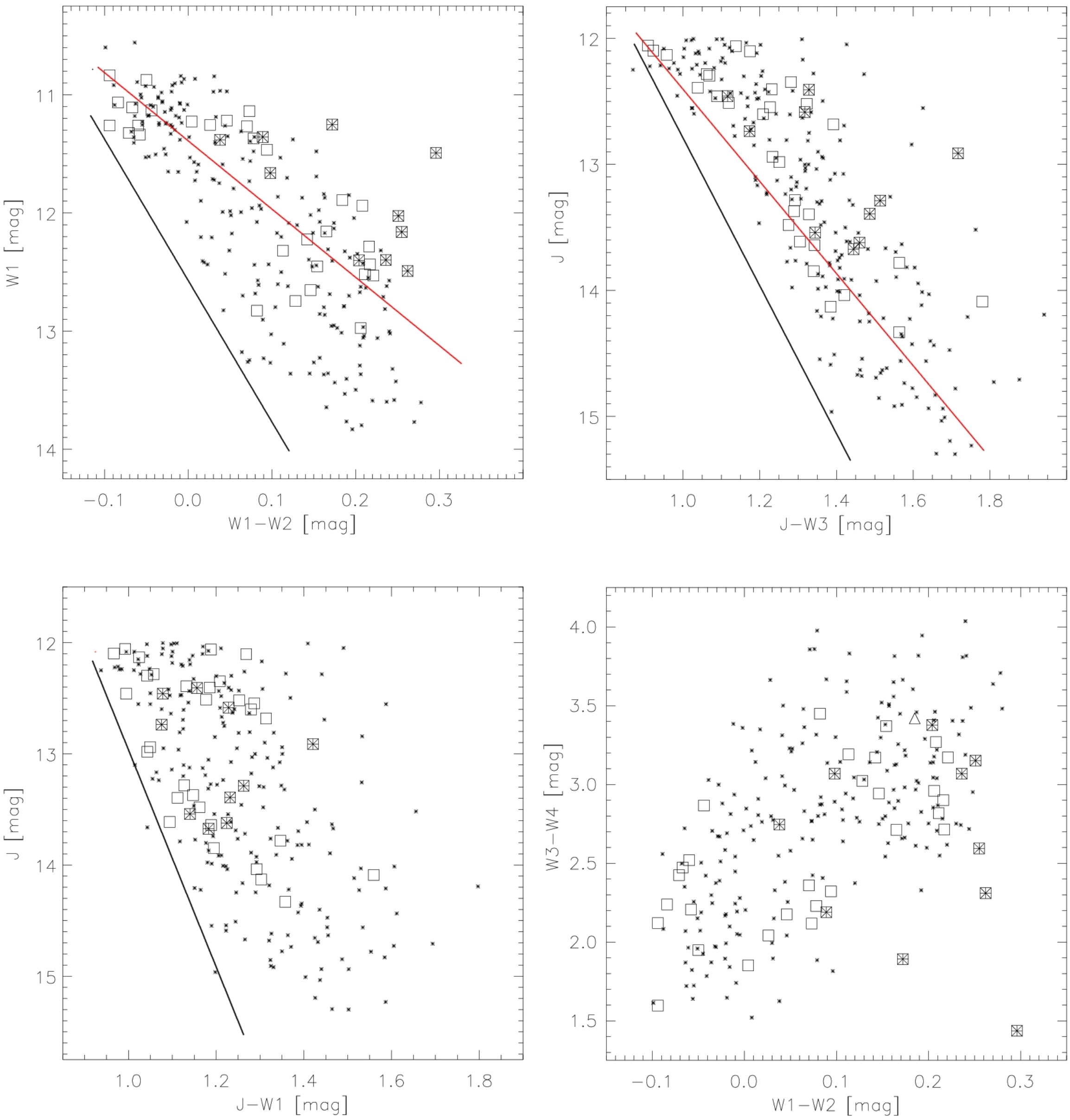

Figure 7.7: We show the data of 253 WISE counterparts of the 272 candidates of the bright and faint LMO Taurus candidate sample (small asterisk). We mark the observed sources (square) and the possible new candidates (square+asterisk). From top left to bottom right, the $W1-W2$ vs. $W1$, the $J-W3$ vs. J, the $J-W1$ vs. J and the $W1-W2$ vs. $W3-W4$ diagram are shown. We indicate possible selection cuts deducted from all 253 sources (black line) and from the 10 possible new members (red). Note: not all data points are shown because the diagrams are scaled to highlight differences.

Chapter 8

Conclusions and future work

8.1 Conclusions

- we searched an area of 25 *sq.deg.* in Taurus located 5 *deg* to the north of its main clouds.
- our extinction maps in Taurus and Orion are of high resolution (1.5 *arcmin*) and help to eliminate the effects of the extinction
- our search for new members in Taurus is the most detailed study of its kind. We used around 40 selection criteria in order to extract every available photometric characteristics of Taurus members.
- in Taurus, we observed 17% of our 253 bright LMO candidates with optical spectroscopy. Of them 26% are identified through spectral analysis as new members. By comparing them to reference spectra, we confirm only 17% as possible new members.
- we assign 36 spectral types to observed stars.
- strong $H\alpha$ emission at 6563 Å and small *NaI* absorption at 7665 and 7699 Å were most useful to probe cloud membership with our observed optical spectra.
- we recover the Taurus disk fraction of 59% by our hydrogen study. 22 of 37 already known Taurus members show strong $H\alpha$ emission at 6563 Å.
- we discover 11 and 4 possible new *M* type WTTS members of Taurus and Orion, respectively. 7 of the them show spectra similar to already known Taurus members. Of them, 6 show adequate UKIDSS GCS DR8 colors.
- in Taurus, the new members are not connected to the molecular clouds. They have moved from their birth site 5 *deg* to the south.
- instead of the former Taurus density of 1 $star \cdot pc^{-2}$ in 60 *sq.deg.*, we estimate a new density of 0.3 $star \cdot pc^{-2}$ in 260 *sq.deg.*.
- our contribution to the MF is small with around 10% and biased in the *M* type region ($0.55 > M > 0.08\ M_{\odot}$). But the existence of our new Taurus members indicates already its incompleteness in that mass range.

- if we use our observational success rate of 17%on our 253 bright LMO candidates, we would expect around 41 new Taurus member in our investigated region. If we account furthermore for the fact, that our region A forms only around 12.5% of the outer regions of Taurus, 328 new Taurus members are expected in the mentioned mass range. In that range, 104 already known Taurus members are located.
- Taurus has many undetected members not any more connected to the main molecular clouds.
- the LMO which are missing in order to change the shape of the Taurus MF towards the universal form are located outside the main clouds of the young and nearby star-forming region Taurus.
- Taurus is more stretched out and of even lower density as previously assumed.
- to answer the question for the uniqueness of the Taurus MF, to find the missing LMO and to fully understand the formation of stars and BD in Taurus, the investigation of its outer parts is essential.
- in Orion, we investigate an area of 15 *sq.deg.* and discover photometrically three stellar associations in the area. Besides σ Orionis and NGC 1981, we find a new loose stellar association consisting of 55 members with $12.0 < J < 18$ *mag* in an area of around 0.35 *sq.deg.*.
- we observed 7 of the 55 objects of the new stellar clump. 4 of them show strong $H\alpha$ emission at 6563 *Å* and small *NaI* absorption at 7665 and 7699 *Å*. Their spectra in the *KI* and *NaI* range do not resemble already known Taurus members. Nevertheless, those sources with spectral types from $M1.0$ to $M3.5$ are considered to be possible members of the region.
- with this membership success rate of 57%, 31 objects would form the new stellar association. Due to the small number of observed objects however, the existence of the association is not yet well established.

8.2 Future work

- to find new members in Taurus we can search for sources showing even lower masses than the already known ones. BD of type T show blue NIR colors and differ by very much from the red colors of the M and L type objects. Up to date there is no such object confirmed in a young and nearby SF region. Therefore, the probability to find one in the low-density region of Taurus or even in our region A is very low.
- another approach to search for disk members in Taurus is the variability of the sources. The idea is to compare the 2MASS and UKIDSS GCS values of the *JHK* photometry. It was done already in σ Orionis by Lodieu et al. (2009).
- our candidate lists should be modified with the insights the additional DR8 data of the 81 already known Taurus members and the WISE data set can deliver.
- our candidate lists should be used for further observations with large telescopes to reach down to the low-mass region. It would be possible to find new member BD in those regions, which could contribute to the question of their formation process.

- with those large 8 to 10*m* telescopes, the candidates of our list should be observed with higher resolution (> 5000) to access better the *KI* and *NaI* doublets. Also, the mentioned *LiI* line at 6708 *Å* could be measured which is another important indicator of youth. The higher resolution would also allow us to measure radial velocities of the candidates and could therefore probe more adequate the membership to the respective region.

- observations should include not only region A, but use the UKIDSS GCS DR8 data also south of 28.3 *deg* in declination.

- in the near future, UKIDSS GCS will cover more off-cloud parts of Taurus. Research and observations should include those parts.

- the UKIDSS GCS might provide second epoch photometry in the near future. The proper motions of the objects calculated by those values would show much smaller errors than the ones calculated by 2MASS. This important selection criteria could then be used more adequately.

- besides the UKIDSS survey, the outer regions of Taurus should be searched for members of the region. The answer to whether Taurus is unique or not is located in those areas.

- all candidates should be observed of our new stellar clump in Orion. Without the confirmation of the membership of a large number of candidates there is no evidence for its existence. For a better view, the observation of objects fainter than $J = 18$ *mag* would be necessary.

Bibliography

Aberasturi, M.; Solano, E.; Martín, E.L., A&A **534**, (2011) 7

Adelman-McCarthy, J.; Agueros, M.A.; Allam, S.S.; et al., ApJS **175**, (2008) 297

Allard, F.; et al., ApJ **556**, (2001) 357

Allen, L.; et al., *Protostars and Planets*, (UoA,USA,2007) 361

Ammler, M.; Joergens, V.; Neuh*ä*user, R., A&A **440**, (2005) 1127

Andre, P.; Ward-Thompson, D.; Barsony, M., ApJ **406**, (1993) 122

Bally, J., *Handbook of Star Forming Regions, Vol.1, The Northern Sky* (San Francisco, CA: ASP, 459, 2008)

Baraffe, I., et al., A&A **327**, (1997) 1054

Baraffe, I., et al., A&A **337**, (1998) 403

Baraffe, I., et al., A&A **382**, (2002) 563

Barrado, D.; et al., A&A **395**, (2002) 813

Barrado, D.; Martín, E.L., AJ **126**, (2003a) 2997

Barrado, D.; et al., A&A **404**, (2003b) 171

Barrado, D.; Huélamo, N.; Morales Calderón, M., AN **326**, (2005) 981

Barrado, D.; et al., ApJ **664**, (2007) 481

Bastian, N.; et al., MNRAS **379**, (2007) 1302

Bastian, N.; et al., MNRAS **389**, (2008) 223

Bastian, N.; Covey, K.R.; Meyer, M.R., A&A **48**, (2010) 339

Batalha, C.C.; et al., ApJS **103**, (1996) 211

Bate, M.R.; Bonnell, I.A.; Bromm, V., MNRAS **339**, (2003) 577

Battinelli, P., A&A **244**, (1991) 69

Bayo, A.; et al., A&A **492**, (2008) 277

Bayo, A.; et al., A&A **536**, (2011) 63

Béjar, V.J.S.; et al., csss **12**, (2003) 651

Béjar, V.J.S.; et al., ApJ **743**, (2011) 64

Bertout, C.; Robinchon, N.; Arenou, F., A&A **352**, (1999) 574

Bihain, G.; et al., A&A **458**, (2006) 805

Blaauw, A., psfe **125**, (1991)

Bok, B.J.; Cordwell, C.S. *Molecules in the Galactic Environment*, (Wiley, NY USA, 1973) 53

Bonnell, I.A.; Bate, M.R.; Vine, S.G., MNRAS **343**, (2003) 413

Bouy, H.; et al., A&A **504**, (2009) 199

Bricе*ñ*o, C.; et al., AJ **115**, (1998) 2074

Brice*ñ*o, C.; et al., ApJ **580**, (2002) 317

Brice*ñ*o, C.; et al., AJ **AJ**, (2005) 907

Brice*ñ*o, C.; et al., ApJ 661, (2007) 1119

Brice*ñ*o, C., *Handbook of Star Forming Regions, Vol.1, The Northern Sky*, (San Francisco, CA: ASP, 31,

2008)
Brown, A.G.A.; de Geus, E.J.; de Zeeuw, P.T., A&A **289**, (1994) 101
Burgess, A.S.M.; et al., A&A **508**, (2009) 823
Caballero, J.A.; et al., A&A **470**, (2007) 903
Caballero, J.A., AIPC **1094**, (2009) 912
Caballero, J.A.; et al., AJ **137**, (2009) 5012
Cargile, P.A.; James, D.J., AJ **140**, (2010) 677
Cartwright, A.; Whitworth, A.P., MNRAS **348**, (2004) 589
Casali, M.; et al., A&A **467**, (2007) 777
Cepa, J.; et al., SPIE **4008**, (2000) 623
Chabrier, G.; et al., ApJ **542**, (2000) 464
Chabrier, G., PASP **115**, (2003) 763
Chabrier, G., ASSL **327**, (2005) 41
Comerón, F.; Testi, L.; Natta, A., A&A **522**, (2010) 47
Cushing, M.C.; et al., ApJ **743** (2011) 50
Cutri, R.M.; et al., *2MASS All Sky Catalog of Point Sources* (NASA/IPAC,USA,2003)
Deacon, N.R.; Hambly, N.C., A&A **416**, (2004) 125
Deacon, N.R.; et al., MNRAS **394**, (2009) 857
de Wit, W.J.; Bouvier, J.; Palla, F., A&A **448**, (2006) 189
Dobashi, K.; et al., PASJ 57, (2005) 1
D'Orazi, V.; Biazzo, K.; Randich, S., A&A **526**, (2011) 103
Downes, J.J.; Briceño, C.; Hernández,J., RMxAC **26**, (2006) 37
Downes, J.J.; Abad, C.; Briceño, C., RMxAC **34**, (2008) 60
Ducourant, C.; et al., A&A **438**, (2005) 769
Fazio, G. G.; et al., ApJSS **154**, (2004) 10
Fender, R., LNP **589**, (2002) 101
Furlan, E.; et al., ApJ **703**, (2009) 1964
Golimowski, D.A.; et al., ApJ **127**, (2004) 3516
Goodman, A.A.; Pineda, J.E.; Schnee, S.L., ApJ **692**, (2009) 91
Güdel, M.; et al., A&A **468**, (2007) 353
Guieu, S.; et al., A&A **446**, (2006) 485
Guieu, S.; et al., A&A **465**, (2007) 855
Gutermuth, R.A.; et al., ApJ **674**, (2008), 336
Gutermuth, R.A.; et al., ApJS **184**, (2009), 18
Greene, T.P., et al., ApJ **434**, (1994) 614
Hauschildt, P.H.; Allard, F.; Baron, E.; Schweitzer, A., ApJ **312**, (1999) 377
Herbig, G.H.; terndrup, D.M., ApJ **307**, (1986) 609
Hernández, J.; et al., ApJ **662**, (2007) 1067
Hewett, P.C., Warren, S.J., Leggett, S.K. & Hodgkin, S.T., MNRAS **367**, (2006) 454
Hillenbrand, L.A.; Carpenter, J.M., ApJ **540**, (2000) 236
Indebetouw. R.; et al., ApJ **619**, (2005) 931
Jayawardhana, R.; Mohnaty, S.; Basri, G., ApJ **592**, (2003) 282
Kenyon, S.J.; Dobrzycka, D.; Hartmann, L., AJ **108**, (1994) 1872
Kenyon, S.J.; Hartmann, L., ApJS **101**, (1995) 117
Kenyon, S.J.; et al., MNRAS **356**, (2005) 89
Kenyon, S.J.; Gómez, M.; Whitney, B.A., *Handbook of Star Forming Regions, Vol.1, The Northern Sky*

(San Francisco, CA: ASP, 405, 2008)
Kharchenko, N.V.; et al., A&A **438**, (2005) 1163
Kirkpatrick, J.D.; et al., ApJS **197**, (2011) 19
Kirkpatrick, J.D.; et al., ApJ **753**, (2012) 156
Koen, C.; et al., MNRAS **403**, (2010) 1949
Kroupa, P., Sci **295**, (2002) 82
Lawrence, A.; et al., MNRAS **379**, (2007) 1599
Lada, C.J., IAUS **115**, (1987) 1
Lada, C.J.; et al., ApJ **429**, (1994) 694
Lada, E.A.; Lada, C.J., AJ **109**, (1995) 1682
Lada, C.J.; et al., AJ **131**, (2006) 1574
Larson, R.B., MNRAS **359**, (2005) 211
Ledrew, G., JRASC **95**, (2001) 32
Lodieu, N.; et al., A&A **436**, (2005) 853
Lodieu, N.; et al., MNRAS **380**, (2007a) 712
Lodieu, N.; et al., MNRAS **374**, (2007b) 372
Lodieu, N.; et al., MNRAS **383**, (2008) 1385
Lodieu, N.; et al., A&A **505**, (2009) 1115
Lodieu, N.; et al., A&A **418**, (2011a) 2604
Lodieu, N.; et al., A&A **532**, (2011b) 103
Lombardi, M.; Alves, J., A&A **377**, (2001) 1023
Lombardi, M., A&A **438**, (2005) 169
Lombardi, M., A&A **493**, (2009) 735
Lombardi, M.; Alves, J., A&A **512**, (2010) 67
Luhman, K., ApJ **544**, (2000) 1044
Luhman, K.; et al., ApJ **593**, (2003a) 1093
Luhman, K.; et al., ApJ **590**, (2003b) 348
Luhman, K., ApJ **617**, (2004a) 1216
Luhman, K., ApJ **602**, (2004b) 816
Luhman, K., ApJ **645**, (2006) 676
Luhman, K.; et al., ApJ **647**, (2006) 1180
Luhman, K., ApJS **173**, (2007) 104
Luhman, K.; et al., ApJ **659**, (2007) 1629
Luhman, K.; Muench, A.A., ApJ **684**, (2008a) 654
Luhman, K.; et al., ApJ **675**, (2008b) 1375
Luhman, K.; et al., ApJ **703**, (2009a) 399
Luhman, K.; et al., ApJ **691**, (2009b) 1265
Luhman, K.L.; et al., ApJ **186**, (2010), 111
Magazzu, A.; Martín, E.L.; Rebolo, R., ApJ **404**, (1993) 17
Maia, F.F.S.; Corradi, W.J.B.; Santos, J.F.C. Jr., MNRAS **407**, (2010) 1875
Manzi, S.; et al., A&A **479**, (2008) 141
Martín, E.L.; Rebolo, R.; Magazzu, A., ApJ **436**, (1994) 262
Martín, E.L.; et al., AJ **118**, (1999) 2466
Martín, E.L.,Delfosse, X. & Guieu, S., AJ **127**, (2004) 449
Martín, E.L.; et al., A&A **517**, (2010) 53
Miller, G.E.; Scalo, J.M., ApJS **41**, (1979) 513

Mohanty, S.; Basri, G.; Jayawardhana, R., AN **326**, (2005) 891

Monin, J.-L.; et al., A&A **515**, (2010) 91

Moraux, E.; et al., A&A **400**, (2003) 891

Morgan, W.W.; Keenan, P.C.; Kellman, E., *An Atlas of Stellar Spectra* (Chicago: University of Chicago Press, 1943)

Morgan, W.W.; Keenan, P.C., A&A **11**, (1973) 29

Muench, A.A.; et al., ApJ **573**, (2002) 366

Muench, A.A.; et al., ApJ **125**, (2003) 2029

Muzerolle, J.; et al., ApJ **592**, (2003a) 266

Muzerolle, J.; et al., ApJ **597**, (2003b) 149

Nakajima, T.; et al., Nature **378**, (1995) 463 Ogura, K.; Sugitani, K., PASA **15**, (1998) 91

Oliveira, J.M.; Jeffries, R.D.; van Loon, J.T., MNRAS **392**, (2009) 1034

Padoan, P.; Nordlund, A., ApJ **576**, (2002) 870

Palla, F.; Baraffe, I., A&A **432**, (2005) 57

Pavlenko, Y.V.; et al., AN **326**, (2005) 934

Pinfield, D.J.; et al., MNRAS **390**, (2008) 304

Portegies Zwart, S.F.; McMillan, S.L.W.; Gieles, M., , ARA&A **48**, (2010) 431

Preibisch, T.; et al., ApJS **160**, (2005) 582

Quanz, S.P.; et al., ApJ **708**, (2010) 770

Rebolo, R.; Martín, E.L.; Magazzu, A., ApJ **389**, (1992) 83

Rebolo, R.; Zapatero Osorio, M.R.; Martín, E.L., Nature **377**, (1995) 129

Rebolo, R.; et al., ApJ **469**, (1996) 53

Rebull, L.M.; et al., ApJS **186**, (2010), 259

Riddick, F.C.; Roche, P.F.; Lucas, P.W., MNRAS **381**, (2007) 1067

Rieke, G.H.; Lebofski, M.J., ApJ **288**, (1985) 618

Reipurth, B.; Clarke, C., AJ **122**, (2001) 432

Rodriguez, D.R.; et al., ApJ **732**, (2011) 29

Salpeter, E.E., ApJ **121**, (1955) 161

Scalo, J.M., FCPh **11**, (1986) 1

Scelsi, L.; et al., A&A **468**, (2007) 405

Scelsi, L.; et al., A&A **490**, (2008) 601

Schmeja, S.; Klessen, R.S., A&A **449**, (2006) 151

Sestito, P.; Palla, F.; Randich, S., A&A **487**, (2008) 965

Slesnick, C.L.; et al., AJ **610**, (2004) 1045

Slesnick, C.L.; et al., AJ **132**, (2006a) 2665

Slesnick, C.L.; Carpenter, J.M.; Hillenbrand, L.A., AJ **131**, (2006b) 3016

Slesnick, C.L.; Hillenbrand, L.A.; Carpenter, J.M., AJ **688**, (2008) 377

Stauffer, J.R.; et al., ApJ **504**, (1998) 805

Stauffer, J.R.; et al., ApJ **527**, (1999) 219

Takita, S.; et al., A&A **519**, (2010) 83

Terada, H.; et al., ApJ **667**, (2007) 303

West, A.A.; et al., AJ **135**, (2008) 785

Williams, J.P.; Blitz, L.; Stark, A.A., ApJ **451** (1995) 252

Williams, J.P.; Blitz, L.; McKee, C.F., *Protostars and Planets IV* (Tucson: University of Arizona Press, 2000)

Whitworth, A.; et al., *The Formation of Brown Dwarfs: Theory*, (UoA,USA,2007) 951

Wright, E.L.; et al., AJ **140**, (2010) 1868
Wu, Z.-Y.; et al., MNRAS **399**, (2009) 2146
Zacharias, N.; et al., yCAT **1297**, (2005) 0
Zapatero Osorio, M.-R., et al., IAUS **211**, (2003) 111

Appendix A

Figures and tables from Chapter 2

This appendix contains the tables and images of Chap. 2, which describes the databases used in this work. We show the photometry of field dwarf model data and the reference spectra used in this work. The data of the 351 already known Taurus members are shown as well as the 82 located in the UKIDSS GCS DR8 region. Additionally, some diagrams analyzing those datasets are put in this chapter.

type	$Z-Y$	$Z-J$	$J-H$	$H-K$	K	type	$Z-Y$	$Z-J$	$J-H$	$H-K$	K
M1.0	0.323	0.842	0.668	0.260	11.031	L6.0	1.616	2.798	1.097	0.884	18.431
M3.0	0.292	0.750	0.593	0.237	13.931	L6.5	1.747	2.976	0.834	0.675	-
M3.5	0.440	1.080	0.541	0.337	13.831	L6.5	1.280	2.468	0.699	0.484	-
M3.5	0.432	0.930	0.543	0.303	13.531	L7.5	1.184	2.309	0.594	0.425	-
M4.0	0.432	0.924	0.514	0.316	13.931	L7.5	1.461	2.621	1.049	0.822	18.631
M4.5	0.559	1.055	0.476	0.288	12.631	L8.0	1.406	2.518	0.928	0.667	18.031
M5.5	0.815	1.443	0.571	0.421	14.731	L9.0	1.631	2.720	0.827	0.618	-
M5.5	0.761	1.428	0.627	0.391	14.131	L9.0	1.470	2.603	0.870	0.653	-
M5.5	0.733	1.427	0.516	0.457	14.231	L9.0	1.542	2.567	0.942	0.688	-
M5.5	1.056	1.774	0.548	0.433	15.231	L9.5	1.664	2.857	0.583	0.698	-
M6.0	1.012	1.710	0.417	0.380	14.431	L9.5	1.738	2.953	0.587	0.546	-
M6.0	0.909	1.680	0.559	0.439	14.831	T0.0	1.410	2.476	0.743	0.506	-
M6.5	1.036	1.830	0.593	0.455	15.431	T0.0	1.513	2.579	0.870	0.730	-
M7.0	0.992	1.788	0.538	0.472	15.431	T0.0	1.517	2.631	0.799	0.550	17.731
M8.5	1.154	2.182	0.747	0.511	-	T1.0	2.133	3.281	0.604	0.472	-
L1.0	1.322	2.515	0.610	0.527	15.731	T1.5	1.787	2.884	0.546	0.224	-
L1.0	1.069	2.545	0.643	0.549	16.231	T2.0	2.020	3.277	0.567	0.332	-
L3.0	1.460	2.749	0.819	0.729	-	T2.0	1.989	3.010	0.534	0.275	18.831
L3.0	1.419	2.831	1.092	0.997	-	T2.5	1.835	2.956	0.414	0.258	-
L3.0	1.385	2.782	0.850	0.718	17.031	T3.0	2.048	3.052	0.255	0.160	-
L3.0	1.503	2.869	0.896	0.665	17.231	T3.0	2.100	3.219	0.287	0.295	-
L4.0	1.458	2.930	0.733	0.550	17.031	T3.0	2.157	3.201	0.234	−0.144	-
L4.5	1.235	2.509	0.899	0.728	-	T3.0	1.991	3.096	0.443	0.183	18.531
L4.5	1.392	2.683	0.902	0.738	-	T3.5	2.608	3.730	0.317	0.062	-
L4.5	1.418	2.681	0.857	0.792	17.131	T4.0	2.447	3.467	0.050	−0.108	-
L5.0	1.359	2.589	0.821	0.643	17.531	T4.5	2.836	3.927	−0.288	−0.251	-
L5.5	1.577	2.960	0.963	0.764	-	T4.5	2.372	3.393	0.001	−0.038	-
L5.5	1.375	2.570	0.778	0.563	-	T4.5	2.526	3.724	−0.090	−0.131	19.431
L5.5	1.443	2.505	0.810	0.636	17.131	T6.0	2.614	3.792	−0.321	−0.152	21.131
L5.5	1.411	2.569	1.186	0.971	18.331	T6.5	2.397	3.538	−0.382	0.066	20.831
L6.0	1.419	2.680	0.730	0.525	-	T7.0	3.006	4.170	−0.399	−0.023	21.331
L6.0	1.286	2.412	0.738	0.669	-	T7.5	3.083	4.029	−0.474	−0.259	22.431
L6.0	1.501	2.747	0.756	0.732	-	T8.0	3.093	4.154	−0.433	−0.152	22.731
L6.0	1.615	2.899	0.885	0.695	16.831						

Table A.1: UKIDSS GCS field star model photometry by Hewett et al. (2006). The data is translated to the Taurus distance and does not include any interstellar reddening.

Table A.2: Data of the 351 already known Taurus members from Luhman et al. 2010 and SIMBAD. Several values are included from literature: Monin et al. 2010, Rebull et al. 2010, Takita et al. 2010, Furlan et al. 2009, Luhman et al. 2009b, 2006, 2004a & 2000, Kenyon et al. 2008 & 1995, Guieu et al. 2007, Slesnick et al. 2006a, Ducourant et al. 2005, Jayawardhana et al. 2003, Muzerolle et al. 2003a & 2003b, Briceño et al. 2002. The objects are sorted by their RA and 2MASS names are shortened. The last two columns (class, α_{IRAC}) get calculated in Chap. 4.1.2. $BVRI$ are from Johnsons filter system, JHK from 2MASS and MIR data are from the IRAC passband system. Values marked with 'lit' were found in the mentioned publications.

* optical spectra observed

** used as reference spectra

name	RA [deg]	Dec [deg]	spectral type	T_{eff} [K]	$\mu_{\alpha,lit}$ [mas/yr]	$\mu_{\delta,lit}$ [mas/yr]	$A_{V,lit}$ [mag]	B [mag]	V [mag]	R [mag]	I [mag]	J [mag]	H [mag]	K [mag]	[3.6] [mag]	[4.5] [mag]	[5.8] [mag]	[8.0] [mag]	[24.0] [mag]	class	α_{IRAC}
J04034930+2610520*	60.955392	26.181072	M3.5	3580	27.0	-36.0	0.2	15.57	14.70	13.50	11.94	10.35	9.74	9.46	9.15	9.11	9.05	9.05	8.67	III	-2.715
J04034997+2620382	60.958250	26.343940	M5.25	3091	-	-	0.0	20.36	-	17.83	-	13.28	12.66	12.34	-	-	-	-	-	-	-
J04035084+2610531	60.961830	26.181440	M2	3580	6.0	-23.0	0.5	15.10	14.30	13.12	11.76	10.40	9.77	9.53	9.33	9.26	9.23	9.23	9.23	III	-2.727
J04043936+2158186	61.164040	21.971830	M3.5	3470	-11.0	8.0	0.3	16.54	15.00	12.46	10.94	10.80	10.17	9.97	9.71	9.69	9.62	9.62	-	III	-2.721
J04043984+2158215*	61.166040	21.972640	M3	3470	-17.0	0.0	0.3	16.60	15.10	12.70	11.19	10.94	10.35	10.10	9.87	9.81	9.76	9.76	-	III	-2.709
J04044307+2618563	61.179462	26.315664	K3	-	-	-	-	20.35	-	16.50	-	14.13	11.91	9.86	6.76	5.46	4.42	3.56	-	I	0.809
J04053087+2151106	61.378670	21.852970	M2	3580	31.0	11.0	0.3	16.04	15.20	13.43	12.13	10.90	10.29	10.06	9.83	9.82	9.76	9.75	9.40	III	-2.733
J04080782+2807280	62.032580	28.124440	M3.75	-	-	-	-	18.32	-	14.97	-	12.45	11.74	11.39	-	-	-	-	-	-	-
J04131414+2819108*	63.308925	28.319678	M4	3270	16.0	-29.0	1.3	15.74	14.00	12.84	11.07	9.60	8.90	8.62	8.52	8.45	8.39	8.44	8.07	III	-2.741
J04132722+2816247	63.363460	28.273560	M0	3850	-	-	3.2	15.03	13.52	12.06	-	8.83	7.79	7.46	7.22	7.18	7.10	7.07	6.94	III	-2.654
J04135328+2811233	63.472042	28.189828	M3.5-M6	3850	-	-	-	-	-	-	18.61	13.64	11.52	10.37	8.97	8.34	7.62	6.52	3.46	I	-0.019
J04135471+2811328	63.477988	28.192472	K6-M3.5	-	-	-	-	-	-	-	-	16.46	13.35	11.06	9.32	8.02	7.08	5.87	1.04	I	1.059
J04135737+2918193	63.485000	29.304200	M0	3415	-	-	4.8	17.44	-	14.43	-	11.31	10.16	9.36	7.46	6.74	6.22	5.49	3.10	II	-0.614
IRAS 04111+2800G	63.549200	28.141400	K6-M3.5	-	-	-	-	-	-	-	-	13.62	11.11	9.55	13.15	11.84	11.10	10.36	3.45	I	0.275
J04141188+2811535	63.549500	28.198190	M6.25	2962	-	-	1.1	18.47	-	17.36	-	13.16	12.33	11.64	11.01	10.35	9.88	8.99	5.83	II	-0.564
J04141291+2812124	63.553840	28.203416	K3	4730	7.0	-23.0	2.8	11.39	10.60	9.97	9.03	7.49	6.64	6.21	6.00	5.55	5.05	4.36	1.56	II	-0.949
J04141358+2812492	63.556592	28.213678	M0	3850	5.0	-36.0	2.4	15.57	14.30	13.14	12.15	10.33	9.39	8.76	8.10	7.63	7.28	6.39	2.91	II	-0.914
J04141458+2827580*	63.560792	28.466128	M5	3125	12.0	-34.0	1.6	16.30	14.60	13.48	-	9.47	8.67	8.19	7.55	7.11	6.64	5.84	2.00	II	-0.878
J04141700+2810578*	63.570846	28.182733	K3	4730	9.0	-27.0	6.9	14.84	14.20	11.75	11.42	9.56	8.24	7.13	5.86	5.38	4.98	4.39	1.61	II	-1.167
J04141760+2806096	63.573380	28.102690	M5.5	3058	-	-	4.6	18.15	-	15.86	14.33	11.73	10.58	9.88	8.64	8.10	7.59	6.57	3.50	II	-0.483
J04142626+2806032	63.609450	28.100903	M2.5	3488	-	-	17.1	21.36	-	18.91	17.84	12.48	9.88	7.78	6.00	5.18	4.63	3.90	0.45	I	-0.475
J04142639+2805597	63.609996	28.099922	M2.5	3488	-	-	0.5	21.36	-	18.91	15.79	11.45	9.25	7.80	7.50	6.61	5.92	4.99	-	I	0.006
J04143054+2805147	63.626750	28.087750	K7	4060	-	-	11.3	20.24	-	16.84	14.49	11.18	9.25	8.24	7.21	6.44	5.69	4.57	0.45	I	0.181
J04144730+2646264*	63.697121	26.774011	M4	3370	14.0	-24.0	0.8	14.81	14.00	12.13	11.33	9.90	9.18	8.87	8.07	7.78	7.58	7.28	4.28	III	-1.947
J04144739+2803055	63.697500	28.051530	M5.25	3091	-	-	0.0	17.33	-	15.09	-	10.80	10.17	9.92	9.61	9.58	9.50	9.50	9.37	III	-2.697
J04144786+2648110	63.699437	26.803058	M2.5	3580	14.0	-23.0	1.4	15.18	13.90	12.63	11.26	9.87	9.05	8.81	8.51	8.01	7.64	6.62	3.38	II	-0.714
J04144797+2752346	63.699888	27.876292	M1	3705	6.0	-21.0	0.7	13.60	12.20	11.05	9.79	8.36	7.63	7.42	7.26	7.28	7.22	7.22	7.09	III	-2.773
J04144928+2812305	63.705371	28.208497	M3.5	3560	3.0	-25.0	3.7	16.97	15.40	13.79	11.85	9.65	8.57	8.12	7.47	7.09	6.72	5.88	2.88	II	-1.030
J04145234+2805598	63.718080	28.099940	M3.25	3379	-	-	0.2	17.30	-	14.20	-	9.53	8.21	7.71	7.40	7.36	7.24	7.21	7.15	III	-2.599
J04150515+2808462	63.771500	28.146170	M5.5	3058	-	-	0.6	17.12	-	14.52	13.55	11.40	10.58	9.09	8.83	8.73	8.67	8.64	8.50	III	-2.623
J04151471+2800096	63.811290	28.002670	M8.5	-	-	-	0.4	-	24.06	-	18.43	15.09	14.25	13.77	13.18	13.04	13.09	13.09	10.61	III	-2.768
J04152409+2910434	63.850420	29.178750	M7	-	-	-	1.2	-	-	18.95	-	13.69	12.89	12.36	11.81	11.71	11.62	11.50	10.06	III	-2.482
J04153916+2818586	63.913178	28.316282	M3.75	3306	-	-	0.2	17.58	-	14.77	-	10.55	9.61	9.24	8.73	8.43	8.23	7.53	4.20	II	-1.496
J04154278+2909597	63.928283	29.166586	M1.25	3669	-	-	0.2	17.30	-	14.30	-	10.71	9.76	9.38	9.09	9.06	8.97	9.05	4.50	III	-2.772
J04155799+2746175	63.991642	27.771547	M5.5	3058	-	-	0.0	18.60	-	16.80	-	11.75	10.99	10.52	9.71	9.37	9.04	8.36	5.78	II	-1.301
J04161210+2756385	64.050420	27.944060	M4.75	3161	-	-	4.6	19.89	-	17.65	-	12.28	11.12	10.34	9.35	8.99	8.69	8.29	5.38	II	-1.631
J04161885+2752155	64.078580	27.870970	M6.25	-	-	-	1.1	20.58	-	18.64	-	12.55	11.78	11.35	10.92	10.74	10.64	10.68	9.95	III	-2.567
J04162725+2053091	64.113580	20.885890	M5	-	-	-	-	18.60	-	16.80	14.90	12.05	11.47	11.11	10.77	10.67	10.65	10.59	-	III	-2.645
J04162810+2807358	64.117121	28.126614	K7	4060	8.0	-24.0	0.8	14.49	12.80	11.71	10.56	9.30	8.50	8.32	8.19	8.17	7.99	8.03	7.96	III	-2.614
J04163048+3037053	64.127040	30.618140	M4.5	3198	-	-	0.1	19.88	-	18.06	-	13.62	12.97	12.62	12.29	12.17	12.16	12.23	-	III	-2.783
J04163911+2858491	64.163000	28.980310	M5.5	-	-	-	2.3	20.35	-	18.73	-	12.72	11.84	11.28	10.46	10.07	9.82	9.41	7.25	II	-1.660
J04173372+2820468	64.390525	28.346347	M1.5	3632	12.0	-24.0	1.7	15.15	13.40	12.50	11.20	9.83	8.97	8.60	7.63	7.25	7.02	6.48	4.41	II	-1.553
J04173893+2833005*	64.412250	28.550142	M2	3560	7.0	-33.0	0.2	15.59	13.60	12.70	11.33	9.98	9.29	9.05	8.90	8.84	8.78	8.76	8.60	III	-2.673
J04174955+2813318*	64.456475	28.225514	M5	-	-3.0	-30.0	1.1	19.10	17.80	16.50	-	11.89	11.14	10.79	10.80	10.29	9.88	8.81	5.93	II	-0.594
J04174965+2829362	64.456870	28.493420	M4	3270	-	-	5.5	17.26	-	14.22	13.78	11.02	9.73	9.08	8.41	7.76	7.39	6.42	3.81	II	-0.623
J04180796+2826036	64.533170	28.434360	M6	2990	-	-	0.8	19.62	18.32	16.92	14.18	12.95	11.66	10.45	9.99	9.91	9.78	9.81	8.74	III	-2.613

Table A.2 – continued from previous page

name	RA	Dec	spectral	T_{eff}	$\mu\alpha$	μ_δ	A_V	B	V	R	I	J	H	K	[3.6]	[4.5]	[5.8]	[8.0]	[24.0]	class	α_{IRAC}
	[deg]	[deg]	type	[K]	[mas/yr]	[mas/yr]	[mag]	[mag]	[mag]	[mag]	[mag]	[mag]	[mag]	[mag]	[mag]	[mag]	[mag]	[mag]	[mag]		
J04181078+2519574	64.544954	25.332630	M1.5	3632	-	-	0.4	15.92	-	12.26	-	10.74	9.59	9.03	8.05	7.70	7.25	6.30	4.49	II	-0.828
J04181710+2828419	64.571290	28.478310	M5.75	3024	-	-	5.9	-	22.18	18.95	16.59	12.95	11.64	10.96	10.20	9.92	9.47	8.80	6.03	II	-1.206
J04182147+1658470	64.589460	16.979720	K5	4350	11.0	-14.0	0.0	14.32	13.60	13.50	12.89	11.18	10.60	10.46	10.39	10.39	10.40	10.33	-	III	-2.772
J04182909+2826191	64.621250	28.438640	M1	3705	-	-	22.9	-	-	-	-	14.90	11.63	9.94	8.92	8.56	8.31	8.37	8.18	III	-2.208
J04183030+2743208	64.626275	27.722453	M5.5	-	13.0	-27.0	0.0	18.90	-	16.10	-	11.89	11.27	11.01	10.66	10.54	10.55	10.49	10.01	III	-2.666
J04183110+2827162	64.629615	28.454480	K7	4060	6.0	-31.0	1.1	11.48	10.80	9.88	9.34	8.45	7.79	7.63	7.37	7.31	7.29	7.24	7.11	III	-2.695
J04183112+2816290*	64.629700	28.274728	M3.5	3415	7.0	-35.0	4.3	15.67	14.60	13.40	11.58	9.83	8.68	7.88	6.45	5.78	5.23	4.42	1.67	II	-0.533
J04183158+2816585	64.631613	28.282925	M3	3415	7.0	-35.0	0.7	16.27	15.50	14.50	12.38	10.52	9.77	9.36	8.46	7.55	6.63	4.95	1.94	I	1.169
J04183203+2831153	64.633460	28.520940	M2.5	3488	-	-	19.0	-	-	-	19.65	15.19	12.37	10.27	7.55	6.99	6.06	5.47	1.82	II	-0.363
J04183444+2830302	64.643540	28.508390	M0	3850	-	-	21.0	-	-	-	-	13.77	10.71	9.22	8.30	8.04	7.77	7.66	3.34	III	-2.091
J04184023+2824245	64.667630	28.406810	M4	3270	-	-	18.0	-	-	-	19.91	13.55	10.93	9.69	8.85	8.58	8.55	8.41	8.20	III	-2.377
J04184061+2819155	64.669250	28.320970	B9	10500	12.0	-30.0	14.3	16.60	15.20	13.96	11.43	8.74	7.02	5.79	6.62	6.10	3.56	3.52	0.45	III	1.198
J04184133+2827250	64.672210	28.456940	K4.5	4470	-	-	24.0	-	-	-	-	16.23	12.92	11.05	9.38	8.82	8.35	7.97	4.64	III	-1.225
J04184250+2818498	64.677080	28.313830	M0.75	3741	-	-	10.3	-	-	18.49	15.92	11.91	10.08	9.26	8.86	8.56	8.37	8.04	5.15	III	-1.918
J04184703+2820073	64.695987	28.335367	K7	4060	11.0	-32.0	2.5	13.34	12.60	11.93	10.65	8.56	7.64	7.29	7.11	7.01	6.98	6.94	6.60	III	-2.653
J04185115+2814332	64.713170	28.242560	M7.5	-	-	-	0.4	-	21.38	18.95	16.44	13.92	13.24	12.75	12.21	12.07	11.96	11.76	9.59	III	-2.328
J04185147+2820264	64.714496	28.340681	M0	3850	28.0	10.0	6.5	19.56	19.30	16.06	15.96	12.87	11.49	10.97	10.19	8.96	7.72	5.84	0.84	I	2.142
J04185170+1723165*	64.715420	17.387940	K7	4060	9.0	-15.0	0.0	12.91	12.50	11.41	10.74	10.02	9.41	9.27	9.24	9.20	9.16	9.13	8.95	III	-2.709
J04185813+2812234	64.742250	28.206530	M5.25	3705	-	-	7.0	20.02	19.15	17.94	16.43	13.78	12.35	11.18	9.26	8.43	7.78	6.92	2.73	I	-0.185
J04190110+2819420	64.754620	28.328330	M5.5	3058	-	-	2.7	18.95	-	16.50	13.48	10.53	9.60	9.13	8.85	8.59	8.49	8.25	3.69	III	-2.180
J04190126+2802487	64.755290	28.046860	M9	-	-	-	0.5	-	23.23	-	-	16.31	15.49	14.93	13.93	13.54	13.17	12.66	10.13	II	-1.385
J04190197+2822332	64.758250	28.375890	M5.5	3058	-	-	5.1	21.28	-	18.48	15.37	11.98	10.78	10.15	9.65	9.58	9.48	9.48	9.08	III	-2.631
J04191281+2829330	64.803379	28.492528	M3	3270	2.0	-32.0	1.1	16.81	15.80	14.33	11.77	10.49	9.70	9.31	8.72	8.35	8.09	7.42	4.82	II	-1.378
J04191583+2906269	64.815980	29.107470	K7	4060	10.6	-29.1	2.1	13.36	-	-	10.45	9.10	8.22	7.74	7.23	6.84	6.61	5.66	2.51	II	-1.091
J04192625+2826142	64.859417	28.437306	K7	4060	9.0	-32.0	1.9	15.26	13.00	12.01	10.45	9.49	8.64	8.42	8.20	8.24	8.13	8.04	6.36	III	-2.625
J04193545+2827218	64.897710	28.456060	M5.25	3091	7.0	-26.0	0.0	17.26	16.20	14.84	-	10.95	10.37	9.97	9.43	8.87	8.32	7.26	4.82	II	-0.364
J04194127+2749484	64.921967	27.830136	M0	4060	5.0	-31.0	1.0	14.23	12.50	11.76	10.58	9.12	8.38	8.26	8.05	8.05	8.01	7.96	7.79	III	-2.726
J04194148+2716070	64.922830	27.268610	K6-M3.5	-	-	-	-	-	-	-	-	14.71	13.41	12.62	11.19	10.36	9.75	9.31	3.25	I	-0.703
IRAS 04166+2706	64.927100	27.227800	K6-M3.5	-	-	-	-	-	-	-	-	14.71	13.41	12.62	12.84	11.26	10.43	9.90	2.90	I	0.430
J04194657+2712552	64.944062	27.215336	M7.5	2795	-	-	2.1	-	-	-	-	-	14.03	11.89	10.27	9.40	8.84	8.16	4.07	I	-0.468
J04195844+2709570	64.993540	27.165860	K6-M3.5	-	-	-	-	-	-	-	-	18.24	14.15	11.58	8.31	7.08	6.21	5.28	0.66	I	0.585
J04201611+2821325	65.067129	28.359041	M6.5	2935	-	-	0.0	20.56	-	18.42	-	13.78	13.12	12.55	11.81	11.40	11.11	10.56	8.20	II	-1.431
J04202144+2813491	65.089345	28.230326	M1	3705	-	-	-	19.20	-	17.20	-	15.83	14.76	14.05	12.71	12.29	12.09	11.56	8.68	II	-1.566
J04202555+2700355	65.106460	27.009860	M5.25	3091	-	-	2.1	20.55	-	18.75	-	12.87	12.01	11.51	10.93	10.68	10.43	9.75	6.07	II	-1.498
J04202583+2819237	65.107642	28.323265	mid-M	-	-	-	-	20.40	-	18.02	-	15.33	13.42	11.72	9.18	8.40	7.91	7.13	3.83	II	-0.541
J04202606+2804089	65.108609	28.069153	M3.5	3342	-	-	0.0	16.41	-	13.90	-	10.61	9.95	9.70	9.29	8.95	8.57	7.03	3.25	I/II	-0.282
J04203918+2717317	65.163250	27.292140	M4.5	3198	6.0	-18.0	0.0	18.15	-	16.22	-	10.50	9.86	9.56	9.40	9.44	9.31	9.31	8.91	III	-2.697
J04205273+1746415	65.219290	17.778140	M5.5	3145	-	-	0.0	17.12	-	15.52	-	11.62	11.04	10.78	10.44	10.35	10.31	10.28	-	III	-2.660
J04210795+2702204	65.283120	27.039000	M5.25	3024	-	-	10.3	-	-	18.85	15.10	13.86	12.06	10.54	7.58	6.59	6.00	5.12	1.50	I	-0.089
J04210934+2750368	65.288930	27.843567	M5.25	3091	-	-	0.0	17.77	-	15.55	-	11.23	10.66	10.36	10.00	9.72	9.58	9.20	7.17	III	-1.951
J04211038+2701372	65.293283	27.027017	K7	-	-	-	-	-	-	-	-	-	13.78	11.05	9.00	8.28	7.60	6.76	2.67	II	-0.273
J04211146+2701094	65.297787	27.019278	M3	3125	-	-	-	-	-	-	-	16.22	12.65	10.34	8.61	7.51	6.69	5.67	1.52	I	0.489
J04213459+2701388	65.394170	27.027440	M5.5	3058	-	-	2.7	20.46	-	17.32	-	11.90	10.97	10.44	9.91	9.61	9.34	8.98	7.19	III	-1.775
J04214013+2814224	65.417250	28.239580	M5.75	3024	-	-	0.0	18.15	-	16.22	-	11.93	11.34	11.03	10.63	10.58	10.54	10.52	-	III	-2.710
J04214323+1934133	65.430170	19.570360	M0	3850	-	-	-	16.99	-	14.86	-	10.19	8.73	8.02	6.96	6.29	5.53	4.36	-	I	0.152
J04214631+2659296	65.442960	26.991560	M5.75	-	-	-	3.6	-	-	-	-	13.82	12.73	12.31	11.53	11.27	11.01	10.58	7.23	II	-1.751
J04215450+2652315	65.477130	26.875420	M8.5	-	-	-	3.0	-	-	-	-	15.54	14.50	13.90	13.17	13.07	12.88	12.84	10.50	III	-2.434
J04215563+2755060*	65.481817	27.918350	M1	3580	22.0	-12.0	2.2	14.98	13.30	11.89	10.42	9.18	8.27	7.80	7.02	6.67	6.35	5.67	2.58	II	-1.304
IRAM 04191+1522	65.487130	15.496080	-	-	-	-	-	-	-	-	-	-	-	-	15.32	13.81	13.23	12.90	6.64	I	-0.202
J04215740+2826355*	65.489208	28.443214	K1	5080	10.0	-29.0	4.8	10.73	10.10	9.62	8.80	7.16	6.13	5.40	6.62	6.10	3.48	3.52	0.45	III	1.220
J04215884+2818066	65.495196	28.301807	G5	5770	8.0	-27.0	0.4	9.44	9.30	8.56	8.10	7.41	7.01	6.87	6.83	6.85	6.76	6.76	6.75	III	-2.732
J04215943+1932063*	65.497583	19.535133	K0	5250	14.0	-12.0	1.8	10.47	10.20	9.19	8.50	7.24	6.24	5.33	-	-	2.65	-	-	-	-
J04220007+1530248	65.500317	15.506903	M6-M8	-	-	-	-	-	-	-	-	10.60	8.01	6.18	12.19	11.23	10.74	9.84	-	I	-0.233
J04220043+1530212	65.501829	15.505892	K6-M3.5	-	-	-	-	-	-	-	-	15.89	13.73	12.26	9.56	8.29	7.31	6.26	1.68	I	0.907
J04220069+2657324	65.502904	26.959025	K5	-	8.0	-17.0	-	-	-	-	-	15.08	13.35	11.75	9.63	8.35	7.16	5.86	1.47	I	1.481

Table A.2 – continued from previous page

name	RA	Dec	spectral	T_{eff}	$\mu\alpha$	μ_δ	A_V	B	V	R	I	J	H	K	[3.6]	[4.5]	[5.8]	[8.0]	[24.0]	class	α_{IRAC}
	[deg]	[deg]	type	[K]	[mas/yr]	[mas/yr]	[mag]	[mag]	[mag]	[mag]	[mag]	[mag]	[mag]	[mag]	[mag]	[mag]	[mag]	[mag]	[mag]		
J04220217+2657304	65.509071	26.958469	M0	3720	4.0	-18.0	6.9	13.78	-	11.33	-	10.71	9.24	8.18	6.76	6.37	5.76	4.89	1.25	II	-0.658
J04220313+2825389	65.513075	28.427497	M3	3470	12.0	-30.0	1.3	15.32	13.60	12.45	-	9.46	8.67	8.45	8.22	8.17	8.13	8.10	7.76	III	-2.699
J04221332+1934392	65.555500	19.577560	M8	-	-	-	-	19.86	-	19.34	-	12.87	12.06	11.53	11.02	10.89	10.82	10.59	-	III	-2.359
J04221568+2657060	65.565341	26.951694	M1	3705	12.0	-16.0	0.1	20.18	-	17.16	-	13.81	12.62	12.03	11.05	10.49	10.20	9.73	3.81	II	-1.373
J04221644+2549118	65.568500	25.819940	M7.75	2300	-	-	0.6	20.49	-	19.07	18.73	13.07	12.37	11.94	11.45	11.26	11.21	11.22	9.51	III	-2.593
J04221675+2654570	65.569830	26.915860	M1.5	2752	-	-	7.7	19.36	17.80	-	-	11.58	10.04	9.01	7.71	7.23	6.79	6.18	3.31	II	-1.090
J04222404+2646258	65.600210	26.773830	M4.75	3161	10.0	-10.0	0.1	18.71	-	15.91	-	11.09	10.19	9.77	9.45	9.36	9.30	9.33	8.98	III	-2.699
J04224786+2645530*	65.699455	26.764736	M1	3850	-	-	0.2	19.56	-	16.10	15.12	11.59	10.15	9.29	8.11	7.55	7.02	6.27	3.25	II	-0.734
J04230607+2801194*	65.775303	28.022081	M6	-	-	-	-	20.20	-	16.98	-	12.24	11.61	11.20	10.58	10.22	9.93	9.35	6.41	II	-1.446
J04230776+2805573	65.782380	28.099250	M2	3785	-	-	8.1	17.71	-	16.66	15.49	13.18	11.60	10.41	8.42	7.74	7.30	6.41	3.26	II	-0.586
J04231822+2641156	65.825957	26.687672	M3.5	-	4.0	-18.0	-	19.58	-	19.34	-	12.66	11.02	10.18	9.39	9.15	8.76	8.12	4.54	II	-1.360
J04233539+2503026	65.897483	25.050739	M7.25	2838	14.0	-26.0	0.2	19.10	-	16.70	-	10.78	9.95	9.32	8.34	7.87	7.33	6.71	4.62	II	-0.952
J04233573+2502596	65.898920	25.049890	M9.25	2350	-	-	0.0	-	-	-	-	15.04	13.91	13.33	12.54	11.93	11.46	10.87	-	II	-0.944
J04233919+2456141	65.913290	24.937250	M3	-	-11.0	-13.0	3.8	15.72	15.00	12.65	-	10.19	9.12	8.60	7.89	7.44	7.12	6.27	3.15	II	-1.019
J04242090+2630511	66.087089	26.514210	M6.5	-	-	-	0.9	20.34	-	18.73	-	13.49	12.81	12.43	11.80	11.41	11.00	10.37	7.48	II	-1.197
J04242646+2649503	66.110250	26.830670	M5.75	-	-	-	0.9	20.59	-	18.30	15.35	12.88	12.19	11.76	11.11	10.80	10.48	9.85	6.79	II	-1.399
J04244457+2610141	66.185750	26.170580	M0.5	3720	-	-	3.4	18.33	-	15.46	-	10.79	9.75	9.05	8.07	7.56	7.07	6.25	3.51	II	-0.761
J04244506+2701447	66.187758	27.029092	M5	3240	2.0	-25.0	0.1	17.62	16.24	15.16	-	11.35	10.72	10.46	10.18	10.14	10.02	10.06	9.49	III	-2.677
J04245708+2711565	66.237833	27.199028	M0	3850	8.0	-26.0	1.9	14.46	13.60	12.70	11.06	9.78	8.89	8.35	7.67	7.38	7.20	6.61	3.46	II	-1.654
J1-4872 A	66.323575	26.297310	M1	4060	19.0	-16.0	3.7	-	13.05	-	-	-	-	-	8.32	8.24	8.30	8.18	7.65	III	-2.708
J1-4872 B	66.323630	26.297330	K7	-	19.0	-16.0	3.7	-	13.86	-	-	-	-	-	9.02	8.95	8.82	8.88	7.65	III	-2.656
J04262939+2624137	66.622460	26.403830	M6	-	-	-	1.6	-	20.24	19.02	15.77	13.32	12.50	12.08	11.39	10.97	10.45	9.70	6.87	II	-0.885
J04263055+2443558	66.627290	24.732190	M8.75	-	-	-	0.0	-	-	-	-	14.66	13.94	13.40	12.56	12.15	11.76	11.06	9.13	II	-1.128
J04265352+2606543	66.723038	26.115103	K5	4350	-7.0	-27.0	8.7	17.47	16.30	14.00	12.72	9.92	8.33	7.44	6.32	5.79	5.20	4.42	1.46	II	-0.648
J04265440+2606510	66.726710	26.114170	M2.5	3342	8.0	-30.0	5.9	18.69	17.20	15.46	13.47	10.80	9.49	8.87	8.03	7.51	6.99	6.28	3.88	II	-0.831
J04265629+2443353	66.734800	24.726500	K6-M3.5	4900	-	-	4.1	-	-	-	-	15.75	12.35	9.99	7.57	6.27	5.34	4.49	0.45	I	0.647
J04265732+2606284	66.738870	26.107890	M5	-	-	-	4.3	19.78	-	16.64	-	11.28	10.17	9.58	8.75	8.32	7.91	7.37	5.30	II	-1.258
J04270266+2605304	66.761080	26.091810	<K6	3955	-	-	-	-	-	19.39	17.66	16.52	13.53	12.04	8.78	7.07	5.72	4.62	0.78	I	1.899
J04270280+2542223*	66.761642	25.706221	M2	3415	12.8	-19.1	2.4	12.96	12.30	-	9.86	8.17	7.26	6.73	6.03	5.36	4.99	4.42	2.23	II	-1.045
J04270469+2606163	66.769575	26.104531	K6	4205	3.0	-24.0	3.2	13.97	12.90	11.40	10.54	8.69	7.72	6.99	6.62	5.05	4.41	3.57	0.45	I	0.502
J04270739+2215037	66.780830	22.251060	M6.75	-	-	-	-	-	-	17.70	15.40	12.27	11.64	11.29	10.90	10.78	10.74	10.73	-	III	-2.653
J04272799+2612052**	66.866670	26.201470	M9.5	-	-	-	2.5	-	24.72	19.70	18.75	15.00	14.02	13.28	12.54	12.32	12.23	12.13	10.66	III	-2.387
J04274538+2357243	66.939080	23.956750	M8.25	2795	-	-	1.3	-	-	-	17.94	14.93	14.24	13.69	13.20	13.05	12.98	13.00	10.55	III	-2.616
J04275730+2619183	66.988790	26.321750	M4.5	3560	-	-	5.8	20.58	-	15.73	14.69	13.24	11.80	11.03	9.78	9.02	8.26	7.11	2.23	I	0.218
J04284263+2714039	67.177630	27.234420	M5.25	3091	-	-	3.7	17.51	-	16.81	-	12.11	11.07	10.46	9.69	9.45	9.19	8.83	6.27	III	-1.848
J04290068+2755033	67.252830	27.917610	M8.25	-	-	-	0.0	-	-	-	-	14.01	13.32	12.85	12.25	11.95	11.58	10.96	8.08	II	-1.351
J04290498+2649073	67.270790	26.818690	K5.5	3240	-	-	9.1	19.97	16.24	18.46	-	14.67	13.02	11.88	10.03	9.34	8.86	8.08	3.35	II	-0.643
J04292071+2633406	67.336290	26.561310	M4	3270	-	-	0.9	16.08	14.58	13.56	-	9.82	9.09	8.79	8.51	8.52	8.45	8.48	8.25	III	-2.783
J04292165+2701259	67.340210	27.023860	M5.25	3240	-	-	5.9	-	15.96	17.96	-	10.80	9.50	8.73	8.07	7.64	7.27	6.64	3.42	II	-1.213
J04292373+2433002*	67.348880	24.550080	K5	4730	-	-	11.9	17.62	16.55	13.13	12.80	11.54	9.59	8.05	6.62	6.10	2.64	3.52	0.45	III	1.444
J04292971+2616532	67.373792	26.281447	M5.5	3058	10.0	-22.0	0.3	17.47	-	14.65	12.38	10.34	9.68	9.39	9.07	8.90	8.90	8.87	7.64	III	-2.637
J04293008+2439550	67.375300	24.665186	M1	3125	-14.0	4.0	9.5	18.40	-	18.42	14.67	13.73	11.98	11.14	10.16	9.40	8.55	6.70	1.09	I	1.115
J04293209+2430597	67.383729	24.516597	K6-M3.5	-	-	-	-	-	-	-	-	-	15.65	13.72	10.36	9.22	8.29	7.31	3.94	I	0.635
J04293606+2435556*	67.400276	24.598793	M3	-	-	-	-	18.32	-	16.17	-	10.78	9.39	8.66	7.99	7.71	7.42	6.96	4.11	II	-1.657
J04294155+2632582	67.423158	26.549519	M1	3705	5.0	-13.0	2.5	14.96	14.00	12.09	11.50	9.77	8.82	8.18	7.60	7.41	7.19	6.81	3.21	III	-1.929
J04294247+2632493	67.426979	26.547031	M0	3850	13.0	-19.0	0.5	14.12	13.00	11.74	10.67	9.32	8.60	8.39	8.22	8.20	8.11	8.10	-	III	-2.682
J04294568+2630468**	67.440330	26.513000	M7.5	-	-	-	0.0	20.56	19.69	18.68	15.08	12.64	11.92	11.54	11.04	10.93	10.89	10.84	9.71	III	-2.619
J04295156+2606448	67.464846	26.112472	M0.5	3778	15.0	-25.0	2.9	15.60	14.10	12.14	11.43	9.42	8.42	7.78	6.73	6.32	6.02	5.46	2.84	II	-1.406
J04295422+1754041*	67.475960	17.901140	M4	-	-	-	-	-	-	-	-	12.65	11.71	11.02	-	-	-	-	-	-	-
J04295950+2433078	67.497960	24.552190	M5	2795	-	-	4.6	20.52	18.50	17.15	15.70	11.69	10.54	9.81	9.03	8.56	8.31	7.80	4.86	II	-1.471
J04300357+1813494	67.514920	18.230420	M2	3705	7.0	-14.0	-	12.04	11.20	10.30	-	9.87	8.95	7.55	8.75	8.75	8.69	8.66	-	III	-2.721
J04300399+1813493	67.516628	18.230386	K5	4900	7.0	-14.0	0.7	12.04	11.20	10.30	-	8.62	7.96	7.55	6.66	6.37	6.16	5.93	1.83	III	-2.011
J04300724+2608207	67.530170	26.139110	M8.5	-	-	-	0.9	-	22.29	19.42	17.90	14.99	14.20	13.69	13.09	12.73	12.41	11.54	9.20	II	-1.085
J04302365+2359129	67.598540	23.986940	M8.25	2555	-	-	1.5	18.14	-	-	17.91	14.96	14.24	13.70	13.21	13.11	13.03	13.02	10.54	III	-2.618
J04302961+2426450	67.623392	24.445847	M1	3720	8.0	-21.0	2.9	15.01	13.50	12.71	10.95	9.39	8.40	7.92	7.17	6.87	6.66	5.94	2.88	II	-1.460

Table A.2 – continued from previous page

name	RA	Dec	spectral	T_{eff}	$\mu\alpha$	μ_δ	A_V	B	V	R	I	J	H	K	[3.6]	[4.5]	[5.8]	[8.0]	[24.0]	class	α_{IRAC}
	[deg]	[deg]	type	[K]	[mas/yr]	[mas/yr]	[mag]	[mag]	[mag]	[mag]	[mag]	[mag]	[mag]	[mag]	[mag]	[mag]	[mag]	[mag]	[mag]		
J04304425+2601244	67.684379	26.023464	K7	4060	6.0	-16.0	2.9	14.17	12.30	11.08	10.46	8.72	7.76	7.10	6.12	5.71	5.39	4.66	1.84	II	-1.191
DK Tau B	67.685040	26.023280	K7	4060	-	-	-	-	-	-	-	-	-	-	7.77	7.41	7.39	6.63	1.84	II	-1.618
J04305028+2300088	67.709500	23.002440	G8	7045	-	-	13.6	17.08	-	14.18	-	8.78	7.04	5.86	6.62	6.10	3.33	3.52	0.45	I	0.508
J04305028+2300088	67.709500	23.002440	M6-M8	-	-	-	-	-	-	-	-	-	-	-	15.33	14.25	13.45	12.37	6.10	III	1.260
J04305171+2441475	67.715475	24.696531	M5	3415	9.0	-28.0	6.9	18.59	17.10	16.28	-	12.84	11.44	10.31	8.06	7.32	6.66	5.72	2.02	II	-0.170
J04305718+2556394**	67.738290	25.944310	M8.25	-	-	-	0.0	-	22.07	19.28	17.16	14.52	13.83	13.27	12.58	12.22	12.00	11.25	8.44	II	-1.355
J04311444+2710179	67.810170	27.171670	M0.5	3785	-	-	0.0	13.77	12.63	12.20	-	9.70	9.03	8.79	8.70	8.72	8.70	8.60	6.72	III	-2.718
J04311578+1820072	67.815783	18.335311	M4.25	3234	13.7	-24.0	0.2	17.66	15.72	15.16	12.95	11.21	10.55	10.30	10.04	9.93	9.86	9.88	9.80	III	-2.655
J04311907+2335047	67.829460	23.584640	M7.75	-	-	-	0.9	-	-	19.43	17.50	13.51	12.72	12.20	11.65	11.52	11.53	11.47	10.59	III	-2.657
J04312382+2410529	67.849258	24.181369	M4.75	3145	7.0	-25.0	0.4	16.12	14.70	13.78	11.46	9.73	9.06	8.77	8.52	8.40	8.37	8.38	8.20	III	-2.689
J04312405+1800215*	67.850250	18.005970	M7	2880	-	-	0.0	20.31	18.68	17.50	14.32	11.65	10.92	10.57	10.12	9.99	9.94	9.93	9.62	III	-2.630
J04312669+2703188	67.861210	27.055220	M7.5	2990	-	-	3.5	-	-	-	17.90	14.83	13.97	13.45	12.88	12.69	12.68	12.68	10.72	III	-2.637
J04313407+1808049	67.891975	18.134681	<K6	-	-	-	-	20.11	-	17.10	-	13.71	11.51	9.82	7.03	5.54	4.16	2.78	-	I	2.035
J04313613+1813432	67.900540	18.228690	K8	3058	8.0	-16.0	1.1	19.40	19.00	16.50	16.05	12.79	10.92	9.69	8.45	7.72	7.12	6.43	2.64	II	-0.539
J04313747+1812244	67.906130	18.206810	M0	4060	-	-	0.8	19.48	19.50	16.77	16.83	15.18	14.24	13.37	12.38	11.81	11.64	11.25	6.40	III	-1.616
J04313843+1813576	67.910170	18.232690	K7	4060	-3.0	-21.0	0.1	16.02	14.60	-	12.56	10.62	9.17	7.41	-	-	3.57	2.93	-	-	-
J04314007+1813571	67.916960	18.232560	G0	-	11.0	-19.0	0.0	15.92	14.60	13.18	11.75	9.91	8.96	8.05	-	5.04	4.40	3.57	-	-	-
J04314444+1808315	67.935210	18.142080	<K6	-	-	-	-	-	-	-	-	16.20	13.28	11.41	8.66	7.06	5.98	5.03	0.55	I	1.256
J04315056+2424180	67.960692	24.405019	M0.5	3778	3.0	-16.0	4.7	17.18	15.20	14.40	12.37	10.45	9.25	8.59	7.68	7.30	7.06	6.55	2.28	II	-1.573
J04315779+1821380	67.990400	18.360300	M0.5	3778	15.0	-6.0	1.9	14.95	13.50	12.70	11.72	9.28	9.11	8.65	7.95	7.55	7.16	6.36	6.40	II	-1.027
J04315779+1821350	67.990830	18.359750	M2	3560	15.0	-6.0	0.1	14.95	13.50	12.70	11.53	10.20	9.23	8.69	8.34	8.13	8.11	7.91	3.67	III	-2.383
J04315844+2543299	67.993500	25.724970	M5.5	3058	-	-	1.2	17.43	15.96	14.91	-	10.59	9.83	9.56	9.29	9.24	9.23	9.27	9.26	III	-2.818
J04315968+1821305	67.998675	18.358472	M1.5	3632	-	-	0.4	19.20	-	16.50	-	12.26	10.92	10.04	8.78	8.24	7.82	7.31	4.50	II	-1.170
J04320329+2528078	68.013710	25.468830	M6.25	-	-	-	0.0	19.71	-	16.84	-	11.72	11.11	10.72	10.27	10.14	10.09	10.09	9.67	III	-2.641
J04320926+1757227	68.038620	17.956330	K7	4060	11.0	-18.0	0.0	13.83	12.20	11.13	10.61	9.71	9.10	8.85	8.79	8.72	8.71	8.67	8.49	III	-2.710
J04321456+1820147	68.060710	18.337420	K7	4060	8.0	-15.0	0.1	14.35	12.50	11.39	10.40	9.12	8.50	8.23	8.12	8.05	8.01	8.02	7.81	III	-2.724
J04321540+2428597	68.064208	24.483264	M0	3850	5.0	-21.0	11.0	18.86	17.70	14.85	13.54	11.24	9.32	8.10	6.30	5.80	5.39	4.74	0.88	II	-1.068
J04321583+1801387	68.066000	18.027420	K7	4060	13.0	-22.0	0.1	14.23	12.20	11.28	10.33	9.16	8.40	8.25	8.04	8.08	8.03	7.97	7.88	III	-2.740
J04321606+1812464*	68.066960	18.212890	M6	2990	-	-	0.1	18.95	17.60	16.36	13.72	11.17	10.54	10.06	9.30	8.95	8.56	7.85	5.64	II	-1.175
J04321786+2422149*	68.074420	24.370830	M5.75	-	-	-	0.0	19.99	18.20	16.73	14.12	11.52	10.79	10.38	9.96	9.81	9.73	9.72	9.69	III	-2.569
J04321885+2422271	68.078575	24.374208	M0.5	3778	4.0	-28.0	3.9	15.59	13.90	12.87	-	9.55	8.44	8.11	7.80	7.75	7.70	7.64	7.58	III	-2.652
J04322210+1827426	68.092120	18.461830	M4.75	3161	-	-	0.1	17.00	-	15.30	13.80	11.78	11.07	10.65	10.01	9.74	9.53	9.06	6.43	II	-1.765
J04322329+2403013	68.097080	24.050390	M7.75	-	-	-	0.0	21.15	-	18.35	-	12.33	11.69	11.33	10.92	10.78	10.84	10.69	9.82	III	-2.616
J04322415+2251083	68.100646	22.852333	M4.5	3198	-	-	0.1	18.75	-	15.95	-	11.62	10.83	10.53	10.03	9.64	9.36	8.47	6.12	II	-1.088
J04322627+1827521*	68.109500	18.464470	M5.25	3091	-	-	0.0	18.06	-	15.96	13.18	11.11	10.46	10.17	9.87	9.79	9.74	9.74	9.82	III	-2.689
J04323028+1731303	68.126040	17.525250	M5.5	-	-	-	-	-	15.20	-	-	9.11	8.23	7.79	9.20	8.80	8.40	7.61	-	II	-1.024
J04323034+1731406	68.126290	17.528060	K7	4060	14.0	-20.0	1.0	12.64	12.20	11.80	10.34	8.67	7.82	7.36	6.62	6.26	5.90	5.03	-	II	-1.030
J04323058+2419572	68.127417	24.332578	K5	4350	1.0	-12.0	5.9	17.37	15.10	13.79	12.40	9.98	8.67	8.05	7.12	6.72	6.45	5.97	3.75	II	-1.545
J04323176+2420029	68.132350	24.334167	M0	3850	8.0	-35.0	7.2	17.11	15.10	13.85	12.38	9.90	8.40	7.35	6.28	5.73	5.24	4.50	1.90	II	-0.810
J04323205+2257266	68.133540	22.957420	K7	3720	-	-	1.5	-	15.19	20.18	-	14.89	11.98	10.14	8.56	7.62	6.81	5.06	1.12	I	1.125
J04324282+2552314	68.178460	25.875390	M2	3560	-	-	0.1	13.41	-	11.37	11.05	9.41	8.00	7.47	7.71	7.38	7.12	6.41	-	II	-1.373
J04324303+2552311	68.179317	25.875314	M1	3705	2.0	-26.0	0.0	13.41	12.90	11.37	11.37	9.14	8.12	7.35	6.41	5.87	5.45	4.59	1.57	II	-0.783
J04324373+1802563	68.182210	18.048970	K7	4060	16.0	-13.0	0.1	15.29	13.30	11.60	11.37	10.20	9.50	9.31	9.19	9.16	9.12	9.10	9.12	III	-2.730
J04324911+2253027	68.204620	22.884110	K6	4205	-	-	5.5	16.54	15.54	13.26	-	10.24	9.00	8.17	7.39	7.13	6.74	5.82	2.54	II	-1.031
J04324938+2253082	68.205751	22.885616	M4.25	3234	-	-	0.3	20.15	-	-	-	11.10	9.81	9.20	8.52	8.17	7.76	7.08	-	II	-1.181
J04325026+2422115	68.209460	24.369890	M7.5	-	-	-	9.2	-	-	-	18.79	13.96	12.22	11.28	10.42	10.22	10.07	10.05	9.42	III	-2.413
J04325119+1730092	68.213330	17.502560	M8.25	2632	-	-	0.0	-	22.58	-	-	14.69	13.99	13.55	-	12.90	-	12.75	-	-	-
J04330197+2421000	68.258250	24.350000	M6	2990	-	-	0.9	19.53	17.95	16.52	13.63	10.86	10.14	9.73	9.26	9.27	9.09	9.10	8.83	III	-2.610
J04330622+2409339	68.275933	24.159442	M2	3632	3.0	-30.0	1.9	14.57	13.10	11.63	10.68	9.11	8.23	7.79	7.06	6.70	6.57	5.99	3.26	II	-1.666
J04330664+2409549	68.277671	24.165275	K5	4060	10.0	-20.0	1.3	11.68	11.30	10.67	9.54	8.15	7.36	6.96	6.45	6.15	5.89	5.50	3.06	III	-1.756
J04330781+2616066	68.282540	26.268500	M6	-	-	-	4.1	-	20.74	18.70	-	11.91	10.81	10.27	9.72	9.64	9.59	9.58	9.21	III	-2.678
J04330945+2246487	68.289420	22.780190	M6	2795	-	-	3.4	-	-	19.92	16.26	13.15	12.14	11.55	10.78	10.56	10.32	9.95	8.25	III	-1.884
J04331003+2433433*	68.291804	24.562050	K7	4060	-8.0	-28.0	0.7	13.33	12.40	10.95	10.51	9.32	8.61	8.42	8.34	8.40	8.32	8.31	8.18	III	-2.774
J04331435+2614235	68.309830	26.239860	M0	3850	-	-	6.5	-	15.54	19.26	17.21	14.64	13.23	12.48	12.04	11.67	11.27	9.55	3.35	I/II	-0.027
J04331650+2253204	68.318750	22.889000	K6-M3.5	3580	-	-	-	-	15.50	18.04	-	14.68	12.15	11.72	10.23	9.97	9.61	9.66	3.46	III	-2.144

Table A.2 – continued from previous page

name	RA	Dec	spectral	T_{eff}	$\mu\alpha$	μ_δ	A_V	B	V	R	I	J	H	K	[3.6]	[4.5]	[5.8]	[8.0]	[24.0]	class	α_{IRAC}
	[deg]	[deg]	type	[K]	[mas/yr]	[mas/yr]	[mag]	[mag]	[mag]	[mag]	[mag]	[mag]	[mag]	[mag]	[mag]	[mag]	[mag]	[mag]	[mag]		
J04331907+2246342	68.328130	22.776330	M0.5	3785	-	-	10.8	20.39	19.15	16.22	15.73	11.10	9.21	7.67	6.16	5.36	4.33	3.67	1.44	II	0.086
J04332621+2245293	68.359210	22.758140	M4	3270	-	-	0.3	20.47	-	17.49	-	11.80	10.50	9.92	9.54	9.39	9.32	9.31	8.27	III	-2.583
J04333278+1800436	68.386625	18.012125	M1	-	-	-	-	-	-	-	-	10.57	9.93	9.60	-	8.71	-	7.33	-	-	-
J04333297+1801004	68.387705	18.016719	B9	-	12.4	-16.7	1.1	6.32	6.25	-	-	5.92	5.81	5.79	-	6.15	-	6.13	-	-	-
J04333297+1801004	68.387705	18.016719	-	4730	-	-	2.3	15.22	13.38	12.28	11.08	9.53	8.25	7.41	-	6.72	-	6.19	-	-	-
J04333405+2421170*	68.391920	24.354720	K7	4060	-4.0	-13.0	2.7	14.79	14.10	11.97	10.89	9.34	8.42	7.89	6.80	6.22	5.74	4.78	2.05	II	-0.551
J04333456+2421058	68.394000	24.351625	K7	4060	17.0	-19.0	2.7	14.01	12.40	12.30	11.20	9.05	8.11	7.47	6.43	6.05	5.72	4.81	1.69	II	-1.007
J04333678+2609492	68.403275	26.163672	M0	4060	9.0	-28.0	3.5	17.44	15.70	14.35	12.55	10.32	9.29	8.64	7.85	7.41	6.95	6.00	3.69	II	-0.726
J04333905+2227207	68.412730	22.455774	M1.75	3596	-	-	0.1	19.08	-	16.13	-	13.13	11.56	10.71	9.97	9.72	9.54	9.17	4.89	III	-1.937
J04333906+2520382	68.412758	25.343953	K7	4060	-3.0	-26.0	2.8	13.81	13.60	11.52	10.89	9.63	8.68	7.96	7.02	6.30	5.84	5.07	2.12	II	-0.652
J04333935+1751523	68.413960	17.864560	K5	4350	15.0	-14.0	1.5	15.50	-	13.31	12.57	10.70	9.47	8.38	6.92	6.22	5.62	4.70	-	II	-0.314
J04334171+1750402	68.423825	17.844508	M4	3270	-	-	0.0	17.20	-	14.80	-	11.27	10.64	10.31	9.97	9.79	9.56	9.07	-	II	-1.804
J04334291+2526470	68.428830	25.446390	M8.75	-	-	-	0.6	-	-	-	-	14.64	13.85	13.33	12.69	12.56	12.47	12.45	11.05	III	-2.564
J04334465+2615005	68.436051	26.250147	M4.75	3161	-	-	0.2	20.23	-	17.91	-	11.64	10.39	9.74	8.80	8.25	7.76	7.14	4.54	II	-0.942
J04334871+1810099*	68.453000	18.169440	M1	3705	11.0	-19.0	0.7	15.61	14.10	13.61	11.77	10.45	9.76	9.52	9.35	9.30	9.25	8.70	-	II	-2.111
J04335200+2250301	68.466688	22.841717	K7	4060	10.0	-16.0	3.6	14.30	13.00	11.85	-	9.48	8.43	7.79	7.03	6.38	6.09	5.37	2.15	II	-1.009
J04335245+2612548	68.468574	26.215237	M8.5	-	-	-	5.2	-	-	-	-	15.80	14.59	13.99	13.18	12.70	12.28	11.52	8.26	II	-0.952
J04335252+2256269	68.468830	22.940810	M5.75	3024	6.0	-10.0	0.0	17.31	-	14.78	-	10.24	9.47	9.11	8.80	8.62	8.61	8.57	8.41	III	-2.602
IT Tau B	68.477460	26.223780	M4	-	-	-	-	-	-	-	-	-	-	-	8.95	8.61	8.08	7.46	3.51	II	-1.093
J04335470+2613275*	68.477921	26.224311	K2	4900	11.0	-17.0	13.4	15.95	13.70	13.06	-	9.87	8.59	7.86	7.27	6.88	6.50	5.91	3.51	II	-1.283
J04335546+1838390	68.480920	18.644280	M3.5	3420	-	-	0.9	16.44	-	14.47	-	10.51	9.92	9.61	9.39	9.37	9.32	9.29	-	III	-2.715
J04341099+2251445	68.545790	22.862360	M1	3720	-	-	1.7	16.68	15.19	13.90	-	10.62	9.78	9.43	9.25	9.25	9.18	9.17	8.64	III	-2.729
J04341527+2250309	68.563630	22.841940	M7	-	-	-	3.1	-	23.43	-	-	13.74	12.54	11.85	11.17	11.04	10.96	10.99	9.94	III	-2.633
J04341803+1830066*	68.575133	18.501817	G8	5520	0.0	-7.0	0.1	14.44	13.70	13.00	11.43	10.60	10.09	9.90	9.82	9.79	9.81	9.76	-	III	-2.779
J04344544+2308027	68.689370	23.134080	M5.25	-	-	-	-	20.20	-	18.20	16.00	12.80	12.02	11.70	11.24	11.19	11.09	11.08	-	III	-2.639
J04345542+2428531*	68.730933	24.481433	K7	4060	-1.0	-24.0	2.2	14.39	12.10	12.02	11.10	9.43	8.55	8.05	7.27	6.78	6.40	5.58	2.78	II	-0.931
J04345693+2258358	68.737218	22.976627	M1.5	3632	4.0	-12.0	0.2	16.00	-	13.46	-	10.47	9.59	9.27	9.05	8.99	8.94	8.94	8.31	III	-2.709
J04350850+2311398	68.785460	23.194420	M6	-	-	-	0.0	20.35	18.40	18.01	14.88	12.53	11.94	11.59	11.19	11.06	11.02	10.98	10.23	III	-2.610
J04352020+2232146	68.834183	22.537389	M0.5	3778	9.0	-17.0	2.6	15.60	14.90	14.06	12.51	11.20	10.20	9.73	8.88	8.49	8.36	7.72	4.90	II	-1.570
J04352089+2254242	68.837092	22.906736	K7	4060	-2.8	-19.7	1.9	15.73	-	12.82	-	9.78	8.93	8.59	8.37	8.37	8.36	8.35	8.25	III	-2.811
J04352450+1751429	68.852146	17.861908	M2	3560	13.9	-19.6	0.1	15.68	14.12	12.92	11.55	10.02	9.33	9.10	8.91	8.88	8.83	8.80	8.75	III	-2.705
J04352737+2414589*	68.864063	24.249703	M0	3850	5.0	-21.0	1.1	13.20	11.80	11.44	10.49	9.14	8.34	8.02	7.43	7.16	6.54	6.00	2.95	II	-1.126
IRAS 04325+2402 A+B	68.897370	24.138750	-	-	-	-	-	-	-	-	-	17.13	13.74	11.60	13.40	12.90	12.40	11.70	-	II	-0.889
J04353539+2408194	68.897460	24.138720	K6-M3.5	-	-	-	-	-	-	-	-	17.10	13.80	11.60	9.90	9.34	9.12	8.52	1.29	II	-1.325
J04354093+2411087	68.920575	24.185767	M1	3705	2.0	-31.0	7.7	18.09	17.30	14.58	-	10.73	9.20	8.41	7.35	6.87	6.42	5.57	3.13	II	-0.812
J04354183+2234115	68.924330	22.569890	M5.75	-	-	-	0.0	20.41	19.26	18.04	15.10	12.96	12.38	11.99	11.60	11.47	11.41	11.45	10.71	III	-2.671
J04354203+2252226	68.925159	22.872963	M4.75	3161	6.0	-20.0	0.1	19.37	-	16.13	-	11.25	10.39	10.00	9.63	9.48	9.39	9.50	8.84	III	-2.688
J04354526+2737130	68.938580	27.620310	M9.25	-	-	-	0.3	-	-	19.43	-	15.01	14.24	13.71	13.12	13.04	12.89	13.04	10.62	III	-2.718
J04354733+2250216	68.947250	22.839360	K2	4900	11.0	-17.0	3.8	13.04	11.50	11.06	-	8.66	7.73	7.14	6.42	5.84	5.36	4.38	1.53	II	-0.529
J04355109+2252401*	68.962917	22.877817	M2.75	-	1.0	-31.0	2.7	17.78	-	15.24	-	11.31	10.35	10.01	9.76	9.69	9.64	9.63	9.71	III	-2.688
J04355143+2249119**	68.964290	22.819970	M8.5	-	-	-	0.0	-	24.92	-	18.76	15.48	14.66	14.19	13.60	13.47	13.56	13.35	10.93	III	-2.601
J04355209+2255039	68.967080	22.917780	M4.5	3198	12.0	-16.0	0.2	18.56	-	15.85	-	11.31	10.23	9.81	9.52	9.43	9.39	9.36	-	III	-2.660
J04355277+2254231	68.969904	22.906419	K3	4730	-9.0	-49.0	4.8	15.22	14.40	12.39	11.21	9.55	8.47	7.63	6.58	6.13	5.73	4.80	1.27	II	-0.821
J04355286+2250585	68.970290	22.849610	M4.25	3234	6.0	-22.0	0.1	18.50	-	15.63	-	10.99	10.11	9.75	9.42	9.29	9.24	9.29	8.93	III	-2.696
J04355349+2254089	68.972920	22.902500	K7	4060	29.0	-3.0	2.2	-	14.90	13.20	11.87	10.05	9.16	8.80	8.61	8.52	8.47	8.48	-	III	-2.691
J04355415+2254134	68.975633	22.903739	G0	6030	11.0	-14.0	2.6	11.66	11.30	10.06	9.32	8.09	7.48	7.23	7.16	7.14	7.05	7.00	-	III	-2.638
J04355684+2254360*	68.986837	22.910006	M3	3125	15.0	-19.0	4.1	18.20	17.30	15.39	-	11.14	10.06	9.53	8.63	8.17	7.79	7.14	4.43	II	-1.148
J04355892+2238353	68.995540	22.643140	M0	3850	8.0	-16.0	0.0	13.90	-	11.44	-	9.32	8.60	8.37	8.11	8.18	8.09	8.06	-	III	-2.748
J04361030+2159364	69.042960	21.993470	M8.5	-	-	-	0.3	-	-	20.16	-	14.85	14.10	13.65	12.99	12.70	12.37	11.79	8.62	II	-1.460
J04361038+2259560	69.043290	22.998890	M7.5	2555	-	-	0.0	-	22.52	19.17	16.81	13.75	12.76	12.17	11.59	11.37	11.38	11.31	10.61	III	-2.558
J04361909+2542589	69.079554	25.716411	M0	3850	4.0	-21.0	0.0	12.18	11.80	10.73	-	9.33	8.71	8.58	8.41	8.47	8.44	8.44	8.19	III	-2.854
J04362151+2351165	69.089655	23.854609	M5.25	-	-	-	-	18.91	-	17.43	-	13.16	12.53	12.24	11.87	11.47	11.12	10.55	7.83	II	-1.336
J04363893+2258119	69.162250	22.969970	M7.75	-	-	-	0.0	-	21.65	19.21	16.88	13.72	12.86	12.37	11.77	11.78	11.53	11.53	8.55	III	-2.503
J04373705+2331080	69.404375	23.518908	L0	2200	-	-	0.0	20.23	-	17.91	-	17.38	16.13	15.44	14.16	13.88	13.59	13.30	-	III	-1.845
J04375670+2546229	69.486267	25.773035	-	-	-	-	-	19.14	-	17.45	-	14.13	13.26	12.70	11.95	11.47	10.71	9.89	7.13	II	-0.420

Table A.2 – continued from previous page

name	RA	Dec	spectral	T_{eff}	$\mu\alpha$	μ_δ	A_V	B	V	R	I	J	H	K	[3.6]	[4.5]	[5.8]	[8.0]	[24.0]	class	α_{IRAC}
	[deg]	[deg]	type	[K]	[mas/yr]	[mas/yr]	[mag]	[mag]	[mag]	[mag]	[mag]	[mag]	[mag]	[mag]	[mag]	[mag]	[mag]	[mag]	[mag]		
J04380083+2558572	69.503500	25.982560	M7.25	2838	-	-	0.6	20.41	-	18.16	14.71	11.54	10.62	10.10	9.57	9.42	9.33	9.34	9.25	III	-2.577
J04381486+2611399	69.561920	26.194420	M7.25	2838	-	-	0.0	19.84	-	19.45	17.84	15.18	14.13	12.98	10.79	10.14	9.61	8.91	5.03	II	-0.702
J04381630+2326402	69.567920	23.444530	M4.75	-	-	-	-	17.70	-	16.20	14.30	11.80	11.24	10.96	-	-	-	-	-	-	-
J04382134+2609137	69.588920	26.153810	M6.5	2935	-	-	4.3	18.39	17.20	16.16	15.04	12.80	11.59	10.63	9.23	8.73	8.40	7.83	5.32	II	-1.266
J04382858+2610494	69.619092	26.180400	M0	3850	5.0	-29.0	4.9	14.61	13.00	12.12	11.30	9.47	8.24	7.30	6.19	5.60	5.14	4.39	0.90	II	-0.801
HV Tau C*	69.633000	26.183000	K6	-	6.0	-43.0	1.9	-	-	-	-	-	13.19	12.32	11.29	10.73	10.21	9.35	3.50	II	-0.626
J04383528+2610386	69.647008	26.177397	M1	3720	6.0	-43.0	2.5	15.02	14.10	11.88	11.41	9.23	8.28	7.91	7.71	7.55	7.44	7.43	-	III	-2.518
J04385859+2336351	69.744170	23.609780	M4.25	-	-	-	0.0	18.40	-	16.80	14.30	11.97	11.36	11.03	10.49	-	9.84	-	6.40	-	-
J04385871+2323595	69.744630	23.399890	M6.5	-	-	-	0.9	19.10	-	17.50	15.30	12.49	11.93	11.59	9.76	-	9.18	-	6.28	-	-
J04390163+2336029	69.756790	23.600830	M6	-	-	-	-	16.70	-	15.20	12.80	11.33	10.59	10.18	9.72	-	9.17	-	6.25	-	-
J04390396+2544264	69.766500	25.740670	M7.25	2838	-	-	0.4	19.99	-	18.92	15.40	12.64	11.84	11.37	10.78	10.37	10.03	9.16	6.44	II	-1.009
J04390525+2337450	69.771877	23.629189	M3.5-M6	-	-	-	-	17.30	-	14.55	-	13.38	12.30	11.55	10.54	10.14	9.73	9.02	3.47	II	-1.099
J04390637+2334179	69.776580	23.571670	M7.5	-	-	-	0.0	19.00	-	17.30	14.60	12.09	11.53	11.19	10.79	-	10.69	-	9.32	-	-
J04391389+2553208	69.807908	25.889064	<K6	-	-	-	-	-	-	-	-	16.44	13.02	10.72	7.95	7.01	6.42	4.77	0.45	I	0.713
J04391741+2247533*	69.822550	22.798167	M0	3850	12.0	-20.0	1.4	14.70	13.60	13.03	11.51	9.97	9.26	8.96	8.61	8.42	8.10	7.42	4.61	II	-1.461
J04391779+2221034	69.824150	22.350967	K5	4350	8.0	-15.0	1.9	12.54	11.60	11.43	10.79	9.42	8.60	8.16	7.70	7.35	7.28	6.59	3.09	II	-1.636
J04392090+2545021	69.837125	25.750586	M2.5	3488	2.0	-21.0	5.7	17.34	15.30	13.76	12.73	10.20	8.89	8.06	7.00	6.50	6.20	5.38	2.83	II	-1.031
J04393364+2359212	69.890187	23.989231	M5	-	-	-	-	18.28	-	15.72	-	11.57	10.81	10.28	9.61	9.16	8.82	7.91	5.23	II	-0.925
J04393519+2541447	69.896630	25.695750	<K6	-	-	-	-	-	-	-	-	16.91	13.76	10.84	7.16	5.73	4.81	4.08	0.45	I	0.628
J04394488+2601527	69.937014	26.031330	M5	-	-	-	-	20.34	-	16.62	-	10.64	9.52	8.95	8.45	8.12	7.69	7.11	3.94	II	-1.284
J04394748+2601407	69.947830	26.028000	M7	2880	-	-	2.6	-	21.56	19.09	15.78	12.17	11.01	10.33	9.47	9.04	8.59	7.80	4.96	II	-0.927
IRAS 04368+2557	69.973290	26.051530	-	-	-	-	-	-	-	-	-	-	-	-	13.51	11.15	9.95	9.56	2.73	I	1.544
J04395574+2545020	69.982290	25.750560	B5	-	-	-	18.0	-	-	19.15	15.91	10.67	8.05	6.28	6.62	6.10	3.43	2.75	0.45	II	2.084
J04400067+2358211	70.002817	23.972546	M6	-	-	-	-	19.45	-	17.35	-	12.43	11.87	11.48	10.90	10.61	10.35	9.69	6.37	II	-1.467
J04400174+2556292	70.007290	25.941440	M5.5	2632	-	-	8.4	-	-	-	17.16	13.22	11.64	10.76	10.13	9.91	9.84	9.81	8.94	III	-2.492
J04400800+2605253	70.033330	26.090390	<M0	-	-	-	13.1	-	-	19.30	17.06	12.41	10.25	8.87	7.92	7.30	6.92	5.91	2.46	II	-0.594
J04403979+2519061	70.165790	25.318360	M5.25	3091	-	-	3.6	20.21	-	17.87	14.80	11.82	10.79	10.24	9.79	9.61	9.62	9.57	7.47	III	-2.619
J04404950+2551191	70.206290	25.855330	M2	3580	-	-	1.5	16.62	15.50	14.26	12.37	10.75	9.92	9.49	8.85	8.50	8.28	7.75	5.19	II	-1.607
J04410424+2557561	70.267683	25.965589	M5	3125	17.0	-19.0	0.6	18.47	-	15.36	13.01	10.94	10.26	9.95	9.58	9.47	9.48	9.44	9.70	III	-2.698
J04410470+2451062	70.269617	24.851733	K7	4060	10.0	-17.0	1.1	14.39	12.60	11.94	10.51	9.24	8.48	8.28	8.10	8.12	8.06	8.03	8.08	III	-2.740
J04410826+2556074	70.284420	25.935420	M3	3415	-	-	8.3	20.43	-	18.63	16.39	13.74	12.15	11.09	9.61	9.04	8.48	7.65	4.40	II	-0.595
J04411078+2555116	70.294920	25.919920	M5.5	3058	-	-	1.8	-	-	19.37	16.43	13.17	12.12	11.45	10.75	10.28	9.89	9.25	6.52	II	-1.136
J04411267+2546354	70.302830	25.776500	K6-M3.5	-	-	-	-	-	-	-	-	17.15	14.14	11.54	9.11	7.77	6.74	5.67	1.33	I	1.066
J04411681+2840000	70.320054	28.666683	M1.5	3720	0.0	-11.0	3.0	-	14.90	12.10	-	10.16	9.08	8.66	8.47	8.39	8.34	8.13	2.30	III	-2.457
J04412464+2543530	70.352685	25.731396	M3.5	-	-	-	-	-	-	-	-	16.71	13.53	11.75	10.48	9.78	9.40	8.87	5.52	II	-1.046
J04413882+2556267	70.411750	25.940780	M0	3778	-	-	9.3	18.84	18.40	15.54	14.50	11.85	10.12	9.20	8.21	7.74	7.09	6.09	1.91	II	-0.381
J04414489+2301513	70.437080	23.030940	M8.5	-	-	-	-	-	-	20.55	-	14.41	13.72	13.16	12.26	11.88	11.53	11.00	-	II	-1.400
J04414565+2301580	70.440217	23.032797	M4.5	3198	-	-	0.0	16.73	-	14.24	-	10.74	10.10	9.85	-	9.48	9.37	9.22	-	-	-
J04414825+2534304	70.451040	25.575140	M7.75	2752	-	-	1.1	20.33	-	19.29	17.03	13.73	12.80	12.22	11.38	10.87	10.47	9.54	6.31	II	-0.762
J04420548+2522562	70.522854	25.382306	M0	4060	0.0	-27.0	4.3	15.55	15.10	11.99	11.99	9.79	8.67	8.23	7.91	7.83	7.73	7.69	7.24	III	-2.577
J04420732+2523032	70.530525	25.384231	M1	3720	8.0	-29.0	4.6	-	15.60	-	12.58	9.59	8.41	7.95	7.59	7.56	7.48	7.50	-	III	-2.719
J04420777+2523118	70.532380	25.386610	K7	4060	15.0	-17.0	5.0	16.51	14.90	13.32	13.33	9.81	8.60	7.94	6.93	6.53	6.06	5.33	2.73	II	-0.995
J04422101+2520343	70.587580	25.342890	M4.75	3560	-	-	1.6	18.84	-	16.22	-	11.40	10.58	10.17	9.52	9.18	8.63	7.79	4.26	II	-0.822
J04423769+2515374	70.657075	25.260406	M0.5	3785	8.0	-21.0	5.6	16.71	14.90	14.03	12.43	11.00	9.69	8.76	7.50	6.85	6.33	5.36	1.85	II	-0.417
J04430309+2520187	70.762896	25.338542	M0	3850	9.0	-27.0	2.3	16.81	15.40	14.24	12.26	10.71	9.77	9.33	9.02	8.61	8.31	7.42	4.35	II	-1.041
J04432023+2940060	70.834308	29.668347	M5	3125	5.0	-21.0	0.3	17.01	-	14.96	12.24	10.40	9.73	9.41	8.90	8.60	8.25	7.53	5.56	II	-1.268
J04442713+2512164*	71.113040	25.204560	M7.25	2838	-	-	0.0	19.27	-	17.00	-	12.20	11.36	10.76	9.52	8.96	8.33	7.43	4.30	II	-0.431
J04455129+1555496	71.463741	15.930472	G5	6030	12.0	-18.0	2.1	12.47	-	10.20	9.35	7.80	7.49	7.28	7.28	7.24	7.29	7.24	-	III	-2.810
J04455134+1555367	71.463960	15.926860	M2.5	3488	-	-	0.1	14.76	13.54	-	-	10.31	9.50	9.10	8.55	8.20	7.80	6.73	2.55	II	-0.764
J04464260+2459034	71.677500	24.984280	M4	3270	-	-	0.0	18.29	-	15.85	-	11.26	10.67	10.34	10.03	9.92	9.97	9.91	9.53	III	-2.731
J04465305+1700001	71.721040	17.000060	M0	3850	0.0	-6.0	1.6	16.28	13.70	12.45	11.27	9.51	8.54	7.98	7.05	6.58	6.07	5.20	-	II	-0.717
Haro 6-37 B	71.745708	17.043917	M1	4205	0.0	-14.0	3.8	14.93	13.50	12.69	11.12	9.24	7.99	7.31	6.64	6.14	5.80	5.24	-	II	-1.263
Haro 6-37 A	71.746208	17.044528	K7	4060	0.0	-14.0	1.3	14.93	13.50	12.69	-	9.20	8.01	7.31	7.85	7.28	7.12	5.99	3.94	I	-0.812
J04470620+1658428	71.775880	16.978560	K5	4060	5.0	-17.0	1.2	12.08	12.00	10.68	10.19	8.85	7.80	6.87	-	5.05	4.47	3.80	-	-	-
J04474859+2925112*	71.952460	29.419780	K5	4350	-	-	1.1	14.00	12.37	11.00	10.80	9.47	8.60	8.04	7.36	6.91	6.65	5.91	-	II	-1.223

Table A.2 – continued from previous page

name	RA	Dec	spectral	T_{eff}	μ_α	μ_δ	A_V	B	V	R	I	J	H	K	[3.6]	[4.5]	[5.8]	[8.0]	[24.0]	class	α_{IRAC}
	[deg]	[deg]	type	[K]	[mas/yr]	[mas/yr]	[mag]	[mag]	[mag]	[mag]	[mag]	[mag]	[mag]	[mag]	[mag]	[mag]	[mag]	[mag]	[mag]		
J04484189+1703374	72.174580	17.060390	M7	-	-	-	-	-	-	19.64	-	13.53	12.93	12.49	12.06	11.94	11.89	11.88	-	III	-2.639
J04514737+3047134	72.947396	30.787072	M0	4060	6.0	-24.0	2.1	12.47	12.30	11.35	10.83	9.13	7.99	7.24	6.08	5.53	4.98	3.92	-	II	-0.374
J04520668+3047175	73.027830	30.788190	M4	3560	-	-	1.0	-	-	-	17.88	14.42	12.02	10.38	8.42	7.68	7.06	6.17	-	II	-0.280
J04551098+3021595	73.795762	30.366539	K7	4730	3.0	-26.0	1.2	13.84	12.10	11.12	10.50	9.34	8.60	8.28	8.04	7.88	7.68	7.07	2.48	II	-1.732
J04552333+3027366	73.847210	30.460170	M6.25	2962	-	-	0.0	-	-	18.63	15.55	13.07	12.39	11.97	11.51	11.39	11.34	11.33	-	III	-2.639
J04553695+3017553	73.904004	30.298664	K0	5250	3.0	-19.0	0.1	11.67	11.00	10.49	9.68	8.87	8.32	8.15	8.12	8.11	8.03	8.05	7.09	III	-2.739
J04554046+3039057	73.918580	30.651580	M5.25	3091	-	-	0.0	19.07	-	17.08	14.71	12.71	12.07	11.77	11.44	11.31	11.27	11.16	-	III	-2.533
J04554535+3019389	73.938960	30.327470	M4.75	3161	-	-	0.0	17.64	-	15.49	13.19	11.44	10.79	10.46	9.92	9.43	9.29	8.65	6.49	II	-1.459
J04554582+3033043	73.941022	30.551191	B9	10500	2.6	-24.7	0.3	7.13	7.06	7.03	6.85	5.94	5.06	4.23	-	-	2.64	-	-	-	-
J04554757+3028077	73.948210	30.468810	M4.75	3161	-	-	0.0	17.26	-	15.17	13.01	11.05	10.31	9.98	9.65	9.52	9.50	9.46	-	III	-2.638
J04554801+3028050	73.950040	30.468060	M5.6	3044	-	-	0.0	20.47	-	16.66	15.20	13.17	12.58	12.15	11.42	11.09	10.75	10.09	7.05	II	-1.319
J04554820+3030160	73.950830	30.504470	M4.5	3198	-	-	0.0	17.67	-	15.80	-	11.89	11.22	10.95	10.67	10.55	10.56	10.38	-	III	-2.534
J04554969+3019400	73.957080	30.327780	M6	2990	-	-	0.0	20.14	-	17.84	15.02	12.81	12.23	11.86	11.36	11.11	10.95	10.66	8.19	III	-2.052
J04555288+3006523	73.970380	30.114530	M5.25	3091	-	-	0.0	17.87	-	15.80	13.70	11.64	11.03	10.73	10.39	10.31	10.26	10.24	-	III	-2.667
J04555605+3036209	73.983540	30.605830	M4	3270	-	-	0.2	15.79	-	12.94	-	10.47	9.66	9.27	8.69	8.37	7.99	7.20	3.77	II	-1.130
J04555636+3049374	73.984880	30.827080	M5	3125	-	-	0.0	18.32	-	16.17	13.85	12.00	11.39	11.09	10.75	10.65	10.58	10.58	-	III	-2.642
J04555938+3034015*	73.997439	30.567089	G2	5860	2.0	-25.0	0.9	9.88	9.40	8.83	8.10	7.20	6.56	5.99	8.73	5.03	4.52	3.79	-	I	2.282
J04560118+3026348	74.004925	30.443008	M3.5	3342	-	-	0.1	16.50	-	15.00	-	11.36	10.55	10.06	9.42	9.02	8.68	8.07	5.81	II	-1.306
J04560201+3021037	74.008400	30.351042	K5	4060	2.0	-26.0	0.1	12.08	11.50	10.67	10.05	8.96	8.32	8.13	8.09	8.05	7.98	8.02	7.55	III	-2.745
J04574903+3015195	74.454290	30.255420	M9.25	2350	-	-	0.0	-	-	-	19.25	15.77	15.12	14.48	13.88	13.76	13.63	13.82	-	III	-2.751
J04584626+2950370	74.692777	29.843611	A2	-	6.3	-23.8	-	7.90	7.73	7.70	-	6.87	6.26	5.53	-	-	-	-	-	-	-
J05030659+2523197	75.777500	25.388810	K7	4060	11.0	-10.0	1.1	14.25	14.00	12.13	11.19	9.91	9.08	8.60	8.30	7.93	7.53	6.82	3.83	II	-1.142
J05044139+2509544	76.172580	25.165890	M3.5	3342	-	-	0.2	17.11	-	14.64	-	10.91	10.01	9.60	9.15	8.86	8.61	7.96	5.18	II	-1.492
J05052286+2531312	76.344960	25.526220	K8	3950	-	-	-	17.04	-	14.09	-	12.81	11.91	11.16	9.17	8.56	7.95	7.02	-	II	-0.377
J05061674+2446102	76.569540	24.770360	M4	3270	-	-	0.0	16.38	-	14.25	-	10.79	10.09	9.82	9.59	9.45	9.44	9.41	-	III	-2.653
J05062332+2432199	76.597040	24.540000	M3.5	3342	-	-	0.1	15.49	-	13.82	-	10.42	9.71	9.46	9.10	8.79	8.47	7.83	-	II	-1.388
J05064662+2104296	76.694290	21.074890	M5.25	-	-	-	-	18.10	-	16.50	14.60	12.05	11.40	11.11	10.73	10.64	10.59	10.57	-	III	-2.658
J05071206+2437163	76.800290	24.621220	K6	4205	-	-	0.1	14.32	-	12.07	11.24	10.14	9.49	9.30	9.23	9.24	9.18	9.14	-	III	-2.719
J05074953+3024050	76.956533	30.401434	K3	4730	4.0	-23.0	0.5	11.07	10.80	10.06	9.45	8.38	7.62	7.02	6.30	5.70	5.23	4.32	-	II	-0.601
J05075496+2500156	76.979040	25.004330	M4	3270	-	-	0.1	15.63	-	14.26	-	11.42	10.71	10.40	10.06	9.84	9.51	8.72	-	II	-1.296

Table A.3: Data of the 82 already known Taurus members in the UKIDSS GCS DR8 region. The first one (2MASSJ04163048+3037053) is the only member located in our region A (see also Tab. A). They are sorted by their RA. 'U' marks the UKIDSS and 'M' the 2MASS value and 2MASS names are shortened.
* optical spectra observed
** used as reference spectra

name	RA_U	Dec_U	$\mu_{\alpha,U}$	$\mu_{\delta,U}$	$\mu_{\alpha,lit}$	$\mu_{\delta,lit}$	$A_{V,YJK}$	$A_{V,JHK}$	$A_{V,lit}$	Z_U	Y_U	J_U	H_U	K_U	J_M	H_M	K_M
	[deg]	[deg]	[mas/yr]	[mas/yr]	[mas/yr]	[mas/yr]	[mag]	[mag]	[mag]	[mag]	[mag]	[mag]	[mag]	[mag]	[mag]	[mag]	[mag]
J04163048+3037053	64.127041	30.618139	1.0	-3.0	-	-	0.2	0.0	0.1	14.90	14.26	13.61	12.99	12.63	13.62	12.97	12.62
J04185115+2814332	64.713177	28.242517	7.0	-15.2	-	-	2.2	-	0.4	15.75	14.70	13.80	-	12.67	13.93	13.24	12.75
J04190126+2802487	64.755304	28.046770	3.4	-27.9	-	-	1.3	-	0.5	19.05	17.55	16.41	-	14.87	16.31	15.48	14.93
J04194127+2749484	64.922066	27.830390	26.3	77.1	5.0	-31.0	-	-	1.0	11.79	11.50	-	-	-	9.13	8.38	8.26
J04202606+2804089	65.108639	28.069076	8.0	-23.2	-	-	0.5	-	0.0	11.66	11.47	10.95	-	10.40	10.61	9.95	9.70
J04210934+2750368	65.288976	27.843471	12.2	-29.1	-	-	0.5	-	0.0	12.57	12.00	11.42	-	10.71	11.23	10.66	10.36
J04211038+2701372	65.293378	27.027015	25.1	-0.2	-	-	-	-	-	-	-	18.72	-	10.86	18.89	13.78	11.09
J04211146+2701094	65.297867	27.019269	21.7	-3.1	-	-	1.6	-	-	-	19.49	16.48	-	10.44	16.22	12.65	10.34
J04213459+2701388	65.394180	27.027415	4.2	-12.9	-	-	1.7	-	2.7	13.82	12.81	11.80	-	10.52	11.90	10.97	10.44
J04214013+2814224	65.417256	28.239502	5.9	-21.5	-	-	0.5	-	0.0	13.20	12.53	11.85	-	11.07	11.93	11.34	11.03
J04214631+2659296	65.442997	26.991478	5.1	-24.1	-	-	1.7	-	3.6	16.06	14.88	13.75	-	12.06	13.82	12.73	12.13
J04215450+2652315	65.477165	26.875410	15.9	-3.8	-	-	1.1	-	3.0	18.25	16.78	15.49	-	13.84	15.54	14.50	13.90
J04215563+2755060*	65.481483	27.918111	-89.3	-72.1	22.0	-12.0	-	-	2.2	11.82	-	-	-	-	9.18	8.27	7.80
J04220217+2657304	65.509126	26.958450	14.9	-5.6	4.0	-18.0	1.8	-	6.9	12.10	11.49	10.48	-	10.21	10.71	9.24	8.18
J04221568+2657060	65.565377	26.951681	9.6	-3.9	12.0	-16.0	1.4	-	0.1	15.18	14.58	13.70	-	11.92	13.81	12.62	12.03
J04221675+2654570	65.569868	26.915853	10.2	-0.6	-	-	1.9	-	7.7	14.41	13.36	12.01	-	10.38	11.58	10.04	9.01
J04222404+2646258	65.600226	26.773856	10.3	6.7	10.0	-10.0	1.5	-	0.1	12.65	11.92	11.11	-	10.24	11.09	10.19	9.77
J04230607+2801194*	65.776299	28.022841	265.5	229.6	-	-	-	-	-	20.45	-	-	-	-	12.24	11.61	11.20
J04230776+2805573	65.782401	28.099189	7.5	-21.9	-	-	-	-	8.1	14.58	-	12.71	-	11.60	13.18	11.60	10.41
J04231822+2641156	65.826002	26.687626	12.1	-13.8	4.0	-18.0	2.3	-	-	15.44	14.05	12.53	-	10.44	12.66	11.02	10.18
J04242090+2630511	66.087137	26.514123	12.9	-26.3	-	-	1.9	-	0.9	14.99	14.10	13.33	-	12.36	13.49	12.81	12.43
J04242646+2649503	66.110294	26.830599	9.8	-17.3	-	-	0.5	-	0.9	14.51	13.59	12.81	-	11.69	12.88	12.19	11.76
J04244457+2610141	66.185795	26.170550	14.2	-10.8	-	-	0.7	-	3.4	12.52	11.99	11.16	-	10.21	10.80	9.75	9.05
J04244506+2701447	66.187801	27.029028	11.6	-19.1	2.0	-25.0	0.6	-	0.1	12.45	11.97	11.33	-	10.47	11.34	10.71	10.46
J04245708+2711565	66.237826	27.198944	-2.3	-25.3	8.0	-26.0	-	-	1.9	11.28	-	10.47	-	10.18	9.78	8.89	8.35
J04262939+2624137	66.622523	26.403777	15.8	-16.2	-	-	1.0	-	1.6	15.16	14.17	13.25	-	12.01	13.32	12.50	12.08
J04265352+2606543	66.723074	26.115060	9.5	-13.1	-7.0	-27.0	1.8	-	8.7	12.15	11.58	10.60	-	9.74	9.92	8.33	7.44
J04265440+2606510	66.726679	26.114127	-5.1	-16.0	8.0	-30.0	1.6	-	5.9	12.65	11.92	10.97	-	10.36	10.80	9.49	8.87
J04265732+2606284	66.738834	26.107844	-6.1	-14.2	-	-	1.4	-	4.3	13.04	12.16	11.26	-	10.19	11.28	10.17	9.58
J04270280+2542223*	66.761685	25.706630	3.9	130.9	12.8	-19.1	-	-	2.4	11.58	11.42	-	-	-	8.17	7.26	6.73
J04284263+2714039	67.177626	27.234399	-5.1	-6.0	-	-	1.1	-	3.7	13.53	12.81	11.99	-	10.42	12.11	11.07	10.46
J04290068+2755033	67.252869	27.917526	8.3	-25.3	-	-	0.4	-	0.0	15.88	14.76	13.85	-	12.80	14.02	13.33	12.85
J04292165+2701259	67.340245	27.023837	6.6	-11.3	-	-	2.0	-	5.9	13.40	12.06	10.74	-	11.38	10.80	9.50	8.73
J04292971+2616532	67.373792	26.281384	-0.1	-19.5	10.0	-22.0	1.0	-	0.3	11.78	11.55	10.75	-	10.44	10.34	9.68	9.39
J04294155+2632582	67.423173	26.549493	4.0	-8.1	5.0	-13.0	0.4	-	2.5	11.15	11.53	10.47	-	10.94	9.77	8.82	8.18
J04294247+2632493	67.427373	26.546956	106.1	-22.6	13.0	-19.0	-	-	0.5	-	11.68	-	-	-	9.32	8.60	8.39

Table A.3 – continued from previous page

name	RA$_U$ [deg]	Dec$_U$ [deg]	$\mu_{\alpha,U}$ [mas/yr]	$\mu_{\delta,U}$ [mas/yr]	$\mu_{\alpha,lit}$ [mas/yr]	$\mu_{\delta,lit}$ [mas/yr]	A$_{V,YJK}$ [mag]	A$_{V,JHK}$ [mag]	$A_{V,lit}$ [mag]	Z_U [mag]	Y_U [mag]	J_U [mag]	H_U [mag]	K_U [mag]	J_M [mag]	H_M [mag]	K_M [mag]
J04294568+2630468[**]	67.440334	26.512921	-0.1	-24.6	-	-	-	-	0.0	14.38	13.35	12.51	-	-	12.64	11.92	11.54
J04295156+2606448	67.464819	26.112428	-6.8	-13.1	15.0	-25.0	0.5	-	2.9	11.32	11.74	10.67	-	9.96	9.42	8.42	7.78
J04300724+2608207	67.530198	26.139047	3.8	-18.9	-	-	0.6	-	0.9	17.00	15.82	14.89	-	13.68	15.00	14.20	13.69
J04304425+2601244	67.684349	26.023463	-8.4	-0.4	6.0	-16.0	0.6	-	2.9	11.32	11.33	11.01	-	11.44	8.72	7.76	7.10
J04305718+2556394[**]	67.738351	25.944253	19.4	-14.4	-	-	0.4	-	0.0	16.42	15.28	14.42	-	13.25	14.52	13.83	13.27
J04311444+2710179	67.809881	27.171660	-77.3	-1.5	-	-	-	-	0.0	-	11.71	-	-	-	9.71	9.04	8.79
J04312669+2703188	67.861262	27.055183	14.4	-12.7	-	-	1.0	-	3.5	16.98	15.82	14.74	-	13.37	14.83	13.97	13.45
J04315844+2543299	67.993541	25.724944	7.1	-10.1	-	-	0.3	-	1.2	12.13	11.84	11.23	-	10.23	10.59	9.83	9.56
J04320329+2528078	68.013732	25.468779	2.0	-18.4	-	-	0.4	-	0.0	13.17	12.29	11.55	-	10.64	11.72	11.11	10.72
J04324282+2552314	68.178597	25.875335	38.3	-17.5	-	-	-	-	0.1	-	13.09	-	-	-	9.41	8.01	7.47
J04330781+2616066	68.282572	26.268460	8.2	-14.8	-	-	2.2	-	4.1	14.10	12.88	11.79	-	10.36	11.91	10.81	10.27
J04333678+2609492	68.403156	26.163637	-32.8	-10.2	9.0	-28.0	-	-	3.5	12.92	-	-	-	-	10.32	9.29	8.64
J04333906+2520382	68.412810	25.343882	15.1	-22.4	-3.0	-26.0	-	-	2.8	11.23	11.97	-	-	9.80	9.63	8.68	7.96
J04334291+2526470	68.428836	25.446308	6.0	-27.6	-	-	0.7	-	0.6	16.93	15.64	14.57	-	13.27	14.64	13.85	13.33
J04335245+2612548	68.468596	26.215209	5.9	-8.4	-	-	1.8	-	5.2	18.36	16.98	15.72	-	14.00	15.81	14.59	13.99
J04335470+2613275[*]	68.477996	26.224277	20.0	-10.5	11.0	-17.0	1.6	-	13.4	11.72	11.61	11.05	-	10.46	9.87	8.59	7.86
J04354526+2737130	68.938650	27.620285	17.7	-6.3	-	-	0.4	-	0.3	17.37	16.03	14.96	-	13.69	15.02	14.24	13.71
J04361909+2542589	69.079595	25.716371	15.8	-2.5	4.0	-21.0	1.2	-	0.0	11.62	11.57	11.05	-	10.62	9.34	8.71	8.58
J04375670+2546229	69.486257	25.773040	-3.1	1.7	-	-	-	-	-	16.36	-	14.83	-	13.55	14.13	13.26	12.70
J04382134+2609137	69.588918	26.153756	0.2	-19.8	-	-	-	-	4.3	13.90	13.00	12.10	-	-	12.80	11.59	10.63
J04382858+2610494	69.619127	26.180360	10.4	-12.8	5.0	-29.0	-	-	4.9	11.20	11.29	10.65	-	-	9.47	8.24	7.30
J04383528+2610386	69.647034	26.177332	7.7	-21.2	6.0	-43.0	-	-	2.5	11.34	11.24	10.50	-	-	9.23	8.28	7.91
J04390396+2544264	69.766507	25.740615	2.0	-18.4	-	-	-	-	0.4	14.60	13.45	12.54	-	-	12.65	11.84	11.37
J04392090+2545021	69.837176	25.750550	15.5	-11.9	2.0	-21.0	-	-	5.7	11.82	11.45	10.60	-	-	10.20	8.89	8.06
J04393364+2359212	69.890221	23.989176	10.2	-18.1	-	-	0.8	-	-	12.92	12.31	11.64	-	10.59	11.57	10.80	10.28
J04394488+2601527	69.937018	26.031254	1.2	-24.8	-	-	2.4	-	-	12.61	11.72	10.87	-	9.99	10.64	9.52	8.95
J04394748+2601407	69.947857	26.027909	2.2	-27.8	-	-	3.0	-	2.6	15.00	13.49	12.18	-	10.94	12.17	11.01	10.33
J04395574+2545020	69.982270	25.750495	-1.4	-23.7	-	-	-	-	18.0	14.93	13.00	10.85	-	-	10.67	8.05	6.28
J04400067+2358211	70.002813	23.972460	-1.1	-28.1	-	-	0.6	-	-	13.93	13.12	12.42	-	11.52	12.43	11.87	11.49
J04400800+2605253	70.033362	26.090334	5.8	-16.2	-	-	-	-	13.1	15.95	14.35	12.41	-	-	12.41	10.25	8.87
J04403979+2519061	70.165806	25.318341	1.2	-8.6	-	-	2.3	-	3.6	13.83	12.84	11.78	-	10.41	11.82	10.79	10.24
J04404950+2551191	70.206305	25.855240	6.1	-28.7	-	-	-	-	1.5	12.12	11.76	11.08	-	-	10.75	9.92	9.49
J04410424+2557561	70.267709	25.965528	8.0	-19.6	17.0	-19.0	-	-	0.6	12.27	11.69	11.03	-	-	10.95	10.26	9.95
J04410470+2451062	70.269593	24.851705	-7.3	-9.4	10.0	-17.0	1.3	-	1.1	11.49	12.12	10.83	-	10.50	9.24	8.48	8.28
J04411078+2555116	70.294955	25.919843	5.6	-19.6	-	-	-	-	1.8	15.68	14.57	13.50	-	-	13.19	12.12	11.45
J04412464+2543530	70.352710	25.731342	7.5	-17.6	-	-	-	-	-	-	19.95	16.88	-	-	16.71	13.54	11.75
J04413882+2556267	70.411789	25.940743	7.8	-7.2	-	-	2.0	-	9.3	13.38	12.39	11.28	-	9.90	11.85	10.12	9.20
J04414825+2534304	70.451044	25.575122	0.4	-5.3	-	-	2.8	-	1.1	16.08	14.78	13.65	-	12.10	13.73	12.80	12.22
J04420548+2522562	70.522879	25.382266	6.7	-12.7	0.0	-27.0	1.1	-	4.3	11.52	11.23	10.54	-	10.72	9.79	8.66	8.23
J04420732+2523032	70.530556	25.384202	9.7	-9.1	8.0	-29.0	1.2	-	4.6	11.34	11.16	10.57	-	9.74	9.58	8.40	7.95
J04420777+2523118	70.532445	25.386603	15.6	-3.0	15.0	-17.0	1.2	-	5.0	11.40	11.36	10.54	-	9.88	9.81	8.60	7.94

Table A.3 – continued from previous page

name	RA$_U$ [deg]	Dec$_U$ [deg]	$\mu_{\alpha,U}$ [mas/yr]	$\mu_{\delta,U}$ [mas/yr]	$\mu_{\alpha,lit}$ [mas/yr]	$\mu_{\delta,lit}$ [mas/yr]	A$_{V,YJK}$ [mag]	A$_{V,JHK}$ [mag]	$A_{V,lit}$ [mag]	Z_U [mag]	Y_U [mag]	J_U [mag]	H_U [mag]	K_U [mag]	J_M [mag]	H_M [mag]	K_M [mag]
J04422101+2520343	70.587596	25.342843	7.0	-13.5	-	-	2.3	-	1.6	12.84	12.14	11.48	-	10.20	11.40	10.58	10.17
J04423769+2515374	70.657078	25.260337	1.5	-22.5	8.0	-21.0	2.3	-	5.6	12.05	11.74	11.07	-	10.15	11.00	9.69	8.76
J04430309+2520187	70.762887	25.338493	-2.0	-16.4	9.0	-27.0	1.9	-	2.3	12.03	11.79	11.22	-	10.01	10.71	9.78	9.33
J04442713+2512164*	71.113093	25.204558	12.5	0.2	-	-	1.3	-	0.0	13.65	12.54	11.91	-	10.66	12.20	11.36	10.76
J04464260+2459034	71.677588	24.984245	22.5	-9.9	-	-	1.0	-	0.0	12.57	12.04	11.49	-	10.52	11.26	10.67	10.34

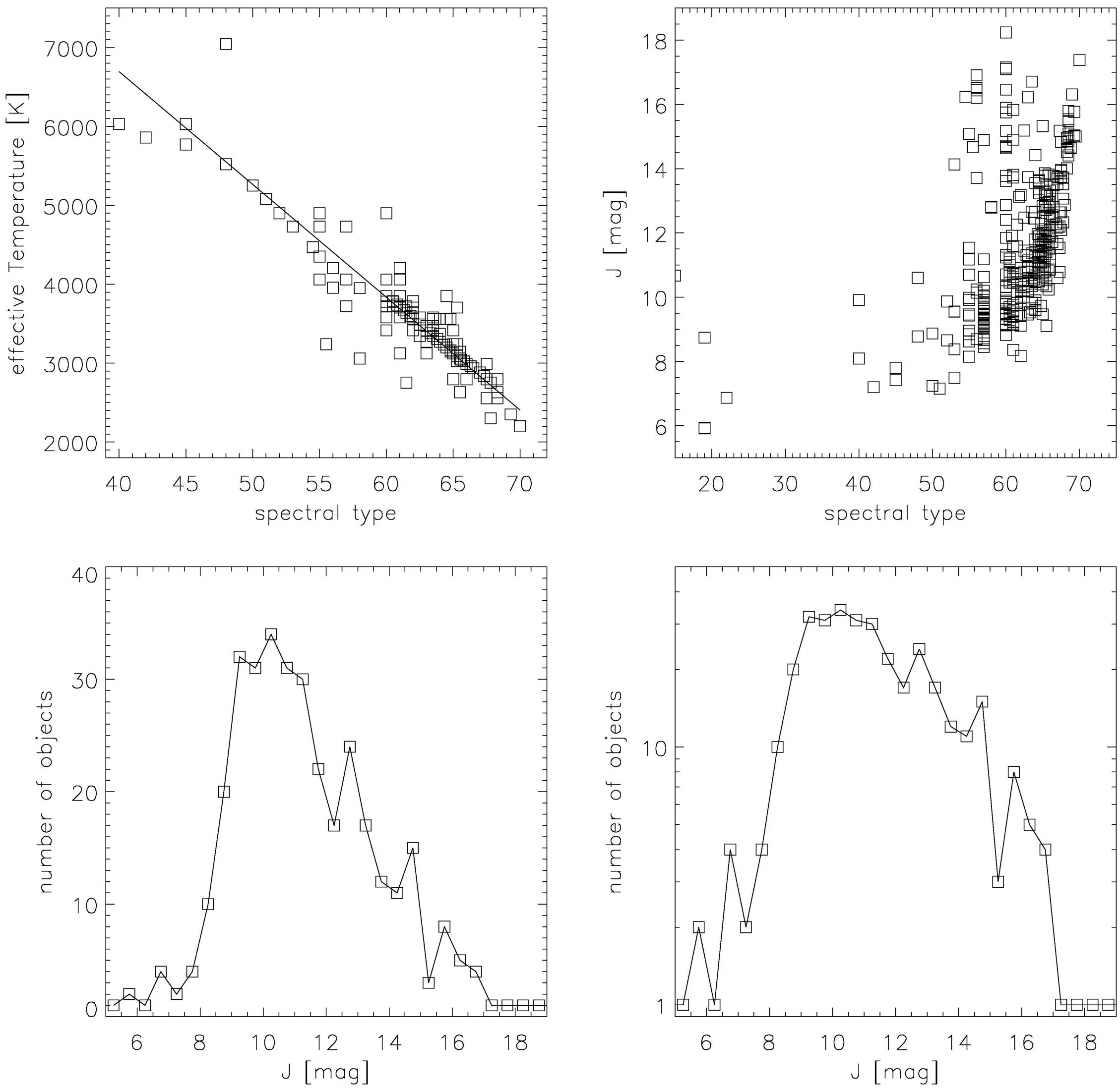

Figure A.1: We show the connection of the spectral types and the effective temperatures of the 351 already known Taurus members (upper left). We find the relation $T_{eff} = -143 \cdot (SpectralType) + 12415\ K$. On the upper right, we show the J band photometry vs. the spectral type. The diagrams on the bottom show the luminosity function of the Taurus members. On the left side, the linear connection is shown. On the right side, the logarithmic values are plotted. We find a peak of $J = 10.25\ mag$, corresponding to masses between 0.8 and 0.9 $M_{\odot}$ following the evolutionary models used in this work.

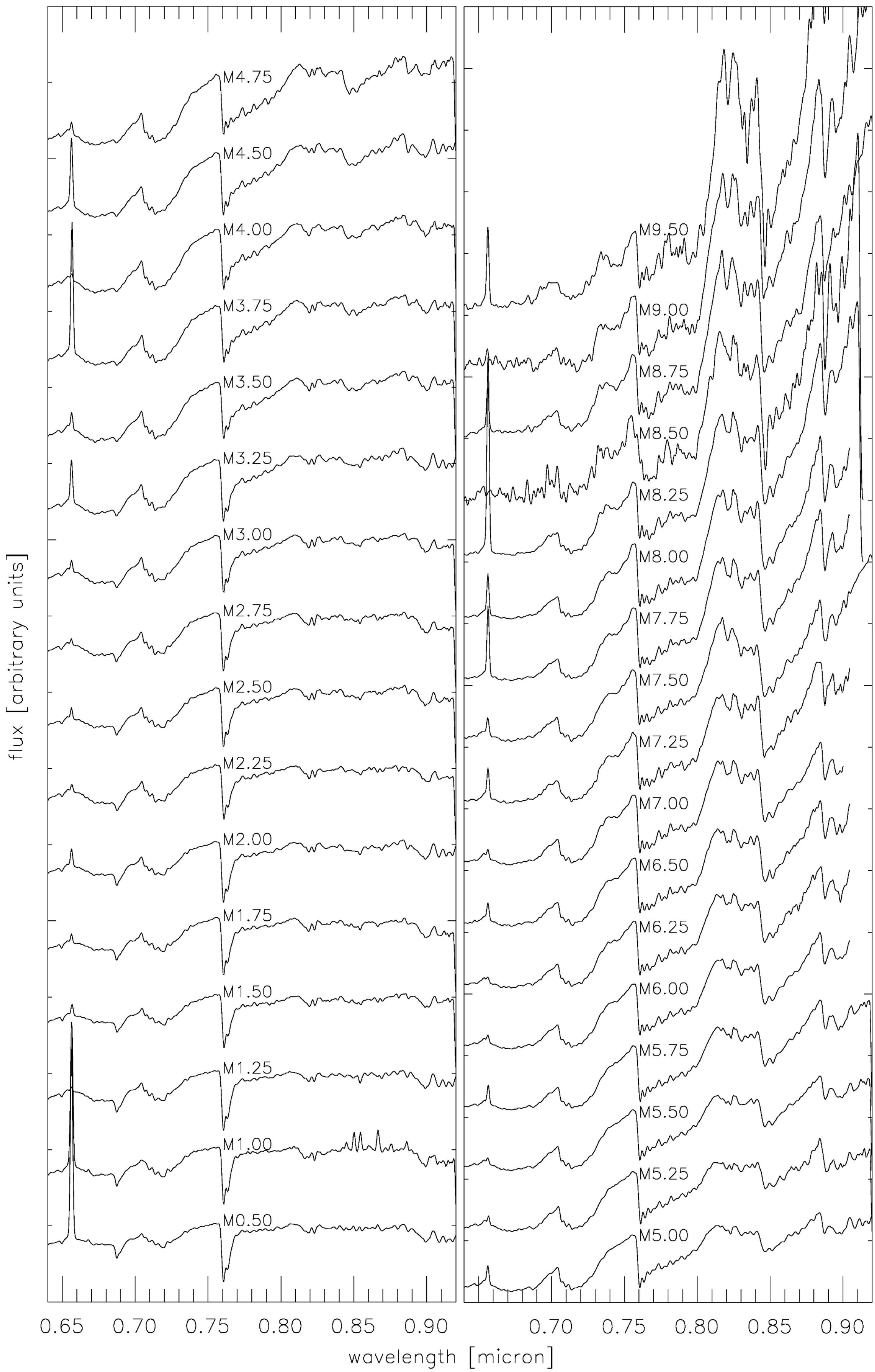

Figure A.2: The 33 reference spectra by K. Luhman

Table A.4: Data of the 33 sources from K. Luhman used as reference spectra. The spectral type is from the authors (Chamaeleon I: Luhman 2004b & 2007, Taurus: Briceño et al. 1998, Upper Sco: Luhman et al. 2007). The other data is collected from the SIMBAD database and shown for completeness purposes. *BVRI* are Johnsons filter system and *JHK* from 2MASS. The sources are sorted by spectral type and 2MASS names are shortened.

spectral type	name	RA [*deg*]	Dec [*deg*]	*B* [*mag*]	*V* [*mag*]	*R* [*mag*]	*I* [*mag*]	*J* [*mag*]	*H* [*mag*]	*K* [*mag*]	region
M0.5	Ass Cha T 2-56	169.404188	-77.077256	13.10	13.50	12.20	-	10.30	9.58	9.23	Chamaeleon I
M1	J11124210-7658400	168.175429	-76.977783	-	-	-	-	10.41	9.72	9.50	Chamaeleon I
M1.25	J11094006-7628391	167.416950	-76.477553	15.68	14.04	12.50	-	10.07	9.23	8.96	Chamaeleon I
M1.5	V* UV Cha	166.469217	-76.307097	14.00	-	12.40	-	10.31	9.59	9.34	Chamaeleon I
M1.75	J11045285-7625514	166.220225	-76.430969	16.51	14.66	-	-	10.72	9.98	9.75	Chamaeleon I
M2	J11091172-7729124	167.298846	-77.486800	12.60	13.17	-	-	9.93	9.15	8.96	Chamaeleon I
M2.25	J11181957-7622013	169.581558	-76.367036	16.46	14.80	-	-	11.25	10.53	10.26	Chamaeleon I
M2.5	J11113474-7636211	167.894775	-76.605872	16.35	14.73	-	-	10.86	10.08	9.80	Chamaeleon I
M2.75	J11145031-7733390	168.709663	-77.560844	15.90	-	12.70	-	10.48	9.75	9.55	Chamaeleon I
M3	J11023265-7729129	165.636058	-77.486939	17.73	15.94	13.50	-	11.27	10.46	10.13	Chamaeleon I
M3.25	J10574219-7659356	164.425833	-76.993239	14.10	-	-	-	10.43	9.56	9.25	Chamaeleon I
M3.5	J11132446-7629227	168.351921	-76.489647	17.50	-	14.60	-	11.86	11.11	10.80	Chamaeleon I
M3.75	Ass Cha T 2-10	165.167596	-76.324464	14.70	-	-	-	11.86	11.24	10.87	Chamaeleon I
M4	J11124861-7647066	168.202546	-76.785186	-	-	-	-	12.14	11.44	11.20	Chamaeleon I
M4.5	J11025504-7721508	165.729375	-77.364114	15.00	-	-	-	11.57	10.86	10.45	Chamaeleon I
M4.75	J11091380-7628396	167.307513	-76.477692	18.20	-	16.00	-	11.85	11.21	10.87	Chamaeleon I
M5	J11120984-7634366	168.041037	-76.576836	15.20	-	14.60	-	10.96	10.18	9.84	Chamaeleon I
M5.25	J11054300-7726517	166.429175	-77.447708	18.71	17.27	-	-	11.26	10.62	10.24	Chamaeleon I
M5.5	J11102852-7716596	167.618850	-77.283233	-	-	-	-	11.73	11.11	10.78	Chamaeleon I
M5.75	J11105597-7645325	167.733225	-76.759047	-	-	-	-	11.16	10.42	9.91	Chamaeleon I
M6	J11041060-7612490	166.044183	-76.213622	-	-	-	-	13.16	12.52	12.12	Chamaeleon I
M6.25	J11082404-7739299	167.100167	-77.658325	22.60	21.60	-	-	14.31	13.58	13.24	Chamaeleon I
M6.5	J11081850-7730408	167.077104	-77.511336	-	-	-	-	14.06	13.47	13.04	Chamaeleon I
M7	J11123099-7653342	168.129154	-76.892844	-	-	-	-	14.07	13.51	13.05	Chamaeleon I
M7.25	J11082927-7739198	167.121958	-77.655511	21.90	19.90	-	-	14.59	13.92	13.55	Chamaeleon I
M7.5	J04294568+2630468	67.440333	26.513003	-	19.69	19.10	15.08	12.64	11.92	11.54	Taurus

Table A.4 – continued from previous page

spectral type	name	RA [*deg*]	Dec [*deg*]	*B* [*mag*]	*V* [*mag*]	*R* [*mag*]	*I* [*mag*]	*J* [*mag*]	*H* [*mag*]	*K* [*mag*]	region
M7.75	J11071668-7735532	166.819537	-77.598136	22.80	21.00	17.90	-	13.34	12.67	12.17	Chamaeleon I
M8	J11102226-7625138	167.592779	-76.420503	18.70	-	16.80	-	13.53	12.90	12.45	Chamaeleon I
M8.25	J04305718+2556394	67.738279	25.944300	-	22.07	-	17.16	14.52	13.83	13.27	Taurus
M8.5	J04355143+2249119	68.964300	22.819986	-	24.92	-	18.76	15.48	14.66	14.19	Taurus
M8.75	Oph J1622-2405B	245.605000	-24.087670	-	-	-	18.98	15.24	14.64	14.03	Upper Sco
M9	J11122250-7714512	168.093792	-77.247567	-	-	22.22	19.57	15.90	14.93	14.43	Chamaeleon I
M9.5	J04272799+2612052	66.866654	26.201464	-	24.72	20.54	18.75	15.00	14.03	13.28	Taurus

Appendix B

Figures and tables from Chapter 4

In this chapter, we put the tables and images of Chap. 4, which describes the searches for new member candidates in Taurus and Orion. The various CMD and CCD of UKIDSS GCS, 2MASS and IRAC photometry are shown, where we applied our selection cuts. We give an overview of all selections made, connecting them to masses and magnitudes. We show the data of the finally observed sources of the different searches and show their UKIDSS *J* band images. Additionally, the SED of the MIR excess candidates are shown.

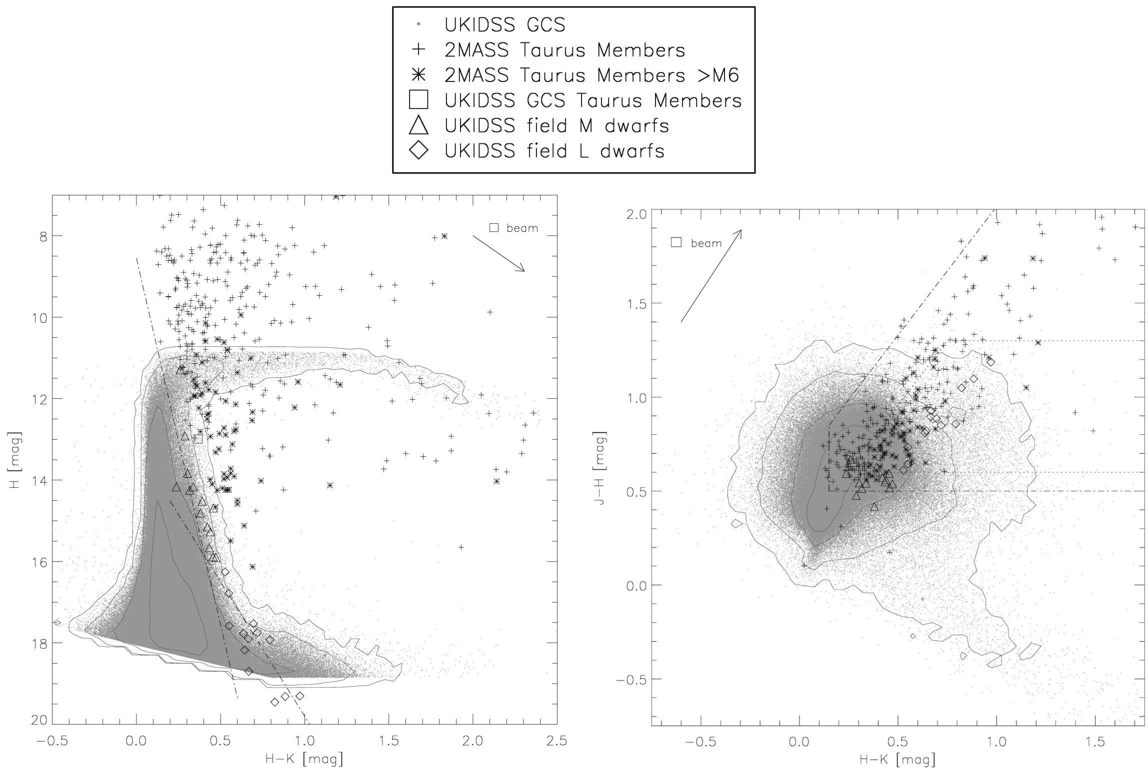

Figure B.1: Selection 1 of the LMO search in Taurus: UKIDSS and 2MASS *JHK* photometry: the $H-K$ vs. H (left) CMD, and the $H-K$ vs. $J-H$ (right) CCD. The signs are like in Fig. 4.1 and 4.2 and get explained at the top of the images. In the CCD, we show the limits given by Luhman et al. (2006) for Taurus members later than $M6$ via the dotted line.

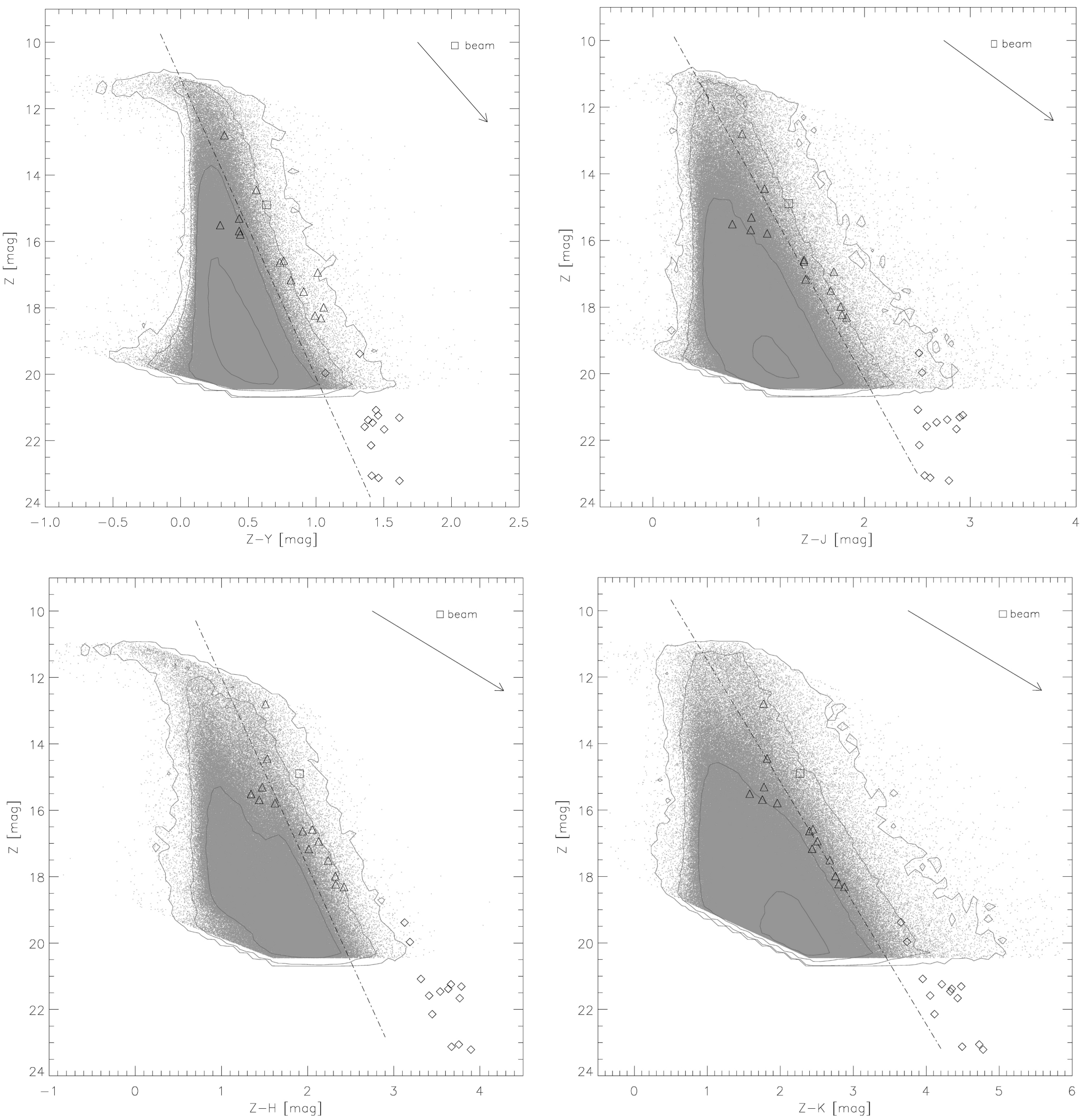

Figure B.2: Selection 2 of the LMO search in Taurus Part I: UKIDSS *ZYJHK* photometry: the $Z-Y$ vs. Z (top left), the $Z-J$ vs. Z (top right), the $Z-H$ vs. Z (bottom left), and the $Z-K$ vs. K (bottom right)) CMD. The signs are like in Fig. 4.1 and 4.2.

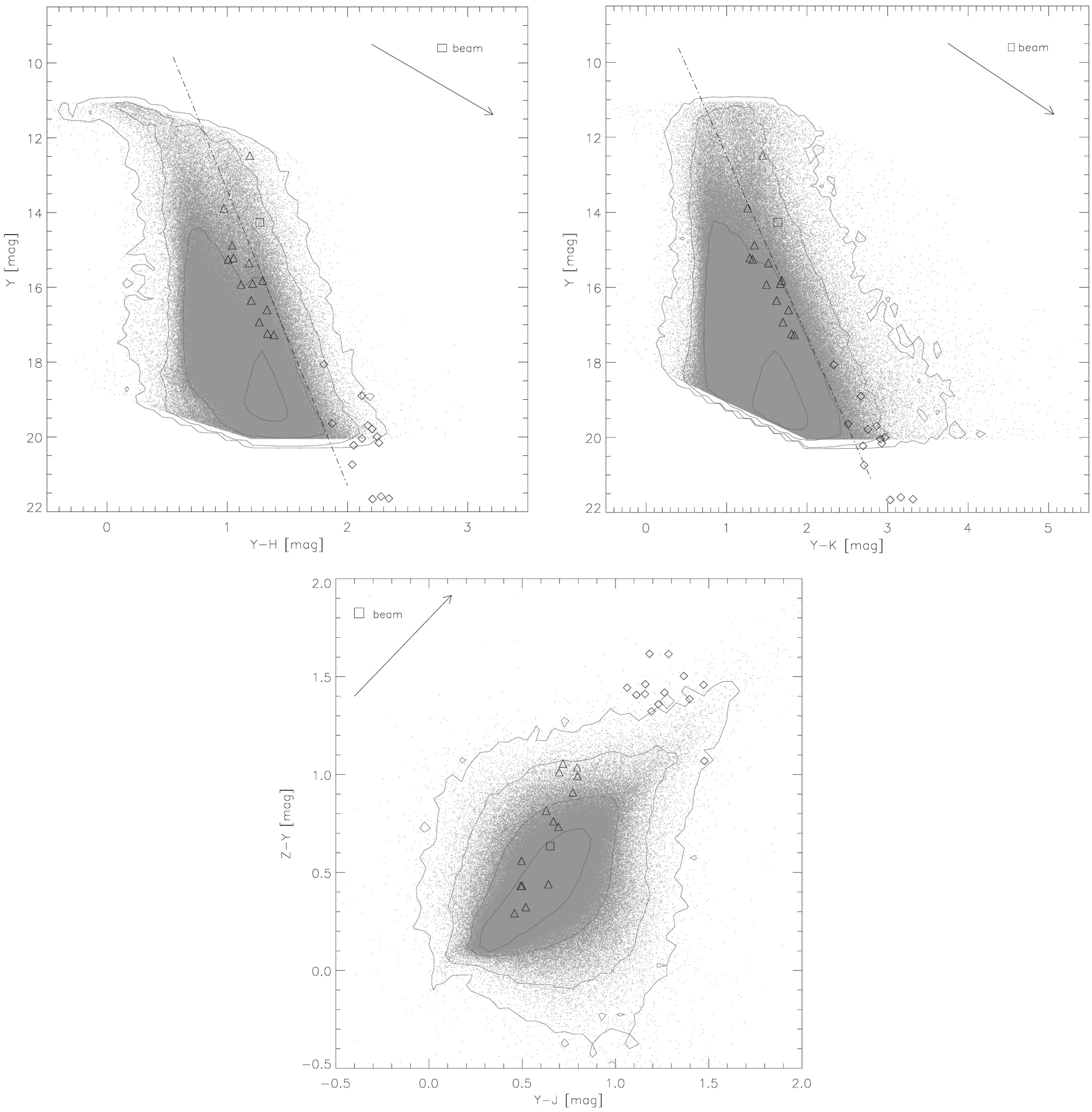

Figure B.3: Selection 2 of the LMO search in Taurus Part II: UKIDSS *ZYJHK* photometry: the $Y-H$ vs. Y (top left) and the $Y-K$ vs. Y (top right) CMD, and the $Y-J$ vs. $Z-Y$ (bottom) CCD (see Fig. B.2).

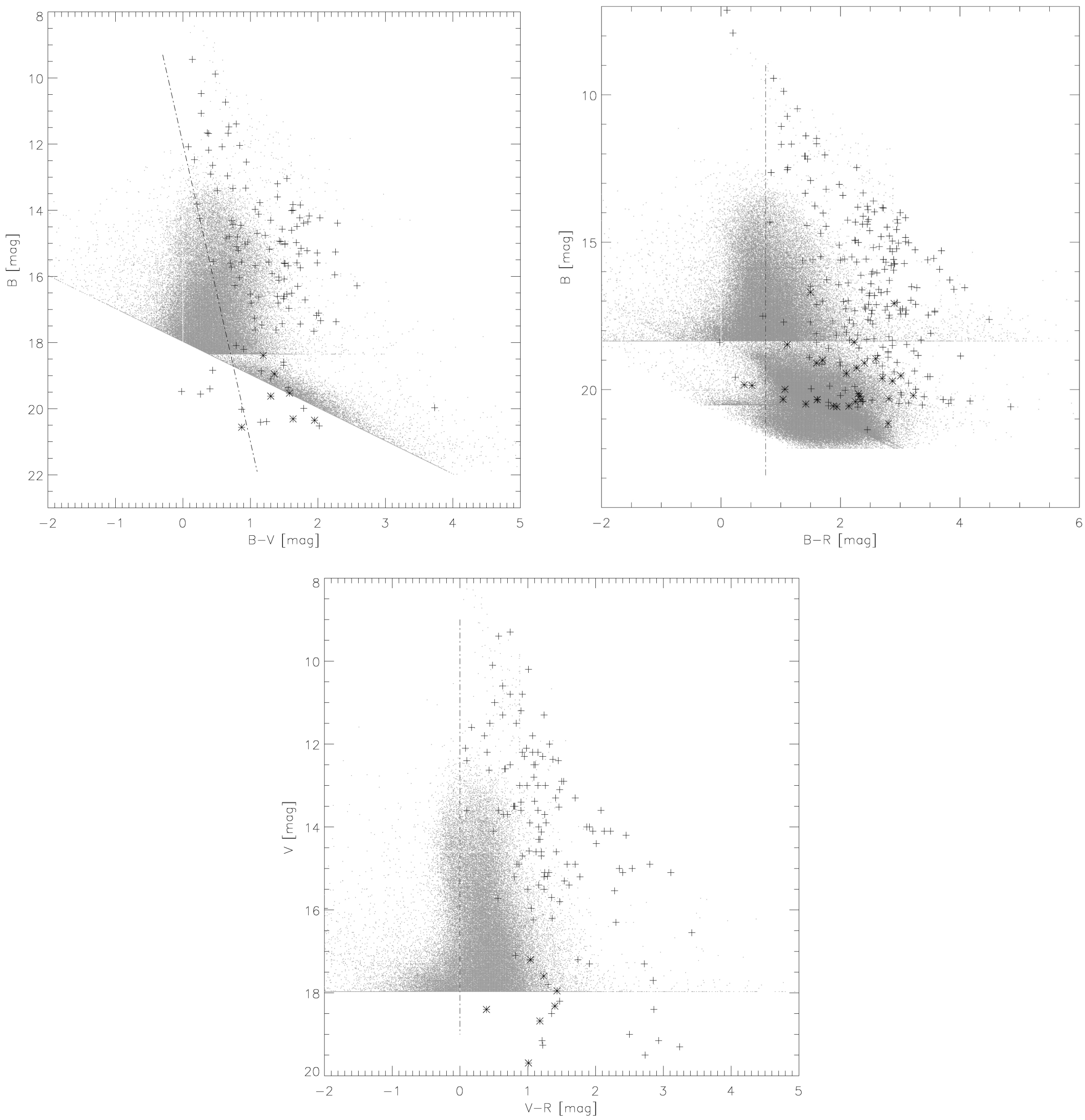

Figure B.4: Selection 4 of the LMO search in Taurus Part I: optical photometry: the $B-V$ vs. B (top left), the $B-R$ vs. B (top right), and the $V-R$ vs. V (bottom) CMD. The signs are like in Fig. 4.2.

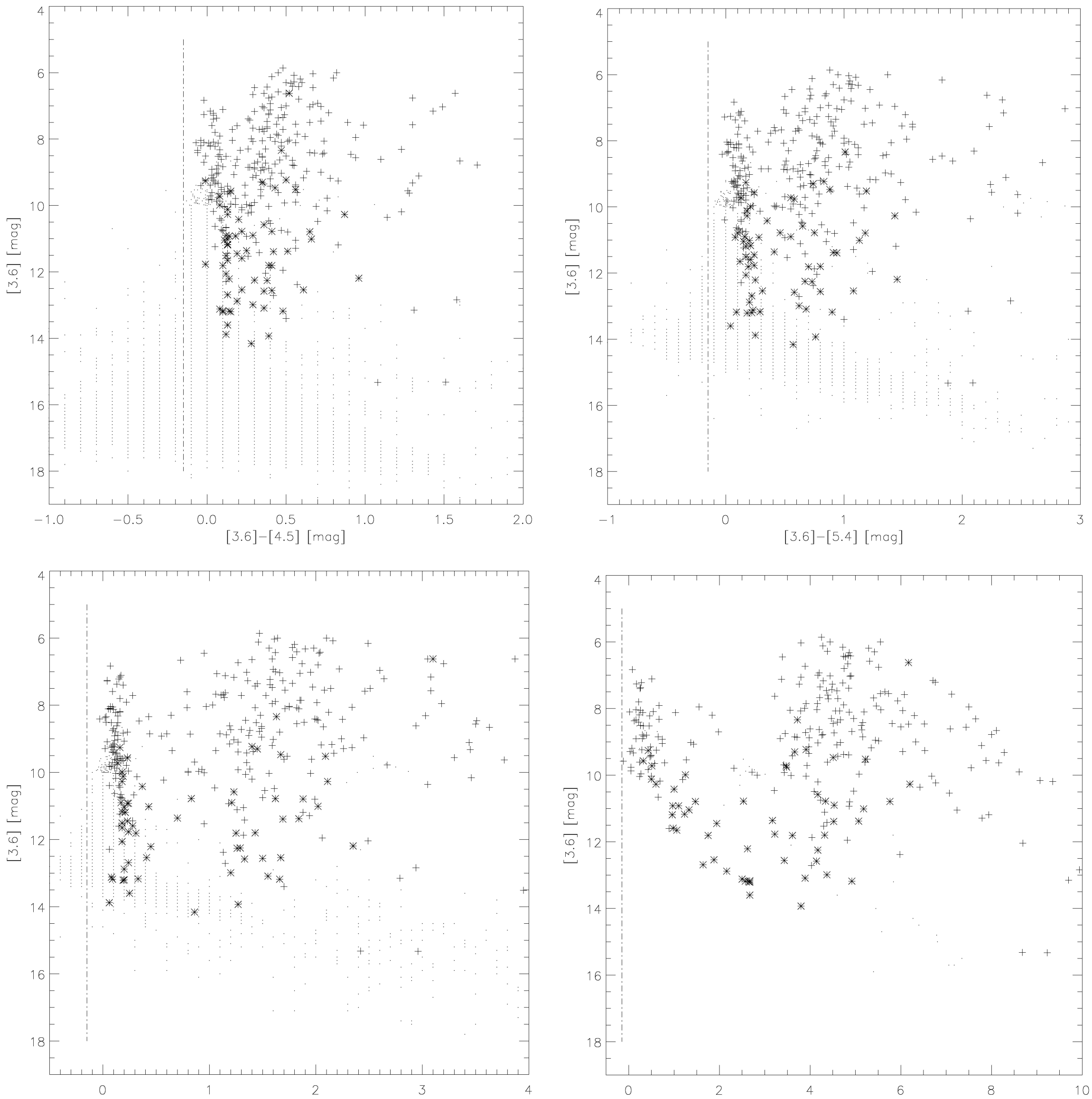

Figure B.5: Selection 4 of the LMO search in Taurus Part II: MIR photometry: the [3.6] − [4.5] vs. [3.6] (top left), the [3.6] − [5.4] vs. [3.6] (top right), the [3.6] − [8.0] vs. [3.6] (bottom left) and the [3.6] − [24.0] vs. [3.6] (bottom right) CMD. Note, that the photometry of those filters is only defined by 0.1 *mag*. The data set appears to be distributed in dotted lines. Only a small part of region A is covered by those filters (see Fig. B.4).

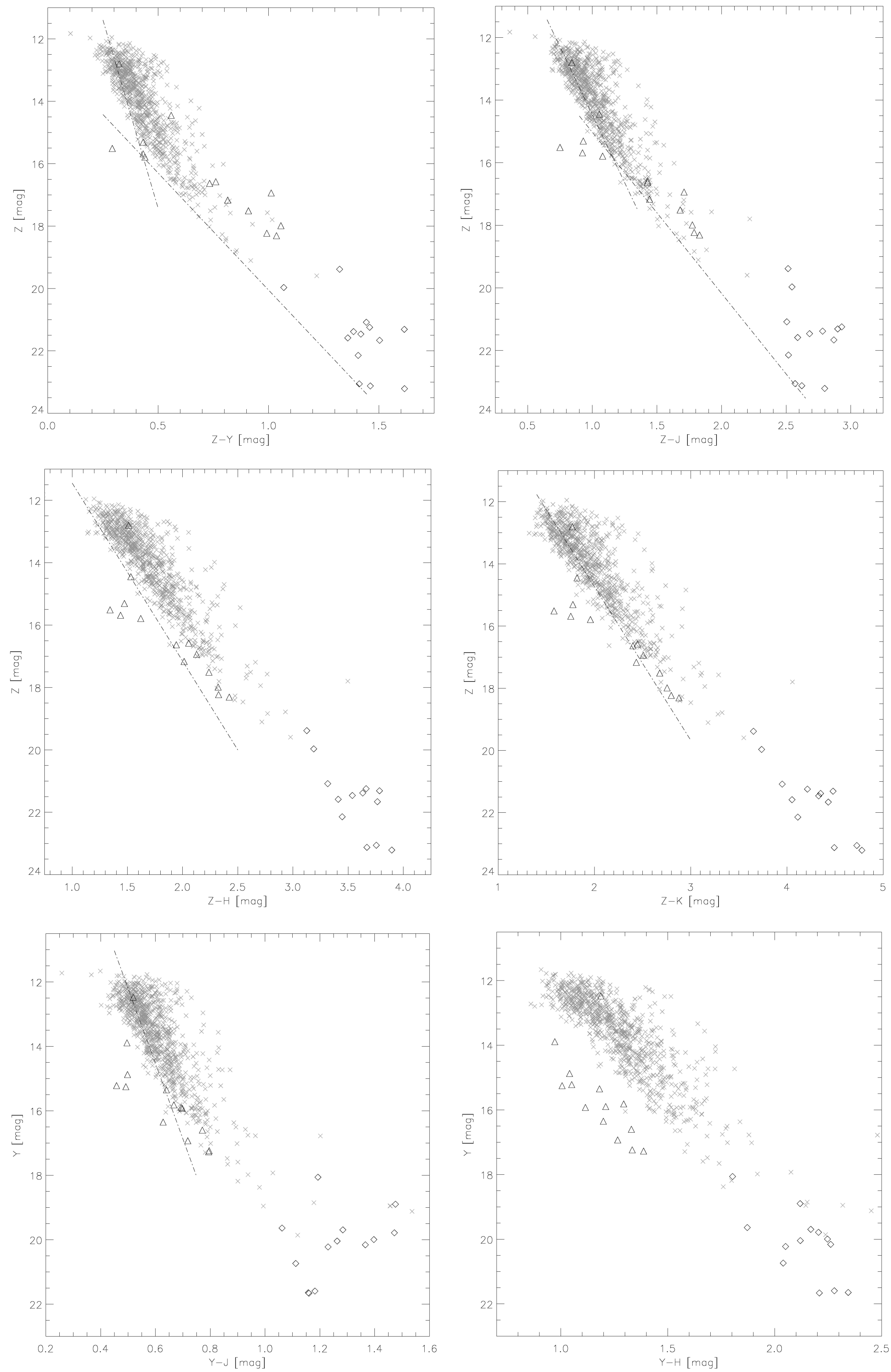

Figure B.6: Selection 5 of the LMO search in Taurus Part I: dereddened *ZYJHK* photometry: we show all CMD for the dereddened UKIDSS GCS photometry of the remaining selection (gray X). The signs are like in Fig.4.2.

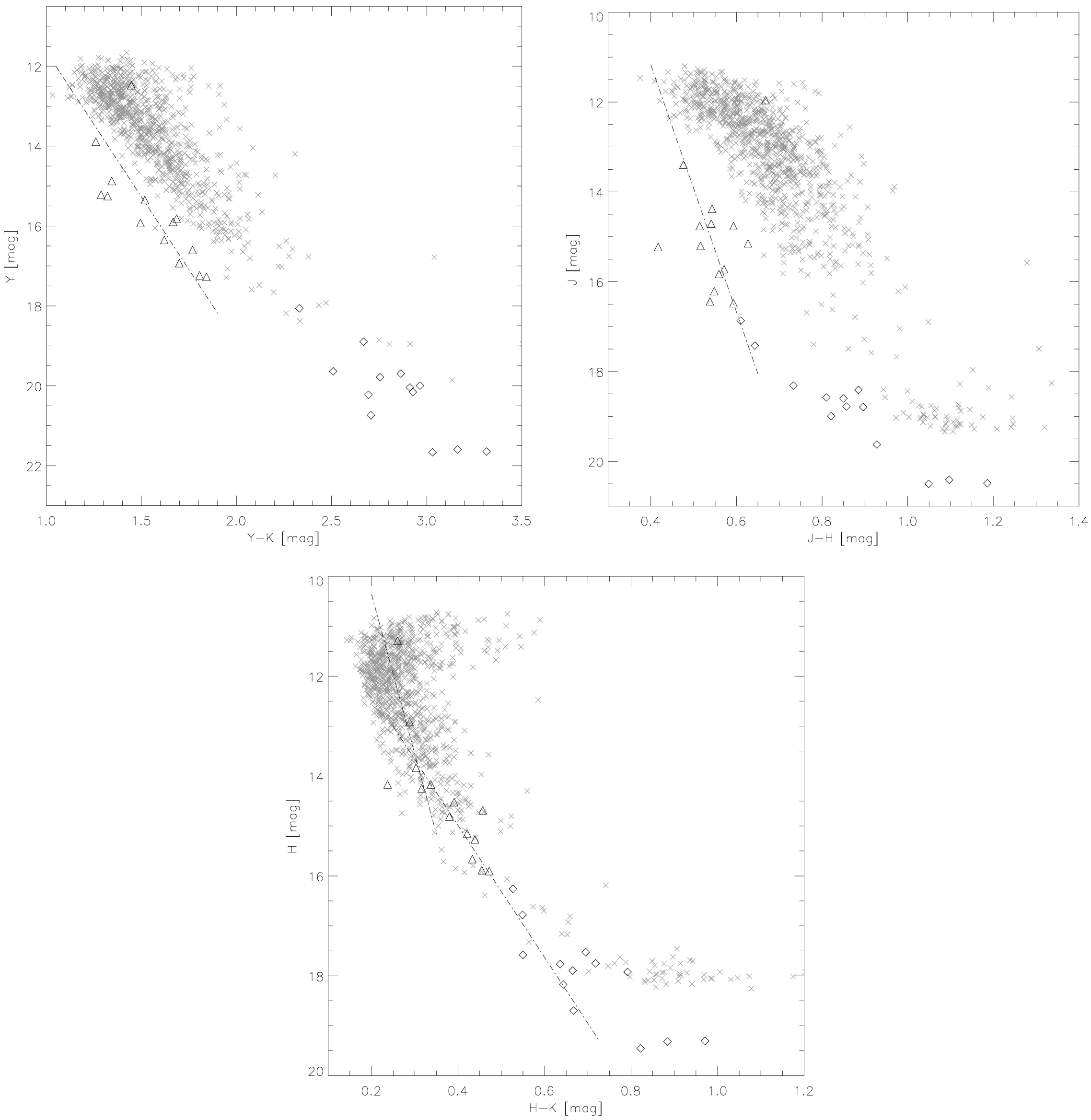

Figure B.7: Selection 5 of the LMO search in Taurus Part II: dereddened *ZYJHK* photometry (see Fig. B.6).

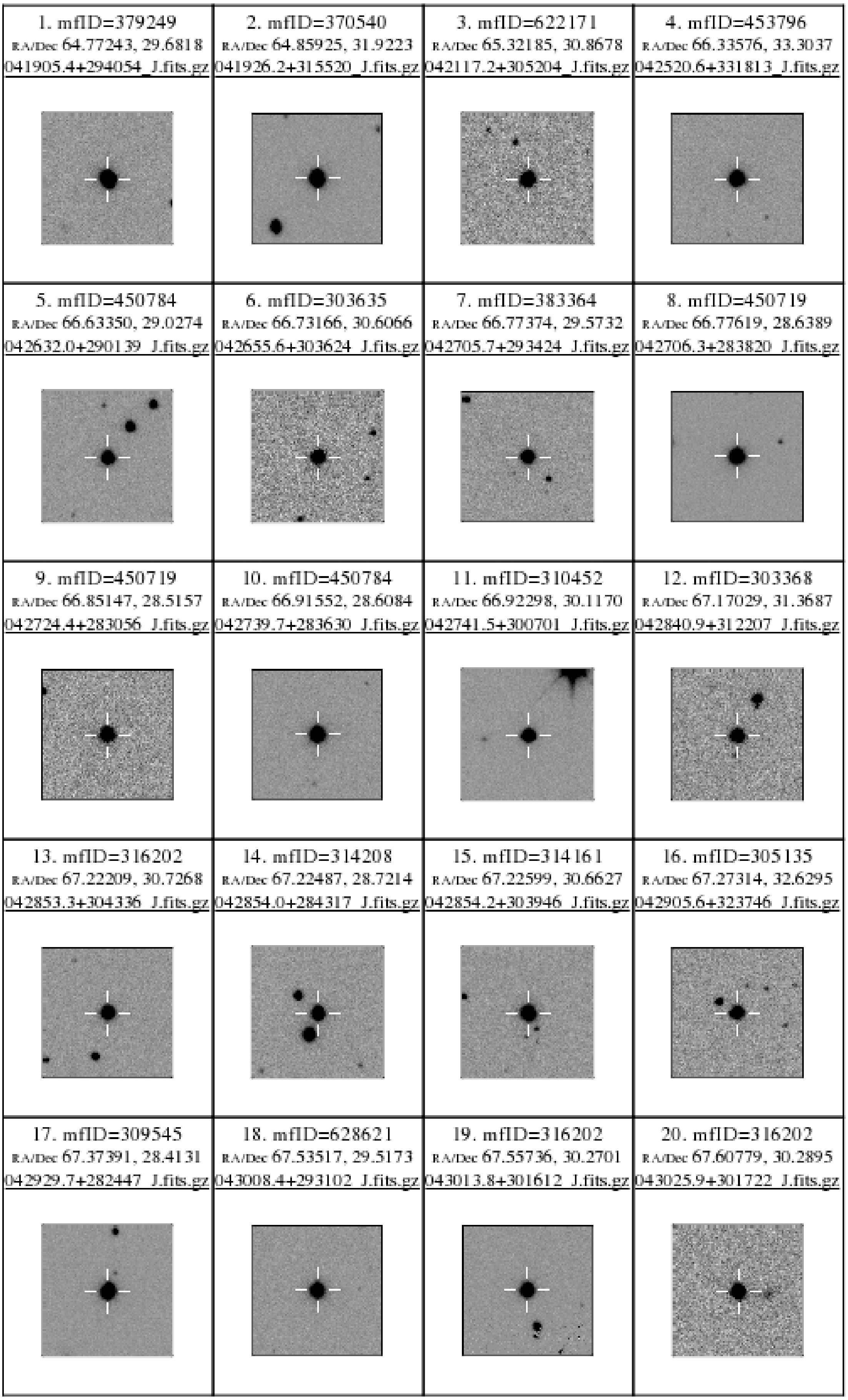

Figure B.8: UKIDSS 30*x*30 $arcsec^2$ J band images of 43 observed bright LMO Taurus member candidates Part I.

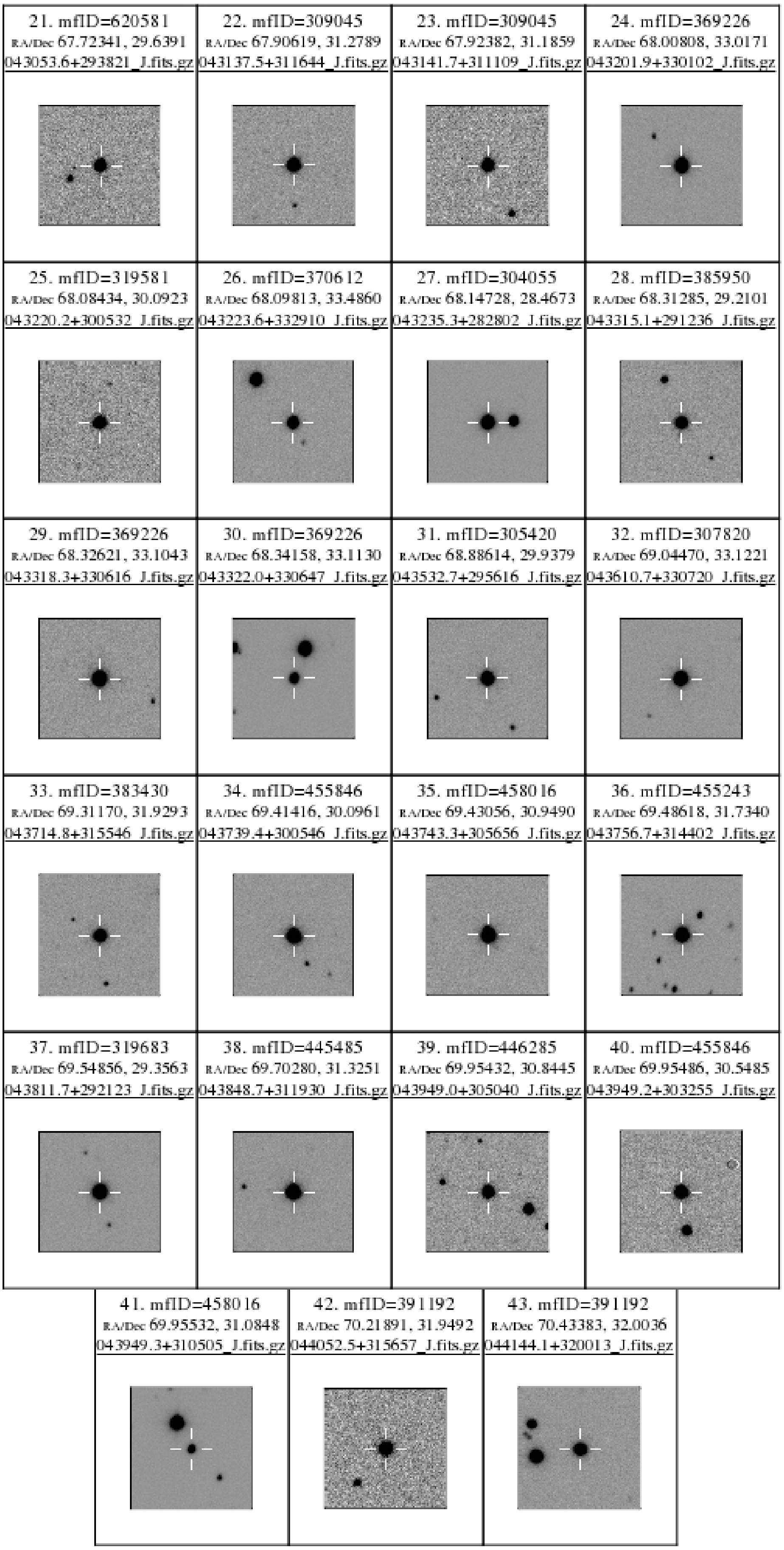

Figure B.9: UKIDSS 30*x*30 *arcsec*^{2} *J* band images of 43 observed bright LMO Taurus member candidates Part II.

Table B.1: Data of 43 observed bright LMO Taurus member candidates Part I. We observed additional NIR spectra for the sources marked by an asterisk.

name	RA_U	Dec_U	B	V	R	Z_U	Y_U	J_U	H_U	K_U	J_M	H_M	K_M	[3.6]	[4.5]	[5.4]	[8.0]
	[deg]	[deg]	[mag]	[mag]	[mag]	[mag]	[mag]	[mag]	[mag]	[mag]	[mag]	[mag]	[mag]	[mag]	[mag]	[mag]	[mag]
UGCSJ0419+2941	64.772426	29.681751	18.35	-	16.39	14.04	13.59	12.94	12.32	12.03	13.00	12.29	12.04	11.70	11.60	11.60	11.50
UGCSJ0419+3155	64.859254	31.922294	-	-	-	-	-	12.28	11.66	11.32	12.34	11.56	11.34	-	-	-	-
UGCSJ0421+3052	65.321851	30.867777	-	-	18.45	14.99	14.38	13.67	13.04	12.67	13.75	13.00	12.67	-	-	-	-
UGCSJ0425+3318	66.335763	33.303691	18.22	16.99	16.68	14.09	13.60	12.98	12.42	12.07	13.03	12.40	12.13	-	-	-	-
UGCSJ0426+2901	66.633504	29.027414	19.05	17.53	16.64	14.44	13.99	13.37	12.71	12.40	13.42	12.69	12.44	-	-	-	-
UGCSJ0426+3036	66.731661	30.606595	19.88	-	17.25	14.73	14.30	13.61	12.96	12.63	13.63	12.95	12.67	-	-	-	-
UGCSJ0427+2935	66.773743	29.573218	19.46	17.97	16.86	14.78	14.29	13.64	12.97	12.64	13.72	12.93	12.68	-	-	-	-
UGCSJ0427+2838	66.776191	28.638935	16.63	15.67	14.83	13.25	12.86	12.30	11.77	11.38	12.37	11.58	11.38	11.20	11.20	11.20	11.10
UGCSJ0427+2830	66.851471	28.515653	20.04	-	17.38	15.06	14.52	13.85	13.11	12.79	13.89	13.17	12.82	12.50	12.40	12.50	12.50
UGCSJ0427+2836	66.915524	28.608425	17.35	16.26	15.66	13.75	13.33	12.74	12.04	11.76	12.78	12.02	11.80	11.50	11.50	11.50	11.60
UGCSJ0427+3007*	66.922979	30.116989	16.67	16.03	15.02	13.45	13.04	12.40	11.70	11.40	12.43	11.61	11.38	-	-	-	-
UGCSJ0428+3122*	67.170288	31.368720	21.43	-	18.30	-	14.50	13.78	13.01	12.62	13.86	12.97	12.62	-	-	-	-
UGCSJ0428+3043	67.222093	30.726782	-	-	-	-	-	12.46	11.84	11.57	12.50	11.79	11.59	-	-	-	-
UGCSJ0428+2843	67.224869	28.721382	18.97	-	16.52	15.03	14.48	13.78	13.11	12.72	13.83	13.01	12.67	12.30	12.30	12.20	12.10
UGCSJ0428+3039*	67.225986	30.662750	-	-	-	-	-	12.41	11.80	11.42	12.43	11.72	11.46	-	-	-	-
UGCSJ0429+3237	67.273143	32.629545	17.93	-	16.82	14.71	14.21	13.54	12.93	12.58	13.59	12.86	12.60	-	-	-	-
UGCSJ0429+2824	67.373913	28.413134	17.73	16.58	15.20	13.45	13.00	12.35	11.66	11.31	12.40	11.57	11.30	10.90	11.00	10.90	11.00
UGCSJ0430+2931*	67.535172	29.517304	-	-	-	13.65	13.18	12.52	11.80	11.41	12.56	11.68	11.38	-	-	-	-
UGCSJ0430+3016	67.557355	30.270062	-	-	-	-	-	12.10	11.56	11.25	12.14	11.45	11.25	-	-	-	-
UGCSJ0430+3017	67.607791	30.289523	-	-	-	-	-	13.40	12.75	12.44	13.47	12.77	12.45	-	-	-	-
UGCSJ0430+2939	67.723409	29.639053	-	-	19.12	15.73	15.00	14.09	13.22	12.76	14.14	13.15	12.79	12.40	12.30	12.30	12.40
UGCSJ0431+3116	67.906190	31.278909	-	-	-	-	-	12.60	11.89	11.49	12.65	11.72	11.45	-	-	-	-
UGCSJ0431+3111	67.923819	31.185879	-	-	-	-	-	13.62	12.93	12.56	13.69	12.88	12.57	-	-	-	-
UGCSJ0432+3301	68.008082	33.017115	15.83	14.53	14.42	-	12.60	12.06	11.53	11.18	12.12	11.38	11.18	-	-	-	-
UGCSJ0432+3005	68.084337	30.092305	19.67	17.52	17.02	14.67	14.14	13.48	12.79	12.47	13.51	12.80	12.49	-	-	-	-
UGCSJ0432+3329	68.098130	33.485994	-	-	-	-	-	13.28	12.65	12.33	13.32	12.64	12.35	-	-	-	-
UGCSJ0432+2828	68.147278	28.467350	16.05	15.47	13.73	13.16	12.72	12.10	11.56	11.08	12.18	11.33	11.08	10.90	11.00	11.00	10.90
UGCSJ0433+2912	68.312853	29.210087	20.43	17.97	17.80	14.75	14.06	13.29	12.60	12.20	13.37	12.63	12.28	11.80	11.80	11.80	11.60
UGCSJ0433+3306A	68.326209	33.104350	-	-	-	-	-	12.39	11.86	11.41	12.45	11.62	11.41	-	-	-	-
UGCSJ0433+3306B	68.341585	33.112994	-	-	-	-	-	12.92	12.33	12.01	12.94	12.21	11.97	-	-	-	-
UGCSJ0435+2959	68.886138	29.937862	17.65	16.53	15.52	13.71	13.20	12.55	11.76	11.44	12.56	11.68	11.41	-	-	-	-
UGCSJ0436+3307	69.044697	33.122114	16.46	15.17	14.63	13.09	12.69	12.13	11.55	11.23	12.21	11.44	11.23	-	-	-	-
UGCSJ0437+3155	69.311695	31.929342	18.35	16.83	16.09	13.92	13.40	12.68	11.93	11.54	12.76	11.87	11.54	-	-	-	-
UGCSJ0437+3005	69.414164	30.096065	17.67	16.62	15.72	13.73	13.25	12.59	11.83	11.52	12.63	11.79	11.53	-	-	-	-
UGCSJ0437+3056	69.430557	30.948983	20.03	17.97	17.05	14.48	13.74	12.91	12.11	11.69	12.98	12.05	11.72	-	-	-	-
UGCSJ0437+3144	69.486177	31.733964	16.87	16.13	15.20	13.59	13.16	12.51	11.81	11.51	12.58	11.69	11.50	-	-	-	-
UGCSJ0438+2921	69.548565	29.356266	17.25	15.64	15.18	13.30	12.78	12.06	11.55	11.03	12.16	11.30	11.02	-	-	-	-
UGCSJ0438+3119	69.702798	31.325123	17.01	15.83	15.14	13.41	13.04	12.46	11.80	11.51	12.50	11.73	11.51	-	-	-	-
UGCSJ0439+3050	69.954321	30.844460	20.12	-	17.23	15.29	14.82	14.13	13.34	13.01	14.16	13.27	12.98	-	-	-	-
UGCSJ0439+3032	69.954857	30.548529	19.91	17.89	17.17	15.23	14.75	14.04	13.26	12.93	14.07	13.30	12.94	-	-	-	-

Table B.1 – continued from previous page

name	RA_U	Dec_U	B	V	R	Z_U	Y_U	J_U	H_U	K_U	J_M	H_M	K_M	[3.6]	[4.5]	[5.4]	[8.0]
	[*deg*]	[*deg*]	[*mag*]	[*mag*]	[*mag*]	[*mag*]	[*mag*]	[*mag*]	[*mag*]	[*mag*]	[*mag*]	[*mag*]	[*mag*]	[*mag*]	[*mag*]	[*mag*]	[*mag*]
UGCSJ0439+3105	69.955318	31.084791	18.23	-	-	15.39	14.84	14.17	13.48	13.14	14.18	13.46	13.17	-	-	-	-
UGCSJ0440+3156	70.218909	31.949154	-	-	18.97	15.88	15.15	14.33	13.59	13.16	14.40	13.57	13.18	-	-	-	-
UGCSJ0441+3200	70.433829	32.003606	20.75	-	18.09	14.82	14.12	13.39	12.74	12.36	13.47	12.73	12.38	-	-	-	-

name	$A_{V,YJK}$	$A_{V,JHK}$	$\mu_{\alpha,U}$	$\mu_{\delta,U}$	$\mu_{\alpha,N}$	$\mu_{\delta,N}$	mem.	Class	α_{IRAC}
	[mag]	[mag]		[mas/yr]			prob.		
UGCSJ0419+2941	0.00	0.00	19.2	-27.7	18.0	-26.0	1	III	-2.628
UGCSJ0419+3155	-	0.20	8.1	-30.1	-	-	1	-	-
UGCSJ0421+3052	0.08	0.25	14.7	-0.1	2.0	-10.0	2	-	-
UGCSJ0425+3318	0.17	0.11	16.4	-21.4	10.0	-22.0	1	-	-
UGCSJ0426+2901	0.15	0.00	-4.7	-20.9	-2.0	-16.0	1	-	-
UGCSJ0426+3036	0.00	0.15	-5.2	-10.8	0.0	0.0	1	-	-
UGCSJ0427+2935	0.59	0.27	-1.7	-3.3	-20.0	-12.0	2	-	-
UGCSJ0427+2838	0.04	0.11	8.1	-6.1	-0.7	-3.9	1	III	-2.726
UGCSJ0427+2830	0.33	0.24	12.1	-13.8	2.0	-10.0	1	III	-2.876
UGCSJ0427+2836	0.42	0.33	-5.6	5.0	0.0	0.0	2	III	-2.947
UGCSJ0427+3007*	0.41	0.16	9.7	-18.1	8.0	-36.0	1	-	-
UGCSJ0428+3122*	0.63	0.47	5.3	-11.1	0.0	0.0	1	-	-
UGCSJ0428+3043	-	0.22	24.9	-15.5	-	-	2	-	-
UGCSJ0428+2843	0.56	0.23	9.2	-44.1	28.0	-58.0	2	III	-2.589
UGCSJ0428+3039*	-	0.00	3.4	-13.0	-	-	1	-	-
UGCSJ0429+3237	0.25	0.27	20.0	-15.2	10.0	-22.0	1	-	-
UGCSJ0429+2824	0.62	0.27	33.4	-2.2	29.2	-15.9	2	III	-2.907
UGCSJ0430+2931*	0.45	0.45	0.3	-12.8	-	-	1	-	-
UGCSJ0430+3016	-	0.33	-7.0	-8.8	-	-	1	-	-
UGCSJ0430+3017	-	0.02	15.7	-14.9	-	-	1	-	-
UGCSJ0430+2939	0.88	0.74	18.3	-14.2	34.0	-30.0	1	III	-2.849
UGCSJ0431+3116	-	0.65	6.7	4.1	-	-	2	-	-
UGCSJ0431+3111	-	0.41	9.9	-6.0	-	-	1	-	-
UGCSJ0432+3301	0.20	0.08	-1.2	2.7	3.5	-9.2	2	-	-
UGCSJ0432+3005	0.41	0.12	27.3	-18.5	24.0	-24.0	2	-	-
UGCSJ0432+3329	-	0.14	18.5	-15.3	-	-	1	-	-
UGCSJ0432+2828	0.37	0.22	-14.2	3.8	0.0	0.0	2	III	-2.823
UGCSJ0433+2912	0.33	0.28	16.1	-19.9	14.0	-18.0	1	III	-2.615
UGCSJ0433+3306A	-	0.18	-1.5	1.3	-	-	2	-	-
UGCSJ0433+3306B	-	0.14	8.7	-5.8	-	-	1	-	-
UGCSJ0435+2959	0.53	0.68	8.1	2.2	-0.2	-2.4	2	-	-
UGCSJ0436+3307	0.41	0.38	-5.6	-3.4	2.9	-10.7	2	-	-
UGCSJ0437+3155	0.66	0.53	16.6	-7.5	10.0	-22.0	1	-	-
UGCSJ0437+3005	0.45	0.50	3.9	-26.8	4.0	-24.0	1	-	-
UGCSJ0437+3056	0.66	0.53	3.3	5.1	0.0	0.0	2	-	-
UGCSJ0437+3144	0.30	0.23	-1.9	-3.2	-8.1	-10.0	2	-	-
UGCSJ0438+2921	0.50	0.35	11.9	-1.3	16.9	-14.3	2	-	-
UGCSJ0438+3119	0.25	0.17	1.0	-13.8	-2.2	-14.5	1	-	-
UGCSJ0439+3050	0.50	0.39	1.0	-8.2	0.0	0.0	1	-	-
UGCSJ0439+3032	0.56	0.47	-8.5	-12.7	0.0	0.0	1	-	-
UGCSJ0439+3105	0.38	0.31	19.3	-26.6	7.4	0.9	1	-	-
UGCSJ0440+3156	0.81	0.59	-4.7	-14.2	0.0	0.0	1	-	-
UGCSJ0441+3200	0.70	0.64	-4.3	-13.3	0.0	0.0	1	-	-

Table B.2: Data of 43 observed bright LMO Taurus member candidates Part II. We observed additional NIR spectra for the sources marked by an asterisk. The membership probability refers to the proper motion selection criteria.

section	selection criteria	sources Region A	sources	Mag. range [*mag*]	mass range [$M_\odot$]
4.1.1	**Taurus LMO via UKIDSS**	620766	967875		
	3 UKIDSS filters	509413	836599		
4.1.1.1	$J < 8.80 \cdot (J-K) + 5.30$			10.0-17.0	0.900-0.040
	$J < 3.70 \cdot (J-K) + 12.15$			17.0-19.5	0.040-0.025
	$J < 15.50 \cdot (J-H) + 4.30$			10.0-18.0	0.900-0.030
	$J < 7.20 \cdot (J-H) + 11.60$			18.0-19.5	0.030-0.025
	$H < 18.00 \cdot (H-K) + 8.55$			10.5-16.0	0.700-0.040
	$H < 6.60 \cdot (H-K) + 13.20$			16.0-19.0	0.040-0.018
	$J - H > 0.50$				
	$H - K > 0.15$				
	$J - H < 1.37 \cdot (H-K) + 0.6445$	20107	53066		
4.1.1.2	$Z < 9.00 \cdot (Z-Y) + 11.10$			11.0-20.5	0.850-0.035
	$Z < 5.70 \cdot (Z-J) + 8.75$			11.0-20.5	0.850-0.035
	$Z < 5.70 \cdot (Z-H) + 6.30$			11.0-20.5	0.850-0.035
	$Z < 3.65 \cdot (Z-K) + 7.85$			11.0-20.5	0.850-0.035
	$Y < 10.00 \cdot (Y-J) + 8.80$			11.0-20.5	0.750-0.027
	$Y < 7.90 \cdot (Y-H) + 5.50$			11.0-20.5	0.750-0.027
	$Y < 4.80 \cdot (Y-K) + 7.70$	2106	15361	11.0-20.5	0.750-0.027
4.1.1.3	(-18.6.-46.4) < ($\mu_\alpha.\mu_\delta$) < (33.4.5.6) mas/yr				
	(-30.0.-60.0) < ($\mu_\alpha.\mu_\delta$) < (40.0.10.0) mas/yr	1368	10492		
4.1.1.4	$B < 9.00 \cdot (B-V) + 12.00$			12.0-22.0	0.950-0.065
	$B - R > 0.75$ mag			12.0-22.0	0.950-0.065
	$V - R > 0.00$ mag			12.0-18.0	0.850-0.180
	$[3.6]-[4.5] >$ -0.15 mag			9.0-18.5	-
	$[3.6]-[5.4] >$ -0.15 mag			9.0-18.5	-
	$[3.6]-[8.0] >$ -0.15 mag			9.0-18.5	-
	$[3.6]-[24.0] >$ -0.15 mag	1295	10419	9.0-18.5	-
4.1.1.5	$Z_d < 24.14 \cdot (Z-Y)_d + 5.36$			12.0-16.0	0.700-0.150
	$Z_d < 7.50 \cdot (Z-Y)_d + 12.55$			16.0-20.0	0.150-0.038
	$Z_d < 8.67 \cdot (Z-J)_d + 5.80$			12.0-16.0	0.700-0.015
	$Z_d < 5.15 \cdot (Z-J)_d + 9.88$			16.0-20.0	0.015-0.038
	$Z_d < 5.70 \cdot (Z-H)_d + 5.75$			12.0-20.0	0.700-0.038
	$Z_d < 4.94 \cdot (Z-K)_d + 4.86$			12.0-20.0	0.700-0.038
	$Y_d < 23.33 \cdot (Y-J)_d + 0.53$			11.5-19.5	0.700-0.032
	$Y_d < 7.27 \cdot (Y-K)_d + 4.36$			11.5-19.5	0.700-0.032
	$J_d < 27.50 \cdot (J-H)_d + 0.18$			11.0-19.5	0.700-0.025
	$J_d < 25.00 \cdot (J-K)_d$ - 7.75			11.0-19.5	0.700-0.025
	$H_d < 32.00 \cdot (H-K)_d + 3.96$			10.5-13.5	0.700-0.200
	$H_d < 13.20 \cdot (H-K)_d + 9.71$	746	9868	13.5-18.5	0.200-0.020
4.1.1.6	$J >$12 mag	377	-	12.0-20.0	0.550-0.024
	Image check	320	-		
	bright sample: $J <$15.5 mag			12.0-15.5	0.550-0.080
	bright sample: 2MASS *JHK*				
	bright sample: error UKIDSS<0.01 mag	**253 (43)**	-		
	faint sample: $J >$15.5 mag	55	-	15.5-20.0	0.800-0.024
	faint sample: no 2MASS *JHK*				
	faint sample: error UKIDSS<0.15 mag	**19 (4)**	-		

section	selection criteria	sources Region A	Mag. range [*mag*]	mass range [$M_\odot$]
4.1.2	**Taurus LMO via IRAC**	42800		
	5 UKIDSS and 4 IRAC filters	2872		
4.1.2.1	$[3.6]-[5.8] > 1.5$			
	$[4.5]-[8.0] < 1.0$			
	$[3.6]-[5.8] > 0.75 \cdot ([4.5]-[8.0]-1.0)$			
	$[4.5]-[5.8] < 1.05$			
	$[5.8]-[8.0] > 1.0$			
	$[4.5]-[5.8] > 0.875 \cdot ([5.8]-[8.0]-1.0)$			
	$[4.5] < 13.5$			
	$[4.5]-[8.0] < 0.5$			
	$[4.5] < 13.5 + ([4.5]-[8.0]-2.3)/0.4$	2637		
4.1.2.2	$\alpha_{IRAC} > -2.62$	712		
4.1.2.3	2MASS *JHK*			
	12< J <15.5 mag		12.0-15.5	0.550-0.080
	error UKIDSS<0.01 mag			
	error IRAC<0.2 mag			
	Image check	**644 (22)**		
4.2	**Orion LMO**	186930		
	$J - K > 0.80$		11.5-15.5	0.700-0.090
	$J < 5.83 \cdot (J-K) + 10.83$		15.5-19.5	0.090-0.030
	$J - H > 0.45$		11.5-15.5	0.700-0.090
	$J < 14.00 \cdot (J-H) + 9.20$		15.5-19.5	0.090-0.040
	$H - K > 0.25$		11.5-13.0	0.600-0.300
	$H < 14.00 \cdot (H-K) + 9.50$		13.0-19.0	0.300-0.026
	$Z < 7.00 \cdot (Z-J) + 7.80$		12.0-20.5	0.800-0.040
	$Y < 15.00 \cdot (Y-J) + 6.00$		12.0-16.5	0.700-0.090
	$Y < 8.33 \cdot (Y-J) + 10.67$		16.5-20.0	0.090-0.040
	$J_d < 15.00 \cdot (J_d - K_d) + 4.00$		11.0-19.5	0.800-0.030
	$J_d - H_d > 0.40$		11.0-16.0	0.800-0.060
	$J_d < 20.00$ .dot $(J_d - H_d) + 8.00$		16.0-19.5	0.060-0.030
	$H_d < 50.00 \cdot (H_d - K_d) + 1.00$		11.0-16.0	0.700-0.050
	$H_d < 15.00$ .dot $(H_d - K_d) + 11.50$		16.0-18.5	0.050-0.027
	$Z_d < 5.00 \cdot (Z_d - J_d) + 12.00$		11.0-20.0	0.900-0.045
	$Y_d < 13.33 \cdot (Y_d - J_d) + 9.33$	3941	11.0-20.0	0.080-0.040
	J <18 mag	1028	11.0-18.0	0.800-0.040
	new stellar clump	**55 (7)**		

Table B.3: Summary of selection criteria for the search for new LMO in Taurus via UKIDSS photometry, via IRAC photometry and the search for LMO in Orion. We indicate the section the selections get explained and show the number of selected candidates in each step. We give an approximation of the validity range in magnitudes and the resulting mass range following the evolutionary models used in this work corrected for the distances of Taurus and Orion, respectively. The number of the final selections are highlighted and the number of observed sources are shown in brackets.

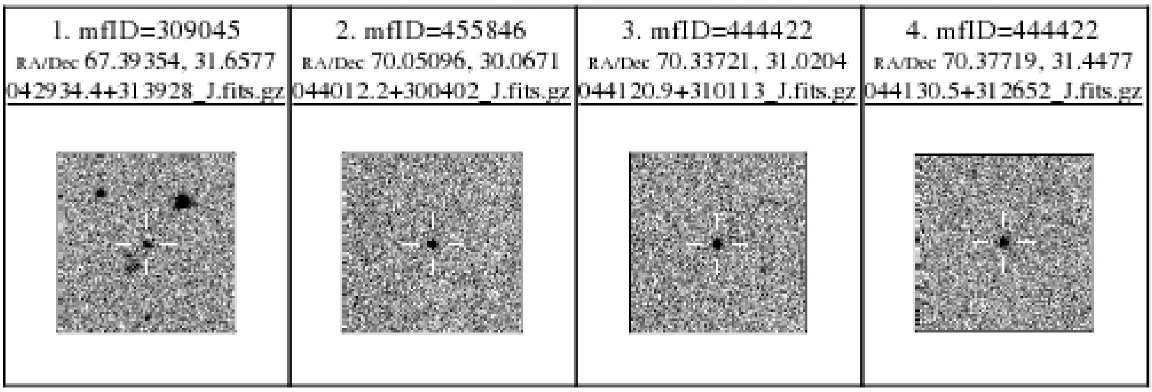

Figure B.10: UKIDSS 30*x*30 $arcsec^2$ *J* band images of 4 observed faint LMO Taurus member candidates.

name	RA_U [*deg*]	Dec_U [*deg*]	Y_U [*mag*]	J_U [*mag*]	H_U [*mag*]	K_U [*mag*]	$A_{V,YJK}$ [*mag*]	$A_{V,JHK}$ [*mag*]
UGCSJ0429+3139	67.393540	31.657711	-	18.408	17.462	16.554	-	0.030
UGCSJ0441+3126	70.377186	31.447661	19.317	18.224	16.979	16.262	1.655	0.956
UGCSJ0441+3101	70.337213	31.020363	19.554	18.182	17.025	16.313	1.782	1.863
UGCSJ0440+3004	70.050963	30.067103	19.875	18.163	17.061	16.317	2.904	2.450

Table B.4: Data of 4 observed faint LMO Taurus member candidates

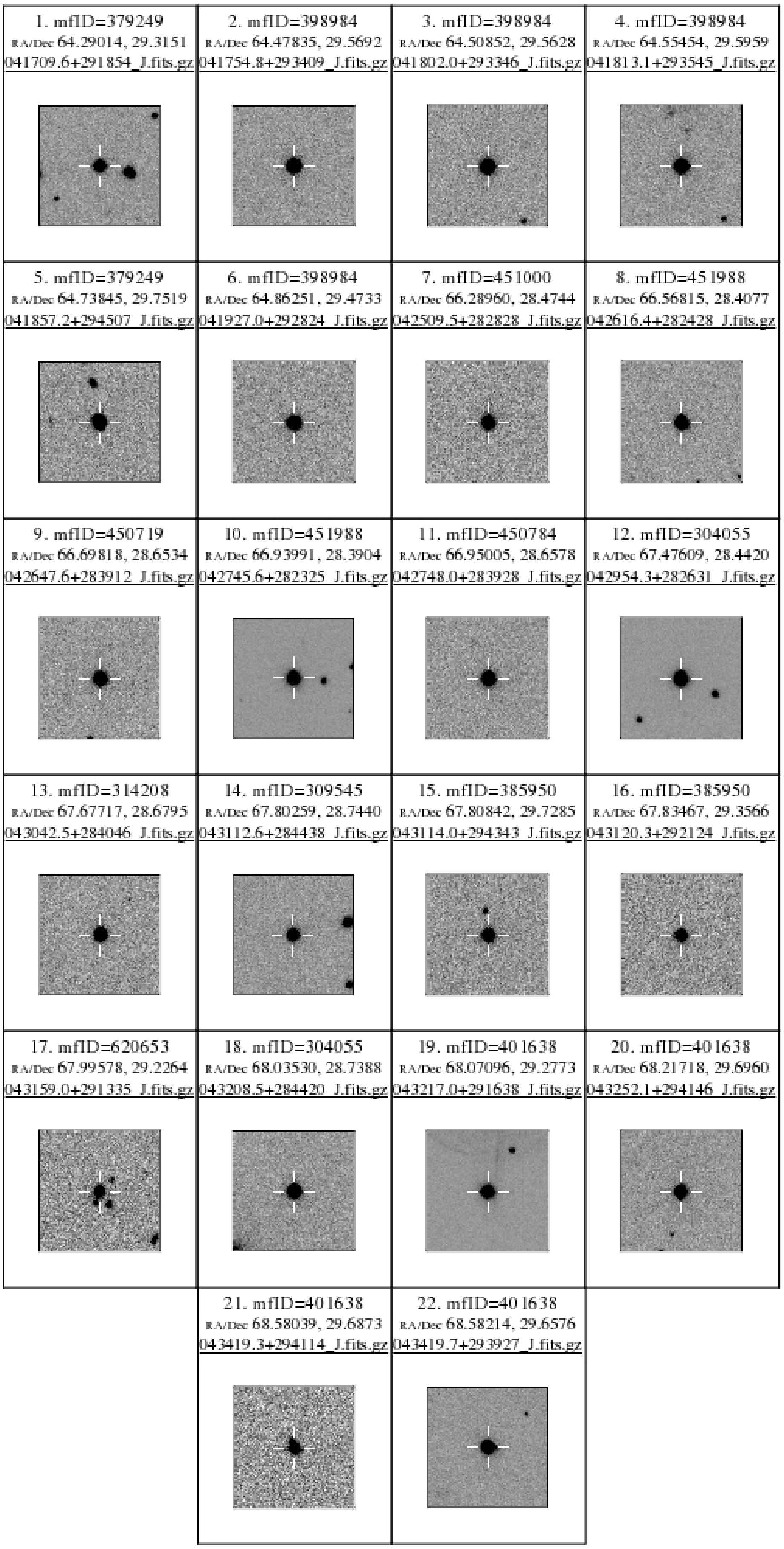

Figure B.11: UKIDSS 30*x*30 *arcsec*^{2} *J* band images of 22 observed MIR excess Taurus member candidates.

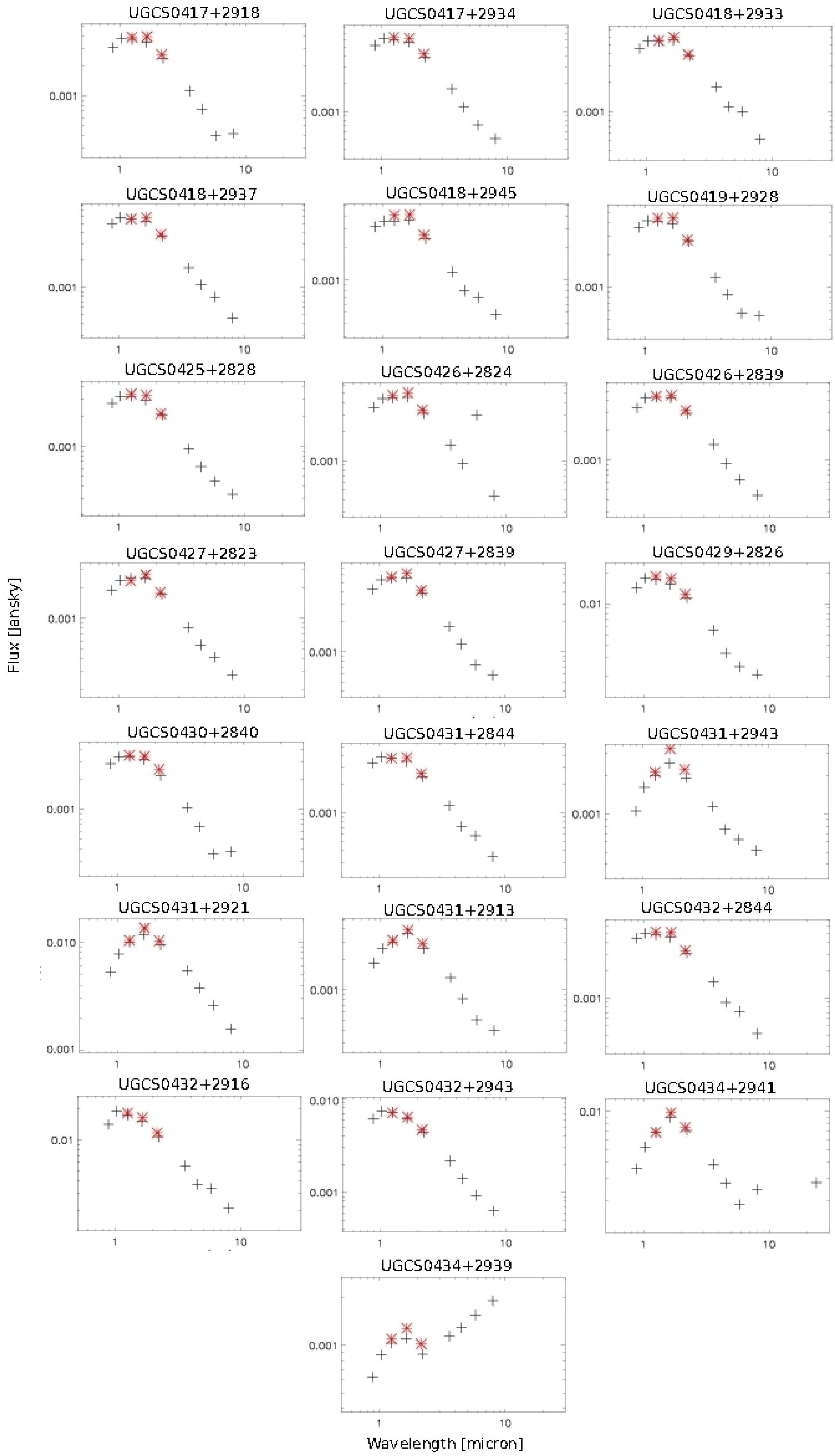

Figure B.12: SED of 22 observed MIR excess Taurus member candidates containing the photometry of UKIDSS and IRAC (black) and 2MASS (red).

name	RA_U [deg]	Dec_U [deg]	B [mag]	V [mag]	R [mag]	Z_U [mag]	Y_U [mag]	J_U [mag]	H_U [mag]	K_U [mag]	J_M [mag]	H_M [mag]	K_M [mag]	[3.6] [mag]	[4.5] [mag]	[5.4] [mag]	[8.0] [mag]	[24.0] [mag]
UGCSJ0417+2918	64.290142	29.315112	16.340	16.240	15.620	14.666	14.409	14.035	13.678	13.563	14.063	13.629	13.531	13.500	13.400	13.600	12.900	-
UGCSJ0417+2934	64.478346	29.569153	15.850	15.540	14.970	14.087	13.885	13.529	13.142	13.033	13.532	13.137	13.009	13.000	13.000	13.000	12.700	-
UGCSJ0418+2933	64.508521	29.562828	16.090	15.890	15.230	14.245	14.031	13.641	13.175	13.055	13.687	13.187	13.084	12.900	13.000	12.600	12.700	-
UGCSJ0418+2937	64.554535	29.595869	15.740	15.710	15.170	14.149	13.950	13.606	13.222	13.115	13.673	13.217	13.121	13.000	13.000	12.900	12.800	-
UGCSJ0418+2945	64.738451	29.751904	16.130	15.710	15.550	14.605	14.438	14.072	13.593	13.502	14.018	13.588	13.514	13.400	13.300	13.000	12.800	-
UGCSJ0419+2928	64.862511	29.473342	16.070	15.600	15.280	14.422	14.275	13.887	13.529	13.432	13.914	13.492	13.460	13.300	13.300	13.200	12.600	-
UGCSJ0425+2828	66.289605	28.474399	16.480	16.150	15.720	14.776	14.580	14.190	13.844	13.713	14.208	13.819	13.741	13.600	13.600	13.500	13.200	-
UGCSJ0426+2824	66.568153	28.407662	16.440	16.130	15.640	14.477	14.234	13.825	13.373	13.269	13.845	13.362	13.250	13.200	13.200	11.400	12.900	-
UGCSJ0426+2839	66.698178	28.653366	16.510	16.020	15.510	14.531	14.277	13.868	13.455	13.329	13.911	13.473	13.308	13.200	13.200	13.100	12.900	-
UGCSJ0427+2823	66.939912	28.390399	15.370	15.060	14.540	13.260	13.013	12.617	12.222	12.094	12.666	12.201	12.106	12.000	12.000	12.000	11.100	-
UGCSJ0427+2839	66.950049	28.657821	16.280	16.260	15.520	14.285	14.042	13.612	13.167	13.026	13.650	13.146	13.025	12.900	12.900	12.900	12.600	-
UGCSJ0429+2826	67.476091	28.441989	15.090	14.740	14.330	12.975	12.724	12.367	12.040	11.852	12.372	12.005	11.842	11.700	11.800	11.600	11.200	-
UGCSJ0430+2840	67.677173	28.679549	16.540	16.400	15.770	14.729	14.550	14.149	13.792	13.683	14.183	13.791	13.569	13.500	13.500	13.700	13.000	-
UGCSJ0431+2844	67.802586	28.744008	16.360	16.420	15.670	14.581	14.379	14.009	13.661	13.542	14.099	13.665	13.536	13.400	13.500	13.200	13.100	-
UGCSJ0431+2943	67.808422	29.728504	16.160	15.870	15.600	14.433	14.225	13.895	13.542	13.408	13.929	13.497	13.361	13.300	13.300	13.200	12.600	-
UGCSJ0431+2921	67.834672	29.356576	19.820	17.970	16.960	15.365	14.902	14.282	13.596	13.331	14.311	13.556	13.339	13.100	13.100	12.800	12.400	-
UGCSJ0431+2913	67.995785	29.226437	19.880	17.890	17.270	15.765	15.305	14.694	14.006	13.773	14.715	13.843	13.699	13.400	13.400	13.100	12.700	-
UGCSJ0432+2844	68.035304	28.738836	15.800	15.810	15.340	14.274	14.093	13.736	13.366	13.264	13.742	13.332	13.276	13.100	13.200	13.000	12.900	-
UGCSJ0432+2916	68.070957	29.277346	14.950	14.820	14.320	12.938	12.634	12.338	12.073	11.896	12.376	12.069	11.897	11.700	11.700	11.300	11.100	-
UGCSJ0432+2943	68.217184	29.696032	16.130	15.730	15.360	13.949	13.697	13.348	13.059	12.912	13.411	13.105	12.896	12.700	12.700	12.700	12.500	-
UGCSJ0434+2941	68.580392	29.687312	20.000	17.970	18.320	16.401	16.009	15.439	14.914	14.648	15.437	14.850	14.546	13.400	12.800	12.100	11.300	-
UGCSJ0434+2939	68.582143	29.657572	18.170	17.460	16.500	14.519	14.051	13.387	12.652	12.380	13.442	12.649	12.380	12.100	12.000	11.900	11.000	8.520

Table B.5: Data of 22 observed MIR excess Taurus member candidates Part I.

name	$A_{V,YJK}$ [mag]	$A_{V,JHK}$ [mag]	$\mu_{\alpha,U}$ [mas/yr]	$\mu_{\delta,U}$ [mas/yr]	$\mu_{\alpha,N}$ [mas/yr]	$\mu_{\delta,N}$ [mas/yr]	Class	α_{IRAC}
UGCSJ0417+2918	0.404	0.258	1.184	-3.155	0.000	0.000	II	-2.239
UGCSJ0417+2934	0.246	0.048	7.384	-1.952	17.700	-8.100	III	-2.505
UGCSJ0418+2933	0.000	0.000	-4.185	0.036	-4.400	-0.900	III	-2.496
UGCSJ0418+2937	0.093	0.219	-14.197	-2.931	-0.800	6.800	III	-2.589
UGCSJ0418+2945	0.011	0.119	23.191	-64.865	22.000	-56.000	III	-2.106
UGCSJ0419+2928	0.337	0.061	-11.356	0.261	0.100	-1.400	II	-2.036
UGCSJ0425+2828	0.248	0.093	0.647	5.739	0.000	0.000	III	-2.368
UGCSJ0426+2824	0.572	0.530	1.592	-0.376	3.100	0.500	III	-2.025
UGCSJ0426+2839	0.526	0.375	10.849	-2.779	-6.500	-1.600	III	-2.478
UGCSJ0427+2823	0.398	0.376	3.188	6.452	-6.300	-1.600	II	-1.842
UGCSJ0427+2839	0.348	0.224	-2.210	-4.449	-9.100	0.200	III	-2.505
UGCSJ0429+2826	0.691	0.564	-2.081	4.499	0.200	-4.700	I/II	-2.218
UGCSJ0430+2840	0.432	0.268	-6.213	4.369	-8.900	-2.800	II	-2.337
UGCSJ0431+2844	0.518	0.248	3.230	-4.968	-8.100	-9.600	III	-2.412
UGCSJ0431+2943	0.531	0.718	-1.271	-0.219	3.000	7.100	II	-2.036
UGCSJ0431+2921	0.699	0.565	-5.762	-14.893	0.000	0.000	II	-1.983
UGCSJ0431+2913	0.852	0.760	-19.116	-18.483	-8.000	-14.000	II	-1.983
UGCSJ0432+2844	0.320	0.144	2.461	2.441	2.100	-14.100	III	-2.549
UGCSJ0432+2916	0.693	0.760	3.359	-1.955	-2.800	-6.700	III	-2.067
UGCSJ0432+2943	0.730	0.570	-10.171	-9.840	-6.200	-8.700	III	-2.615
UGCSJ0434+2941	0.870	0.781	1.822	8.638	0.000	0.000	II	-0.407
UGCSJ0434+2939	0.923	0.976	-0.974	10.150	0.000	0.000	II	-1.607

Table B.6: Data of 22 observed MIR excess Taurus member candidates Part II.

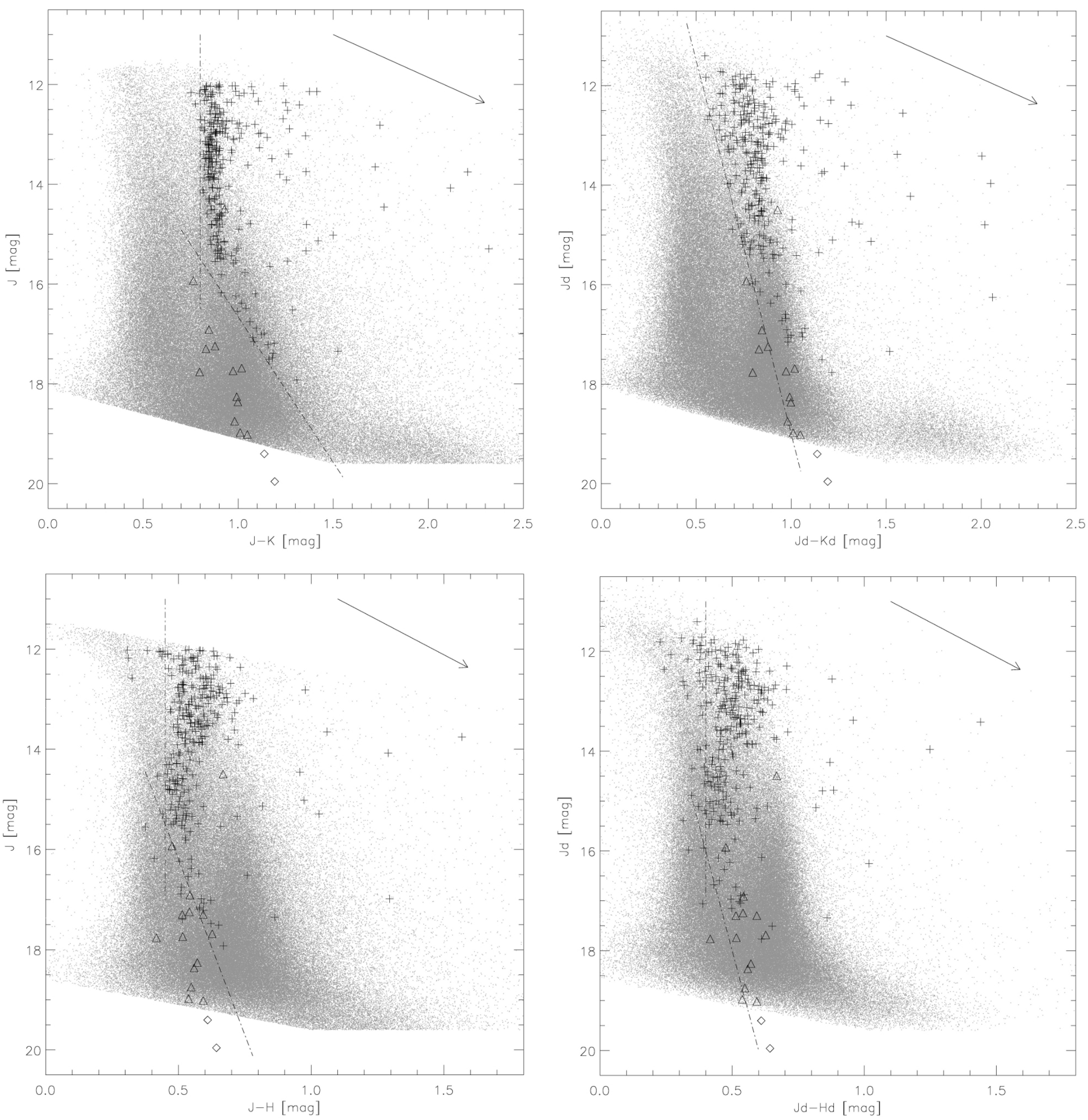

Figure B.13: Selection of Orion candidates Part I: the $J-K$ vs. J (top) & the $J-H$ vs. J (bottom) CMD. On the left side, the observed photometry is shown. On the right side, the dereddened values are plotted. The plus signs show the candidates of the σ Orionis Cluster by N. Lodieu. The other signs are like in Fig. 4.2.

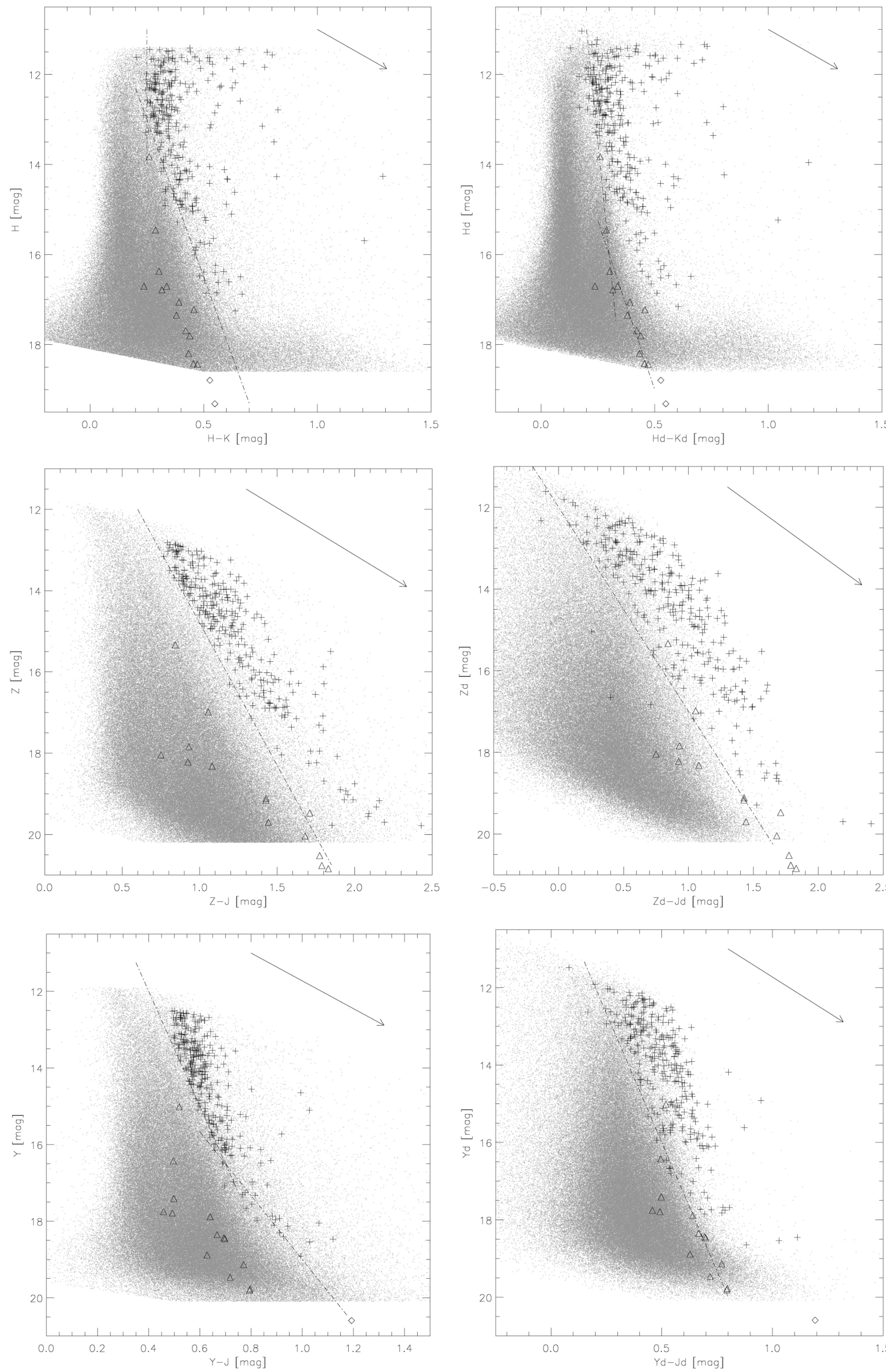

Figure B.14: Selection of Orion candidates Part II: the $H-K$ vs. H (top), the $Z-J$ vs. Z (middle) & the $Y-J$ vs. Y (bottom) CMD (see Fig. B.13).

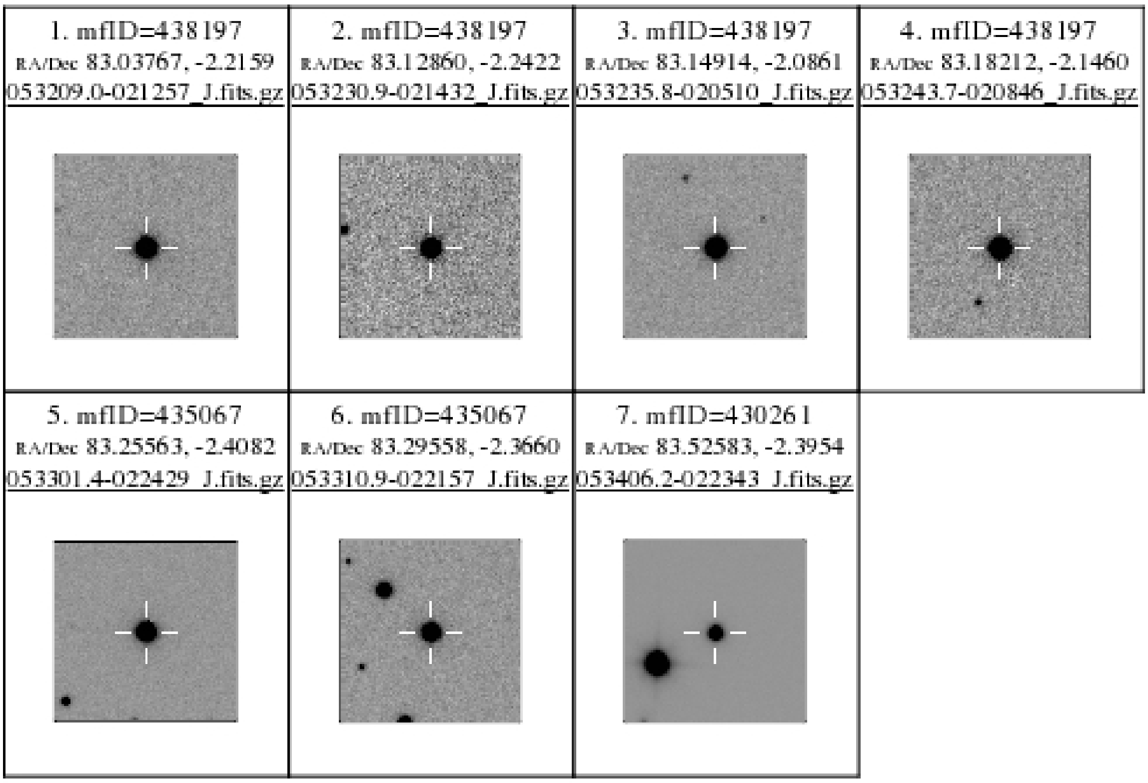

Figure B.15: UKIDSS 30*x*30 *arcsec*^{2} *J* band images of 7 Orion member candidates.

name	RA [deg]	Dec [deg]	Z_U [mag]	Y_U [mag]	J_U [mag]	H_U [mag]	K_U [mag]	J_M [mag]	H_M [mag]	K_K [mag]	$A_{V,calc}$ [mag]	$\mu_{\alpha,U}$ [mas/yr]	$\mu_{\delta,U}$ [mas/yr]
UGCSJ0532-0212	83.037675	-2.215901	13.477	13.087	12.523	11.935	11.669	12.619	11.928	11.709	0.025	-7.83	-3.22
UGCSJ0532-0214	83.128602	-2.242225	14.548	14.159	13.551	12.898	12.615	13.611	12.808	12.622	0.007	-10.53	8.36
UGCSJ0532-0205	83.149136	-2.086078	13.459	13.034	12.489	12.010	11.659	12.568	11.931	11.697	0.000	12.80	-1.47
UGCSJ0532-0208	83.182117	-2.145996	14.012	13.638	13.011	12.365	12.088	13.064	12.360	12.094	0.475	0.12	-0.12
UGCSJ0533-0224	83.255635	-2.408156	13.455	13.037	12.456	11.887	11.590	12.509	11.808	11.610	0.542	-0.70	5.13
UGCSJ0533-0221	83.295579	-2.365958	14.167	13.710	13.129	12.539	12.255	13.230	12.582	12.267	0.690	2.00	10.81
UGCSJ0534-0223	83.525833	-2.395352	12.828	12.502	11.996	11.447	11.167	12.046	11.320	11.173	0.000	-3.57	-1.35

Table B.7: Data of 7 observed Orion member candidates.

Appendix C

Figures and tables from Chapter 5

In this chapter, we show the tables and images of Chap. 5, which describes the observations done in this work. We put the observational logs of the different candidate selections and show the data and spectra of the observed field dwarfs and standard stars.

name	spectral type	RA [deg]	Dec [deg]	B [mag]	V [mag]	R [mag]	I [mag]	J_M [mag]	H_M [mag]	K_M [mag]	$\mu_{\alpha,lit}$ [mas/yr]	$\mu_{\delta,lit}$ [mas/yr]
J00000099-1929557	K3	0.004265	-19.498840	10.80	9.00	-	-	7.40	6.98	6.81	181.2	-0.9
HIP 18	K5	0.052829	-4.053680	12.30	10.50	-	-	-	-	-	-127.2	23.8
J00001280+3818144	G5	0.053309	38.304050	7.47	6.53	-	-	5.00	4.57	4.33	-2.5	-15.1
J00001512+2331451	G0	0.063046	23.529228	8.95	8.50	-	-	7.52	7.31	7.26	36.0	-23.0
J00005477+3249321	M0	0.228214	32.825654	10.76	-	-	-	5.22	4.43	4.16	-2.0	-8.5
J00010057+2753109	K0	0.252428	27.886330	10.37	9.56	9.10	8.70	8.10	7.72	7.60	225.6	-5.5
J00082573+0637004	G2	2.107273	6.616805	8.22	7.60	-	-	6.42	6.15	6.12	87.3	-0.9
J00170635+4056538	K7	4.276561	40.948295	10.36	8.94	8.20	7.50	6.39	5.75	5.58	567.9	82.8
J00180010+4400293	M5	4.500420	44.008170	12.84	11.04	-	-	11.00	10.56	10.41	-	-
J00181659+1012100	M1.5	4.569119	10.202783	12.10	10.88	-	-	7.56	6.92	6.74	-0.7	-32.3
J00322970+6714080	M2.5	8.122640	67.235669	11.83	10.29	9.60	-	6.84	6.27	6.04	1739.0	-224.9
J00385879+3036583	M2.5	9.746012	30.616242	12.60	11.06	10.60	10.00	7.45	6.86	6.61	1556.4	31.9
J00450489+0147077	K2	11.270393	1.785521	9.03	8.03	7.40	6.90	6.31	5.87	5.74	-49.0	-573.1
J00482326+6057422	G8	12.096954	60.961692	9.47	8.44	-	-	6.46	5.85	5.72	1.3	-28.8
J00512963+5818071	M2	12.874318	58.302027	11.95	10.64	9.80	9.10	7.83	7.24	7.05	1566.9	405.0
J01012006+6121560	M2	15.333630	61.365580	12.26	10.87	10.00	9.20	7.27	6.71	6.48	370.0	-824.0
J01592349+5831162	M4	29.847978	58.521133	12.90	12.04	11.80	-	7.79	7.22	6.96	321.8	-195.3
GJ 83.1	M4.5	30.127381	13.088910	14.08	12.26	10.91	9.41	7.51	6.97	6.65	1092.0	-1772.9
J03205965+1854233	M8	50.248554	18.906475	20.50	19.21	17.20	14.00	11.76	11.07	10.64	360.0	-252.0
HIP 16242	K7	52.332482	-11.678367	11.42	9.99	-	-	-	-	-	60.9	-304.1
J03542950+3203013	G0	58.622960	32.050390	12.71	11.85	-	-	10.08	9.71	9.58	-	-
HBC 353	G5	58.625692	32.051242	13.25	12.31	-	-	-	-	-	-	-
J03543556+2537111	K3	58.648300	25.620000	14.90	13.79	-	-	11.79	11.23	11.10	-	-
J03543597+2537081	K2	58.649880	25.618920	13.59	12.67	-	-	10.81	10.34	10.21	-	-
HBC 357	K2	60.808150	25.883267	13.96	12.91	-	-	-	-	-	-	-
J04271056+1750425	K1	66.794050	17.845178	11.00	10.24	10.20	-	8.78	8.39	8.30	0.8	-12.4

J04312717+1706249	K5	67.863210	17.106920	13.71	12.51	11.40	-	10.28	9.71	9.50	-	-
J04391586+3032074*	M3.5	69.816080	30.535390	17.46	16.41	15.76	-	12.68	12.07	11.83	-	-
J23340328+0010452	M4	353.513884	0.179413	12.62	11.17	10.15	8.89	7.66	7.07	6.83	-997.0	-936.2
J23351050-0223214	M5.5	353.793750	-2.389280	16.60	14.69	-	-	9.14	8.51	8.18	850.0	-957.0
J23415498+4410407	M6	355.479120	44.178000	14.19	12.28	11.10	9.00	6.88	6.25	5.93	111.0	-1584.0

Table C.1: Data of 31 observed field dwarfs. The one marked with an asterisk is the TTS located in the Taurus region (see Chap. 2.2.3). The 2MASS names are shortened.

telescope/ instrument	date of observation	target name	J_U [mag]	I_{calc} [mag]	t_{exp} [s]	number of exposures	t_{tot} [s]
CAHA2.2/CAFOS	10.11.2009	UGCSJ0419+2941	12.94	14.32	900	1	900
CAHA2.2/CAFOS	11.11.2009	UGCSJ0419+3155	12.28	13.39	600	1	600
CAHA2.2/CAFOS	10.11.2009	UGCSJ0421+3052	13.67	15.34	1500	1	1500
CAHA2.2/CAFOS	10.11.2009	UGCSJ0425+3318	12.98	14.37	900	1	900
CAHA2.2/CAFOS	10.11.2009	UGCSJ0426+2901	13.37	14.92	900	1	900
CAHA2.2/CAFOS	11.11.2009	UGCSJ0426+3036	13.61	15.25	1200	1	1200
NOT/ALFOSC	19.12.2009	UGCSJ0427+2830	13.85	15.59	900	1	900
CAHA2.2/CAFOS	10.11.2009	UGCSJ0427+2836	12.74	14.04	900;900	2	1800
CAHA2.2/CAFOS	10.11.2009	UGCSJ0427+2838	12.30	13.42	600	1	600
CAHA2.2/CAFOS	11.11.2009	UGCSJ0427+2935	13.64	15.3	900;900	2	1800
CAHA2.2/CAFOS	10.11.2009	UGCSJ0427+3007*	12.40	13.56	900	1	900
CAHA2.2/CAFOS	11.11.2009	UGCSJ0428+2843	13.78	15.49	900;900	2	1800
CAHA2.2/CAFOS	11.11.2009	UGCSJ0428+3039*	12.41	13.57	600;600	2	1200
CAHA2.2/CAFOS	11.11.2009	UGCSJ0428+3043	12.46	13.64	600;600	2	1200
NOT/ALFOSC	19.12.2009	UGCSJ0428+3122*	13.78	15.49	600	1	600
CAHA2.2/CAFOS	10.11.2009	UGCSJ0429+2824	12.35	13.49	900	1	900
CAHA2.2/CAFOS	11.11.2009	UGCSJ0429+3237	13.54	15.16	1200	1	1200
WHT/ISIS	23.12.2008	UGCSJ0430+2931*	12.51	13.71	1200;1200	2	2400
NOT/ALFOSC	24.08.2009	UGCSJ0430+2939	14.09	15.93	1200	1	1200
CAHA2.2/CAFOS	11.11.2009	UGCSJ0430+3016	12.10	13.14	600	1	600
NOT/ALFOSC	19.12.2009	UGCSJ0430+3017	13.40	14.96	700	1	700
NOT/ALFOSC	19.12.2009	UGCSJ0431+3111	13.62	15.27	900	1	900
CAHA2.2/CAFOS	11.11.2009	UGCSJ0431+3116	12.60	13.84	600	1	600
CAHA2.2/CAFOS	10.11.2009	UGCSJ0432+2828	12.10	13.14	900	1	900
CAHA2.2/CAFOS	11.11.2009	UGCSJ0432+3005	13.48	15.07	1500	1	1500
CAHA2.2/CAFOS	11.11.2009	UGCSJ0432+3301	12.06	13.08	600	1	600
CAHA2.2/CAFOS	11.11.2009	UGCSJ0432+3329	13.28	14.79	900	1	900
NOT/ALFOSC	24.08.2009	UGCSJ0433+2912	13.31	14.83	360;90	2	450
CAHA2.2/CAFOS	11.11.2009	UGCSJ0433+3306A	12.39	13.55	600	1	600
CAHA2.2/CAFOS	11.11.2009	UGCSJ0433+3306B	12.92	14.29	600;600	2	1200
CAHA2.2/CAFOS	10.11.2009	UGCSJ0435+2959	12.55	13.77	900	1	900
CAHA2.2/CAFOS	10.11.2009	UGCSJ0436+3307	12.13	13.18	600	1	600
CAHA2.2/CAFOS	10.11.2009	UGCSJ0437+3005	12.59	13.83	900	1	900
CAHA2.2/CAFOS	10.11.2009	UGCSJ0437+3056	12.91	14.27	1200;1200	2	2400
CAHA2.2/CAFOS	10.11.2009	UGCSJ0437+3144	12.51	13.71	900	1	900
WHT/ISIS	23.12.2008	UGCSJ0437+3155	12.69	13.97	1200	1	1200
CAHA2.2/CAFOS	10.11.2009	UGCSJ0438+2921	12.06	13.08	900	1	900
CAHA2.2/CAFOS	10.11.2009	UGCSJ0438+3119	12.46	13.64	900	1	900
NOT/ALFOSC	19.12.2009	UGCSJ0439+3032a	14.04	15.86	900	1	900
CAHA2.2/CAFOS	11.11.2009	UGCSJ0439+3032b	14.04	15.86	1200	1	1200
NOT/ALFOSC	19.12.2009	UGCSJ0439+3050	14.13	15.98	900	1	900
NOT/ALFOSC	19.12.2009	UGCSJ0439+3105	14.17	16.04	600	1	600
NOT/ALFOSC	24.08.2009	UGCSJ0440+3156a	14.33	16.26	1600	1	1600
NOT/ALFOSC	19.12.2009	UGCSJ0440+3156b	14.33	16.26	900	1	900
NOT/ALFOSC	24.08.2009	UGCSJ0441+3200	13.39	14.95	440;110	2	550

Table C.2: Observation log of 45 observed optical spectra of 43 bright LMO candidate members. Note, that the annotation with capital letters A and B stand for different types of objects. Small letters a and b stand for same objects, but different telescope configurations. We have obtained additional NIR spectra for the four sources marked with an asterisk. The *I* band magnitudes got calculated by the formula explained in the text.

telescope/ instrument	date of observation	target name	J_U [mag]	I_{calc} [mag]	t_{exp} [s]	# exp.	t_{tot} [s]	λ [μm]	res.	STD
GTC/OSIRIS	08.01.2010	UGCSJ0429+3139	18.41	21.97	600;600;600;600	4	2400	-	-	J23195840-0509561
GTC/OSIRIS	06.12.2009	UGCSJ0440+3004A	18.16	21.63	600;600	2	1200	0.55 0.93	1100	GD 108
GTC/OSIRIS	06.12.2009	UGCSJ0440+3004B	18.16	21.63	600;600	2	1200	0.55 1.05	900	J05053062+5249519
GTC/OSIRIS	08.01.2010	UGCSJ0441+3101a	18.18	21.65	500;500;500;500	4	2000	0.55 1.05	900	J05053062+5249519
GTC/OSIRIS	05.01.2010	UGCSJ0441+3101b	18.18	21.65	635;635;635	3	1905	0.53 1.05	900	J11370512+2947581
GTC/OSIRIS	06.12.2009	UGCSJ0441+3126	18.22	2171	600;600;700	3	1900	0.56 1.05	900	J05053062+5249519

Table C.3: Observational log of 6 observed optical spectra of 4 faint LMO candidate members. Note, that the annotation A and B for UGCSJ0440+3004 stand for the usage of different standard star spectra resulting in different resolutions and wavelength ranges. The small letters a and b for UGCSJ0441+3101 stand for different spectra which we could not add together.

telescope/ instrument	date of observation	target name	J_U [mag]	I_{calc} [mag]	t_{exp} [s]	number of exposures	t_{tot} [s]
CAHA/CAFOS	11.11.2009	UGCSJ0417+2918	14.03	15.85	600;600	2	1200
CAHA/CAFOS	10.11.2009	UGCSJ0417+2934	13.53	15.14	900	1	900
CAHA/CAFOS	10.11.2009	UGCSJ0418+2933	13.64	15.30	1200	1	1200
CAHA/CAFOS	10.11.2009	UGCSJ0418+2937	13.61	15.25	900	1	900
WHT/ISIS	01.11.2009	UGCSJ0418+2945	14.08	15.91	450	1	450
WHT/ISIS	31.10.2009	UGCSJ0419+2928	13.91	15.68	240	1	240
CAHA/CAFOS	11.11.2009	UGCSJ0425+2828	14.19	16.07	600	1	600
WHT/ISIS	01.11.2009	UGCSJ0426+2824	13.84	15.58	450	1	450
CAHA/CAFOS	11.11.2009	UGCSJ0426+2839	13.87	15.61	600	1	600
WHT/ISIS	31.10.2009	UGCSJ0427+2823	12.63	13.89	180	1	180
CAHA/CAFOS	11.11.2009	UGCSJ0427+2839	13.61	15.26	600	1	600
WHT/ISIS	31.10.2009	UGCSJ0429+2826	12.38	13.53	180	1	180
CAHA/CAFOS	11.11.2009	UGCSJ0430+2840	14.15	16.01	600	1	600
CAHA/CAFOS	11.11.2009	UGCSJ0431+2844	14.01	15.81	600	1	600
WHT/ISIS	31.10.2009	UGCSJ0431+2943	13.89	15.65	180	1	180
WHT/ISIS	01.11.2009	UGCSJ0431+2921	14.26	16.17	600	1	600
WHT/ISIS	01.11.2009	UGCSJ0431+2913	14.72	16.80	600	1	600
CAHA/CAFOS	10.11.2009	UGCSJ0432+2844	13.74	15.43	900	1	900
WHT/ISIS	31.10.2009	UGCSJ0432+2916	12.35	13.49	180	1	180
CAHA/CAFOS	10.11.2009	UGCSJ0432+2943	13.35	14.89	900	1	900
WHT/ISIS	31.10.2009	UGCSJ0434+2941	15.43	17.80	900	1	900
WHT/ISIS	01.11.2009	UGCSJ0434+2939	13.37	14.92	300	1	300

Table C.4: Observational log of 22 observed optical spectra of the MIR excess candidate members

telescope/ instrument	date of observation	target name	J_U [mag]	t_{tot} [s]
LICK/Gemini	08.11.2008	UGCSJ0427+3007	12.42	180 (JH), 90 (K)
LICK/Gemini	08.11.2008	UGCSJ0428+3122	13.77	180 (JH), 90 (K)
LICK/Gemini	08.11.2008	UGCSJ0428+3039	12.40	180 (JH), 90 (K)
LICK/Gemini	08.11.2008	UGCSJ0430+2931	12.51	180 (JH), 90 (K)

Table C.5: Observational log of 4 observed NIR spectra of bright LMO candidate members

telescope/ instrument	date of observation	target name	J_U [mag]	I_{calc} [mag]	t_{tot} [s]
CAHA/CAFOS	02.12.2007	J04034930+2610520	10.35	10.69	200
CAHA/CAFOS	04.12.2007	J04043936+2158186	10.80	11.32	200
CAHA/TWIN	24.11.2005	J04131414+2819108	9.60	9.64	60
CAHA/CAFOS	03.12.2007	J04141458+2827580	9.47	9.46	200
CAHA/CAFOS	02.12.2007	J04141700+2810578	9.56	9.58	100
CAHA/CAFOS	04.12.2007	J04144730+2646264	9.90	10.06	150
CAHA/CAFOS	01.12.2007	J04173893+2833005	11.89	12.85	100
CAHA/TWIN	24.11.2005	J04174955+2813318	11.02	11.63	300
CAHA/CAFOS	01.12.2007	J04183112+2816290	9.83	9.96	50
CAHA/CAFOS	02.12.2007	J04185170+1723165	10.02	10.23	200
CAHA/CAFOS	03.12.2007	J04215563+2755060	9.18	9.05	200
CAHA/CAFOS	03.12.2007	J04215740+2826355	7.16	6.22	50
CAHA/CAFOS	04.12.2007	J04215943+1932063	7.24	6.34	50
CAHA/CAFOS	10.11.2009	J04224786+2645530	11.59	12.42	1200
CAHA/CAFOS	11.11.2009	J04230607+2801194	12.24	13.34	1200
CAHA/CAFOS	03.12.2007	J04270280+2542223	8.17	7.64	300
CAHA/CAFOS	02.12.2007	J04292373+2433002	11.54	12.36	80
CAHA/CAFOS	10.11.2009	J04293606+2435556	10.78	11.29	1200
CAHA/CAFOS	10.11.2009	J04295422+1754041	12.65	13.91	1200
CAHA/TWIN	22.11.2006	J04312405+1800215	11.65	12.51	300
CAHA/CAFOS	01.12.2007	J04321606+1812464	11.17	11.84	900
WHT/ISIS	23.12.2008	J04321786+2422149	11.52	12.33	1200
CAHA/CAFOS	01.12.2007	J04322627+1827521	11.11	11.75	250
CAHA/CAFOS	30.11.2007	J04331003+2433433	9.32	9.25	300
CAHA/CAFOS	02.12.2007	J04333405+2421170	9.34	9.28	100
CAHA/CAFOS	30.11.2007	J04334871+1810099	10.41	10.77	250
CAHA/CAFOS	03.12.2007	J04335470+2613275	9.87	10.01	300
CAHA/CAFOS	04.12.2007	J04341803+1830066	10.52	10.93	200
CAHA/CAFOS	03.12.2007	J04345542+2428531	9.43	9.41	200
CAHA/CAFOS	30.11.2007	J04352737+2414589	9.14	8.99	250
CAHA/TWIN	24.11.2005	J04355109+2252401	11.31	12.03	300
CAHA/CAFOS	03.12.2007	J04355684+2254360	11.14	11.8	300
CAHA/CAFOS	04.12.2007	HV Tau C	9.23	9.12	150
CAHA/CAFOS	04.12.2007	J04391741+2247533	9.97	10.16	50
CAHA/TWIN	22.11.2006	J04442713+2512164	12.20	13.28	600
CAHA/CAFOS	02.12.2007	J04474859+2925112	9.47	9.45	50
CAHA/CAFOS	03.12.2007	J04555938+3034015	7.20	6.28	10

Table C.6: Observational log of 37 observed optical spectra of already known Taurus members. All objects were observed in one exposure. 2MASS names are shortened.

telescope/ instrument	date of observation	target name	J_U $[mag]$	I_{calc} $[mag]$	t_{tot} $[s]$
CAHA/CAFOS	04.12.2007	J00000099-1929557	7.40	6.56	5
CAHA/CAFOS	03.12.2007	HIP 18	-	-	50
CAHA/CAFOS	03.12.2007	J00001280+3818144	5.00	3.20	2
CAHA/CAFOS	03.12.2007	J00001512+2331451	7.52	6.73	1
CAHA/CAFOS	03.12.2007	J00005477+3249321	5.22	3.51	5
CAHA/CAFOS	03.12.2007	J00010057+2753109	8.10	7.55	10
CAHA/CAFOS	04.12.2007	J00082573+0637004	6.42	5.19	5
CAHA/TWIN	24.11.2005	J00170635+4056538	6.39	5.14	10
CAHA/TWIN	24.11.2005	J00180010+4400293	11.00	11.59	5
CAHA/TWIN	24.11.2005	J00181659+1012100	7.56	6.79	30
CAHA/TWIN	24.11.2005	J00322970+6714080	6.84	5.78	15
CAHA/TWIN	24.11.2005	J00385879+3036583	7.45	6.63	30
CAHA/CAFOS	04.12.2007	J00450489+0147077	6.31	5.03	5
CAHA/CAFOS	04.12.2007	J00482326+6057422	6.46	5.24	10
CAHA/TWIN	24.11.2005	J00512963+5818071	7.83	7.16	15
CAHA/TWIN	24.11.2005	J01012006+6121560	7.27	6.38	15
CAHA/CAFOS	04.12.2007	J01592349+5831162	7.79	7.11	150
CAHA/TWIN	24.11.2005	GJ 83.1	7.51	6.72	120
CAHA/TWIN	24.11.2005	J03205965+1854233b	11.76	12.66	300
CAHA/TWIN	22.11.2005	J03205965+1854233a	11.76	12.66	300
CAHA/CAFOS	04.12.2007	HIP 16242	-	-	10
CAHA/CAFOS	02.12.2007	J03542950+3203013	10.08	10.32	200
CAHA/CAFOS	02.12.2007	HBC 353	-	-3.80	200
CAHA/CAFOS	04.12.2007	J03543556+2537111	11.79	12.71	150
CAHA/CAFOS	04.12.2007	J03543597+2537081	10.81	11.34	150
CAHA/CAFOS	04.12.2007	HBC 357	-	-	150
CAHA/CAFOS	02.12.2007	J04271056+1750425	8.78	8.50	102
CAHA/CAFOS	04.12.2007	J04312717+1706249	10.28	10.59	200
CAHA/CAFOS	11.11.2009	J04391586+3032074	12.68	13.95	900
CAHA/TWIN	24.11.2005	J23340328+0010452	7.66	6.93	60
CAHA/TWIN	24.11.2005	J23351050-0223214	9.14	9.00	300
CAHA/TWIN	24.11.2005	J23415498+4410407	6.88	5.84	100

Table C.7: Observational log of 32 observed optical spectra of 31 probable field dwarfs. All objects were observed in one exposure. 2MASS names are shortened.

telescope/ instrument	date of observation	target name	J_U $[mag]$	I_{calc} $[mag]$	t_{tot} $[s]$
NOT/ALFOSC	19.12.2009	UGCSJ0532-0212	12.52	13.73	600
NOT/ALFOSC	19.12.2009	UGCSJ0532-0214	13.55	15.17	900
NOT/ALFOSC	19.12.2009	UGCSJ0532-0205	12.49	13.69	600
NOT/ALFOSC	19.12.2009	UGCSJ0532-0208	13.01	14.41	600
NOT/ALFOSC	19.12.2009	UGCSJ0533-0224	12.46	13.64	600
NOT/ALFOSC	19.12.2009	UGCSJ0533-0221	13.13	14.58	600
NOT/ALFOSC	19.12.2009	UGCSJ0534-0223	12.00	13.00	600

Table C.8: Observation log of 7 observed optical spectra of Orion member candidates. All objects were observed in one exposure.

telescope/ instrument	date of observation	target name	J_U $[mag]$	I_{calc} $[mag]$	t_{tot} $[s]$	λ $[\mu m]$	res.
WHT/ISIS	23.12.2008	J02350758+0343567	11.27	11.97	120	0.48-1.05	2100
WHT/ISIS	01.11.2009	J04043412+2508517	13.91	15.67	180	0.58-0.76	1700
LICK/Gemini	08.11.2008	J04412412+4818033	5.66	4.13	1.52 (JHK)	1.08-2.45	-
GTC/OSIRIS	06.12.2009	J05053062+5249519	12.54	13.76	15	0.55-1.05	900
GTC/OSIRIS	07.01.2010	J05053062+5249519	12.54	13.76	7	0.55-1.05	900
GTC/OSIRIS	06.12.2009	J05053062+5249519	12.54	13.76	15	0.55-1.05	900
NOT/ALFOSC	19.12.2009	J09485609+1344395	7.36	6.50	6	0.50-0.90	2400
GTC/OSIRIS	27.11.2009	GD 108	-	-	60	0.55-0.93	1100
GTC/OSIRIS	05.01.2010	J11370512+2947581	12.99	14.39	30	0.53-1.05	900
NOT/ALFOSC	24.08.2009	J22113136+1805341	8.44	8.01	20	0.51-1.00	2400
CAHA/CAFOS	10.11.2007	J23195840-0509561	12.55	13.77	500	0.62-1.02	1800
GTC/OSIRIS	07.01.2010	J23195840-0509561	12.55	13.77	7	-	-

Table C.9: Observational log of 9 standard stars. All objects were observed in one exposure. 2MASS names are shortened.

name	spectral type	RA [deg]	Dec [deg]	B [mag]	V [mag]	R [mag]	I [mag]	J_M [mag]	H_M [mag]	K_M [mag]	$\mu_{\alpha,lit}$ [mas/yr]	$\mu_{\delta,lit}$ [mas/yr]
J02350758+0343567	A1	38.781641	3.732444	12.210	12.400	-	-	11.265	10.733	10.557	82.02	5.49
J04043412+2508517	A4	61.142192	25.147711	13.920	13.800	14.100	13.600	13.910	13.968	14.001	131.00	-227.00
J04412412+4818033	A0	70.350536	48.300879	5.649	5.648	-	-	5.663	5.668	5.649	44.65	-45.24
J05053062+5249519	A	76.377553	52.831099	11.455	11.781	11.930	12.108	12.543	12.669	12.764	7.45	-89.54
J09485609+1344395	F5	147.233742	13.744257	8.690	8.280	8.100	7.900	7.359	7.121	7.062	373.05	-774.38
GD 108	B	150.197370	-7.558470	13.330	13.560	-	-	-	-	-	-	-
J11370512+2947581	A3	174.271267	29.799540	12.406	12.492	12.598	12.714	12.993	13.105	13.183	-148.21	-5.30
J22113136+1805341	F8	332.880724	18.092826	9.886	9.454	9.166	8.846	8.435	8.108	8.075	511.75	59.91
J23195840-0509561	A	349.993326	-5.165600	11.527	11.832	11.970	12.145	12.548	12.663	12.796	-10.68	0.31

Table C.10: Data of 9 standard stars. 2MASS names are shortened.

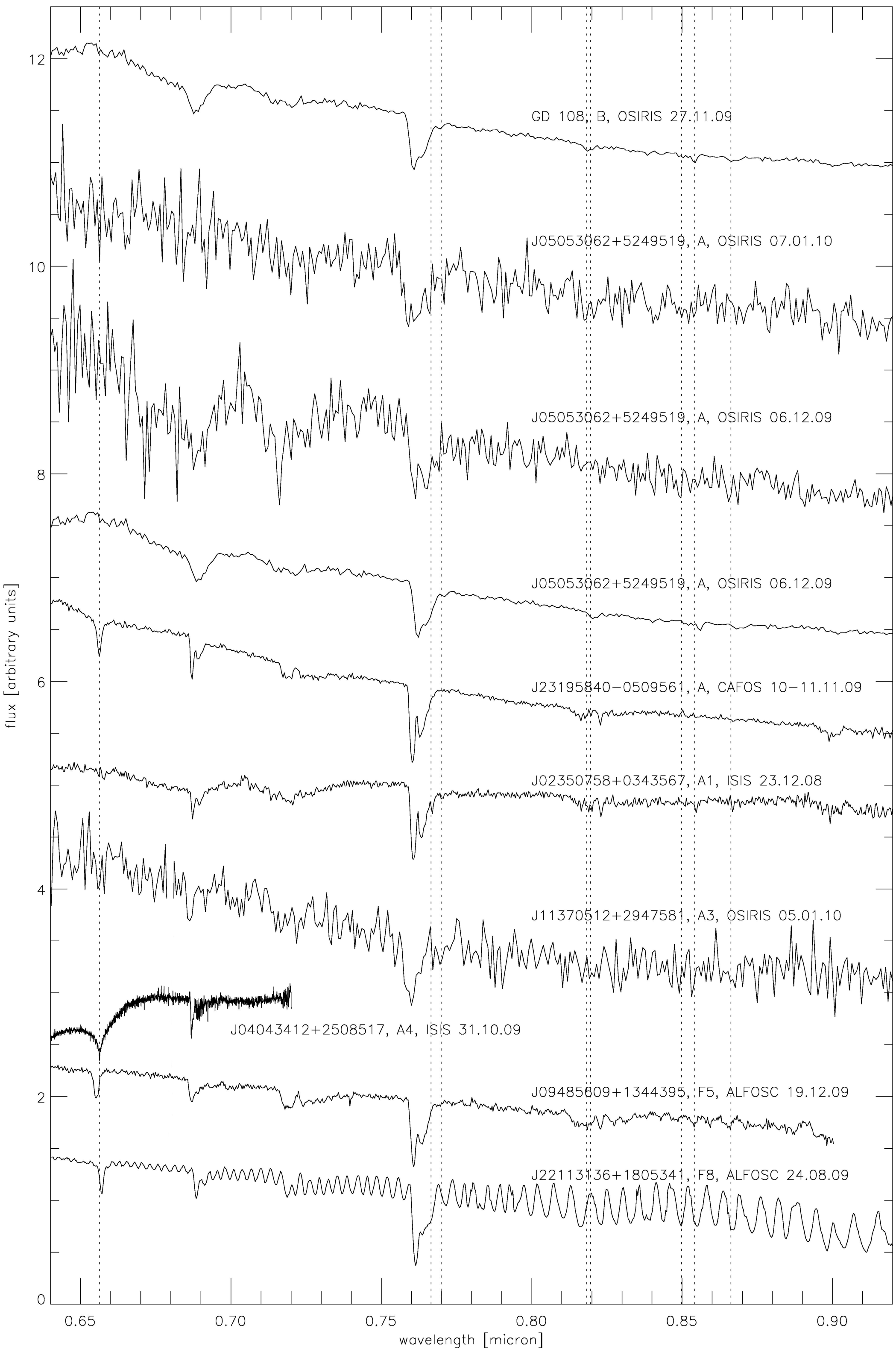

Figure C.1: Spectra of 9 standard stars used in the optical observations. The sources are sorted by their spectral type, which we indicate together with their name, the observational date and the instrument with which they were observed. Most of the OSIRIS standard stars are very noisy and were of no use for our data reduction process.

Appendix D

Figures and tables from Chapter 6

In this chapter, we show the tables and images of Chap. 6, which describes the analysis of this work. Besides the fully reduced spectra of all observed sources, this includes the data tables of the spectral types and the EW of the line features. We show the spectral indices and the diagrams of those not considered in this work. The outcome of the VOSA tool includes the data table and the SED of all observed sources. For the research done in Orion, we show the MST applied for the three clusters identified in the UKIDSS GCS and their LF.

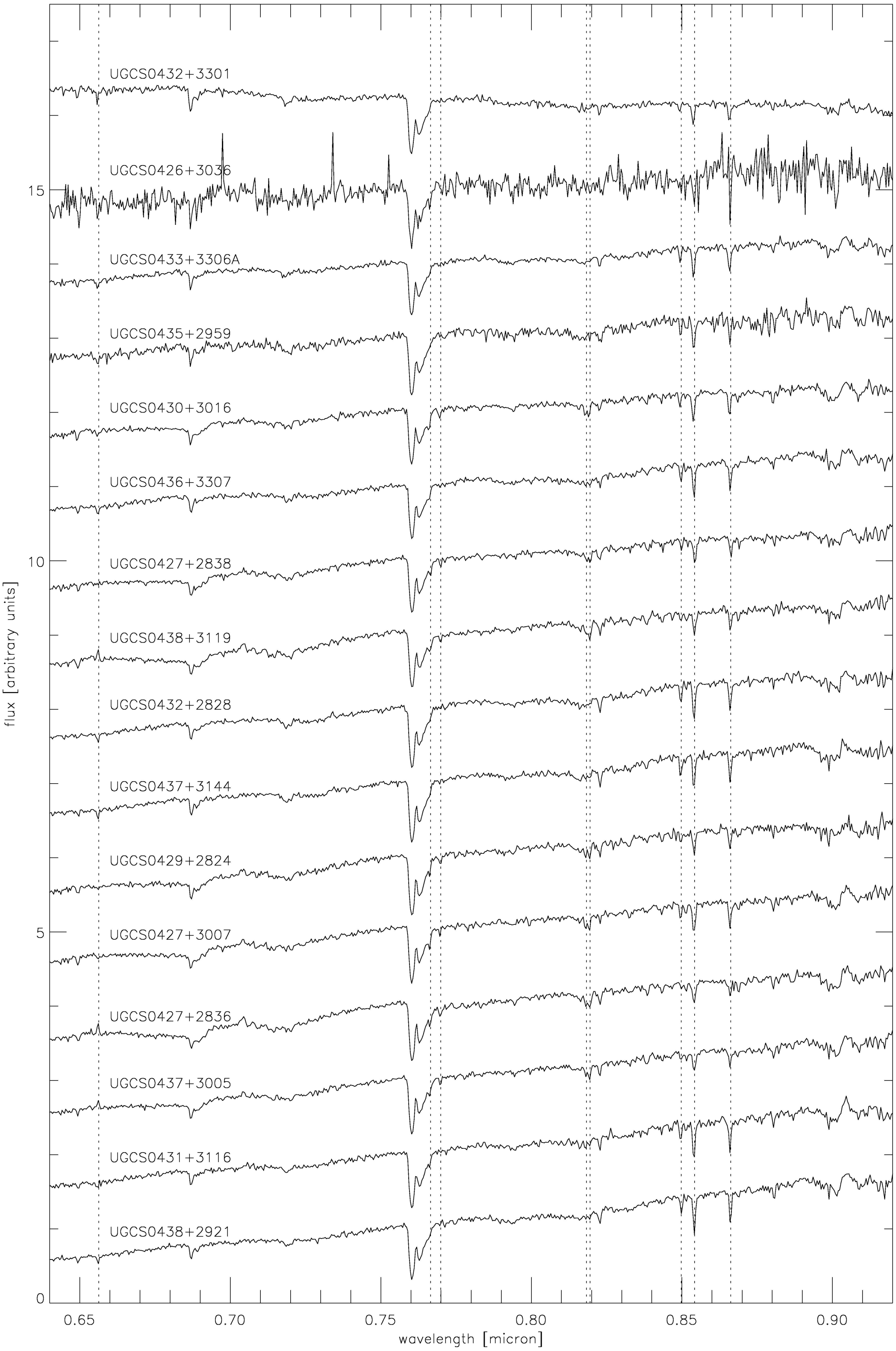

Figure D.1: Optical spectra of the observed bright LMO candidates of type $< M0.5$ sorted by their type. We mark each spectrum with the name of the source. The horizontal lines mark from left to right the wavelengths of the $H\alpha$ line, the *KI* and *NaI* doublets and the *CaII* triplet (see as well Fig. 6.1).

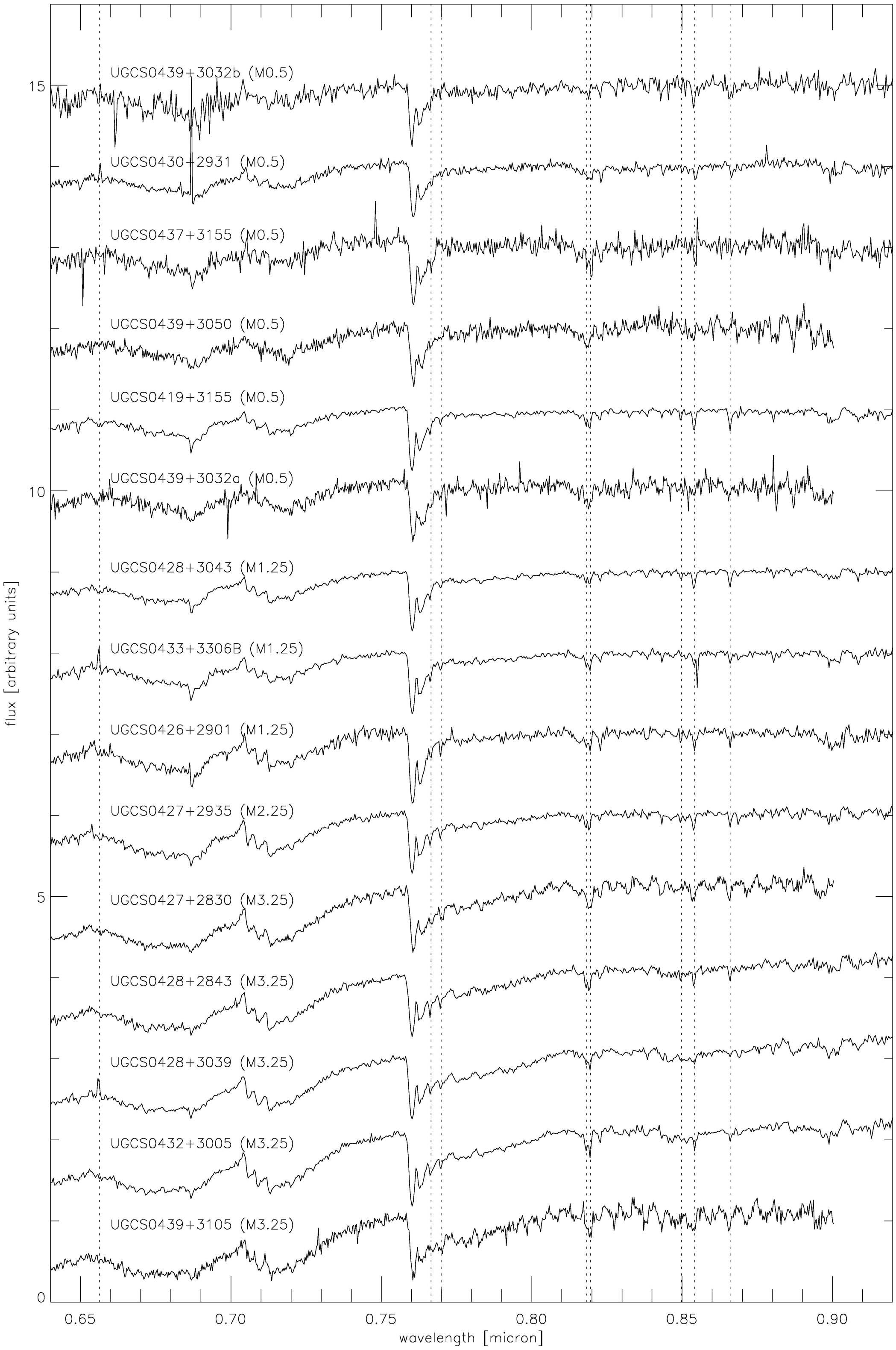

Figure D.2: Optical spectra of the observed bright LMO candidates of type $> M0.5$, part I. The spectral type derived from the reference spectra and adapted in this work are indicated in brackets (see Fig. D.1).

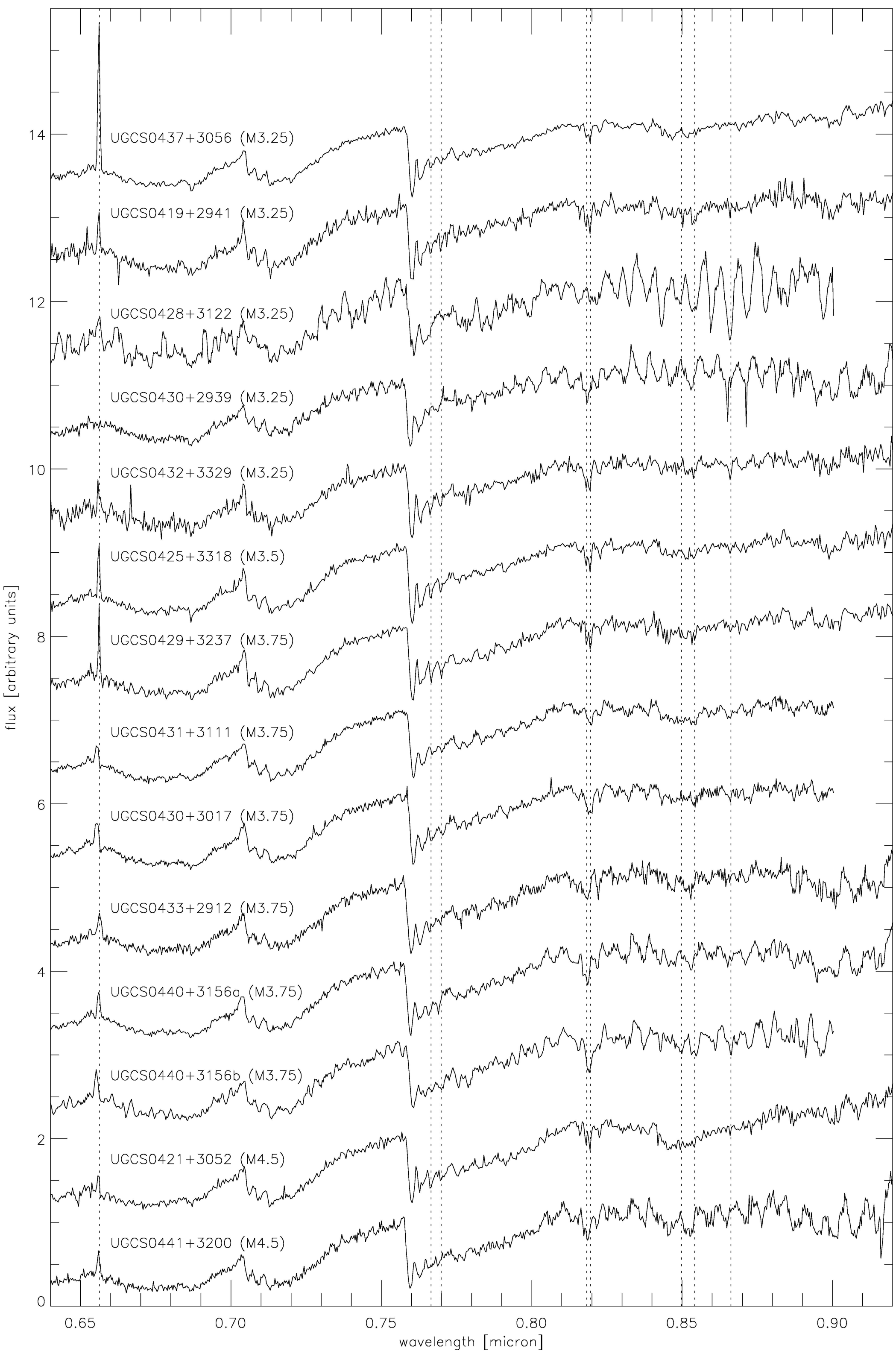

Figure D.3: Optical spectra of the observed bright LMO candidates of type $> M0.5$, part II (see Fig. D.2).

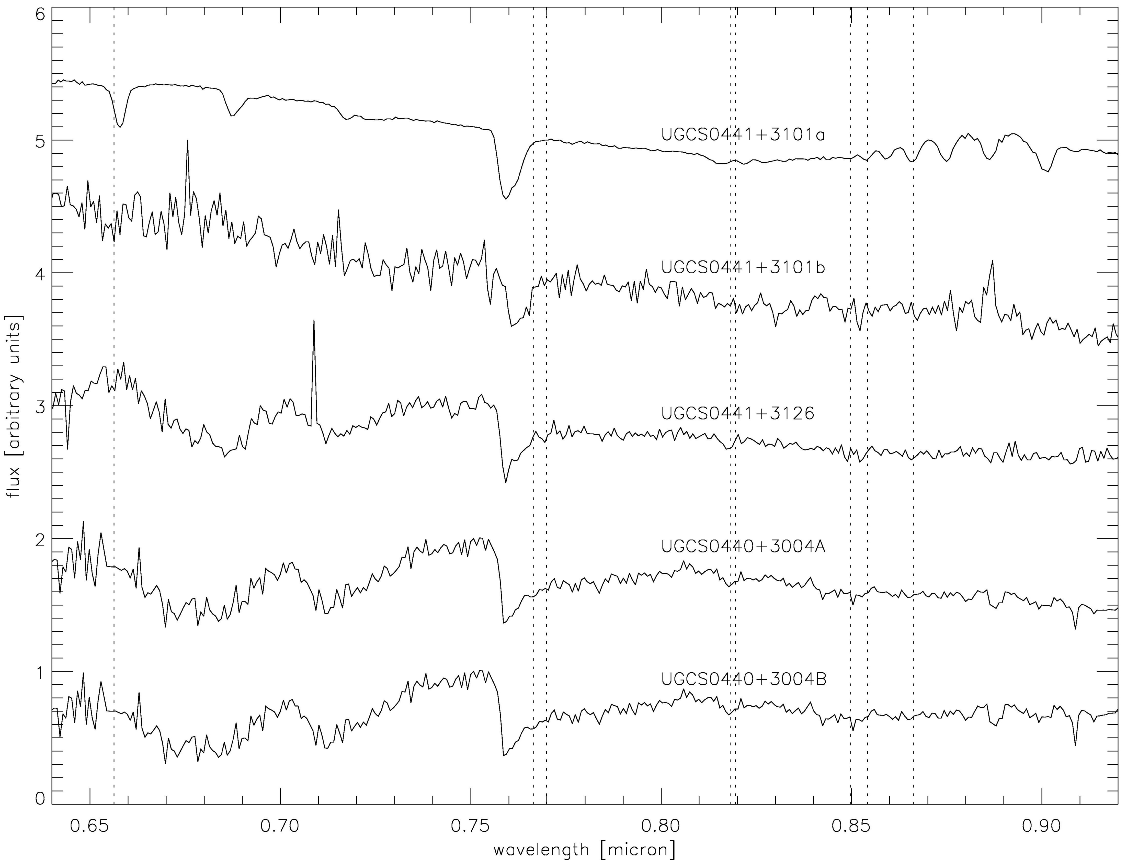

Figure D.4: Optical spectra of the observed faint LMO candidates (see Fig. D.1).

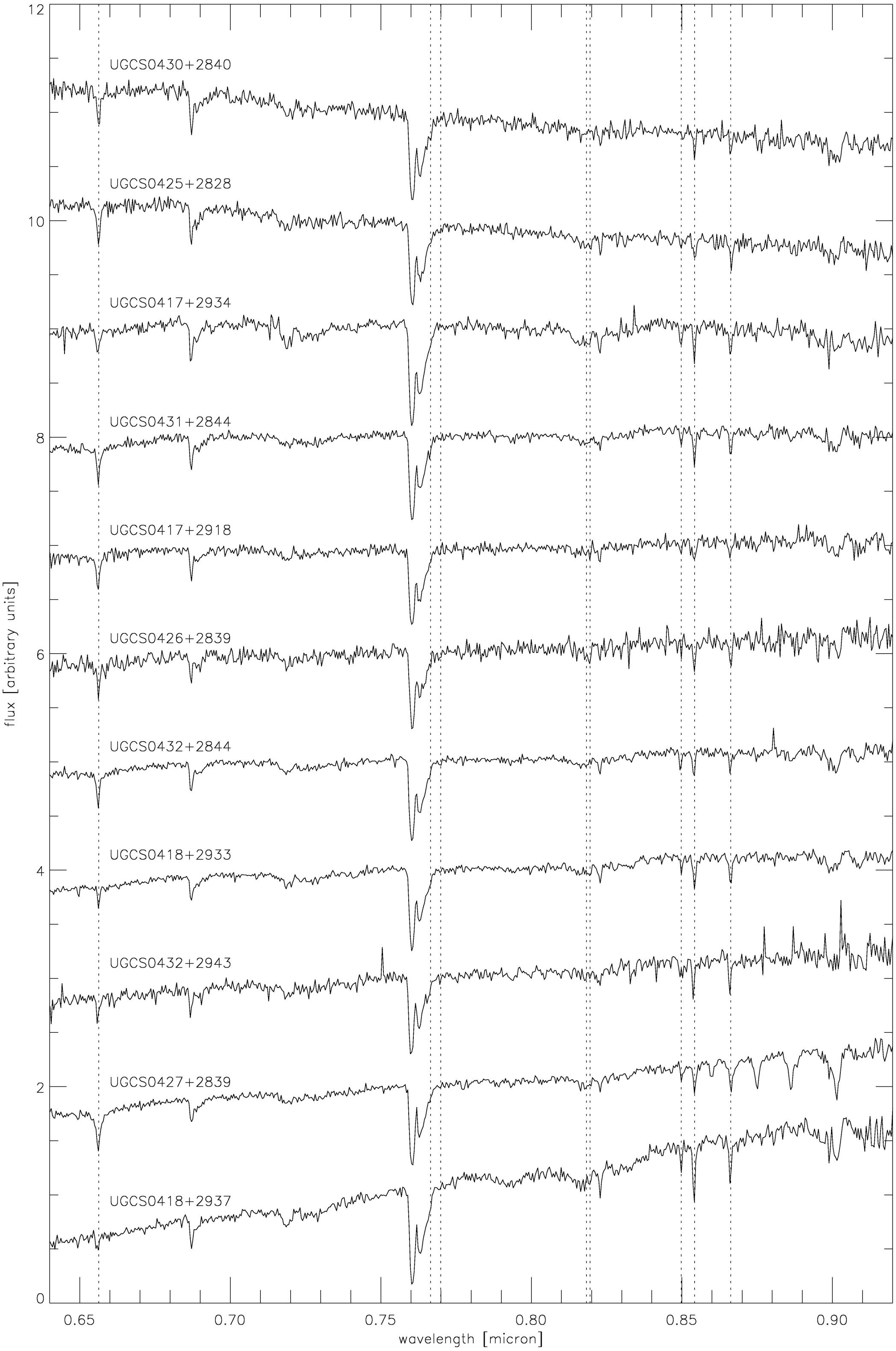

Figure D.5: Optical spectra of the observed MIR excess candidates, part I (see Fig. D.1).

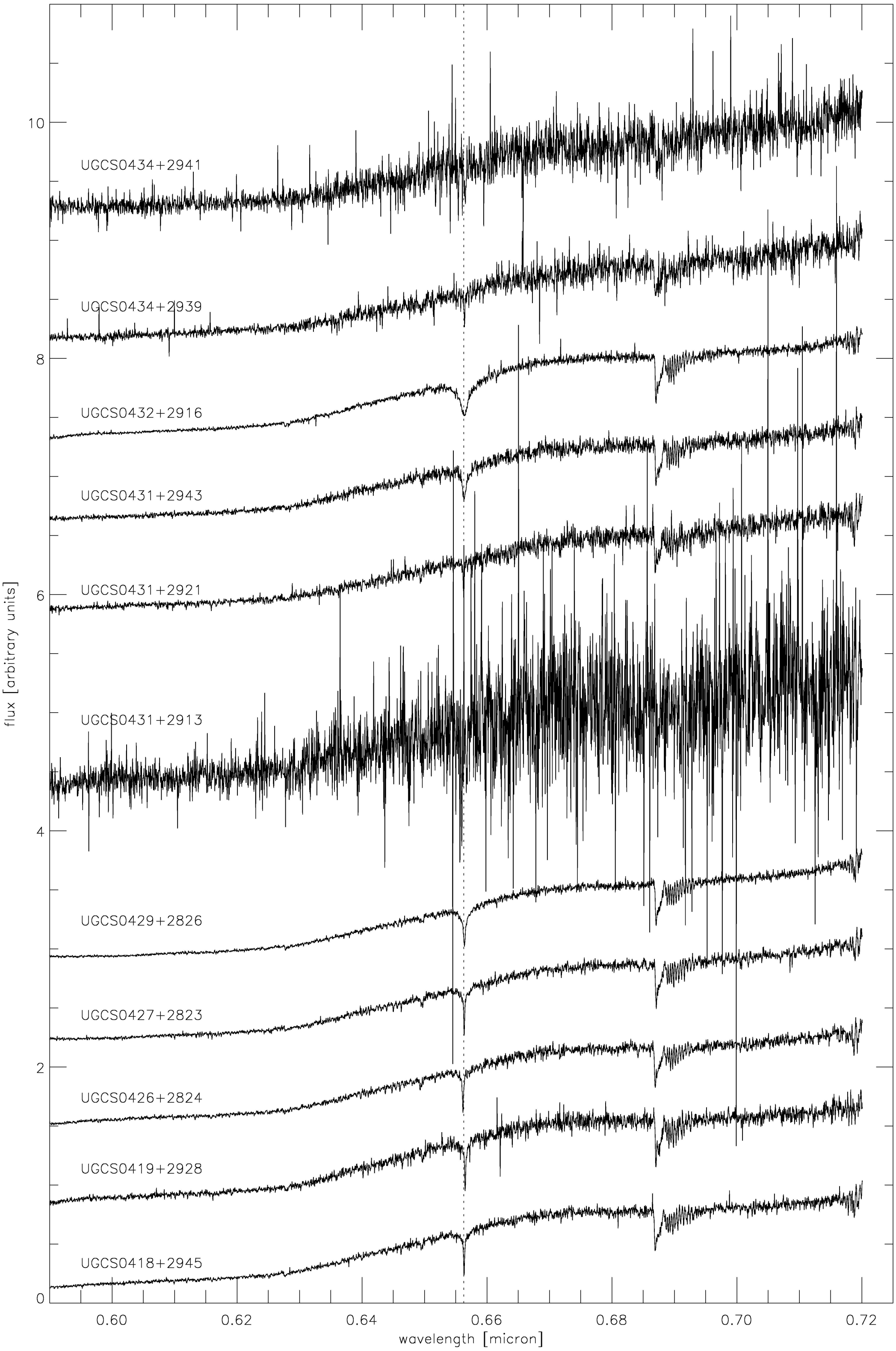

Figure D.6: Optical spectra of the observed MIR excess candidates, part II (see Fig. D.1). Note the different wavelength range.

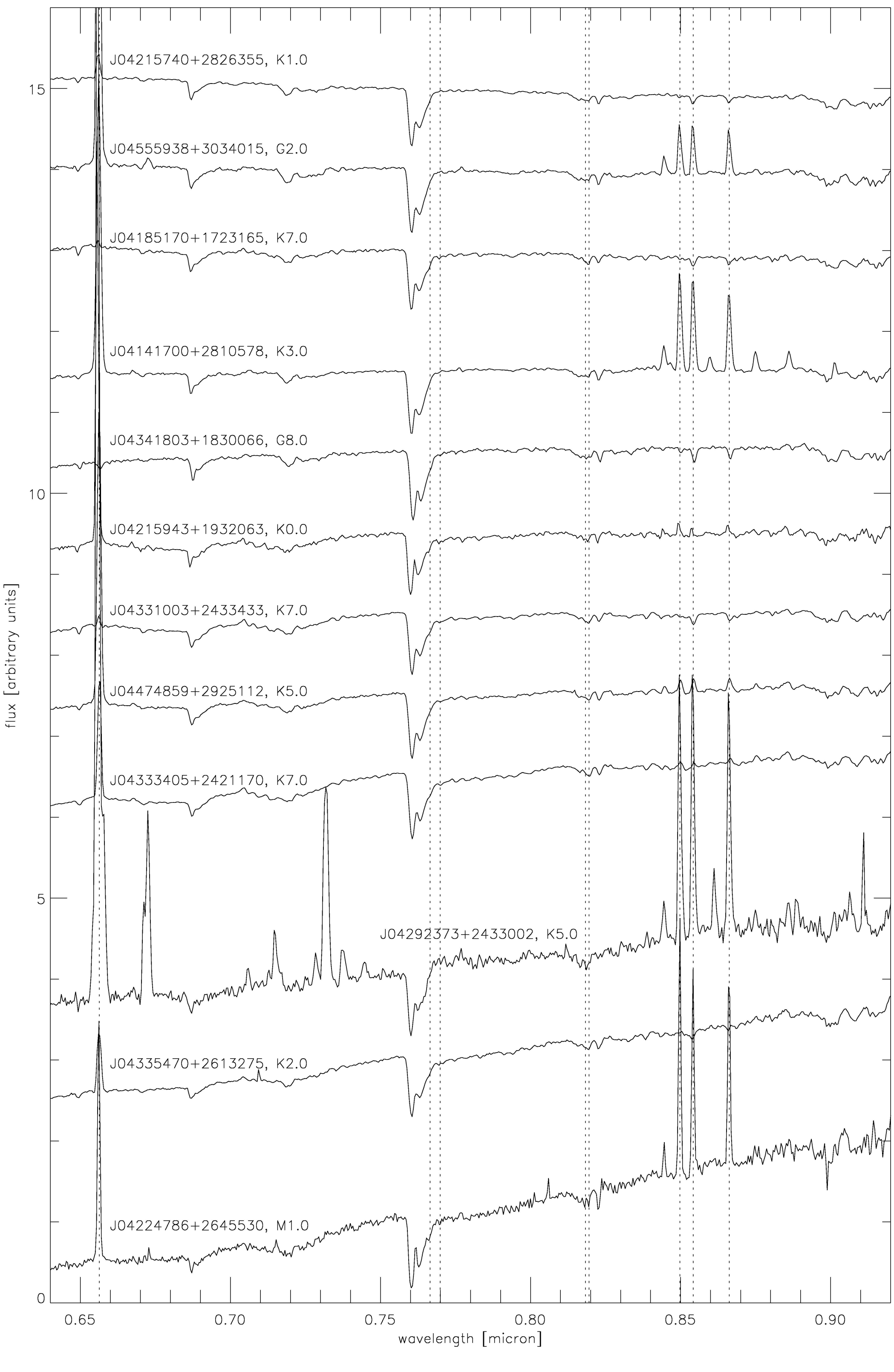

Figure D.7: Optical spectra of the Taurus members of type $< M0.5$ (see Fig. D.1). The spectral types indicated in literature are given.

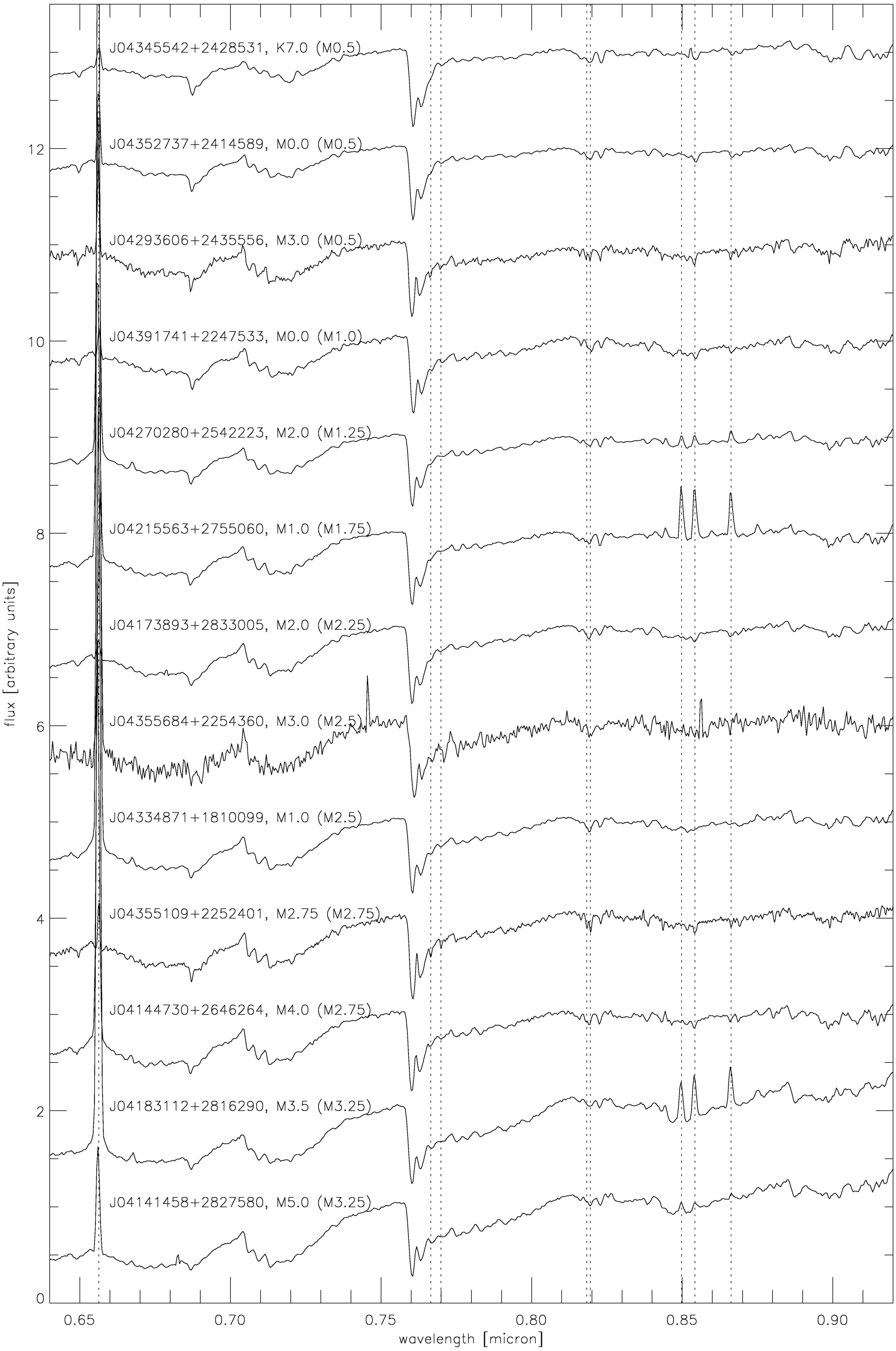

Figure D.8: Optical spectra of the Taurus members of type $> M0.5$, part I (see Fig. D.1 and Fig. D.7).

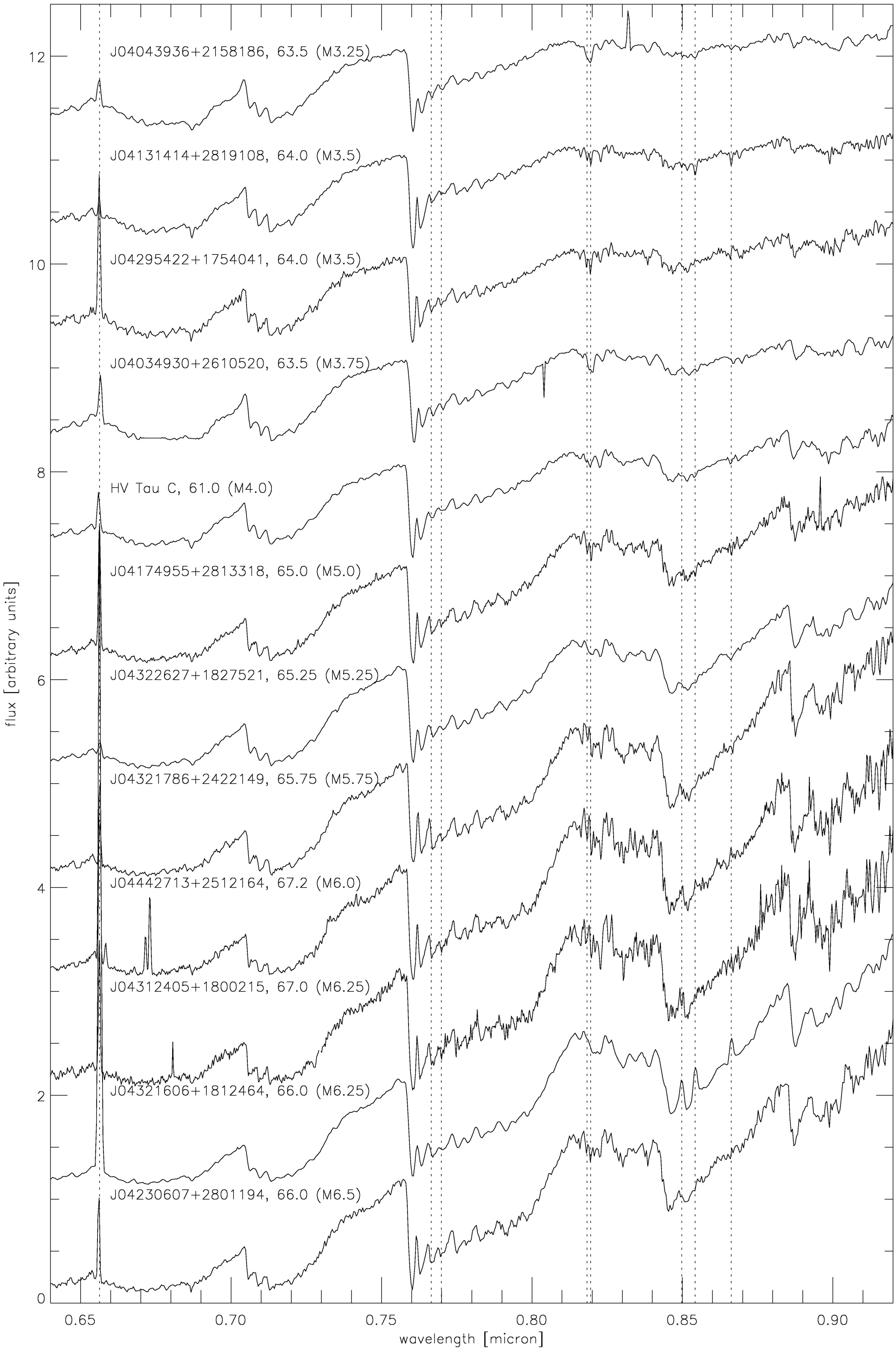

Figure D.9: Optical spectra of the Taurus members of type $> M0.5$, part II (see Fig. D.8).

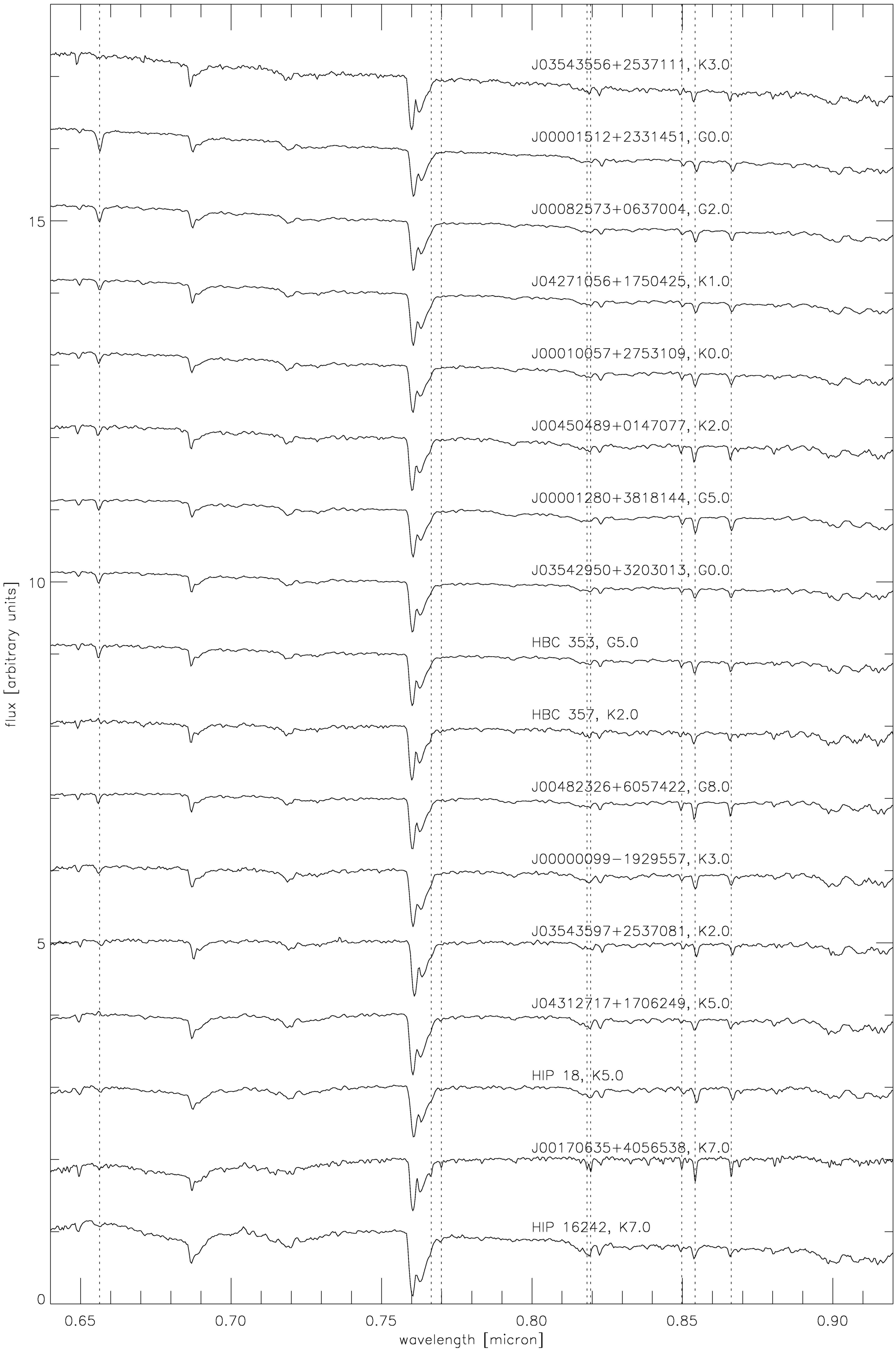

Figure D.10: Optical spectra of the field dwarfs of type $< M0.5$ (see Fig. D.1).

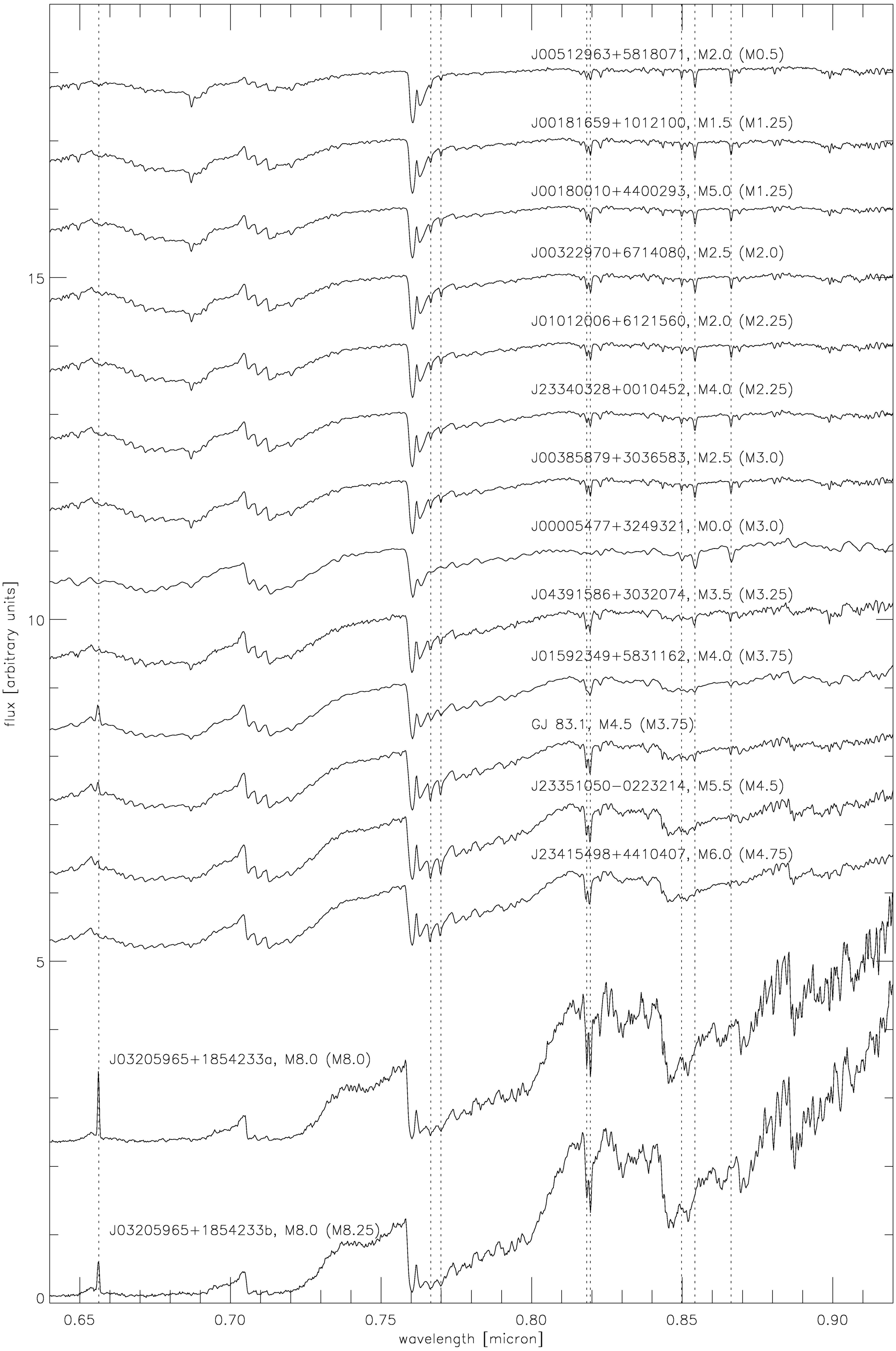

Figure D.11: Optical spectra of the field dwarfs of type $> M0.5$ (see Fig. D.8).

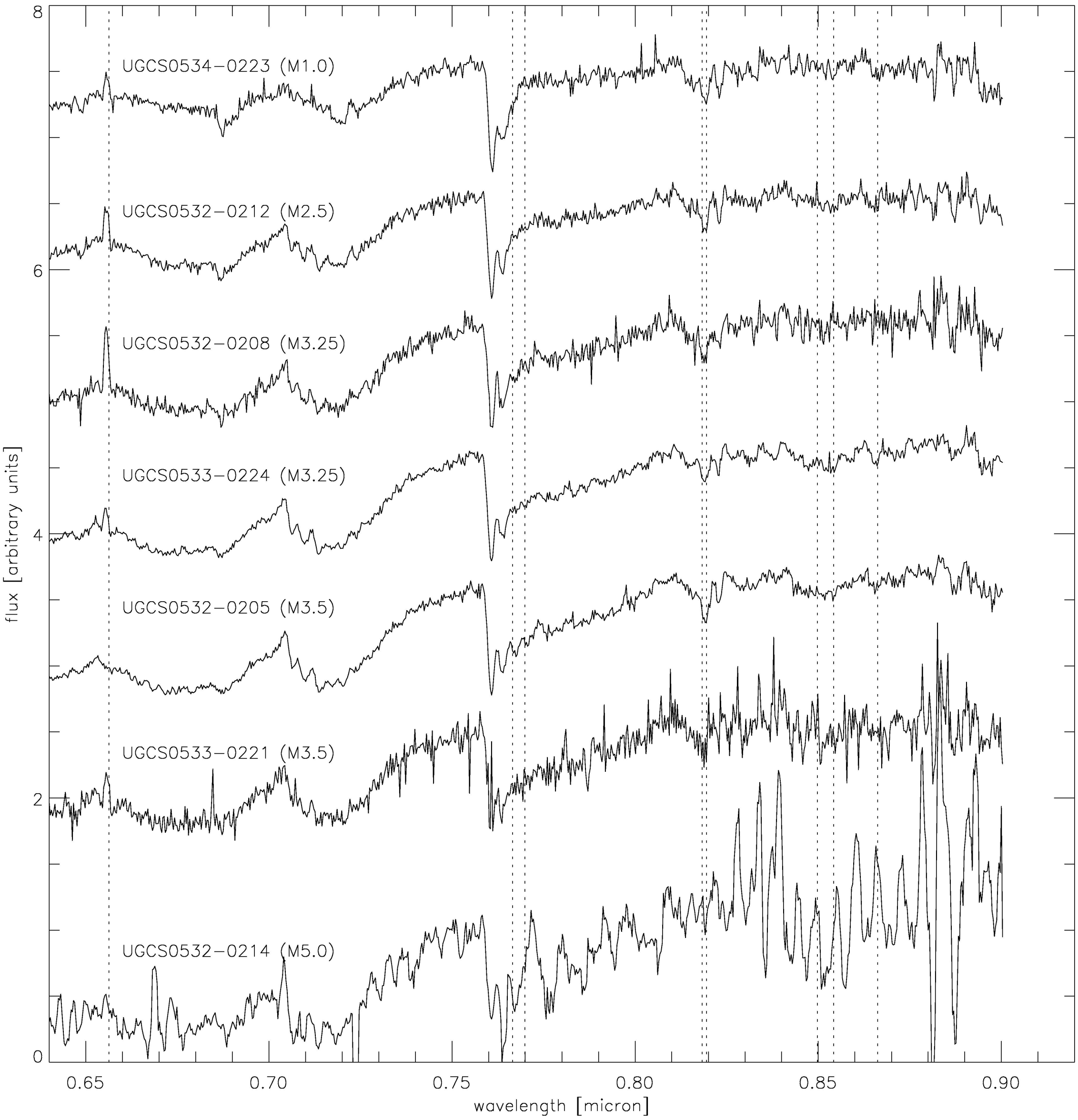

Figure D.12: Optical spectra of the Orion sources (see Fig. D.2).

Table D.1: The spectral types derived from the spectral indices, from the visual comparison with the reference spectra and the literature types. Also, we put the visual extinctions used to resemble the reference spectra. We show only those values matching the validity range of each index. The table is divided from top to bottom into observed candidates, Taurus members and field dwarfs. 2MASS names are shortened.

name	A_V	$TiO6$	$PC2$	$TiO7$	$R1$	$R3$	$c81$	$R2$	$TiO8465$	$TiOb$	VOb	lit.	visual
UGCSJ0419+2941	3.0	63.04	64.16	63.26	63.17	62.86	63.21	-	63.41	63.46	64.26	-	63.25
UGCSJ0419+3155	1.6	60.22	-	-	-	-	-	-	-	-	63.14	-	60.50
UGCSJ0421+3052	1.8	64.23	64.66	64.58	64.92	64.27	64.43	64.18	64.11	64.93	64.58	-	64.50
UGCSJ0425+3318	3.1	63.62	64.51	63.52	64.05	63.75	63.36	63.04	63.59	63.74	63.92	-	63.50
UGCSJ0426+2901	3.4	-	62.78	-	62.54	-	-	-	-	-	-	-	61.25
UGCSJ0427+2830	1.0	62.79	62.92	-	63.36	62.66	62.57	-	63.12	63.02	-	-	63.25
UGCSJ0427+2935	3.2	61.38	62.91	62.10	63.14	63.06	-	-	63.01	-	63.33	-	62.25
UGCSJ0428+2843	2.7	62.59	63.81	62.00	63.05	62.90	62.97	-	-	-	-	-	63.25
UGCSJ0428+3039	2.0	63.02	63.51	63.22	63.83	63.53	63.23	63.09	63.48	63.51	64.03	-	63.25
UGCSJ0428+3043	1.8	60.59	-	-	62.55	62.64	-	-	-	-	-	-	61.25
UGCSJ0428+3122	2.0	64.09	64.99	62.72	63.94	-	63.12	-	-	64.31	64.87	-	63.25
UGCSJ0429+3237	3.2	63.69	64.39	63.59	64.37	63.18	63.60	-	63.50	64.16	64.29	-	63.75
UGCSJ0430+2931	2.5	60.45	62.43	-	62.88	62.89	-	-	-	-	-	-	60.50
UGCSJ0430+2939	2.9	61.36	64.36	-	64.79	64.31	-	63.06	-	-	-	-	63.25
UGCSJ0430+3017	1.1	63.49	63.82	63.12	63.67	63.40	63.22	63.10	63.54	63.45	63.34	-	63.75
UGCSJ0431+3111	1.8	63.90	64.59	63.69	63.76	63.36	63.68	63.17	63.84	63.86	63.60	-	63.75
UGCSJ0432+3005	3.1	62.88	64.13	63.08	63.96	63.84	63.10	63.07	63.57	63.32	63.44	-	63.25
UGCSJ0432+3329	4.0	63.01	64.53	-	64.70	63.47	62.87	-	-	-	63.37	-	63.25
UGCSJ0433+2912	2.0	63.79	64.88	63.22	64.11	64.20	63.26	63.50	63.74	63.34	-	-	63.75
UGCSJ0433+3306B	2.7	60.32	62.19	-	62.75	62.67	-	-	-	-	63.23	-	61.25
UGCSJ0437+3056	3.6	63.13	64.42	63.48	63.86	63.83	63.23	63.37	63.59	63.70	63.87	-	63.25
UGCSJ0437+3155	2.5	-	63.04	-	64.10	62.74	-	-	-	-	-	-	60.50
UGCSJ0439+3032a	2.3	-	62.40	-	-	62.72	-	-	-	-	-	-	60.50
UGCSJ0439+3032b	4.0	-	62.47	-	63.39	-	-	-	-	-	63.16	-	60.50
UGCSJ0439+3050	1.9	-	62.20	-	-	-	-	-	63.22	-	-	-	60.50
UGCSJ0439+3105	1.3	63.27	63.68	62.41	63.72	63.36	63.07	63.03	63.22	63.41	-	-	63.25
UGCSJ0440+3156a	2.2	63.33	64.78	62.58	64.55	63.66	63.05	-	63.16	63.02	63.97	-	63.75
UGCSJ0440+3156b	2.2	63.96	64.90	62.22	64.45	63.46	63.25	-	63.17	-	-	-	63.75
UGCSJ0441+3200	1.4	64.10	65.22	63.82	65.26	64.27	63.95	63.56	63.62	63.88	64.60	-	64.50
UGCSJ0532-0212	0.2	61.99	62.10	62.60	-	-	62.50	-	63.13	63.29	-	-	62.50
UGCSJ0532-0214	-	67.86	63.53	-	-	65.56	64.49	-	64.51	-	-	-	65.00
UGCSJ0532-0205	-	63.44	63.33	63.61	63.30	63.29	63.17	-	63.81	63.67	-	-	63.50
UGCSJ0532-0208	0.3	62.73	62.83	63.15	63.53	63.31	-	-	63.25	63.30	63.79	-	63.25
UGCSJ0533-0224	-	63.54	63.27	63.12	63.59	63.67	62.98	63.20	63.58	63.53	63.17	-	63.25
UGCSJ0533-0221	-	63.60	62.85	64.55	64.83	64.23	63.30	63.88	64.22	64.76	-	-	63.50
UGCSJ0534-0223	-	61.45	-	62.45	-	62.68	-	-	63.19	-	63.30	-	61.00
J04034930+2610520	0.7	63.90	63.63	63.81	63.39	63.74	64.03	63.94	63.94	63.68	63.69	63.50	63.75
J04043936+2158186	0.2	63.41	63.01	63.10	63.19	63.14	63.48	63.38	63.36	63.43	63.14	63.50	63.25
J04131414+2819108	-	63.76	63.10	63.75	63.50	63.58	63.75	63.85	63.79	63.84	63.46	64.00	63.50
J04141458+2827580	0.8	63.60	63.37	63.92	63.80	63.74	63.63	63.78	63.89	63.90	63.97	65.00	63.25
J04144730+2646264	0.7	62.78	62.22	62.24	62.90	63.16	62.99	63.18	63.10	-	63.27	64.00	62.75
J04173893+2833005	0.5	62.65	-	62.97	62.99	62.93	63.15	63.19	63.24	63.32	63.44	62.00	62.25
J04174955+2813318	0.8	64.80	65.22	65.12	65.16	65.04	65.11	64.96	65.10	65.13	65.13	65.00	65.00
J04183112+2816290	1.5	63.71	63.74	63.28	64.25	64.32	63.43	64.12	64.02	63.45	64.42	63.50	63.25
J04215563+2755060	-	62.22	-	-	62.79	62.94	-	-	-	-	63.00	61.00	61.75
J04230607+2801194	-	66.61	65.69	66.06	65.94	65.80	65.97	65.86	65.83	66.20	65.86	66.00	66.50
J04270280+2542223	1.2	62.32	-	-	62.87	63.14	62.69	-	63.12	-	63.29	62.00	61.25
J04293606+2435556	6.3	60.97	64.08	62.34	63.46	63.16	62.58	-	-	-	63.93	63.00	60.50
J04295422+1754041	2.7	63.71	64.36	63.91	63.86	63.74	63.75	63.52	63.87	63.96	63.81	64.00	63.50
J04312405+1800215	-	-	65.94	66.82	66.31	66.01	66.66	66.09	66.46	66.81	66.40	67.00	66.25
J04321606+1812464	-	66.76	65.68	65.65	65.78	65.88	66.02	66.09	66.01	65.77	65.77	66.00	66.25
J04321786+2422149	0.7	66.43	65.85	66.02	65.73	65.91	66.02	66.05	66.30	66.02	65.68	65.75	65.75
J04322627+1827521	-	65.71	65.14	65.24	65.07	65.14	65.36	65.37	65.31	65.32	65.19	65.25	65.25
J04334871+1810099	0.6	62.93	62.07	62.75	63.03	63.06	63.19	63.21	63.27	63.14	63.42	61.00	62.50
J04345542+2428531	0.8	61.04	-	-	-	62.53	-	-	-	-	63.28	57.00	60.50
J04352737+2414589	0.9	61.34	-	62.01	-	62.52	62.57	-	-	-	63.25	60.00	60.50
J04355109+2252401	3.6	62.14	63.80	62.60	63.44	63.16	63.20	-	63.23	63.11	63.86	62.75	62.75
J04355684+2254360	3.8	62.22	63.67	62.46	63.93	62.77	63.02	-	63.17	63.05	-	63.00	62.50
HV TauC	1.3	63.93	64.32	64.55	64.26	64.14	64.16	64.20	64.23	64.57	64.48	61.00	64.00
J04391741+2247533	2.0	62.47	62.30	63.21	63.23	63.37	63.33	63.44	63.48	63.42	63.83	60.00	61.00
J04442713+2512164	-	66.87	65.69	66.68	66.23	66.02	66.61	66.17	66.36	66.74	66.07	67.20	66.00
J00005477+3249321	0.2	62.97	-	62.95	-	62.58	62.96	63.07	63.24	63.29	-	60.00	63.00

Table D.1 – continued from previous page

name	A_V	$TiO6$	$PC2$	$TiO7$	$R1$	$R3$	$c81$	$R2$	$TiO8465$	$TiOb$	VOb	lit.	visual
J00180010+4400293	0.7	61.28	-	-	-	-	62.65	-	-	-	-	65.00	61.25
J00181659+1012100	1.0	61.29	-	-	-	-	62.56	-	-	-	-	61.50	61.25
J00322970+6714080	1.4	61.62	62.05	-	62.65	62.61	62.74	-	-	-	63.03	62.50	62.00
J00385879+3036583	1.2	62.25	62.28	62.08	62.78	62.83	62.93	-	-	-	-	62.50	63.00
J00512963+5818071	-	-	-	-	-	-	-	-	-	-	63.01	62.00	60.50
J01012006+6121560	1.1	61.75	-	-	62.55	62.60	62.75	-	-	-	-	62.00	62.25
J01592349+5831162	0.7	63.78	63.53	63.88	63.64	63.59	63.86	63.73	63.78	63.92	63.72	64.00	63.75
GJ83.1	1.5	63.73	63.92	64.11	63.96	63.89	63.95	63.83	63.96	64.06	63.82	64.50	63.75
J03205965+1854233b	0.3	67.98	66.67	67.12	67.02	66.43	67.04	66.27	66.74	67.13	67.26	68.00	68.25
J03205965+1854233a	0.4	-	66.59	67.38	67.39	67.03	66.68	66.57	67.19	67.33	67.54	68.00	68.00
J04391586+3032074	1.9	63.00	63.40	63.15	62.99	63.16	63.15	63.05	63.41	63.41	63.45	63.50	63.25
J23340328+0010452	1.5	62.36	62.23	62.03	62.84	62.83	62.96	-	-	-	63.01	64.00	62.25
J23351050-0223214	3.0	64.48	65.07	65.13	65.02	64.86	64.85	64.70	64.94	65.16	65.16	65.50	64.50
J23415498+4410407	1.5	64.52	64.74	65.14	65.05	64.86	64.95	64.85	64.89	65.20	65.19	66.00	64.75

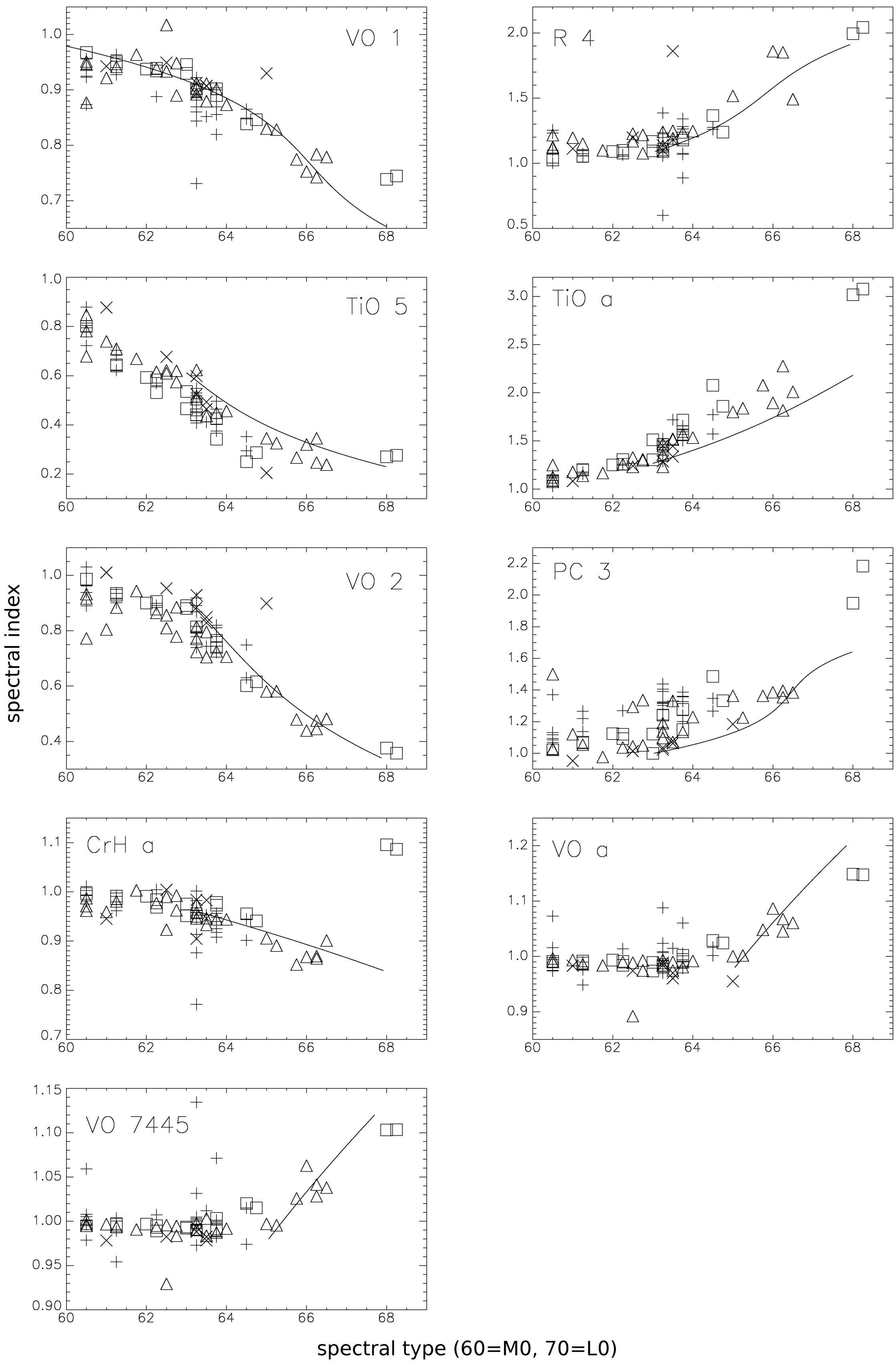

Figure D.13: The spectral indices not used to calculate spectral types (see Fig. 6.3).

Table D.2: We show in this table the values of the EW of the line features. For a better overview we put the visual extinction and the spectral types derived by the visual comparison and the literature types. The EW of the *NaI* and *KI* doublets and the *CaII* triplet are the sum of the single EW. The table is divided from top to bottom into observed bright LMO candidates, faint LMO candidates, MIR excess candidates, Orion candidates, already known Taurus members and field dwarfs. 2MASS names are shortened.

name	A_V [mag]	$EW(H_\alpha)$ [Å]	$EW(KI)$ [Å]	$EW(NaI)$ [Å]	$EW_{CaII(8662)}$ [Å]	EW_{CaII} [Å]	lit. type	visual type
UGCSJ0419+2941	3.0	-7.57	3.57	5.50	0.97	3.93	-	63.25
UGCSJ0419+3155	1.6	-	1.03	3.41	2.77	6.15	-	60.50
UGCSJ0421+3052	1.8	-6.83	8.01	3.98	-	-	-	64.50
UGCSJ0425+3318	3.1	-11.35	5.18	5.43	-	-	-	63.50
UGCSJ0426+2901	3.4	-	2.15	4.20	2.27	6.50	-	61.25
UGCSJ0426+3036	-	1.93	3.02	-	-	-	-	-
UGCSJ0427+2830	1.0	-	3.81	5.28	2.08	5.16	-	63.25
UGCSJ0427+2836	-	-2.38	2.69	3.47	1.77	5.77	-	-
UGCSJ0427+2838	-	-	1.58	2.38	1.74	6.01	-	-
UGCSJ0427+2935	3.2	-	2.60	3.27	1.62	4.53	-	62.25
UGCSJ0427+3007	-	-	1.33	3.51	2.46	6.84	-	-
UGCSJ0428+2843	2.7	-	3.29	3.87	1.24	3.14	-	63.25
UGCSJ0428+3039	2.0	-4.37	2.87	2.89	0.99	2.22	-	63.25
UGCSJ0428+3043	1.8	-	2.07	2.58	2.26	5.07	-	61.25
UGCSJ0428+3122	2.0	-	2.98	-	-	-	-	63.25
UGCSJ0429+2824	-	-	1.94	2.57	1.92	5.06	-	-
UGCSJ0429+3237	3.2	-17.27	7.17	4.67	-	-	-	63.75
UGCSJ0430+2931	2.5	-2.38	1.62	4.43	1.19	3.85	-	60.50
UGCSJ0430+2939	2.9	-	2.22	1.23	-	-	-	63.25
UGCSJ0430+3016	-	1.65	1.94	3.11	2.08	6.21	-	-
UGCSJ0430+3017	1.1	-9.24	5.49	5.45	0.74	2.35	-	63.75
UGCSJ0431+3111	1.8	-6.82	3.30	3.24	-	-	-	63.75
UGCSJ0431+3116	-	-	0.74	1.63	2.70	8.14	-	-
UGCSJ0432+2828	-	1.57	-	-	2.57	8.35	-	-
UGCSJ0432+3005	3.1	-	4.27	4.83	0.47	2.20	-	63.25
UGCSJ0432+3301	-	0.68	-	3.60	2.94	6.62	-	-
UGCSJ0432+3329	4.0	-8.70	5.77	6.11	1.87	3.24	-	63.25
UGCSJ0433+2912	2.0	-9.84	2.24	3.96	-	-	-	63.75
UGCSJ0433+3306A	-	0.68	-	-	3.27	8.34	-	-
UGCSJ0433+3306B	2.7	-3.13	2.13	2.96	1.19	3.04	-	61.25
UGCSJ0435+2959	-	1.04	-	0.92	2.41	7.81	-	-
UGCSJ0436+3307	-	1.42	-	1.80	1.77	6.46	-	-
UGCSJ0437+3005	-	-2.10	1.55	2.33	1.85	3.68	-	-
UGCSJ0437+3056	3.6	-26.30	3.29	3.52	-	-	-	63.25
UGCSJ0437+3144	-	1.25	-	2.59	2.37	7.08	-	-
UGCSJ0437+3155	2.5	-	0.89	9.76	-	-	-	60.50
UGCSJ0438+2921	-	0.85	-	0.72	2.04	6.32	-	-
UGCSJ0438+3119	-	-1.86	2.00	3.49	1.51	3.86	-	-
UGCSJ0439+3032a	2.3	-	3.17	8.13	-	-	-	60.50
UGCSJ0439+3032b	4.0	-	1.87	1.93	-	-	-	60.50
UGCSJ0439+3050	1.9	-	2.29	3.72	-	-	-	60.50
UGCSJ0439+3105	1.3	-	2.28	10.55	-	-	-	63.25
UGCSJ0440+3156a	2.2	-7.74	5.33	8.36	-	-	-	63.75

Table D.2 – continued from previous page

name	A_V [mag]	$EW(H_\alpha)$ [$\AA$]	$EW(KI)$ [$\AA$]	$EW(NaI)$ [$\AA$]	$EW_{CaII(8662)}$ [$\AA$]	EW_{CaII} [$\AA$]	lit. type	visual type
UGCSJ0440+3156b	2.2	-9.93	2.27	5.53	-	-	-	63.75
UGCSJ0441+3200	1.4	-9.59	7.46	2.24	-	-	-	64.50
UGCSJ0429+3139	-	-	-	-	-	-	-	-
UGCSJ0440+3004A	-	-	1.56	3.61	1.24	2.40	-	-
UGCSJ0440+3004B	-	-	1.56	3.52	1.19	2.63	-	-
UGCSJ0441+3101a	-	8.61	-	-	5.31	6.99	-	-
UGCSJ0441+3101b	-	-	1.28	1.40	2.00	4.76	-	-
UGCSJ0441+3126	-	-	0.67	7.38	2.36	7.21	-	-
UGCSJ0417+2918	-	4.15	1.29	2.99	1.67	5.64	-	-
UGCSJ0417+2934	-	3.31	-	3.05	1.75	6.68	-	-
UGCSJ0418+2933	-	2.06	0.24	2.08	2.87	6.28	-	-
UGCSJ0418+2937	-	3.40	0.50	1.42	2.14	6.96	-	-
UGCSJ0418+2945	-	1.41	-	-	-	-	-	-
UGCSJ0419+2928	-	1.49	-	-	-	-	-	-
UGCSJ0425+2828	-	3.96	-	2.27	3.57	7.68	-	-
UGCSJ0426+2824	-	1.41	-	-	-	-	-	-
UGCSJ0426+2839	-	2.80	0.72	3.70	2.87	5.80	-	-
UGCSJ0427+2823	-	1.87	-	-	-	-	-	-
UGCSJ0427+2839	-	3.34	1.83	2.03	2.35	8.12	-	-
UGCSJ0429+2826	-	3.83	-	-	-	-	-	-
UGCSJ0430+2840	-	2.55	-	-	2.66	6.10	-	-
UGCSJ0431+2844	-	4.06	1.16	0.89	0.32	4.06	-	-
UGCSJ0431+2943	-	3.11	-	-	-	-	-	-
UGCSJ0431+2921	-	1.14	-	-	-	-	-	-
UGCSJ0431+2913	-	-4.39	-	-	-	-	-	-
UGCSJ0432+2844	-	3.86	-	0.85	1.29	4.88	-	-
UGCSJ0432+2916	-	7.35	-	-	-	-	-	-
UGCSJ0432+2943	-	5.82	0.30	2.73	3.68	7.14	-	-
UGCSJ0434+2941	-	0.92	-	-	-	-	-	-
UGCSJ0434+2939	-	-	-	-	-	-	-	-
UGCSJ0532-0212	0.2	-6.40	1.66	4.98	-	-	-	62.50
UGCSJ0532-0214	-	-	-	4.27	-	-	-	65.00
UGCSJ0532-0205	-	-	2.58	5.94	0.40	1.02	-	63.50
UGCSJ0532-0208	0.3	-12.31	2.76	3.60	-	-	-	63.25
UGCSJ0533-0224	-	-5.51	0.59	4.00	-	-	-	63.25
UGCSJ0533-0221	-	-11.06	2.08	1.86	-	-	-	63.50
UGCSJ0534-0223	-	-5.41	1.22	3.56	-	2.13	-	61.00
J04034930+2610520	0.7	-10.23	3.11	3.22	-	-	63.50	63.75
J04043936+2158186	0.2	-5.68	2.89	3.02	-	-	63.50	63.25
J04131414+2819108	-	-3.27	3.41	1.41	0.84	2.25	64.00	63.50
J04141458+2827580	0.8	-26.62	-	0.94	-0.82	-3.47	65.00	63.25
J04141700+2810578	-	-68.67	-	0.39	-14.66	-48.89	53.00	-
J04144730+2646264	0.7	-70.71	1.13	2.06	-	-	64.00	62.75
J04173893+2833005	0.5	-3.86	-	2.08	-	-	62.00	62.25
J04174955+2813318	0.8	-34.32	5.01	1.72	-	-	65.00	65.00
J04183112+2816290	1.5	-220.70	-	1.36	-6.28	-21.22	63.50	63.25
J04185170+1723165	-	-0.88	0.17	2.01	1.54	3.39	57.00	-

Table D.2 – continued from previous page

name	A_V [mag]	$EW(H_\alpha)$ [Å]	$EW(KI)$ [Å]	$EW(NaI)$ [Å]	$EW_{CaII(8662)}$ [Å]	EW_{CaII} [Å]	lit. type	visual type
J04215563+2755060	-	-62.71	-	1.64	-6.45	-21.91	61.00	61.75
J04215740+2826355	-	-3.73	-	1.00	1.45	3.69	51.00	-
J04215943+1932063	-	-56.75	1.04	0.42	-1.71	-4.79	50.00	-
J04224786+2645530	-	-54.07	1.18	1.29	-14.03	-47.59	61.00	-
J04230607+2801194	-	-30.37	7.81	1.11	-	-	66.00	66.50
J04270280+2542223	1.2	-62.56	-	1.43	-1.86	-5.77	62.00	61.25
J04292373+2433002	-	-75.57	0.81	1.73	-27.33	-82.26	55.00	-
J04293606+2435556	6.3	-10.03	1.24	2.21	0.91	2.37	63.00	60.50
J04295422+1754041	2.7	-25.08	1.94	2.94	-	-	64.00	63.50
J04312405+1800215	-	-40.91	2.74	2.39	-	-	67.00	66.25
J04321606+1812464	-	-192.90	0.75	0.28	-1.99	-11.89	66.00	66.25
J04321786+2422149	0.7	-15.15	21.42	1.66	-	-	65.75	65.75
J04322627+1827521	-	-6.08	5.14	1.35	-	-	65.25	65.25
J04331003+2433433	-	-1.75	0.12	1.86	1.20	2.97	57.00	-
J04333405+2421170	-	-27.15	0.25	1.73	-1.01	-3.32	57.00	-
J04334871+1810099	0.6	-206.50	1.54	2.09	-	-	61.00	62.50
J04335470+2613275	-	-20.71	-	1.42	-	-	52.00	-
J04341803+1830066	-	-	-	1.29	1.76	4.89	48.00	-
J04345542+2428531	0.8	-4.08	0.41	1.73	-	-	57.00	60.50
J04352737+2414589	0.9	-10.70	0.62	1.80	-	-	60.00	60.50
J04355109+2252401	3.6	-5.38	1.61	2.80	0.76	1.56	62.75	62.75
J04355684+2254360	3.8	-62.33	3.65	2.24	-	-	63.00	62.50
HV TauC	1.3	-9.17	3.56	1.79	-	-	61.00	64.00
J04391741+2247533	2.0	-4.07	1.04	2.39	0.93	2.19	60.00	61.00
J04442713+2512164	-	-113.10	3.23	2.67	-	-	67.20	66.00
J04474859+2925112	-	-62.07	-	1.48	-2.56	-7.81	55.00	-
J04555938+3034015	-	-85.94	-	1.22	-8.32	-26.23	42.00	-
J00000099-1929557	-	1.85	-	1.36	2.06	5.82	53.00	-
HIP18	-	1.59	0.33	1.42	2.28	7.04	55.00	-
J00001280+3818144	-	1.97	-	0.72	3.33	8.11	45.00	-
J00001512+2331451	-	3.85	-	0.53	2.50	6.07	40.00	-
J00005477+3249321	0.2	-	1.46	0.52	2.91	7.69	60.00	63.00
J00010057+2753109	-	1.58	-	1.03	2.41	6.39	50.00	-
J00082573+0637004	-	2.96	-	0.77	2.16	5.82	42.00	-
J00170635+4056538	-	-	1.06	2.71	1.84	5.93	57.00	-
J00180010+4400293	0.7	-	2.08	3.21	1.33	3.81	65.00	61.25
J00181659+1012100	1.0	-	1.62	3.12	1.27	4.05	61.50	61.25
J00322970+6714080	1.4	-	2.09	3.59	1.12	3.40	62.50	62.00
J00385879+3036583	1.2	-	2.21	3.22	1.12	3.23	62.50	63.00
J00450489+0147077	-	1.48	-	1.47	2.30	6.55	52.00	-
J00482326+6057422	-	1.50	-	0.86	2.16	6.18	48.00	-
J00512963+5818071	-	-	1.13	2.16	1.51	4.61	62.00	60.50
J01012006+6121560	1.1	-	2.42	3.37	1.22	3.59	62.00	62.25
J01592349+5831162	0.7	-5.55	3.83	4.12	-	-	64.00	63.75
GJ83.1	1.5	-2.82	8.00	6.09	-	-	64.50	63.75
J03205965+1854233b	0.3	-19.32	8.07	6.73	-	-	68.00	68.25
J03205965+1854233a	0.4	-33.26	9.54	7.42	-	-	68.00	68.00

Table D.2 – continued from previous page

name	A_V [mag]	$EW(H_\alpha)$ [$\AA$]	$EW(KI)$ [$\AA$]	$EW(NaI)$ [$\AA$]	$EW_{CaII(8662)}$ [$\AA$]	EW_{CaII} [$\AA$]	lit. type	visual type
HIP16242	-	-	0.56	3.28	1.86	6.43	57.00	-
J03542950+3203013	-	2.25	-	0.71	1.95	4.92	40.00	-
HBC353	-	2.66	-	1.02	1.75	5.55	45.00	-
J03543556+2537111	-	-	-	1.58	1.49	3.56	53.00	-
J03543597+2537081	-	1.42	-	1.38	1.76	4.89	52.00	-
HBC357	-	-	-	1.73	1.04	3.53	52.00	-
J04271056+1750425	-	1.88	-	0.87	2.06	5.12	51.00	-
J04312717+1706249	-	-0.64	0.34	2.12	1.67	4.40	55.00	-
J04391586+3032074	1.9	-	2.76	4.86	0.83	2.43	63.50	63.25
J23340328+0010452	1.5	-	1.84	2.81	1.24	3.60	64.00	62.25
J23351050-0223214	3.0	-1.41	11.71	6.17	-	-	65.50	64.50
J23415498+4410407	1.5	-	9.44	6.09	-	-	66.00	64.75

Table D.3: We show the outcome, i.e. best fit, of VOSA sorted by RA. Only for few sources an age and mass could be estimated in the range of the model parameters. For the calculation of the spectral type via T_{eff} we use the relation found by the Taurus members, where $(spectraltype) = (12415 - T_{eff})/143$ (see Chap. 2.2.2 and Fig. A.1). The values get compared to the ones found by the visual comparison in this chapter. The asterisk marks the best candidates. Note, that VOSA only operates with an input of more than 3 photometric filters.

object	model	T_{eff} [K]	$logg$	L_{bol} [$L_\odot$]	log(L_{bol}) [$L_\odot$]	age [Myr]	mass [$M_\odot$]	J [mag]	type calc.	type vis.
UGCSJ0417+2918	NextGen	5000	4.0	0.00915±0.00022	-2.039±0.024	-	-	14.03	51.85	-
UGCSJ0417+2934	NextGen	4800	3.5	0.01537±0.00036	-1.813±0.023	-	-	13.53	53.25	-
UGCSJ0418+2933	NextGen	4600	3.5	0.01300±0.00016	-1.886±0.013	-	-	13.64	54.65	-
UGCSJ0418+2937	NextGen	4800	3.5	0.01423±0.00019	-1.847±0.013	-	-	13.61	53.25	-
UGCSJ0418+2945	NextGen	4600	3.5	0.00995±0.00019	-2.002±0.019	-	-	14.07	54.65	-
UGCSJ0419+2928	NextGen	5200	4.0	0.01156±0.00021	-1.937±0.018	-	-	13.89	50.45	-
UGCSJ0419+2941	NextGen	3200	5.5	0.01662±0.00013	-1.779±0.008	15.8	0.15	12.94	64.44	63.25
UGCSJ0419+3155	NextGen	2600	5.5	0.02490±0.00019	-1.604±0.007	-	-	12.28	68.64	60.50
UGCSJ0421+3052*	NextGen	2800	5.5	0.00749±0.00006	-2.126±0.009	6.0	0.04	13.67	67.24	64.50
UGCSJ0425+2828	NextGen	4800	3.5	0.00817±0.00016	-2.088±0.020	-	-	14.19	53.25	-
UGCSJ0425+3318	DUSTY00	3000	6.0	0.01554±0.00013	-1.808±0.009	-	0.07	12.98	65.84	63.50
UGCSJ0426+2824	NextGen	4800	4.0	0.01036±0.00022	-1.985±0.021	-	-	13.83	53.25	-
UGCSJ0426+2839	NextGen	4600	3.5	0.01015±0.00016	-1.993±0.016	-	-	13.87	54.65	-
UGCSJ0426+2901	COND00	3300	3.5	0.01095±0.00010	-1.961±0.010	-	-	13.37	63.74	61.25
UGCSJ0426+3036	COND00	3300	3.5	0.00847±0.00010	-2.072±0.011	-	-	13.61	63.74	-
UGCSJ0427+2823	NextGen	4600	3.5	0.03018±0.00031	-1.520±0.010	-	-	12.62	54.65	-
UGCSJ0427+2830	COND00	3300	3.0	0.00692±0.00006	-2.160±0.009	-	-	13.85	63.74	63.25
UGCSJ0427+2836*	COND00	3600	4.0	0.02151±0.00020	-1.667±0.009	-	-	12.74	61.64	-
UGCSJ0427+2838	NextGen	3400	5.5	0.03361±0.00031	-1.474±0.009	25.0	0.30	12.30	63.04	-
UGCSJ0427+2839	NextGen	4600	5.5	0.01191±0.00016	-1.924±0.013	-	-	13.61	54.65	-
UGCSJ0427+2935	COND00	3300	3.5	0.00848±0.00008	-2.072±0.010	-	-	13.64	63.74	62.25
UGCSJ0427+3007	NextGen	3500	4.0	0.03084±0.00030	-1.511±0.010	50.3	0.40	12.40	62.34	-
UGCSJ0428+2843	NextGen	3400	4.0	0.00834±0.00002	-2.079±0.002	-	-	13.54	63.04	63.25
UGCSJ0428+3039*	NextGen	3100	4.0	0.02687±0.00023	-1.571±0.009	5.0	0.11	12.41	65.14	63.25
UGCSJ0428+3043	NextGen	3600	4.5	0.02944±0.00019	-1.531±0.006	768.8	0.46	12.46	61.64	61.25
UGCSJ0428+3122	NextGen	2600	5.0	0.00696±0.00008	-2.157±0.011	-	-	13.78	68.64	63.25
UGCSJ0429+2824	NextGen	3400	4.0	0.03071±0.00024	-1.513±0.008	25.9	0.30	12.10	63.04	-
UGCSJ0429+2826	NextGen	4800	3.5	0.03892±0.00041	-1.410±0.011	-	-	12.37	53.25	-
UGCSJ0429+3237*	NextGen	3300	4.0	0.00978±0.00011	-2.010±0.011	63.0	0.20	12.35	63.74	63.75
UGCSJ0430+2840	NextGen	4800	3.5	0.00814±0.00013	-2.089±0.016	-	-	14.15	53.25	-
UGCSJ0430+2931	NextGen	3200	3.5	0.02402±0.00020	-1.619±0.008	10.1	0.16	12.52	64.44	60.50
UGCSJ0430+2939	DUSTY00	2200	6.0	0.00578±0.00006	-2.238±0.010	-	-	14.09	71.43	63.25
UGCSJ0430+3016	NextGen	3600	5.5	0.04207±0.00021	-1.376±0.005	62.7	0.50	12.60	61.64	-
UGCSJ0430+3017	NextGen	3300	4.0	0.01118±0.00007	-1.952±0.007	50.2	0.20	13.40	63.74	63.75

Table D.3 – continued from previous page

object	model	T_{eff}	$logg$	L_{bol}	log(L_{bol})	age	mass	J	type	
		$[K]$		$[L_\odot]$	$[L_\odot]$	$[Myr]$	$[M_\odot]$	$[mag]$	calc	
UGCSJ0431+2844	NextGen	4800	3.5	0.00912±0.00016	-2.040±0.017	-	-	14.01	53.25	-
UGCSJ0431+2913	NextGen	3600	4.0	0.00369±0.00007	-2.433±0.018	-	-	14.69	61.64	-
UGCSJ0431+2921	NextGen	3500	4.0	0.00520±0.00006	-2.284±0.011	-	-	14.28	62.34	-
UGCSJ0431+2943	NextGen	4800	3.5	0.01067±0.00016	-1.972±0.015	-	-	13.89	53.25	-
UGCSJ0431+3111*	NextGen	3100	3.5	0.00871±0.00006	-2.060±0.007	19.3	0.10	13.62	65.14	63.75
UGCSJ0431+3116	DUSTY00	2100	6.0	0.02141±0.00015	-1.669±0.007	-	-	12.06	72.13	-
UGCSJ0432+2828	NextGen	3200	5.0	0.04472±0.00048	-1.349±0.011	5.1	0.17	12.39	64.44	-
UGCSJ0432+2844	NextGen	4800	3.5	0.01272±0.00021	-1.896±0.017	-	-	13.74	53.25	-
UGCSJ0432+2916	NextGen	5200	5.5	0.03950±0.00041	-1.403±0.010	-	-	12.34	50.45	-
UGCSJ0432+2943	NextGen	4800	3.5	0.01520±0.00019	-1.818±0.012	-	-	13.35	53.25	-
UGCSJ0432+3005	NextGen	3100	5.0	0.01025±0.00008	-1.989±0.008	15.5	0.10	13.28	65.14	63.25
UGCSJ0432+3301	NextGen	3500	5.5	0.04508±0.00040	-1.346±0.009	31.6	0.41	13.48	62.34	-
UGCSJ0432+3329	NextGen	3200	4.0	0.01225±0.00007	-1.912±0.006	22.7	0.14	12.10	64.44	63.25
UGCSJ0433+2912*	NextGen	2800	5.5	0.01074±0.00009	-1.969±0.008	3.9	0.04	13.29	67.24	63.75
UGCSJ0433+3306A	DUSTY00	2200	5.5	0.02269±0.00015	-1.644±0.007	-	-	12.92	71.43	-
UGCSJ0433+3306B*	NextGen	3300	5.5	0.01846±0.00001	-1.734±0.001	25.5	0.20	12.92	63.74	61.25
UGCSJ0434+2939	COND00	3500	3.0	0.01158±0.00011	-1.936±0.010	-	-	13.39	62.34	-
UGCSJ0434+2941	COND00	3400	4.5	0.00185±0.00005	-2.734±0.030	-	-	15.44	63.04	-
UGCSJ0435+2959	COND00	3500	2.5	0.02661±0.00022	-1.575±0.008	-	-	12.55	62.34	-
UGCSJ0436+3307	NextGen	3400	5.5	0.03980±0.00046	-1.400±0.011	20.3	0.31	12.13	63.04	-
UGCSJ0437+3005*	COND00	3500	2.5	0.02471±0.00025	-1.607±0.010	-	-	12.59	62.34	-
UGCSJ0437+3056*	NextGen	2700	5.5	0.01626±0.00016	-1.789±0.010	-	-	12.91	67.94	63.25
UGCSJ0437+3144	NextGen	3500	4.0	0.02759±0.00029	-1.559±0.011	62.0	0.40	12.51	62.34	-
UGCSJ0437+3155	NextGen	3200	3.5	0.02180±0.00020	-1.662±0.009	12.2	0.15	12.68	64.44	60.50
UGCSJ0438+2921	NextGen	3100	4.5	0.03796±0.00027	-1.421±0.007	4.0	0.13	12.06	65.14	-
UGCSJ0438+3119*	NextGen	3500	4.5	0.02943±0.00031	-1.531±0.010	53.8	0.40	12.46	62.34	-
UGCSJ0439+3032	COND00	3500	2.5	0.00673±0.00008	-2.172±0.012	-	-	14.04	62.34	60.50
UGCSJ0439+3050	COND00	3500	2.5	0.00607±0.00006	-2.217±0.010	-	-	14.13	62.34	60.50
UGCSJ0439+3105	NextGen	3900	3.5	0.00596±0.00001	-2.225±0.002	-	-	14.17	59.55	63.25
UGCSJ0440+3004	DUSTY00	1800	5.0	0.00019±0.00000	-3.715±0.003	51.5	0.02	18.01	74.23	-
UGCSJ0440+3156	NextGen	2700	5.0	0.00423±0.00005	-2.373±0.012	7.9	0.03	18.01	67.94	63.75
UGCSJ0441+3101	DUSTY00	1800	5.0	0.00020±0.00000	-3.707±0.003	50.9	0.02	14.33	74.23	63.75
UGCSJ0441+3126	DUSTY00	1800	5.0	0.00020±0.00000	-3.691±0.003	54.6	0.02	14.33	74.23	-
UGCSJ0441+3200*	NextGen	2900	5.5	0.00987±0.00009	-2.006±0.010	6.3	0.06	13.39	66.54	64.50
UGCSJ0532-0205	COND00	3300	5.0	0.27610±0.00018	-0.559±0.001	-	-	12.49	63.74	63.50
UGCSJ0532-0208*	NextGen	3500	4.5	0.18003±0.00012	-0.745±0.001	4.9	0.45	13.01	62.34	63.25
UGCSJ0532-0212	NextGen	3500	5.0	0.27967±0.00018	-0.553±0.001	2.6	0.48	12.52	62.34	62.50
UGCSJ0532-0214	NextGen	3500	4.5	0.11133±0.00012	-0.953±0.001	9.3	0.45	13.55	62.34	65.00
UGCSJ0533-0221*	NextGen	3500	4.5	0.15449±0.00015	-0.811±0.001	5.9	0.45	13.13	62.34	63.50
UGCSJ0533-0224*	NextGen	3400	5.5	0.29218±0.00019	-0.534±0.001	1.6	0.40	12.46	63.04	63.25
UGCSJ0534-0223*	NextGen	3800	5.0	0.50583±0.00017	-0.296±0.000	4.0	0.90	12.00	60.24	61.00

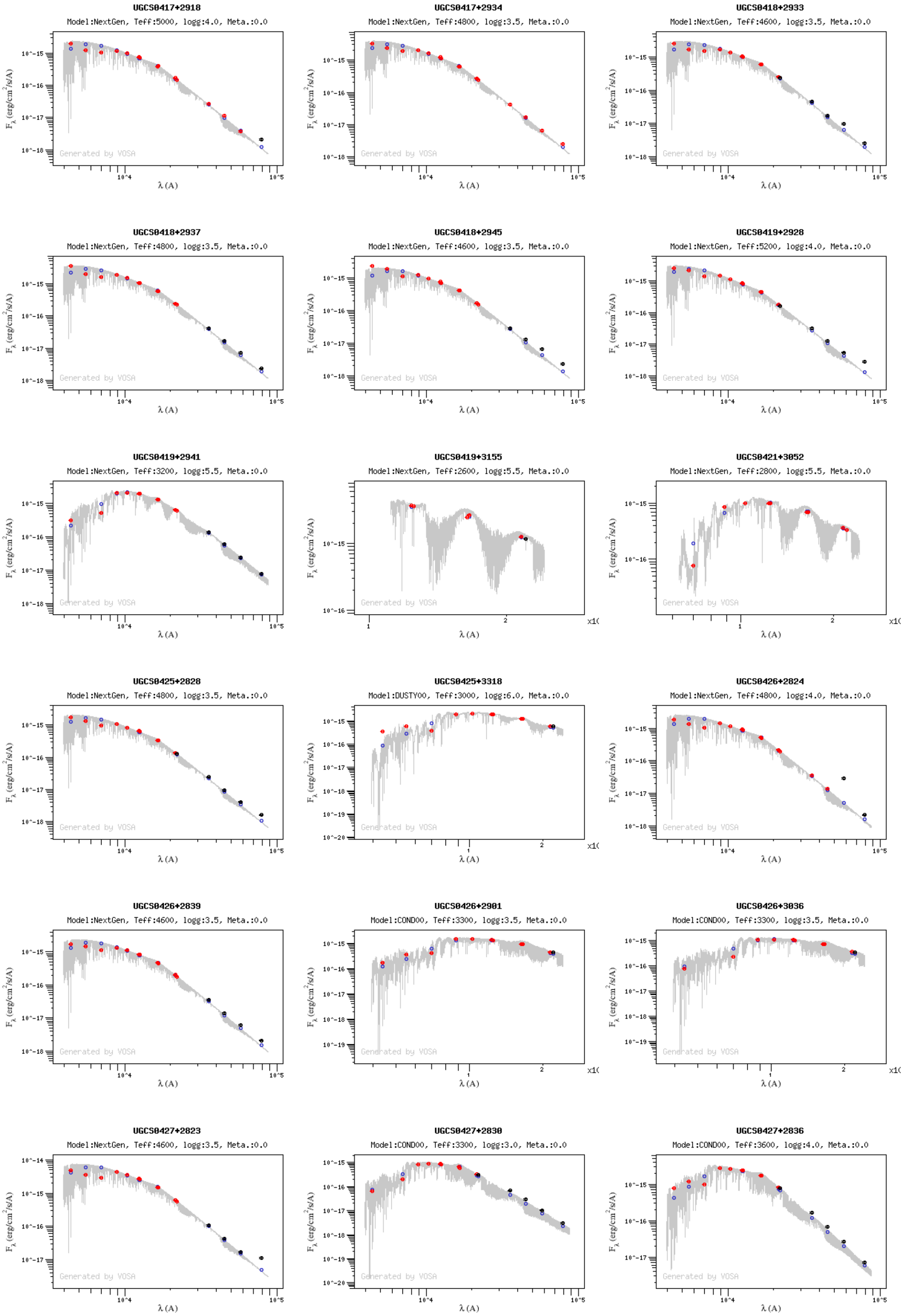

Figure D.14: Best fit SED (gray) for the observed objects by VOSA, part I. The red circle mark the photometry of BVR NOMAD, $ZYJHK$ UKIDSS GCS, JHK 2MASS, and the four IRAC filters and their errors. If the data point is black, VOSA identifies an excess in this filter compared to the best fitted model, which is shown by the blue circles. The model data of the best fit and object name is shown above each diagram. Note, that VOSA only operates with an input of more than 4 photometric filters, which is why UGCSJ0429+3139 has no fit (see Fig. D.15).

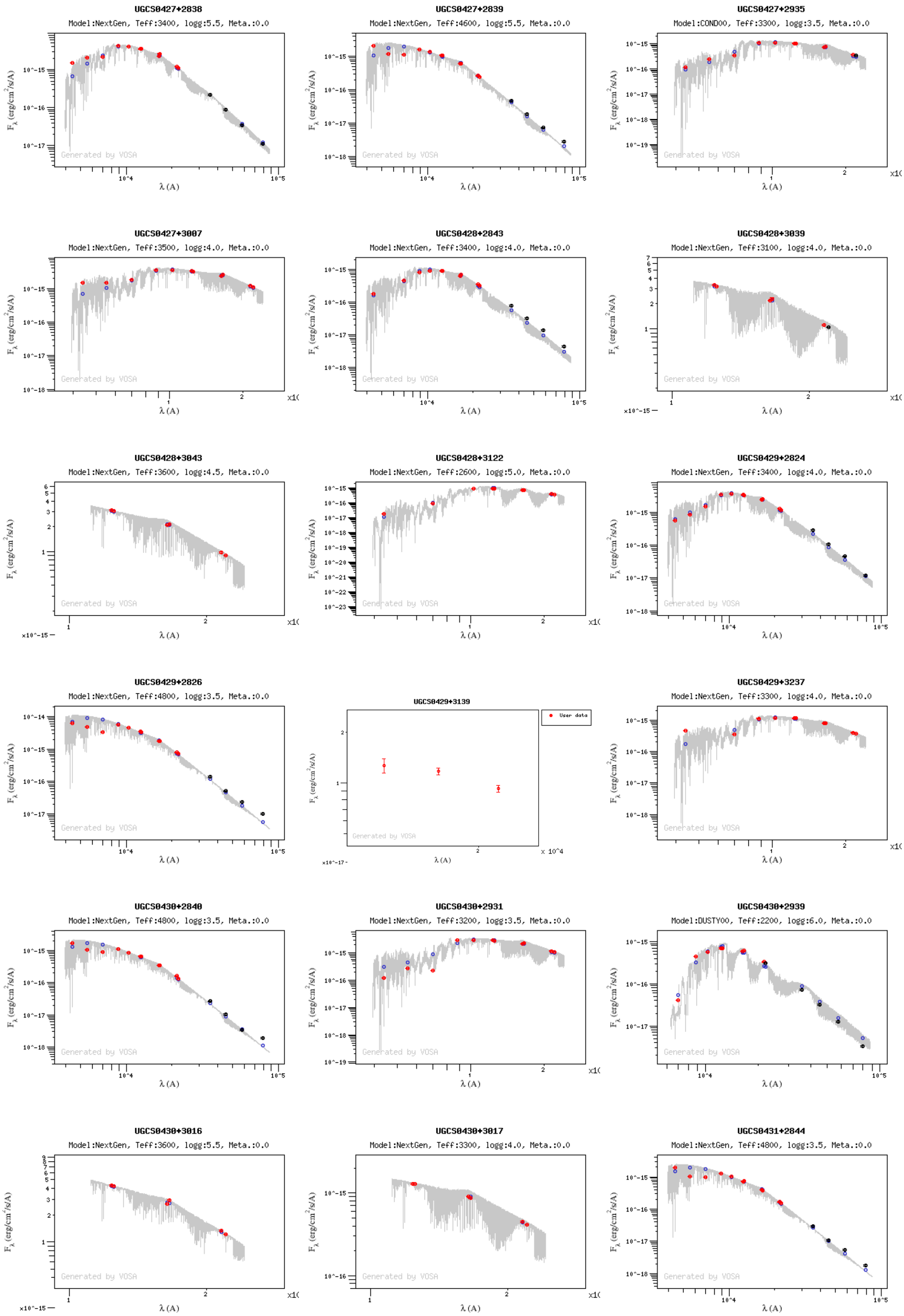

Figure D.15: Best fit SED for the observed objects by VOSA, part II (see Fig. D.14).

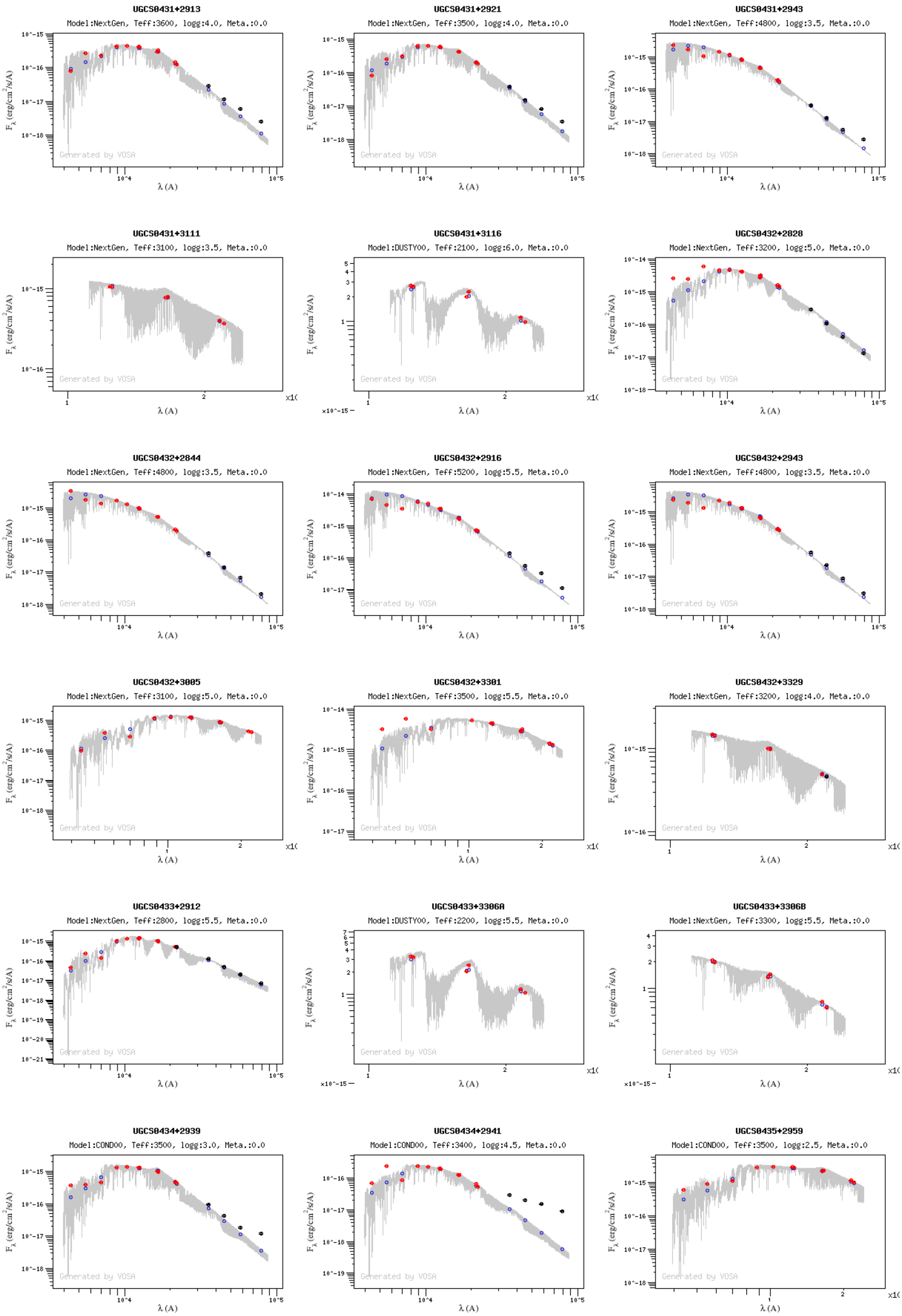

Figure D.16: Best fit SED for the observed objects by VOSA, part III (see Fig. D.14).

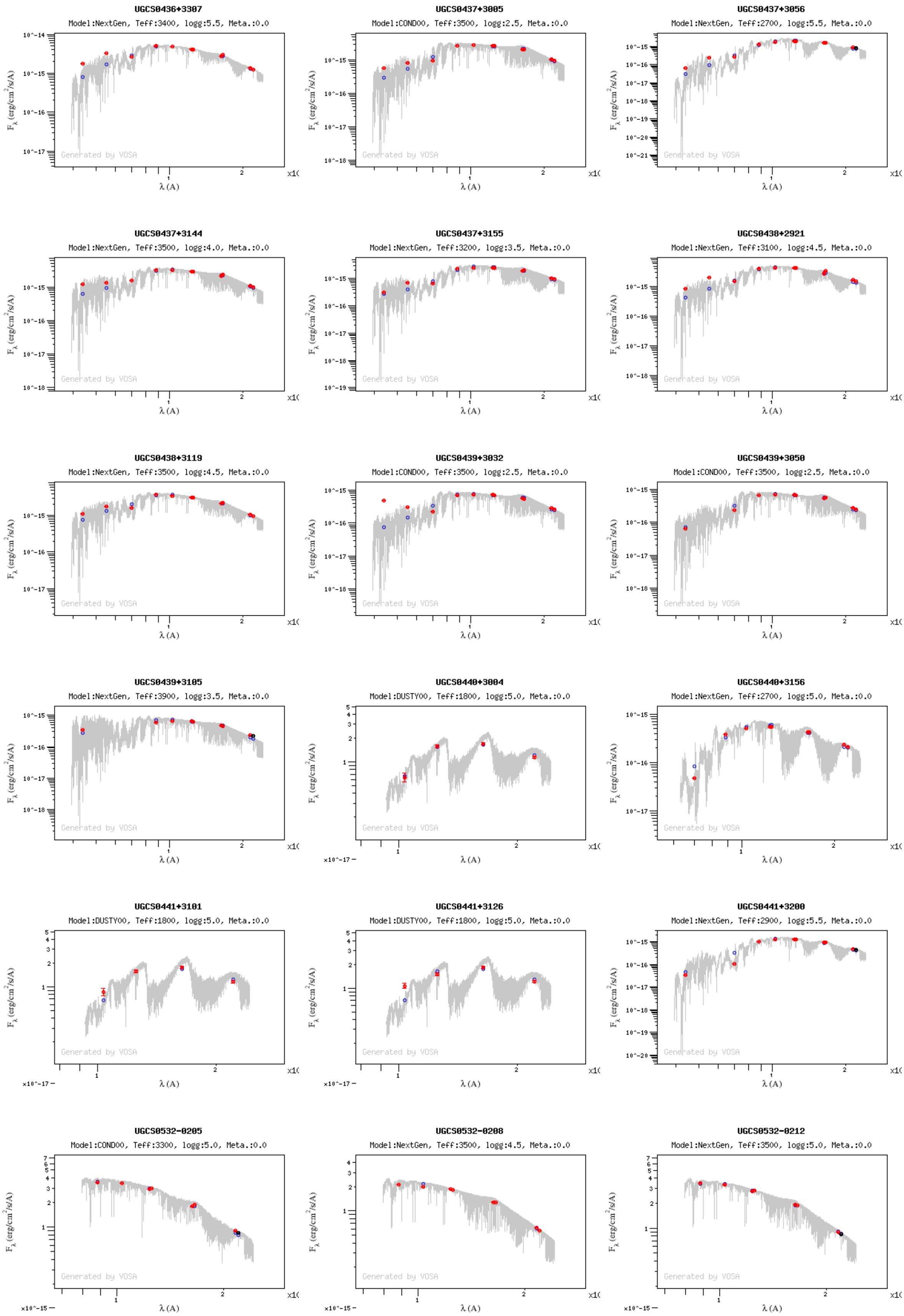

Figure D.17: Best fit SED for the observed objects by VOSA, part IV (see Fig. D.14).

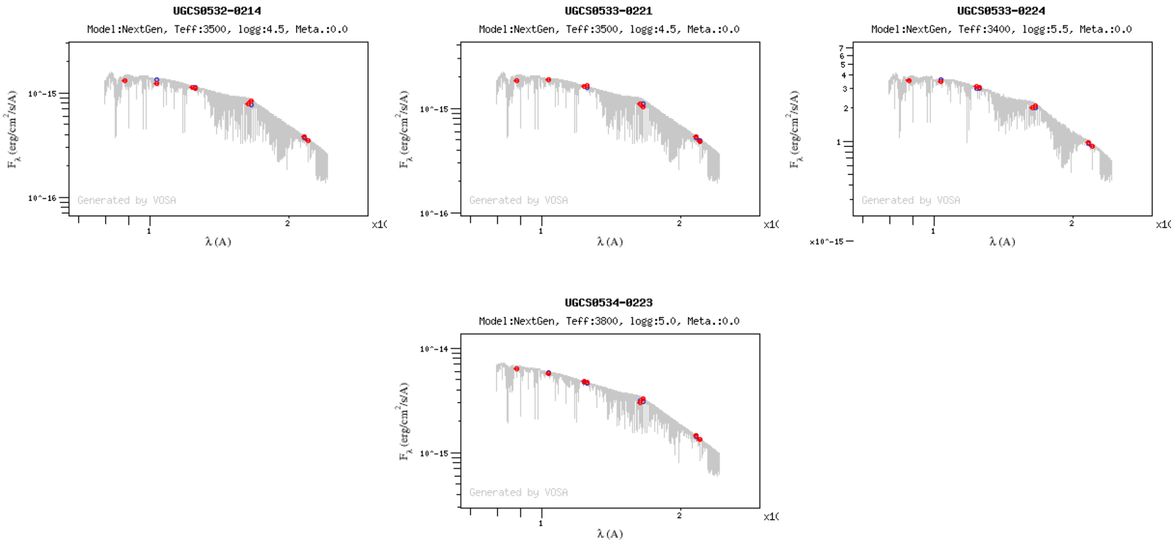

Figure D.18: Best fit SED for the observed objects by VOSA, part V (see Fig. D.14).

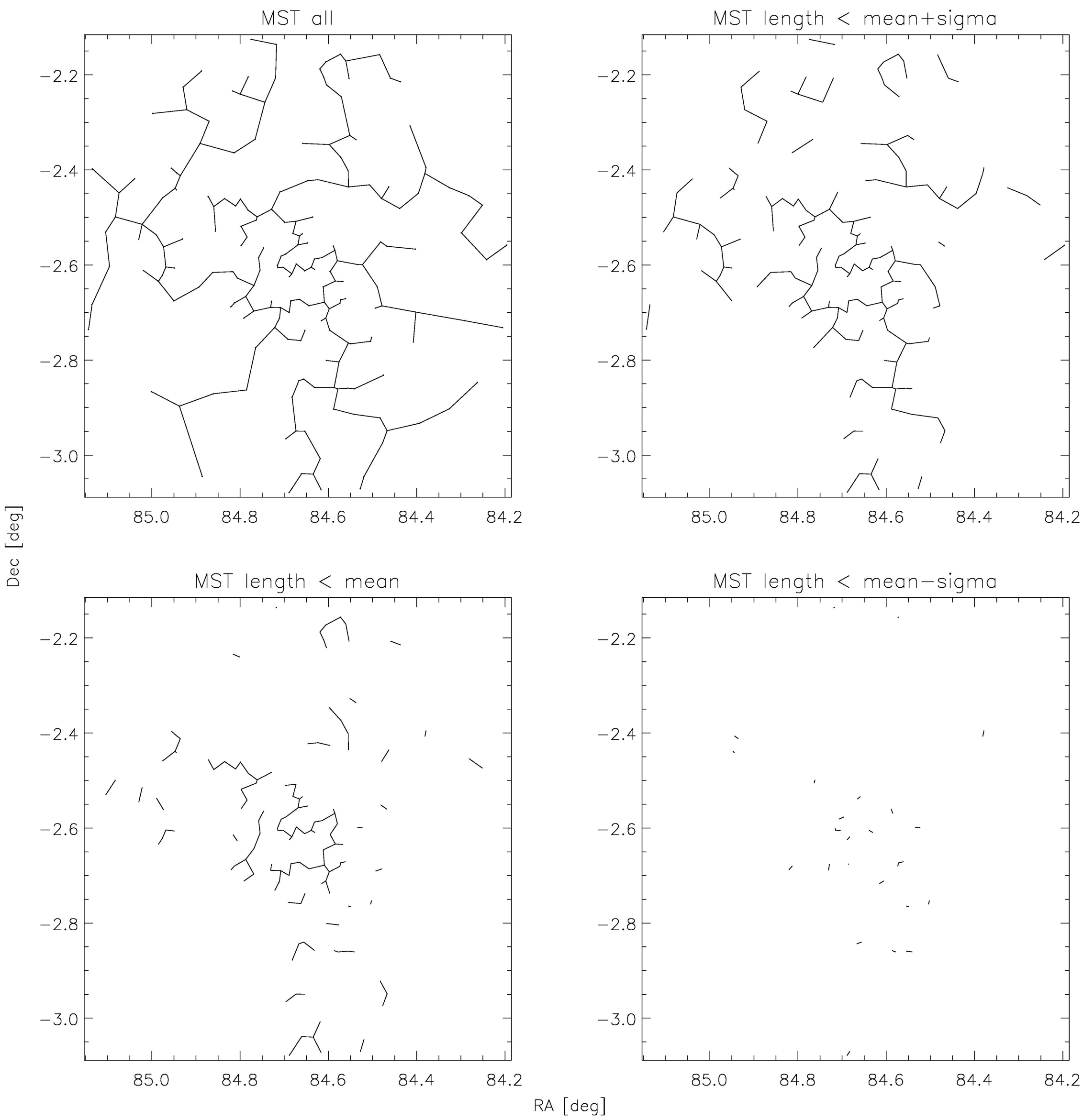

Figure D.19: The MST of the σ Orionis cluster with all its branches (top left). We show the MST showing lengths of the mean values plus 1σ (top right), the mean value (bottom left), and the mean values minus 1σ (bottom right).

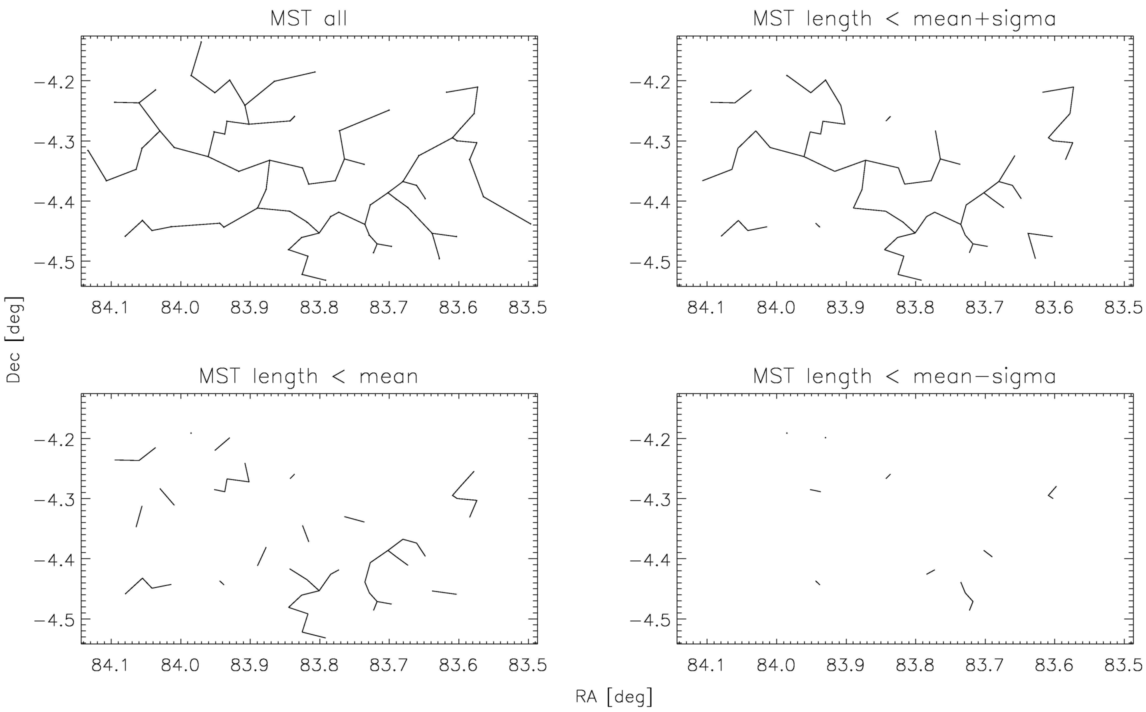

Figure D.20: The MST of NGC 1981. For explanation of the four diagrams see Fig. D.19.

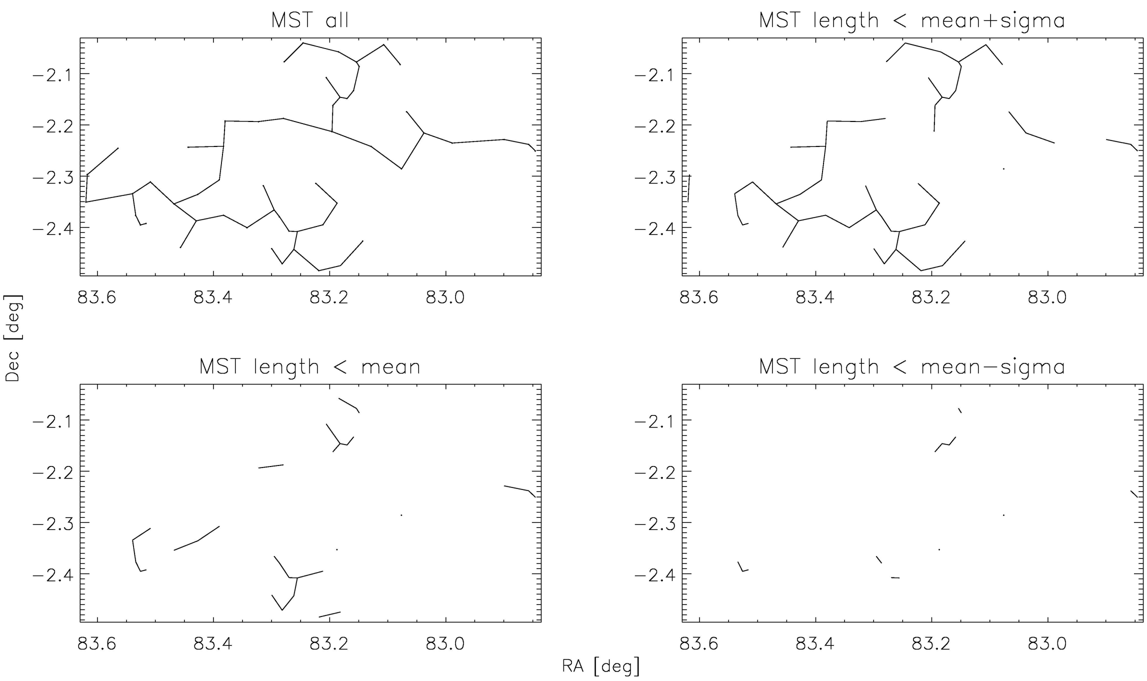

Figure D.21: The MST of the new star cluster. For explanation of the four diagrams see Fig. D.19.

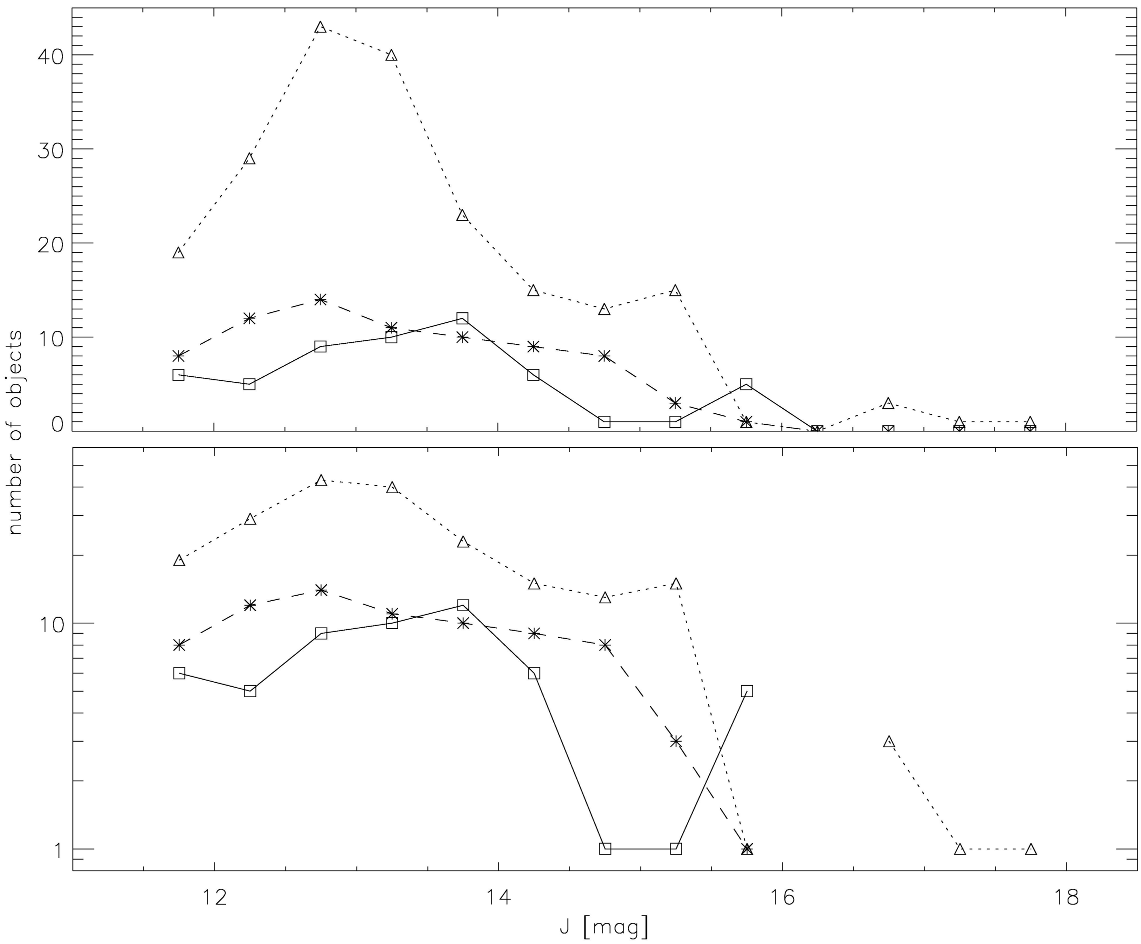

Figure D.22: top: the linear luminosity function of the three clusters σ Orionis (triangle), NGC 1981 (asterisk) and the newly found one (square). bottom: the logarithmic distribution of the three clusters. We find a peak of $J = 12.75$ *mag* for the first two and $J = 13.75$ *mag* for the newly found one. This corresponds to masses between 0.8 and 0.9 $M_{\odot}$ & 0.6 and 0.7 $M_{\odot}$, respectively, following the evolutionary models used in this work. For comparison see also the LF of Taurus in Fig. A.1.